GROUND PENETRATING RADAR SURVEY OF HISTORIC MASONRY ARCH BRIDGES OF GALICIA (SPAIN)

Mª Mercedes Solla Carracelas

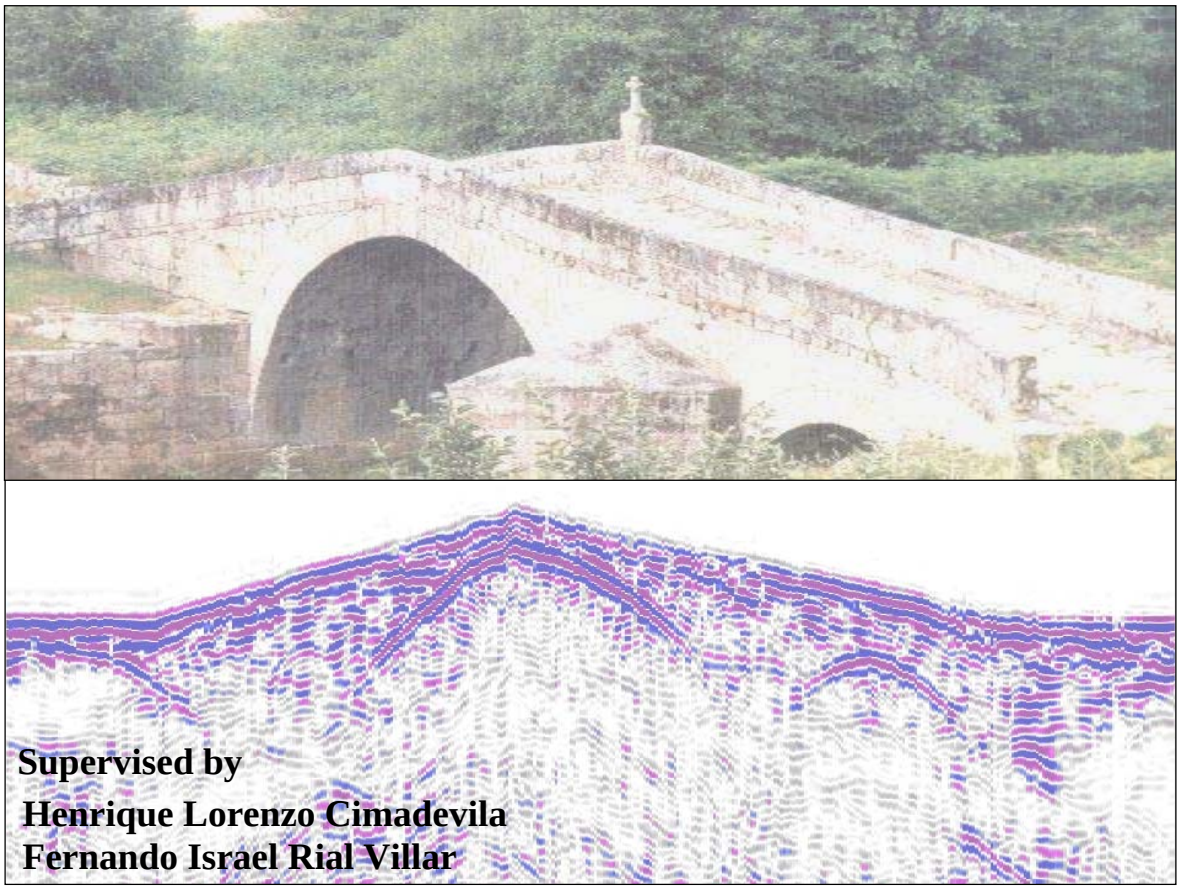

Supervised by
Henrique Lorenzo Cimadevila
Fernando Israel Rial Villar

Department of Natural Resources & Environmental Engineering
University of Vigo

– OPTA AL DOCTORADO EUROPEO –

Pontevedra, 2010

Abstract

Historical bridges represent an integral part of the traditional architectonic heritage of a region. These ancient structures require special attention because many of them have lost their original utility and now have different functionalities, often supporting special tension conditions such as strong loads and intense vibrations. Therefore, a constant diagnosis of their structure is required to provide information on their preservation and restoration using methods that will not change the historical character of the structure.

This thesis presents the results of the application of GPR as a non-destructive technique for evaluating the state of conservation of 36 Roman or medieval bridges selected from around the whole Galician territory (NW Spain). A field methodology was proposed in this work to analyze the viability and effectiveness of GPR for obtaining internal information on ancient masonry arch bridges from three points of view: historical, structural and archaeological. As a result, an inventory was developed including the most relevant information obtained for their characterization and diagnosis. This information can be useful for engineers in planning maintenance or rehabilitation tasks as well as in designing legal regulations for heritage protection.

Owing to the heterogeneity of these structures, the analysis and interpretation of GPR data can be complex. In such circumstances, a sophisticated numerical modelling was employed to facilitate GPR data interpretation. The GPR numerical modelling allowed the study of the attributes of reflected signals from various targets within the bridge structure. The GPR numerical analysis was undertaken using the finite-difference time-domain (FDTD) method and the synthetic models were created from the accurate external geometry of the bridges provided by photogrammetric and 3D laser scanning methods.

The contents of this work are organized as follows:

Chapter 1 provides the motivation taken into account for this dissertation together with the main purposes and scope established, concluded by brief comments on each chapter.

Chapter 2 provides some general background information on masonry arch bridges. A brief summary of their evolution and construction materials is given as well as details on the typical damages that historical bridges suffer. A significant part of this chapter focuses on the most common NDT methods employed for the detection of these problems with particular attention to GPR. The main applications and the basic fundamentals of GPR are outlined, and, finally, a brief historical review of GPR applications to masonry arch bridges is presented.

In Chapter 3, the survey methodology proposed in this work for assessing historical bridges is described. The GPR and the topographic surveys as well as the methods used to obtain the external geometries of the structures are briefly explained. Some guidelines for GPR signal processing are also presented. Finally, some guidelines for FDTD modelling are provided. In addition, the theory of FDTD numerical modelling is outlined with a particular emphasis on the GprMax software.

Chapter 4 presents the GPR results obtained for the 36 selected historical bridges. This chapter is divided in two parts. The first one includes an inventory with a brief summary concerning the GPR results acquired for all of them. The second part consists of a selection of four case studies representative of the most interesting results acquired where the results are analyzed in more detail and compared with synthetic models. The extracted results revealed noteworthy information from historical, archaeological and structural points of view.

Finally, the general conclusions of the thesis are summarized in Chapter 5, including some recommendations for future works.

Resumen

Los puentes históricos representan una parte integral del patrimonio arqueológico de una región. Estas construcciones requieren una especial atención puesto que muchas de ellas han perdido su utilidad original y en la actualidad, se encuentran desempeñando una funcionalidad diferente para la que han sido diseñados. Normalmente se encuentran expuestos a especiales situaciones de tensión como pueden ser las fuertes cargas e intensas vibraciones derivadas del tránsito de vehículos. Por lo tanto, se requiere de medidas de evaluación y diagnóstico constantes encaminadas a su conservación y rehabilitación, utilizando métodos que no alteren el carácter histórico de estas estructuras.

En el presente trabajo se analiza la aplicación del GPR como una técnica no destructiva para la evaluación del estado de conservación de 36 puentes históricos, romanos o medievales, de la Comunidad Autónoma de Galicia (Noroeste de España). Para ello, se ha propuesto una metodología de campo con el objetivo de evaluar la aplicabilidad y efectividad del GPR para obtener información interna de puentes históricos de mampostería desde tres puntos de vista: histórico, estructural y arqueológico. Como resultado, se ha desarrollado un inventario en el cual se ha incluido la información más relevante adquirida para su caracterización y diagnosis, lo cual puede ser útil para los ingenieros en cuanto a decidir futuras tareas de mantenimiento o rehabilitación o incluso poder diseñar adecuadas normas de protección del patrimonio histórico-arqueológico.

Debido a la heterogeneidad que suele caracterizar a estas estructuras, el análisis e interpretación de datos GPR pueden llegar a ser muy complejos. Para estos casos, fueron requeridas simulaciones numéricas sofisticadas en cuanto a poder establecer una adecuada interpretación de los datos obtenidos. Mediante el empleo de estas simulaciones, ha sido posible el estudio de la naturaleza de algunas de las señales reflejadas dentro del puente. Para la realización de este análisis GPR numérico se ha aplicado el método de diferencias finitas en el dominio del tiempo (FDTD) y los modelos sintéticos fueron elaborados a partir de la geometría externa precisa obtenida mediante Fotogrametría o 3D Láser Scanner.

Los contenidos de cada capítulo de esta tesis son los siguientes:

El Capítulo 1 presenta la motivación tenida en cuenta para el desarrollo de este trabajo así como, los principales objetivos y ámbito de aplicación establecidos. La última parte de este capítulo está compuesta por un breve comentario para cada uno de los restantes capítulos.

En el capítulo 2 se recoge información general sobre los puentes mampostería y arco. Se presenta un breve resumen sobre su evolución y materiales constructivos así como a los daños típicos que se suelen observar en puentes históricos. Una parte significativa de este capítulo se centra en los métodos no destructivos más comúnmente empleados para la detección de estos problemas, con una atención excepcional al GPR. Las principales aplicaciones y los fundamentos básicos del GPR son brevemente expuestas y, finalmente, se presenta una breve revisión histórica en la aplicación del GPR al estudio de este tipo de construcciones.

En el capítulo 3 se describe la metodología de trabajo propuesta en este trabajo para evaluación de puentes históricos. Se detallan brevemente los estudios con GPR y topográficos así como los métodos empleados para obtener la geometría externa de la estructura son brevemente detallados. Además, se presentan se presentan algunas pautas para la simulación numérica, con una breve introducción a la teoría de la análisis numérico FDTD y una breve descripción al software GprMax empleado para generar los modelos sintéticos.

En el Capítulo 4 se muestran los resultados obtenidos para los 36 puentes históricos seleccionados. Este capítulo está dividido en dos partes. Una primera parte incluye un inventario en el que se recoge un breve resumen de los datos adquiridos para cada uno de estos puentes. La segunda parte del capítulo está compuesta por una selección de cuatro casos de estudio representativos de los resultados más interesantes que se han observado. En esta sección, los resultados son analizados con más detalle y comparados con modelos sintéticos con el fin de poder realizar una interpretación más exhaustiva. De este modo, la interpretación realizada para cada uno de ellos ha revelado información de importancia desde el punto de vista histórico, arqueológico y estructural.

Por último, las conclusiones generales del trabajo en su conjunto se resumen en el Capítulo 5 junto con algunas sugerencias y propuestas para futuras investigaciones en este tema.

Acknowledgements

I would like to thank to my supervisors Dr. Henrique Lorenzo and Dr. Fernando I. Rial for their guidance, support, and tireless enthusiasm for this project. Their advices and comments have strengthened all aspects of this thesis. I would also like to thank my lab mates Dr. Alexandre Novo and Dr. Manuel Pereira for their always helping hands in the field and entertaining discussions. Likewise, thanks go to Dr. Pedro Arias, Dr. Julia Armesto and Belén Riveiro for collaborating with the accurate geometrical data by photogrammetry and laser scanning – especially to Belén for her collaboration and lasting friendship. As well, Till Sonnemann, Santi and Simón are thanked for their help during data adquistion.

I wish to show my appreciation to Dr. Antonios Giannopoulos for his advice, help and reception during my stay in the School of Engineering at the University of Edinburgh, supported by the HPC-Europa project (European Commission) and the Spanish Ministry of Science and Innovation.

I also want to show my gratitude towards Dr. Manuel Durán for the interesting discussions and the valuable information provided for a better understanding in matter of historical bridges. Also, Dr. Dean Goodman is thanked for his guidance in terms of data acquisition and understanding of the GPR-Slice software package.

Lastly and most importantly, my gratitude goes to my family for supporting my ambition to follow my dreams and for providing me with their dedication, patience and encouragement along these four long years. It would take up much space to thank all my friends who supported me with their care. However, I would like to name my friends Carmen, Julia, Ana, Jorge, Kata, Elena, Sandriña, Rebe, Noe, Maria, Ángeles, Sesi, Yoli and Sandra as well as, Cardi, Baby, Isabel and Miguel for their endless support.

This research has been partially supported by Xunta de Galicia (PGIDIT06CSC37101PR) and MICINN (BIA2006-10259). Additionally, I want to mention the support of a pre-doctoral grant from DXID-Xunta de Galicia.

List of Symbols

B	Magnetic flux density (Wb/m^2)
D	Electric flux density (C/m^2)
E	Electric field intensity (V/m)
H	Intensity of the magnetic field (A/m)
J	Current density (A/m^2)
c	Velocity of light in free space (30 cm/ns)
d	Depth (m)
f	Frequency (Hz)
t	Time (s)
λ	Wavelength (m)
ε	Electric permittivity (F/m)
ε_0	Permittivity of free space (8.854×10^{-12} F/m)
ε_r	Relative permittivity or relative dielectric constant
μ	Magnetic permeabiliby (H/m)
μ_0	Magnetic permeability of free space ($4\pi \times 10^{-7}$ H/m)
μ_r	Relative magnetic permeability
q	Electric charge density (C/m^3)
σ	Electrical conductivity (S/m)
v	Velocity (m/s)

List of Abbreviations

2D	Two Dimensional
3D	Three Dimensional
BAM	Federal Institute for Materials Research and Testing
CDP	Common Depth Point
CMP	Common Mid Point
CO	Common Offset
EM	Electromagnetic Field
FDTD	Finite-Difference Time-Domain
FEM	Finite Element Analysis
FFT	Fast Fourier Transform
GPR	Ground Penetrating Radar
GSSI	Geophysical Survey Systems, Inc.
ICOMOS	International Council on Monuments and Sites
IDS	Ingegneria Dei Sistemi
MALA	Måla GeoScience
NDT	Non-Destructive Testing
S & S	Sensors & Software Inc.
SI	International System of Units
UNESCO	United Nations Educational, Scientific and Cultural Organization
WARR	Wide Angle Reflection and Refraction
RTK	Real Time Kinematic
GPS	Global Positioning System

Contents

1

Introduction

1.1.- MOTIVATION OF THIS THESIS

As there has been a continuous increase in the use of non-destructive testing (NDT) methods to detect defects and anomalies in various civil engineering structures from the 1990s to the present (Peters and Young, 1994; Saarenketo et al., 1995; Martin et al., 1998; Grandjean et al., 2000; Maierhofer and Leipold, 2001; Wiggenhauser, 2002; Chong et al., 2003; Lataste et al., 2003; Popovics, 2003; Tavukçuoğlu et al., 2005; Leucci et al., 2007; Bavusi et al., 2009; Al-Qadi et al., 2010), several organizations dedicated to the conservation, protection, enhancement and appreciation of cultural heritage such as ICOMOS and UNESCO have asserted the importance of NDT technology to evaluate historical monuments, reflecting societal concern for their maintenance and conservation (Icomos, 2001; Lourenço, 2004; Genovese, 2005). Consequently, some studies on the assessment of historical buildings with NDT methods have been reported in recent years (Maierhofer et al., 2003b; Ranalli et al., 2004; García et al., 2007; Orlando and Slob, 2009; Pérez-Gracia et al., 2009). In this sense, it is possible to mention the important value of historical bridges from several points of view: architectural, historic, economic, symbolic and aesthetic (Fernández, 1995). This has posed an important task for engineers and scientists in terms of determining the state of conservation of historical bridges and to provide information about their preservation and restoration using methods that will not change the historical character of the structure (Lourenço and Oliveira, 2006; Melbourne et al., 2006; Bień and Kamiński, 2007; Orbán et al., 2008; Ural et al., 2008).

Many of these bridges have lost their original utility and now have different functionalities than those for which they were originally designed (Forde, 1998; Clark and Forde, 2003a; Orbán, 2006; Senker, 2007), but they continue to provide a visual surprise of the first order, mainly if as often happens they are located in beautiful rural places. They can characterize the landscape of a region (Rusnak and Boothby, 1998) and represent an integral part of its traditional architectonic heritage (Mullett et al., 2006; Fraile and Gamallo, 2007). These constructions require special attention due to their vulnerability because, normally, they are subjected to special tension conditions such as road traffic, great avenues, seismic movements, etc., besides suffering from possible engineering errors made during their construction and the ordinary human and natural actions over the centuries, producing a deterioration that demands a constant conservation (Alvarado et al., 1989; Oliveira and Lourenço, 2004). When this conservation stops, ruin and destruction soon set in. A number of the remaining bridges are at a risk of total loss, not to mention those that are in the process of being destroyed or are submerged in reservoirs. Some of them are part of the road infrastructure, requiring a constant evaluation of their structures due to the strong loads and intense vibrations they support (Clark and Forde, 2003b; Bhandari, 2006).

While ground penetrating radar (GPR) is one of the most recommended NDT methods in bridge inspection (Carrión et al., 2003; Orbán et al., 2008), the specialized literature does not contain many examples of GPR surveys in evaluations of historical bridges, probably because non-destructive testing on ancient civil engineering structures with GPR is a relatively new subject (Flint et al., 1999). Thus, GPR studies applied to the evaluation of masonry arch bridges are not yet widespread, with only a few selected examples found in recent years (Colla et al., 1997a; Flint et al., 1999; Pérez-Gracia, 2001; Colombo et al., 2002; Fernandes, 2006; Orbán, 2006; Arias et al., 2007; Lorenzo et al., 2007; Diamanti et al., 2008; Orbán et al., 2008; Riveiro et al., 2008; Solla et al., 2008a,b,c; Orbán and Gutermann, 2009; Lubowiecka et al., 2009; Solla et al., 2009).

The distribution of historical bridges in Galicia (NW Spain) is very extensive and a Roman or medieval bridge can be found in any village, valley or stream. At the moment, there are about 250 historical bridges catalogued in the Galician territory (Alvarado et al., 1989). This work presents an extending methodology in the non-destructive and non-invasive evaluation of historical bridges in Galicia by GPR. This technique was chosen because improvements in its understanding and its use on masonry arch bridges are expected in the

near future due to its quick data acquisition and real-time data interpretation. Construction details, modifications and problems arising over time are elucidated. This inner structural information, along with external measurements, could be useful for civil engineers in verifying the structural stability of a bridge in terms of conservation and restoration.

1.2.- SCOPE AND OBJECTIVES OF THE RESEARCH

This thesis is agreed with the objectives, contents and investigation activities developed in two Research Projects entitled:

"*Advanced Methodologies on Close Range Photogrammetry, Laser Scanner and Radar Applied to Historical Bridge Evaluation and Documentation*", with financial support of Xunta de Galicia (PGIDIT06CSC37101PR).

"Geomatic Techniques for the Structural and Dimensional Analysis of Historical Bridges and their Conservation", with financial support of the Spanish Ministry of Science and Education (BIA2006-10259).

The main general goal of this work was to analyze the viability and effectiveness of GPR (as an NDT method), for obtaining internal information from ancient masonry arch bridges from three points of view: documentary, structural and archaeological. It will allow for improved knowledge of the state of conservation in a number of representative historical bridges in Galicia from the Roman and Medieval periods, the majority of which have been rehabilitated or partially reconstructed over the years.

In particular, this study attempted to assess the feasibility of GPR to: 1) locate and measure structural elements inside the bridges such as hidden arches or inner reinforcements; 2) document and position failures such as cracks or voids; and 3) detect different filling zones with respect to the construction materials used and their homogeneity or/and density, changes often related to rehabilitation or reconstruction activities. The final purpose was to develop synergies for creating or improving the processes and services related to the value of this cultural heritage by means of conservation activities, especially in aspects of durability and security, environmental concerns and, in particular, for the evaluation, rehabilitation and maintenance of historical bridges. To this end, a database was created including all information obtained from the GPR surveys conducted.

Sometimes, because of the heterogeneity of these structures, the identification of interesting construction details can be difficult due to the confluence of many reflections, e.g., multiples, corner reflections and reflections from the foundations and filling material between the arches. In such circumstances sophisticated numerical modelling is required. For an exhaustive interpretation of the GPR results, the proposal implemented the application of GPR together with close-range photogrammetry and 3D laser scanning methods. The accurate three-dimensional data obtained on the external geometry of the bridges was used as inputs to create synthetic radargrams using GprMax, an electromagnetic wave simulator for GPR, developed using the finite difference time domain (FDTD) method to aid in GPR data interpretation (Giannopoulos, 2006).

1.3.- OUTLINE OF THIS THESIS

Chapter 2 provides some general information on masonry arch bridges. A brief summary of the evolution of these structures throughout history, as well as their construction materials and their main structural damages are described. A significant part of this chapter reviews the most common NDT techniques employed to evaluate masonry arch bridges with a special attention to GPR. A short history of GPR and its main applications is presented in addition to its basic principles and the fundamental equations governing the propagation of electromagnetic signals. Finally, the range of GPR applications in evaluating masonry arch bridges is summarized.

The survey methodology proposed for evaluating historical bridges is described in Chapter 3. The GPR and topographic surveys as well as the methods used to acquire the external geometry of the structures are explained. The usual GPR signal processing applied is also presented. Finally, some guidelines for FDTD modelling are provided. This numerical simulation can represent an important tool in GPR data interpretation.

Chapter 4 shows the GPR results obtained for the historical bridges selected around the Galician territory. This chapter is divided in two parts. The first one includes an inventory with a brief summary concerning to the GPR results gathered for all bridges surveyed. This inventory maintains a balanced representation of the four Galician provinces. The second part is composed by a selection of four case studies representative of the most interesting results acquired.

Finally, the general conclusions of the thesis are summarized in Chapter 5, including some recommendations for future works.

2

Masonry arch bridges

This chapter is divided in two parts; the first part provides information about masonry arch bridges history as well as the evolution of their different construction materials used throughout time and the main structural damages caused in masonry bridges, while the second part is an introduction to the most common NDT methods employed to analyze their state of conservation with a special attention to GPR.

2.1.- HISTORICAL EVOLUTION OF MASONRY ARCH BRIDGES

The bridges origin takes place in the prehistory. Bridges are useful structures which have suffered a historical transformation according to the conditions of transportation and technical limitations. Possibly, the first bridge made by the most primitive human communities was a simple fallen tree to serve as a plank when streams need to be crossed. The following bridges were spans of wooden logs or planks and eventually stones, using a simple support and crossbeam arrangement in order to connect both margins of a river. Maybe the oldest existing arch bridge is the Mycenaean Arkadiko bridge in Greece from about 1300 b.C. This is a stone corbel arch bridge (Fig. 2.1). Although true arches were already known by the Etruscans and ancient Greeks, the Romans were –as with the vault and the dome– the first to fully realize the potential of arches for bridge construction. Roman arch bridges were usually semicircular –barrel arch–, although a few were segmental –elliptical and segmented arches–. Gothic pointed arches were introduced at medieval period (Fernández, 2005). While medieval bridges adopted a double-sloped

elevation, roman bridges had a horizontal road surface modified only by the minimum gradient necessary for road drainage (Durán, 2004). Figure 2.2 illustrates a variety of arch geometries and Figure 2.3 shows the components of a masonry arch bridge and the terminology employed for its different parts.

Figure 2.1.- Illustration of Arkadiko bridge in Greece. (*From Wikipedia, 2009*)

Figure 2.2.- Different arch geometries.

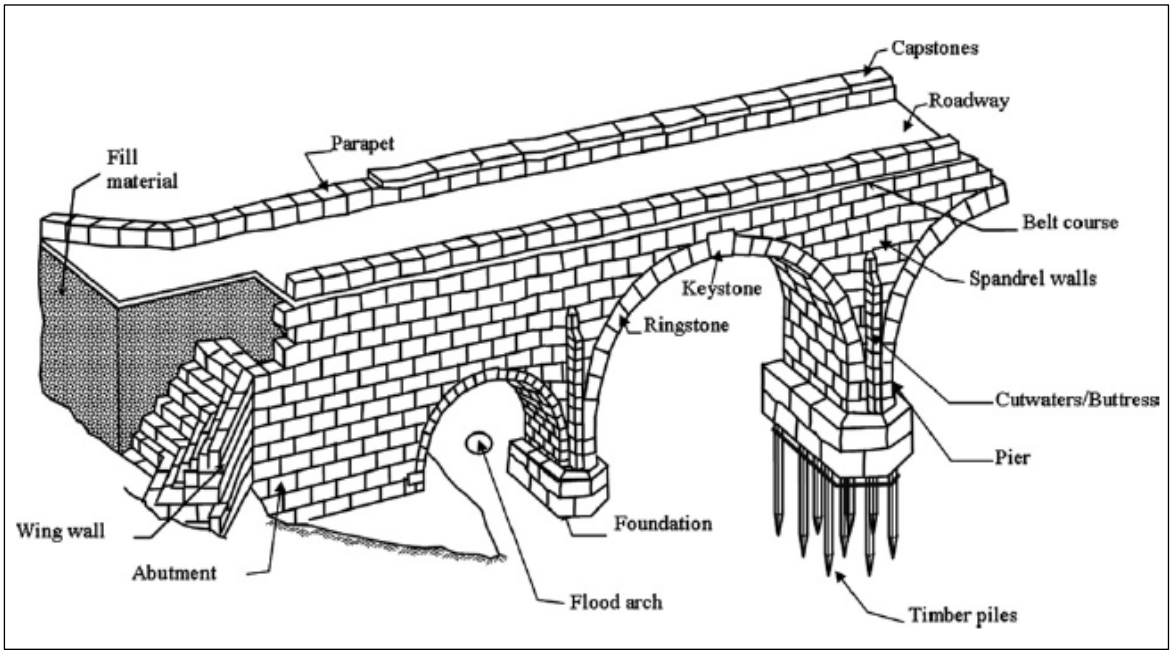

Figure 2.3.- Component parts and definitions used in masonry arch bridges. (*From Ural et al., 2008*)

Bridges have been constructed throughout history using different materials. When Rome began to conquer the World, they were constructing wooden bridges and it was when they started to build paved roads that they constructed stone bridges. Roman engineers were the first and until the industrial revolution the only ones to construct bridges with concrete. This concrete were called "*Opus caementicium*" which is made from a mix of aggregate and a binder –as gypsum, lime and volcanic dusts in some cases– which, when mixed with water, hardens over time. It was used from the beginning of the Roman Republic through the whole history of the Roman Empire. Brick and mortar bridges were built after the Roman Era, as the technology for cement was lost then later rediscovered. The main materials that were used for bridges construction are stone, timber, steel, reinforce concrete, pre-stressed concrete and post-stressed concrete. More recently –with the Industrial Revolution in the 19th century–, iron bridges were developed.

Typical historical bridges are stone arch bridges (Durán, 2002; Ural et al., 2008). Ever since man got to control the arch technique, this type of bridges dominated during centuries. Only the industrial revolution with incipient construction techniques using iron could restrain this dominion. In more modern times, stone and brick bridges continued to be built by many civil engineers but different materials as iron, steel and concrete have been increasingly used in the construction of arch bridges due to their low cost. Many historic bridges have been destroyed because of their strategic value, reconstructed or widened due to the new needs of transport, or abandoned owing to the construction of other further bridges.

The quality of masonry arch bridges depends on the materials employed. The habitual materials for the construction of historical bridges are stone, with or without the presence of mortar being a mixture of cement, sand and lime and occasionally of other ingredients. In the early masonry bridge structures, mortar was not present in the building arrengement since it was constructed from cut and perfectly fitted stone blocks. In the case of less well-shaped stone blocks, mortar layers were used to fill the gaps between the stone units to provide a uniform contact surface. Mortar has a very significant influence on the structural behavior of the masonry construction. Therefore, a number of important mortar properties, such as ability to spread easily, water retain-ability, resistance to cracking, water penetration, frost and chemical attack, need to be considered (Hendry et al., 1997). In addition, puddle clay was often used in construction, depending on clay availability at the location where the bridge was built. This clay layer was employed to increase the

durability and the load carrying capacity of the bridge by serving as a waterproof backing to arches and therefore, preventing water penetration in the masonry structure and possible damage of the mortar joints (McKinbbins et al., 2006). Despite the usual external uniform surface of the stone ashlars, the internal structure of these stone blocks is very irregular. This effect is called internal anathyrosis (Durán, 2005). Also the internal staircase shape of ring stone could be observed in some cases as shown in Figure 2.4a. Furthermore, the filling within the bridge structure is composed by irregular and heterogeneous granular materials (Fig. 2.4b).

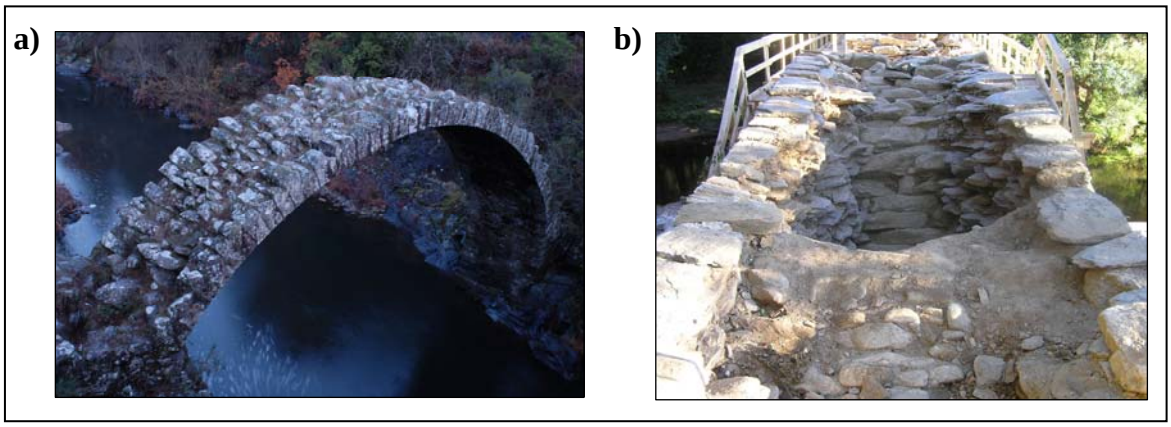

Figure 2.4.- a) Internal staircase shape of ring stones in Carixa bridge (Vila de Cruces, Pontevedra), and b) Filling material within San Alberte bridge during the restoration actuations performed (Guitiriz, Lugo).

In the Autonomous Community of Galicia, a significant number of masonry arch bridges were constructed between the roman period and the early 19th century. The stones mainly used were igneous rocks, such as granite, and metamorphic rocks, such as shale, depending on the material availability at the area of the construction. However, at the end of the 19th century, with the coming of age of the railway, big metal bridges appear. First iron, then forged iron and finally steel or reinforced concrete –at the beginning of the 20th century– allowed the development of bridges with great spans, this factor becoming a fundamental condition for the conception and design of bridges (Alvarado et al., 1989).

2.2.- DAMAGES TO MASONRY ARCH BRIDGES

During centuries, the construction of bridges represented a feat since it required an enormous economic effort and specialized technical skills. They were considered to be in a permanent state of construction and transformation for centuries (Alvarado et al., 1989; Oliveira and Lourenço, 2004). Masonry arch bridges are the oldest structures still in use in

the transport infrastructure and as a result of ageing, their materials degrade and they suffer a number of damages (Page, 1993). The typical damages for historic masonry have been divided into two main groups: 1) damages due to material deterioration such as moisture, erosion and other damages due to wind and air pollution; 2) damages due to mechanical effects on the structure including increase and decrease of loads, traffic, differential settlements, thermal deformation, earthquakes or explosions (Maierhofer et al., 2003b). The main cause of those damages is due to water. Insufficient or damaged waterproofing causes the initiation of the decay process which in addition to adverse weather conditions, results in the deterioration of the masonry unit (Frunzio et al., 2001). In addition, the increase in traffic loads and age of these structures has resulted in structural decay (Bhandari and Kumar, 2006). Some of the most typical damages in masonry arch bridges are shown below in Figure 2.5.

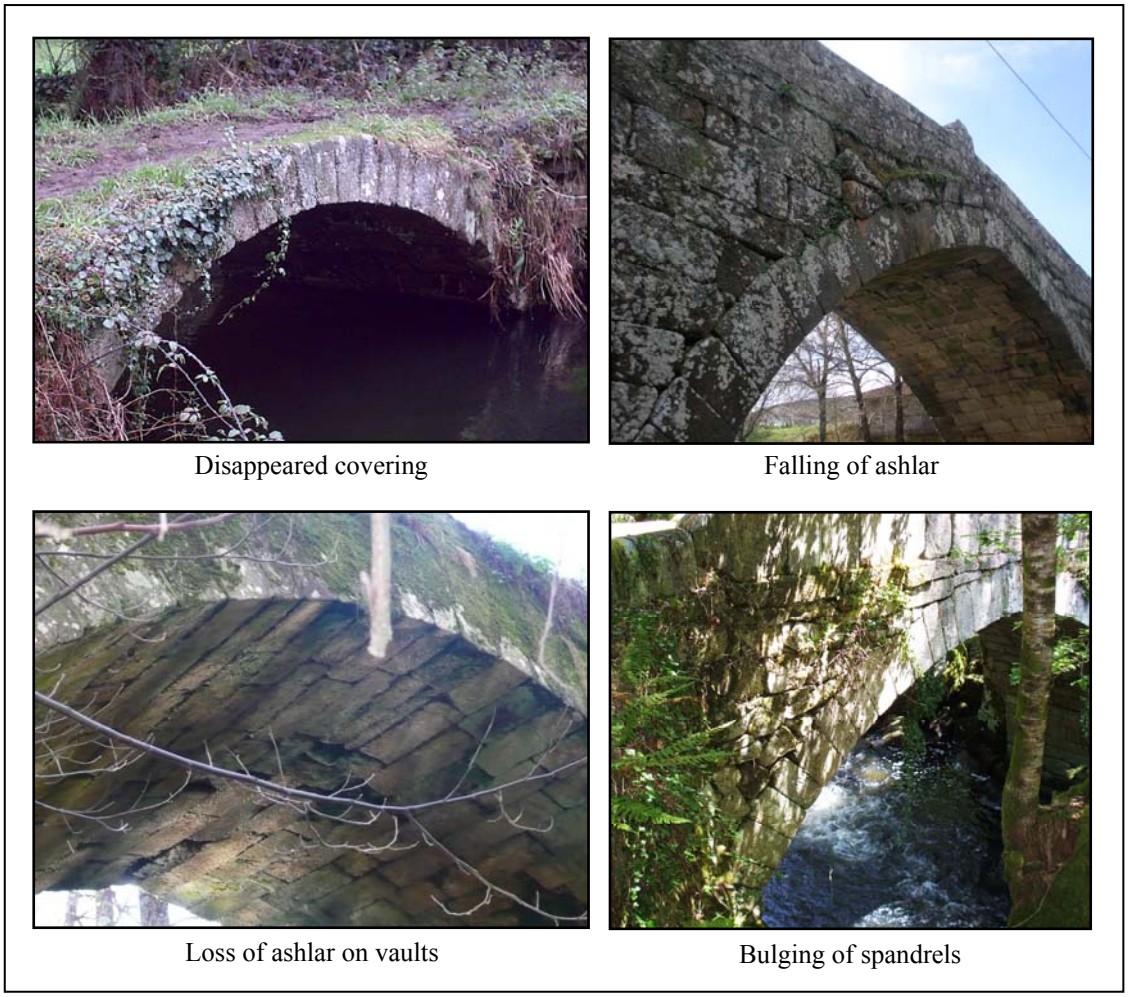

Fig 2.5.- Frequent damages on masonry arch bridges.

A masonry arch bridge responds to traffic loading in two directions: parallel to the span and transverse to the span. The cracks in the transverse direction may result in separation

of the arch barrel from the collapse of a spandrel walls or wing wall (Fanning et al., 2001). Thus, longitudinal cracks have the potential to seriously reduce the carrying capacity of the bridge. Besides, a crack in arch barrel may have its origin in deficient foundation behaviour (Mathur et al., 2006). The foundation damages can be produced due to the construction material or soil-foundation degradation. Even superstructures damages can be produced resulting from a bad resistance performance –gravitational actions, imposed movements, abutment overturn by excessive earth pressure, bulging of spandrels, damages in wing walls, stepped cracking, arch mechanism failure and loss or dislocation of pieces– or a deficient durability –climatic and/or weather conditions, as well as growth of vegetation or even improper maintenance of drainage– (Ozaeta and Martín-Caro, 2006).

2.3.- NDT METHODS FOR ASSESSING MASONRY ARCH BRIDGES

Many masonry arch bridges are listed historical monuments, valued tourist attractions or local landmarks (Mabon, 2002). NDT methods are required for assessing their state of conservation in support of preserving the historical character of these structures (Lourenço and Oliveira, 2006; Ural et al., 2008). Some reasons for using NDT methods are (Orbán, 2007): 1) to determine hidden dimensions such as barrel thickness, level of filling, presence of dovetailed clamps, internal voids, pier geometry, depth and condition of foundations, etc.; 2) to investigate variations in type and quality of materials throughout the structure; 3) to identify damages such as cracks, voids, ring separation, fill leaching, insulation, etc.; 4) to identify and control previous interventions such as new lining, injections, etc.; and 5) to identify services such as buried services, presence of metal, abandoned ducts, etc.

There are different NDT techniques employed in the evaluation and testing of masonry arch bridges such as sonic/ultrasonic, electromagnetic and electrical methods as well as infrared thermography (Colla, 1997; Colla et al., 1997a; Flint et al., 1999; Pérez-Gracia, 2001; Colombo et al., 2002; Perret et al., 2002; Clark et al., 2003; Clark and Forde, 2003a,b; Fernandes, 2006; Orbán, 2006; Arias et al., 2007; Lorenzo et al., 2007; Aperio, 2008; Diamanti, 2008; Forde, 2008; Orbán et al., 2008; Riveiro et al., 2008; Solla et al., 2008a,b,c; Lubowiecka et al., 2009; Orbán and Gutermann, 2009; Solla et al., 2009). Each NDT method provides different information regarding the physical properties of the masonry structure. These properties, such as compressional and shear wave velocities,

electrical resistivity and so on, have to be interpreted in terms of the stonework of the bridge and its engineering properties (McCann and Forde, 2001). Besides their varying applicability, the advantages and disadvantages of appropriate NDT methods applied to masonry arch bridge assessment have been analyzed in several works (McCann and Forde, 2001; Carrión et al., 2003; Gupta, 2005; Bhandari and Kumar, 2006). A summary of this analysis is presented in Table 2.1.

NDT method	Information obtained	Advantages	Disadvantages
Impact-echo	Voids, delamination, cracks and masonry thickness.	- Easily repeatable. - Map of discontinuities.	- Difficult to interpret. - Lost of small voids. - Difficulties for complicated geometries.
Conductivity	Moisture and salt content, masonry thickness, voids, in-homogeneities, pipes, drains, construction materials composite, presence of metal reinforcements.	- Relative quick. - Gives relative conductivities over a large area.	- Limited depth penetration of 1.5 m. - Complements radar.
Sonic	Internal voids, cracks, damaged parts, and controlling the effectiveness of repair interventions.	- High penetration depth. - Gives an overall qualitative view.	- Specialist required for interpretation. - Slow
Infrared thermography	Cavities and delamination, detection of inclusions of different materials, presence of moisture.	- Gives an overall qualitative view.	- Low penetration depth. - Specialist required for interpretation. - Susceptible to surface conditions.
Georadar	Voids, hidden geometry, inclusions of different materials, rings detachment, structural irregularities, backfill conditions, moisture level.	- High penetration depth. - Gives an overall qualitative view. - Relatively quick.	- Specialist required for interpretation. - Not applicable in conductive environments.

Table 2.1.- Overview on the main applied test methods for masonry arch bridges assessment. (*Adapted from McCann and Forde, 2001; Orbán, 2006; Orbán and Gutermann, 2009*)

It is possible to consider five main factors on the use and optimal selection of the accuracy NDT method for the appraisal (McCann and Forde, 2001): 1) depth of penetration required; 2) vertical and lateral resolution demanded; 3) the contrast in physical properties between the target and the filling; 4) signal to noise ratio for the physical property measured; 5) historical information concerning the methods used in the construction of the bridge. The fundamental principles of the most common NDT methods used for bridge assessment are described and illustrated below. In addition, brief case studies from the literature are mentioned.

2.3.1.- The impact-echo system

The impact-echo test method (Sansalone and Streett, 1997) has been developed over the past 20 years (Gibson and Popovics, 2005) and it was originally developed to measure concrete thickness and integrity from one surface (McCann and Forde, 2001). Employing the impact-echo technique, a mechanical impact is generated by using a small instrumented impulse hammer to hit the surface of the structure to be tested in a specific location and the reflected energy, when a difference in acoustic impedance is encountered, close to the impact location is recorded by an accelerometer or a displacement transducer (Fig. 2.6). The method can operate either by acquiring single point measurements, which is not an area of the structure, employing automated hardware developments for fast data collection (Colla, 2003). Since the time-domain reflected waveforms are complex and hard to interpret, the recorded signal is converted into the frequency-domain using the fast Fourier transform (FFT).

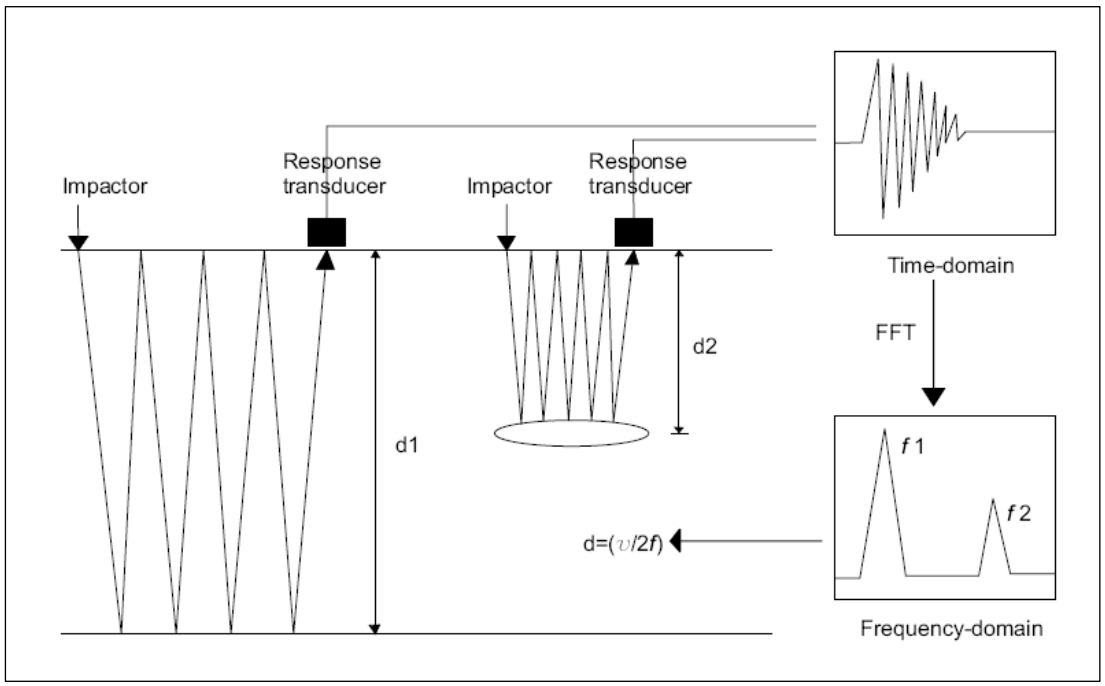

Figure 2.6.- Set-up for impact-echo test. (*From Diamanti et al., 2008*)

Reflections or echoes of the compressional wave energy are indicated by pronounced resonant frequency peaks in the frequency spectrum record (Fig. 2.7). These peaks correspond to the thickness or flaw depth resonant frequencies and knowing the compressional wave velocity of propagation in the construction material, the depth to the corresponding flaw can be calculated. The depth of the reflector will correspond to the wall thickness if the material used in construction is sound.

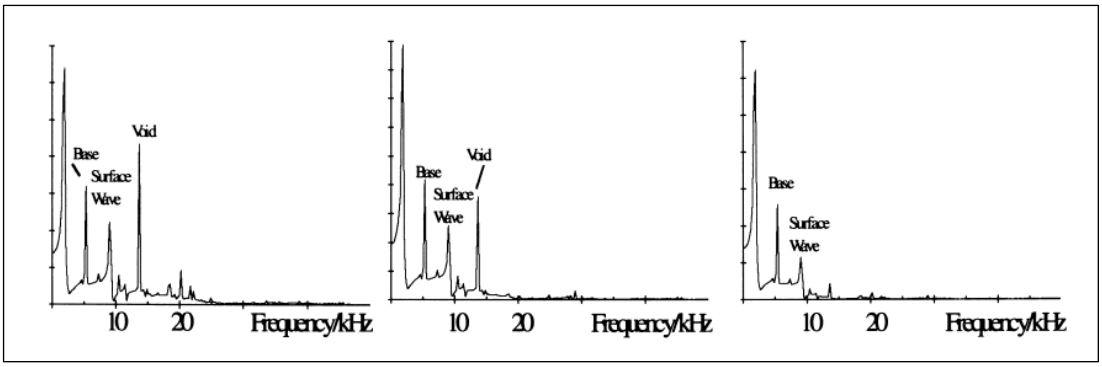

Figure 2.7.- Frequency spectrum obtained. (*From Martin et al., 1998*)

Williams et al. (1997) have shown, through numerical simulations of the impact-echo response of masonry units, as well as from laboratory and field tests; that the impact-echo method can be used to locate voids in masonry where the brick or stone units are bonded together with mortar.

2.3.2.- Conductivity measurements

Conductivity is a recent application in the civil engineering field (Colla et al., 1997a). The technique involves the use of a transmitter coil energized with an alternating current and a receiver coil located a short distance away. The time-varying magnetic field arising from the alternating current induces very small electric currents in the structure. These currents generate a secondary magnetic field, which is sensed, together with the primary field, by the receiver coil that is located close to the transmitter (Fig. 2.8).

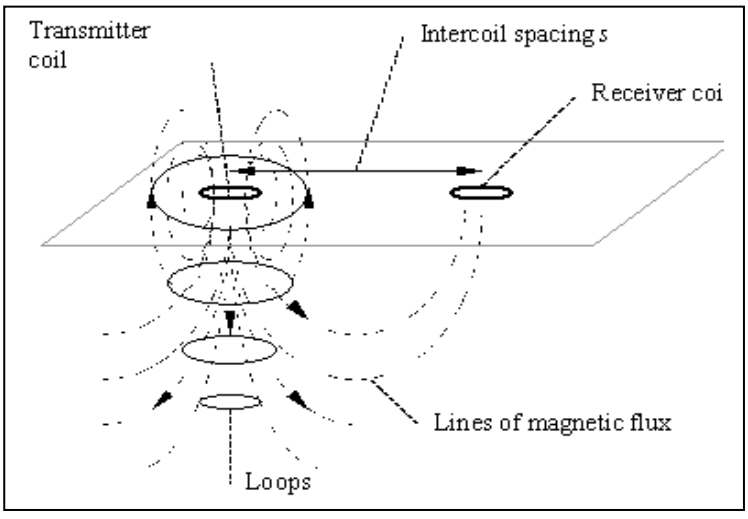

Figure 2.8.- Induced current flow in a homogeneous half-space with coils working in a vertical dipole mode.
(*From Colla, 1997*)

The conductivity equipment permits the measurement of near surface average conductivity. It should be noted that the results are averaged over the depth of penetration. This secondary field is a function of the inter-coil spacing, the operating frequency and the conductivity of the materials, and reveals the presence of a conductor and provides information on its geometry and electrical properties (McNeill, 1980). The ratio of the secondary to the primary magnetic field is therefore linearly proportional to the material conductivity.

Colla et al. (1997a) have used conductivity on a masonry bridge with moisture-drainage problems, in order to acquire important information on the moisture/water distribution in the structure, as well as, on the thickness of the masonry wall. The laboratory and field works performed by Clark and Forde (2003b) show that electrical conductivity measurements can be used to determine the moisture content within the fill of a masonry arch bridge.

2.3.3.- Sonic methods

The application of sonic methods to masonry structures date back to 1960 (Bhandari and Kumar, 2006). The sonic transmission method involves the passing of a compressional wave at frequencies between 500 Hz and 10 kHz through the structure under investigation. The signal is transmitted by an impact hammer and received on the opposite side by an accelerometer positioned directly opposite the hammer (Fig. 2.9).

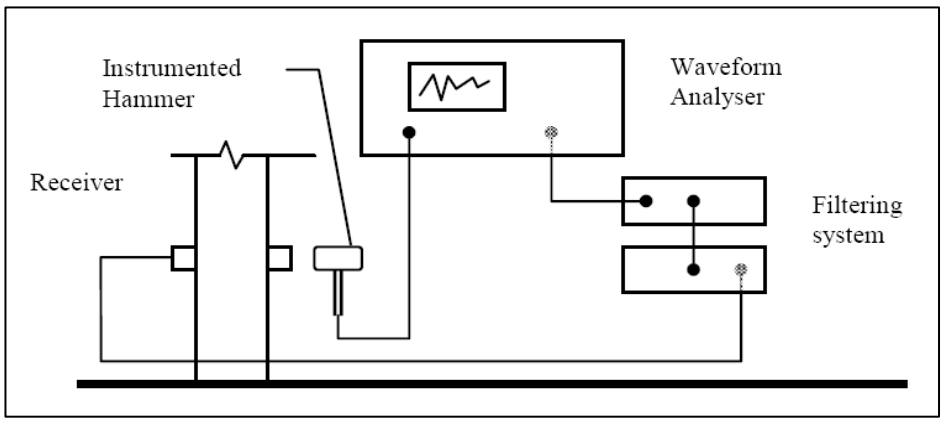

Figure 2.9.- The sonic test equipment. (*From Bhandari and Kumar, 2006*)

The results obtained are relatively simpler to interpret since it provides a defined path length through the structure. However, the resulting velocity is an average of the local velocity along the path of the wave and hence it is not possible to evaluate material

uniformity and/or inhomogeneity. Sonic tomography can be considered as the improvement of the sonic transmission method because tests are performed not only in the direct mode but also along paths which are not perpendicular to the wall surfaces. With sonic tomography, a 3D reconstruction of the velocity distribution across the structure is built up. The masonry section under investigation is divided into square pixels and the velocity reconstruction provides a mean value of the sonic velocity for each masonry fragment. Those velocities can be associated with material densities that can be related to material inhomogeneity or flaws in the masonry bridges. The velocity reconstruction image is affected by a number of factors such as the strength and the nature of the hammer impact generating the initial signal, the interpretation experience of the operator and the coupling of the receiving transducer to the masonry structure (McCann and Forde, 2001).

Colla et al. (1997a) applied the sonic methods to stone masonry bridges and have proved that the masonry wall thickness could be identified when great attention is paid to recording the data. Perret et al. (2002) performed sonic tomography tests in order to check the effectiveness of the grout injection for the restoration of a masonry bridge. Sonic tomography surveys that were carried out before the grouting revealed zones with low propagation velocities, which is an indication of problematic zones often associated to the presence of flaws and defect patterns, while sonic tests performed after the injection grouting provided evidence of the overall improvement of the masonry unit under investigation.

2.3.4.- Infrared thermography

The origin of infrared thermography comes from the early 1800s when the invisible light later called infrared was discovered. Thanks to the studies of many other scientists in successive years, infrared thermography has become a useful technique of surface temperature mapping (Meola and Carlomagno, 2004). In civil engineering, impulse-thermography has recently been applied (Maierhofer et al., 2005) and its application was mostly limited to passive investigations of the quality of thermal insulation of building envelopes (Brink et al., 2002). Nowadays, this method represents a powerful NDT tool to be used for quick periodic inspection (Meola, 2007). Infrared thermography is a technique that converts the radiated heat from an object (infrared energy in the region of the electromagnetic spectrum visible light and microwaves (Fig. 2.10)) into a visual image using specialized scanning cameras. The principle of thermograph is that any body temperature above the absolute zero emits radiation in the form of heat, with a spectral

distribution as a function of temperature. The radiated heat is dependent on a number of different factors, such as the surface emissivity, the thermal conductivity of the object, surface convection, and external radiation (Clark and Forde, 2003a).

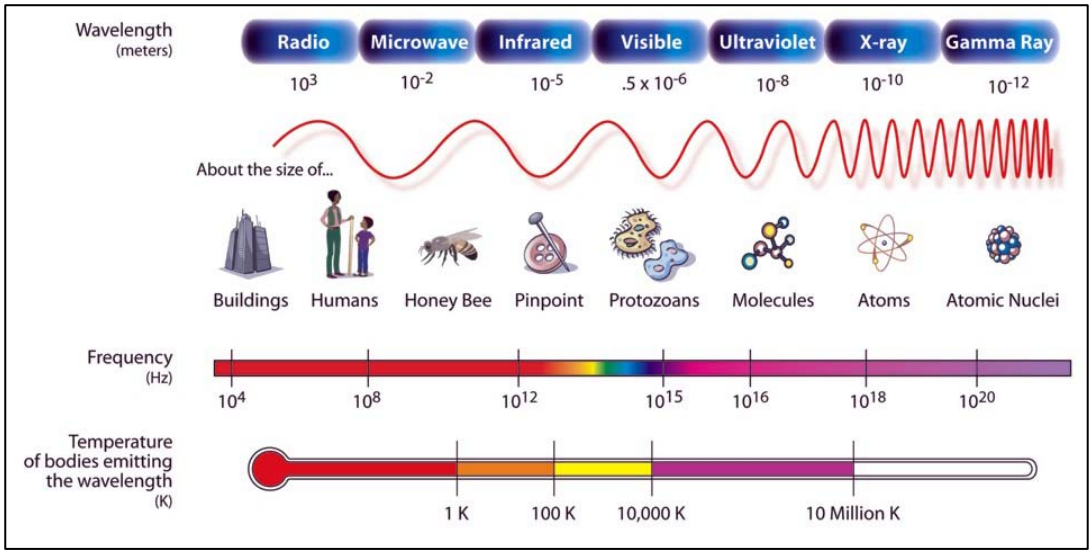

Figure 2.10.- The electromagnetic spectrum (*From NASA, 2009*).

Woodham (2002) employed infrared imaging in order to examine internal brick wall construction, and locate internal voids to be filled with injectable mortar in order to extract salts from walls. In addition, Clark et al. (2003) applied effectively, the infrared thermography method on a masonry arch bridge to investigate the presence of moisture into the bridge.

2.4.- GPR FOR MASONRY ARCH BRIDGES EVALUATION

A short history of GPR and the main applications are described in this subchapter as well as an introduction to the basic principles of GPR presenting the fundamental electromagnetic equations that govern the propagation of the GPR waves. Also the interaction of the electromagnetic pulses with the materials encountered is examined. Finally, a review on the application of GPR to evaluate masonry arch bridges is presented.

2.4.1.- Historical notes and applications of GPR

The use of radar to detect metal and dielectric objects through the reflection of electromagnetic waves was experimentally verified by Hertz in 1886 (Skolnik, 1981). Later, in 1904, the German engineer Hulsmeyer was the first to employ electromagnetic signals to detect remote terrestrial metal objects (Ulriksen, 1982). However, the first patent to locate buried objects using electromagnetic waves was obtained in 1910 by Leimbach and Lowy (Daniels et al., 1988). Additional experiments using pulse radar for the investigation of buried features were performed by Hülsenbeck (1926). After the mid-twenties and during the thirties, the radar technique was constantly developing. Pioneering works in the field of mineral and ore exploration in Sweden were carried out by Sundberg (1931). The first GPR survey was performed by W. Stern in Austria in 1929 to sound the depth of a glacier.

Later on, in the early seventies, the interest in the radar method picked up again in order to help lunar investigations and landings. Civil engineering applications of GPR started to appear in the mid 1970-1980's (Bungey and Millard, 1993; Forde and McCavitt, 1993). Bertram et al. (1974) reported one of the very first studies on the use of GPR related to civil engineering. Since then, the applications of radar have been broadened in a number of fields. A comprehensive history of development of GPR has been compiled by Daniels et al. (1988) and Cook (1995).

Some of the main applications of GPR are in engineering investigations including NDT services, such as road and concrete evaluation and bridge inspection, masonry structures investigation, utility and void detection. In addition, earth and environmental sciences use GPR to study bedrock, soil, snow, ice, glacier and moreover, groundwater contamination and remediation sites. Furthermore, GPR is employed in archaeological investigations, mineshaft, land mines, pipes and cable detection. Forensic experts are also using GPR to detect buried human bodies in order to help criminal investigations. With the continuous progress of the technology and the growing experience of the scientific community, more and better equipment is available. Since then, many specialized radar companies have appeared with similar products such as Måla GeoScience (MALA), ERA Technology, Sensors & Software Inc. (S&S), Geophysical Survey Systems Inc. (GSSI), Ingegneria Dei Sistemi (IDS) and Radar Systems Inc.

2.4.2.- GPR fundamentals

RADAR is an acronym for RAdio Detection And Ranging (Buderi, 1998). The name reflects the importance placed by the early workers in this field on the need for a device to detect the presence of a target and to measure its range. Although modern radar can extract more information from a target's echo signal than its range, the measurement of its range is, in general, one of the most important functions. It's important to note that radar engineers use the term range to mean distance, which is not the definition of range in some dictionaries (Skolnik, 2001).

2.4.2.1.- Basic principles

The ground penetrating radar is a geophysical method based on the propagation of a very short electromagnetic pulse (1-20 ns) in the frequency band of 10 MHz – 2.5 GHz. A radar system consists of four main parts; a transmitting and a receiving antenna, a control unit and a portable computer unit. Using the GPR method, a transmitting antenna emits an electromagnetic pulse into the ground which is partly reflected when it encounters media with different dielectric properties, and partly transmitted into deeper layers. Then, the reflected signal is recorded from a receiving antenna; which is either in a separate antenna box, or in the same antenna box as the transmitter (Fig. 2.11).

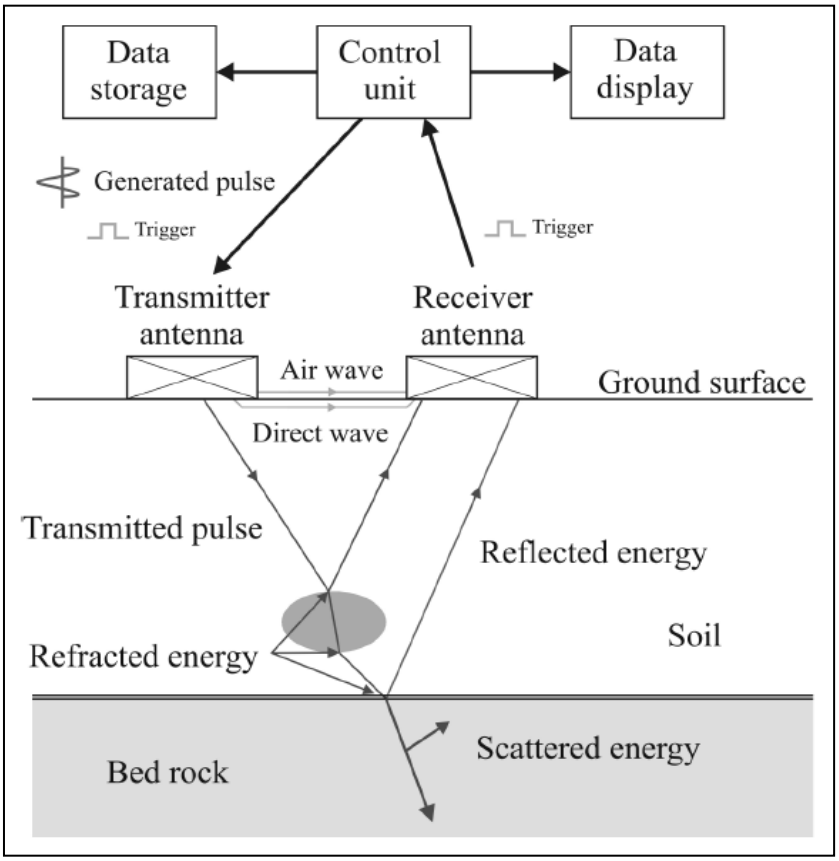

Figure 2.11.- Components and basic principles of a modern GPR system (*From Fernandes, 2006*).

By moving the antenna over the ground, an image of the shallow subsurface under the displacement line is obtained (Fig. 2.12). These two dimensional (2D) images, called radargrams, are XZ graphic representations of the reflections detected. The X axis represents the antenna displacement along the survey line and the Z axis represents the two-way travel time of the pulse emitted (in terms of nanoseconds). If the time for the electromagnetic pulse to go from the transmitting antenna to the reflector into the ground and return to the receiving antenna is measured and the velocity of this pulse in the subsurface medium is known, then the position of the reflector can be determined. The average velocity of GPR pulse in dry masonry is reported in the literature as 0.14-0.15 m/ns (Colla et al., 1997b; Maierhofer et al., 2003a) but important velocity changes can be observed depending on the presence of inhomogeneities in the masonry and the moisture content (Binda et al., 2003a).

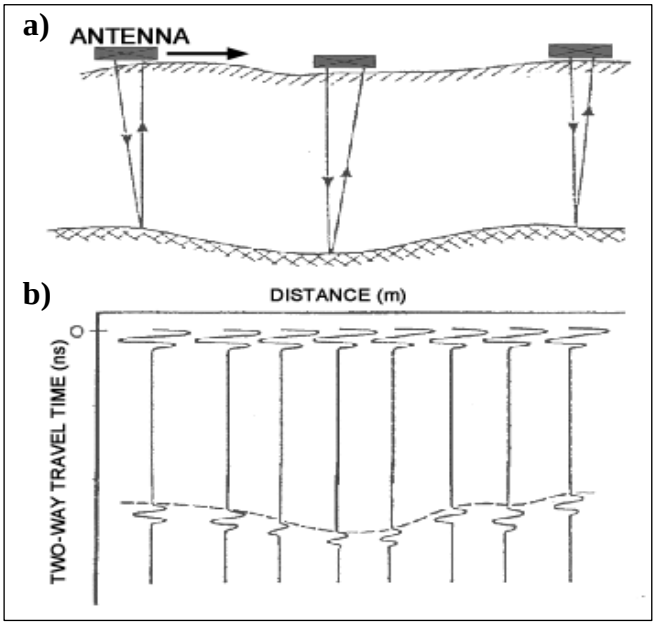

Figura 2.12.- Data acquisition procedure, a) methodology and b) radargram displayed as wiggle traces.

Propagation media of electromagnetic waves can be of quite variable nature since GPR surveys can be performed virtually in every material which permits the transmission of electromagnetic energy. Among them, numerous natural materials can be found such as dry soil, rocks, ice and water (only in certain conditions), and construction materials, like brick and stone masonry, concrete, asphalt, etc. However, care should be taken when applying the GPR method to structures that might include highly conductive materials. Since the electromagnetic signal attenuates rapidly in the presence of soils that have high electrical conductivity, such as clays, silts and saline soils, the penetration depth of GPR is

greatly reduced. Furthermore, another important parameter controlling the depth range of GPR, is the transmitting antenna frequency. The antenna frequency employed at a GPR survey should be very carefully chosen since there is a balance to be kept between a low frequency antenna, that gives deeper signal penetration but poorer resolution, and a higher frequency antenna, which gives better resolution but shallower penetration. Antennas with a 200 MHz - 1 GHz centre frequency are best suited for the study of historical masonry bridges. 500 MHz antennas have limited ground penetration, but they give a very high resolution map of the subsoil in the first 2-3 meters. Below this depth, lower frequency antennas work better, but those with a centre frequency below 100 MHz may have insufficient vertical resolution. 1 GHz antennas are suited for very shallow studies, and they are an especially effective tool for structure inspection: detection of cracks in buildings, estimation of wall thickness, moisture content inside structures, etc.

2.4.2.2.- Data acquisition modes

Three modes of deployment are usually considered with GPR: common offset mode, common depth point mode and common midpoint mode (Fig. 2.13).

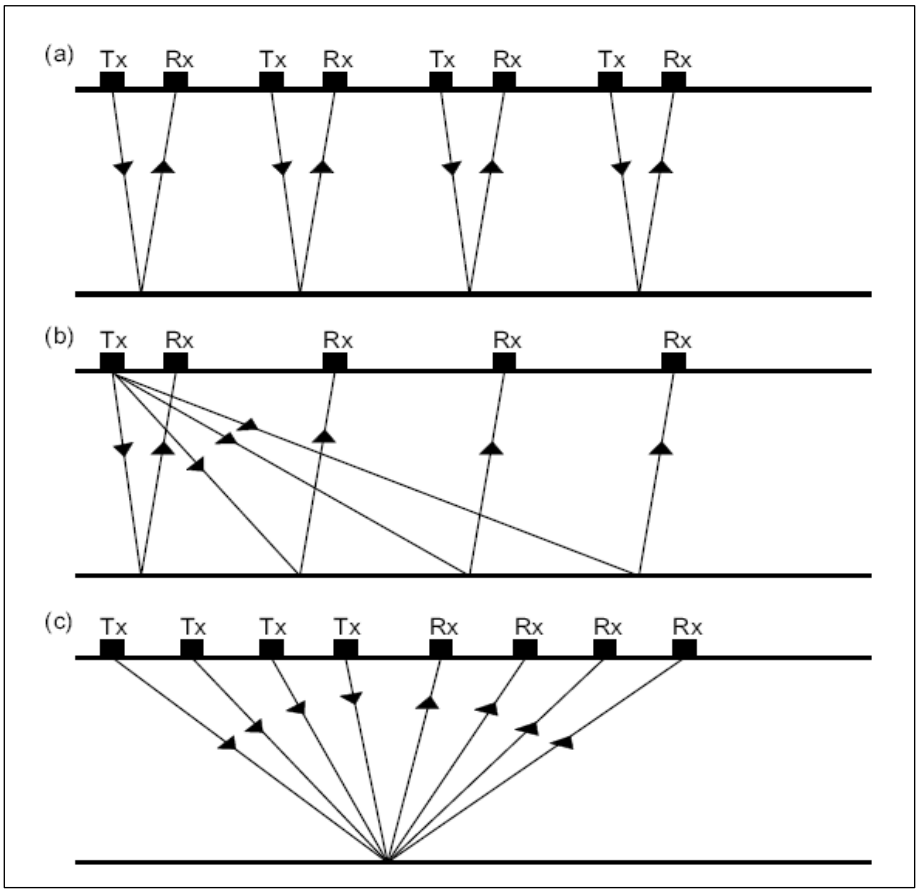

Figure 2.13.- GPR data acquisition modes. (a) Common offset mode, (b) Common depth point mode and (c) Common midpoint mode (*From Diamanti, 2008*).

Each acquisition mode has its particularities and differs considerably in terms of required equipment. Similarly, the results obtained are substantially different, being the reflection mode the most frequent method, as the simplest and fastest way of acquiring data with a radar system. Using the common offset (CO) mode (Fig. 2.13a), one or two antennas are required to be moved over the investigation medium along a specific direction by keeping constant the distance between transmitter and receiver. In most GPR surveys, this procedure is repeated at regular intervals and for a number of survey lines, which are usually located parallel to each other. Generally, survey lines should be designed to run perpendicular to the preferred strike direction of the features under investigation.

Another possible survey mode is the common depth point (CDP) mode, which is also called the reflection and refraction (WARR) mode. Employing the CDP mode for a GPR survey, the transmitting or receiving antenna is kept stable at a fixed location while the second antenna is moved along a survey line in constant step intervals (Fig. 2.13b). Finally, in the common midpoint (CMP) acquisition mode, both the transmitting and receiving antennas are moved apart about a common fixed centre point along the survey line at a constant step (Fig. 2.13c). For both the CDP and CMP modes the antenna spacing is varied at a fixed location and the change of the two-way travel time of the electromagnetic wave from the reflectors is measured. Therefore, those two operative modes can be used to calculate an estimate of the radar signal velocity versus depth in the ground.

2.4.2.3.- Maxwell's equations

GPR signals are electromagnetic (EM) fields. The nature of the electromagnetic field was described by the physicist James Clark Maxwell in 1864, who defined the basic principles of Electromagnetism by means of four fundamentals expressions, known as *Maxwell's Equations*. These equations can be expressed as follows:

$$\nabla \times \mathbf{E} = -\frac{\partial \mathbf{B}}{\partial t} \qquad \text{Faraday's law} \qquad (2.1)$$

$$\nabla \times \mathbf{H} = \mathbf{J} + \frac{\partial \mathbf{D}}{\partial t} \qquad \text{Ampere-Maxwell's law} \qquad (2.2)$$

$$\nabla \cdot \mathbf{D} = q \qquad \text{Gauss's law for the electric field} \qquad (2.3)$$

$$\nabla \cdot \mathbf{B} = 0 \qquad \text{Gauss's law for the magnetic field} \qquad (2.4)$$

Where, E is the electric field intensity in volts per meters (V/m), B is the magnetic flux density in webers per square meters (Wb/m^2), H is the intensity of the magnetic field in amperes per meters (A/m), D is the electric flux density in coulombs per square meters (C/m^2), J is the current density in amperes per square meters (A/m^2) and q is the electric charge density in coulombs per meters cubed (C/m^3).

The associated constitutive relations introduce the relevant material property parameters of permittivity, magnetic permeability and conductivity. These are the following:

$$\mathbf{J} = \sigma\mathbf{E} \tag{2.5}$$

$$\mathbf{D} = \varepsilon\mathbf{E} \tag{2.6}$$

$$\mathbf{B} = \mu\mathbf{H} \tag{2.7}$$

Where σ is the conductivity of the material in Siemens per meters (S/m), ε is the permittivity of the material in Farads per meters (F/m), and μ is the permeability of the material in Henrys per meters (H/m). In Equations (2.5)-(2.7), the properties are shown as simple constants. This is for the ideal case of uniform, homogeneous materials.

2.4.2.4.- Electromagnetic properties of media

The GPR technique is based on a solid theorical background. In order to understand how electromagnetic signals propagate, attenuate and reflect at material interfaces, a brief description of the most important properties is addressed in this section. In general, the properties that govern the propagation and loss of electromagnetic energy through natural and artificial materials are primarily associated to dielectric properties of those materials. These properties deal with the composition and water content of natural and artificial materials, namely geological and building materials.

An electromagnetic wave consists of a disturbance in space constituted by an electrical intensity (E) and a magnetic force (H) in a plane perpendicular to the direction of travel (polarized) and variable in time (Fig. 2.14). These electromagnetic waves have the particularity to propagate at the speed of light *c* (30 cm/ns) through space without the need of solid matter. The main components of an electromagnetic wave are: frequency (*f*), wave or pulse period (1/*f*), wavelength (λ) and amplitude.

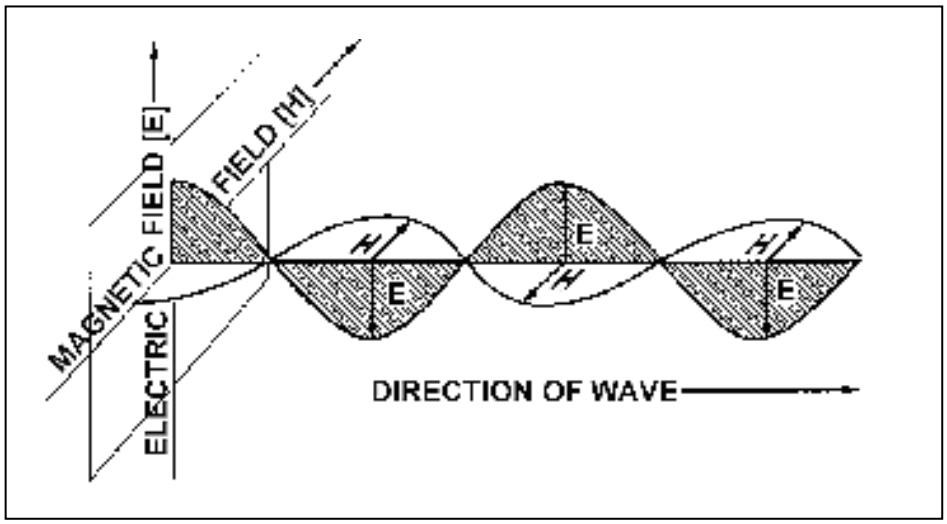

Figure 2.14.- An electromagnetic harmonic plane wave with the polarized electric and magnetic fields.

The velocity (v) can be obtained by means of the frequency and wavelength by the following expression:

$$v = f \cdot \lambda \tag{2.8}$$

The velocity of electromagnetic waves through vacuum is not the same as when they propagate through solid mater, being given by the relation:

$$v = \frac{1}{\sqrt{\varepsilon_0 \mu_0}} \tag{2.9}$$

Where the constant ε_0 represents the permittivity of free space (8.854×10^{-12} F/m) and μ_0 the magnetic permeability of free space ($4\pi \times 10^{-7}$ H/m). F/m (Farads per meter) and H/m (Henrys per meter) represent the SI units to measure, respectively, the permittivity and the permeability.

The speed of radiowaves in air is equal to the speed of light in vacuum, namely, 30 cm/ns. However, when a radiowave propagates through a solid material, the velocity is expressed as:

$$v = \frac{1}{\sqrt{\frac{\mu\varepsilon}{2}\left(\sqrt{1+\left(\frac{\sigma}{\omega\varepsilon}\right)^2}+1\right)}} \tag{2.10}$$

This expression for the speed of propagation can be simplified when the radiowaves propagate through a low-loss material at radar usual frequencies, such as construction materials and most dry soils. This means that the material's conductivity σ is very low and close to zero. Consequently, the term $\sigma/w\varepsilon$, designed by "loss factor", is considered to be null. In non-magnetic materials, the relative magnetic permeability (μ_r) is equal to one. Thus, the general expression for wave velocity can be further simplified for low-loss materials by using the following relation:

$$v = \frac{c}{\sqrt{\varepsilon_r}} \tag{2.11}$$

Where c is the velocity of an electromagnetic wave in the vacuum and ε_r is the relative permittivity of materials.

Dielectric properties include the electrical conductivity (σ), the magnetic permeability (μ) and the permittivity (ε) of materials. These properties constitute fundamental parameters and can influence the way radiowaves propagate, reflect and attenuate through different earth and construction materials. The magnetic properties are only relevant where magnetic materials are present. Therefore, usual building materials such as concrete and masonry are characterized by a relative permittivity or relative dielectric constant (ε_r), which is described by:

$$\varepsilon_r = \frac{\varepsilon}{\varepsilon_0} \tag{2.12}$$

Where (ε) represents the electric permittivity and (ε_0) the permittivity of free space of the particular material. Materials that allow the propagation of an electromagnetic field are designated as dielectrics, and are defined as poor conductors of electricity, but efficient supporters of electrostatic fields.

However, despite the term "constant" in the definition of ε_r, the value of the relative dielectric constant of building materials depends on physical properties, water content and the proportion of its constituents. Table 2.2 shows typical values of dielectric constant for materials of interest in this thesis, such as granite, shale and concrete.

Material	Relative dielectric constant (ε_r)	Electrical conductivity (mS/m)	Radiowave velocity x 10^8 (m/s)
Air	1	0	3.00
Fresh water	81	1	0.33
Sand	3-6 (dry) 25-30 (wet)	10^{-4}-1 (dry) 1-10 (wet)	1.20-1.70 (dry) 0.55-0.6 (wet)
Granite	4-5 (dry) 7-8 (wet)	10^{-5} (dry) 1 (wet)	1.20-1.50 (dry) 1.06-1.12 (wet)
Shale	5-15	1-100	0.9
Concrete	4-6 (dry) 11-12 (wet)	1 (dry) 10-50 (wet)	1.30 (dry) 0.9 (wet)

Table 2.2.- Relative dielectric constant, electrical conductivity and velocities for different materials (*Adapted from David and Annan, 1989; Reynolds, 2002; Clark and Crabb, 2003; Forde, 2004*).

2.4.3.- GPR on masonry arch bridges

GPR has shown good potential for providing valuable information on the evaluation of masonry arch bridges. Internal geometrical data and hidden characteristics such as the presence of internal voids, ancient arches, restorations, moisture content, etc. can be obtained. This additional information can be useful for engineers as it provides a better structural knowledge of the bridge. Despite its effectiveness for bridge investigation, to date there have not been many contributions to the literature. Pérez-Gracia (2001) applied GPR for assessing historical bridges to reach their foundations. In addition, the results obtained with 100 and 500 MHz antennas provided information about the water table and sub-bottom geological structure near riverbed level. In another study, Fernandes (2006) performed a GPR investigation on a nineteenth century masonry bridge using 250 and 500 MHz antennas. The purpose was to obtain the ring stone thickness and the location of drainage channels and drainpipes under the pavement along the bridge. This aim was achieved with good accuracy and the presence of significant moisture content within the

whole structure was also determined. Also, GPR surveys were carried out by Solla et al. (2008a) to determine the state of conservation of several Roman bridges using 250 and 500 MHz antennas. It was possible to identify relevant structural information concerning ring stone thickness, foundation conditions, the presence of reinforcement elements, etc. Other studies have employed GPR together with photogrammetric techniques to study the internal structure of historical bridges (Lorenzo et al., 2007; Solla et al., 2008b; Riveiro et al., 2009). The metric information obtained by a photogrammetric survey allows for the calculation of the average velocity of a radar pulse for the filling and the masonry within the bridge, providing better GPR data interpretation. In addition, several authors (Arias et al., 2007; Lubowiecka et al., 2009) have presented a multidisciplinary approach utilizing laser scanning or photogrammetric methods and GPR as well as finite element analysis (FEM) for evaluating historical bridges. The complex external geometry of the structure is elucidated using the data collected by a laser scanner. The accurate geometry obtained can be useful in performing an exhaustive interpretation of the GPR data and obtaining information about the bridges' internal composition. The resulting information is used to define a hypothesis for the numerical model and the finite element structural analysis, which describes the structural behavior of the bridge.

Other authors have recommended a combination of different NDT techniques for the structural evaluation of historical masonry bridges (Bhandari and Kumar, 2006; Orbán, 2007). This complementary testing provides an exhaustive knowledge regarding their state of conservation. Many structural problems can be best analyzed by a particular NDT method owing to the physical properties of their construction materials. Colla et al. (1997a) employed radar, sonic and conductivity methods for assessing an historical stone masonry bridge. These tests have demonstrated the ability to achieve inhomogeneity identification and layering within the bridge together with moisture-drainage problems. Furthermore, Flint et al (1999), combined seismic, radar and electrical resistivity tomography methods to evaluate changes in the internal condition of a masonry viaduct. The response of these techniques shown to be useful in monitoring the presence of voids into the structure as well as changes in internal moisture content. Some bibliographic contributions (Orbán, 2006; Orbán et al., 2008; Orbán and Gutermann, 2009) have analyzed the use of GPR, infrared thermography and sonic methods in the assessment of masonry arch bridges. These techniques have shown their joint effectiveness for obtaining unknown geometric data and finding hidden characteristics such as voids, moisture content, inhomogeneous filling materials, etc.

In complex and heterogeneous structures, the interpretation and analysis of GPR data is often complicated. Numerical modelling has become an affective interpretational tool used in conjunction with GPR (Cassidy, 2005). According to these recommendation, Diamanti et al. (2008) conducted laboratory experiments and FDTD numerical analysis with GPR to investigate ring separation in brick masonry arch bridges. GPR numerical models were created to help understand the complex real data acquired owing to the heterogeneity of these structures. Good correlations were obtained between numerical and laboratory experiments. A mortar loss between ring stones could be determined. However, hairline delimitations among mortar and brick masonry could not be detected using a 1.5 GHz antenna. Other researches (Solla et al., 2008c; Solla et al., 2009) have employed the joint use of GPR and FDTD modelling for the internal diagnostics of masonry arch bridges. Numerical modelling has been shown to be an important tool for interpreting the complex pattern of reflections obtained in the radar data d the heterogeneity of the filling material in the bridge.

3

Survey Methodology

This chapter describes the survey proposed methodology for assessing the selected historical bridges. A brief overview of the procedures developed in this work for evaluating historical bridges is illustrated in the flowchart shown in Figure 3.1.

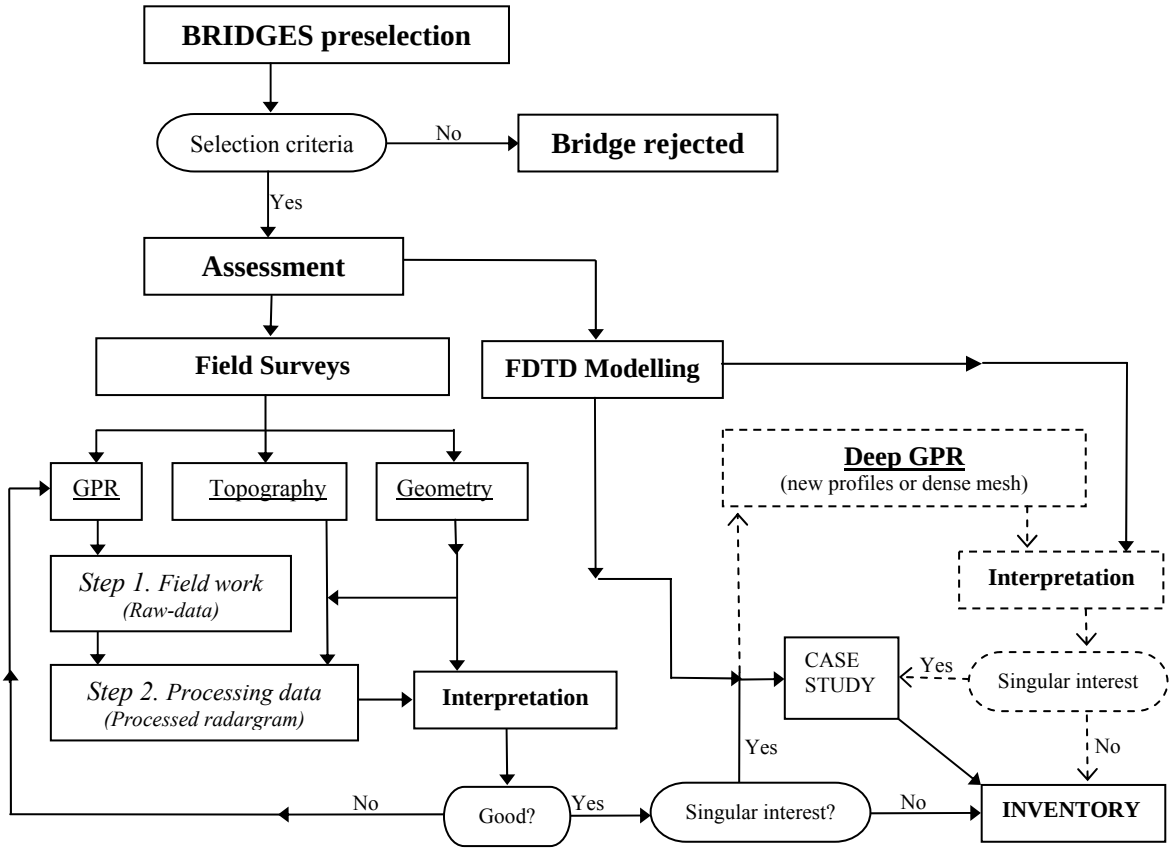

Figure 3.1.- The flowchart for survey methodology.

The selection criteria defined to select the historical bridges for inventory are mentioned. The first section evaluates the methodologies established for the GPR and topographic surveys as well as the methods used to obtain the external geometry of the structures. The second section presents the most common signal processing applied to the GPR results obtained before interpretation. Furthermore, the guidelines for the numerical modelling of GPR are described in the third section. Numerical simulation using the FDTD method can be an important tool to aid GPR data interpretation in some cases. Several pitfalls in GPR data interpretation are also mentioned and illustrated in the fourth section.

3.0.- SELECTION CRITERIA

The General Galician Heritage Inventory was reviewed to select a number of historical bridges for the GPR surveys. This inventory includes a total of 275 historical and modern bridges. The selection criteria were defined to select a representative sample of unique bridges with respect to their structural and architectonic typologies. According to these criteria, they should be stone arch bridges –granite or slate masonry– built before the 18th century. Preferably, they must present some risk of being lost to deterioration as well as the necessity of any intervention for their maintenance and conservation. Considering these recommendations, a total of 36 historical bridges were chosen from around the whole Galician territory.

3.1.- FIELD WORK

3.1.1.- GPR Survey

3.1.1.1.- Equipment

The radar system used for this research is a RAMAC/GPR system from the Swedish manufacturer MALÅ Geoscience. The equipment belongs to the Close Range Remote Sensing and Photogrammetry Group (TF-1) of the University of Vigo (Fig. 3.2). This system is composed by a "Toughbook" Panasonic laptop adapted for field surveys, a UCII control unit with a MC4 expansion module for multi-channel mode, two shielded antennas of 250 and 500 MHz and an unshielded antenna of 200 MHz.

Figure 3.2.- RAMAC/GPR equipment. 200, 250 and 500 MHz antennas together with the interchangeable electronics, control unit, odometer wheel and field laptop.

The UCII unit is the main part of the system as it controls the data acquisition, generates and synchronizes the pulses and all the needed control signals. It is connected to the laptop through the parallel port. The UCII allows the communication in ECP mode in order to ensure a high data transmission rate. GroundVision software (also developed by MALÅ) is used as interface for choosing data acquisition settings and data display. The 200 MHz unshielded antenna is used for high penetration studies whereas the 250 and 500 MHz antenna are used for high-medium resolution studies. The shielded antennas are modified bowtie placed inside a box for shielding of external radiant elements and focusing the energy on the right direction. The transmitter is located in the front part of the frame whereas the receiver is in the back. In the backside of the frame an odometer wheel can be attached for triggering at equal space intervals. The communication with the control unit is through optic fiber cables (two for signaling (T and R) and the third one for data sending (D)). Another cable transmits the information sent by the odometer wheel. The odometer wheel (also called survey wheel or measuring wheel), is employed for measuring the profile length when the acquisition is based on constant distance intervals. The measuring wheel for the RAMAC/GPR equipment uses an optical encoder which transmits electrical pulses to the control unit. The control unit reads a calibration file in order to convert the number of pulses to correct length.

3.1.1.2.- GPR methodology

In this work, a common methodology to assess the selected masonry arch bridges by means of GPR is proposed. The GPR surveys were performed using 250 and 500 MHz antennas. These frequencies were selected as the most suitable for this work due to their optimum compromise between penetration and resolution. The main purpose was to reach the bridge foundations and to obtain information concerning the shallower filling material. Two longitudinal parallel profiles in opposite directions along the bridge were gathered with each antenna as shown in Figure 3.3. The survey parameters usually selected with the 250 MHz antenna were 5 cm in-line spacing and time windows of 200 ns, whereas these acquisition parameters for the 500 MHz antenna were 2 cm in-line spacing and time windows of 100 ns.

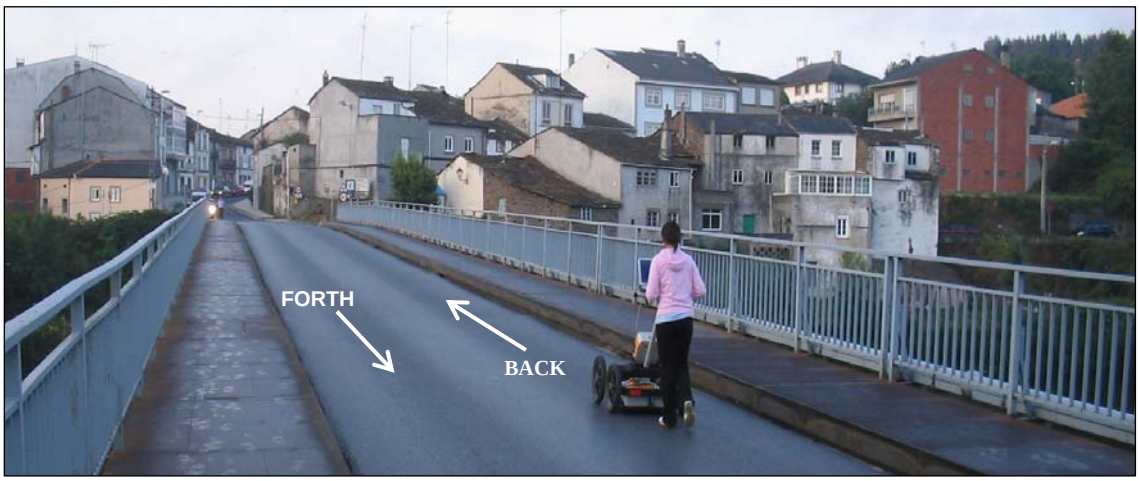

Figure 3.3.- General methodology used to GPR data acquisition composed by two parallel profiles through the bridge, back and forth.

Sometimes, owing to the bridge height, the use of a lower frequency was required to obtain information from the foundation. In these cases, the 200 MHz unshielded antenna was employed with a distance interval of from 2 to 10 cm in-line spacing and time windows between 250 and 300 ns.

The GPR data acquisition was based on constant distance intervals following the common offset mode described. An odometer wheel or a tape measure was used for measuring the profile length depending on the antenna used and the surface conditions (Fig. 3.4). Some of the historical bridges surveyed had intact ancient flagstone paths built of large irregular blocks. This ground condition can make measurements difficult as the continuous movement of the survey wheel can be interrupted. Different forms of GPR transport were employed to manage this problem (Fig. 3.4). Before starting the survey, calibration of the

wheel is recommended to mitigate this factor, which affects the accuracy of radar-trace location. The odometer wheel was calibrated for each particular surface condition in the profile direction over at least 50 meters to maximize accuracy.

Figure 3.4.- Example of different GPR procedures for measuring the profile lenght concerning to historical bridges assessment.

Field markers were collected coinciding with the tops of the bridge arches during the GPR data acquisition to perform a first estimation of the arch-air interface locations. They were registered when the system was placed upon the keystone of the arches. Sometimes, due to a low signal response, the identification of reflections from the arches was very complex, so markers were useful to verify the interface locations, as shown in Figure 3.5.

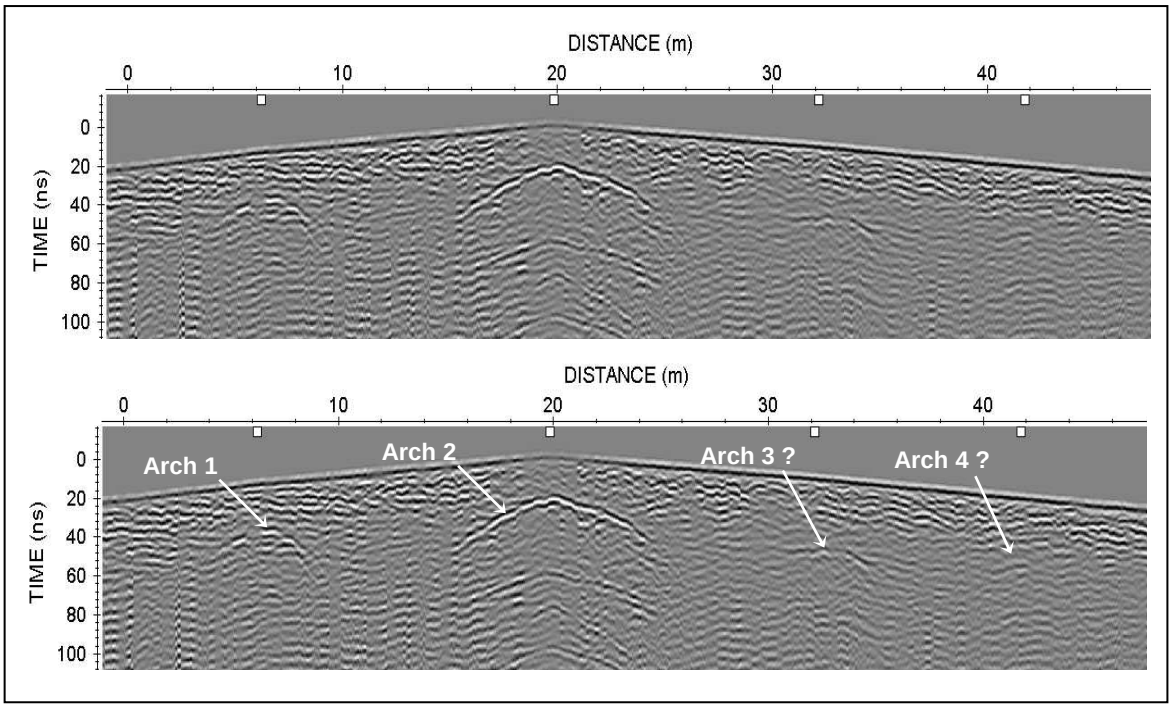

Figure 3.5.- The effectiveness of using field markers (at the top of the radargram) to locate the reflections generated in the arch-air interfaces.

In some cases, when the results were unsatisfactory, a new GPR survey was performed with the same characteristics as the first one. On the contrary, when the results presented an interesting interpretation a deeper survey was carried out to obtain more profiles, and to realize an exhaustive analysis.

3.1.2.- Topographic measurements

Historical bridges usually present a medieval pointed profile. In these cases, a topographic survey was required to obtain the variations in elevation of the GPR profiles acquired along the bridge. It was carried out by means of a total station model Leica TCR110 (Fig. 3.6). Sometimes, these variations in elevation were measured with a RTK GPS model Settop AL-TOP (Fig. 3.7). The (x,y,z) data collected allowed for the correction of GPR data for topography and the tilt of the antenna. Static corrections are recommended to improve accuracy in imaging subsurface features (Goodman et al., 2006).

Figure 3.6.- Example of topographic survey with a total station in Navea bridge.

Figure 3.7.- Example of topographic survey connecting a differential GPS to the GPR system.

GPS seems to be the best topographic method due to its centimeter accuracy (theoretically 1-2 cm) and real-time positioning without the need to process the GPS data or apply further modifications to coordinate files. Groundvision software allows simultaneous GPR-GPS data acquisition through a laptop which is connected to the CUII by a parallel port and to the GPS by a serial port. During data acquisition, the software interface displays both GPS coordinates and GPR data in real time. However, it has shown considerable limitations. GPS antenna position and stability during GPR-GPS data collection are critical to achieve high accuracy in data processing. A lower placement for the GPS antenna over the GPR antenna can produce bad satellite coverage and multipath problems which

strongly reduce GPS data accuracy. Conversely, if the GPS antenna is placed too high, stability is an issue during data acquisition as most historical bridges have a rough stone pathway. Thus, GPR data acquisition takes additional time. Additionally, historical bridges are usually located in wooden areas which impede good coverage for continuous RTK precision so GPS connection to GPR should be avoided. Therefore, GPS is more convenient for long profiles and open areas. Finally, the GPS data acquisition software used (Groundvision v. 1.4.1) can pose some problems for the acquisition of position information when a consistent latency time is required (Novo, 2009). Although a topographic survey with a total station requires post-processing to coordinate the files, it has proven to be a fast and simple data correction. The (x,y,z) data collected together with field markers and expeditious measurements with a tape measure have confirmed it to be the easiest methodology and to provide suitable information.

3.1.3.- External geometry measurements

3.1.3.1.- Expeditious measurements with a tape measure

To locate the usual reflections and perform a first data interpretation prior to the accurate external geometry obtained from the photogrammetric or laser scanning methods, several measurements were made by hand using a tape measure (Fig. 3.8). The basic geometry measured included the distance between pathway and arch-air interface as well as arch-air and air-water interfaces, river depth, external ring stone thickness, distance between arches and arch spans (Fig. 3.9). The distance between the arch-air and air-water interfaces as well as the river depth under the arches is variable information that depends on climatic factors. According to this, it is important to measure this information at the time of the GPR survey to obtain a suitable distance.

Figure 3.8.- Geometric measurement from a tape measure.

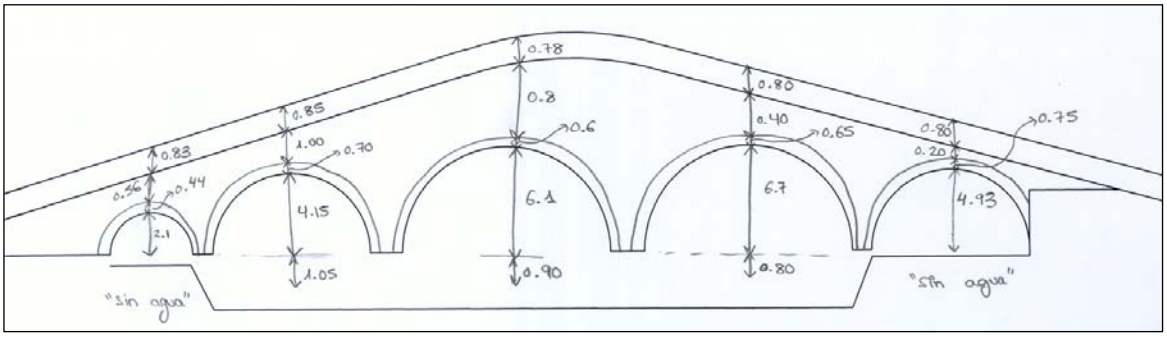

Figure 3.9.- Example of a field sketch with basic geometry measured for Cernadela bridge.

3.1.3.2.- Accurate measures from photogrammetric or laser scanning methods

Close range photogrammetry and laser scanning techniques were employed in some of the historical bridges surveyed with GPR aiming to develop both investigation projects previously mentioned (Fig. 3.10). The 3D model of the bridge acquired by these methods provided accurate metric data related to the external geometry of the bridge. This information also provided an accurate knowledge of the arch geometries and the distance between the pathway and the arches. Therefore, in bridges surveyed by photogrammetric or laser scanning methods the topography survey and the field geometry measurements were omitted. Only the distance between the arch-air and air-water interfaces and the river depth under the arches are required at the time of the GPR survey, as these are variable measures. The accurate geometry obtained can be used to estimate the average values of radar pulse velocity for the filling and masonry in the bridge to perform an exhaustive interpretation of GPR data.

Figure 3.10.- 3D Laser Scanner equipment.

The accurate external geometric measures of the bridges as well as the orthophoto obtained from the photorealistic models (Fig. 3.11) generated by laser scanning or photogrammetry were also used as inputs to create synthetic radargrams using GprMax –an electromagnetic wave simulator for ground penetrating radar, developed using the Finite Difference Time Domain method (FDTD)–. The synthetic results can supply important additional information for the advanced interpretation of GPR data by rendering the complex pattern of reflections obtained.

Figure 3.11.- Orthophoto of Loña bridge generated by laser scanning data.

3.2.- GPR DATA PROCESSING

GPR processing filters are employed in order to reduce clutter or any unwanted noise in the raw-data, enhance the extraction of information from the signals received and produce an image of the subsurface including all the features and/or targets of interest which will make easier the interpretation by survey operators. However, it is important to point out that the effectiveness of the various signal processing filters depends on the quality and nature of the raw-data. In most cases, features of interest are detectable even without the application of any data processing filter. Nevertheless, signal processing is an essential tool for noise reduction and better data presentation. It is important to note that appropriate signal processing should be carefully chosen and applied in a way that the data are not extremely distorted and spurious features are not introduced.

ReflexW software was mainly used for data processing of the results presented in this dissertation. From a large number of possible signal processing filters, the most commonly employed for GPR data processing in this work will be briefly discussed below.

3.2.1.- 1D Filters

3.2.1.1.- Time Zero

Traces require adjusting to a common time-zero position since thermal drift, electronic, instability, cable length differences or variations in antenna air gap can cause "jumps" in the air/ground wavelet first arrival time (Olhoeft, 2000; Rial, 2007). This is usually achieved using some particular criteria such as the air wave first break point or the maximum amplitude peak of the trace (Yelf, 2004; Rial et al., 2006). Time-zero is often calculated automatically by the processing software. This adjustment of the signal is advisable before other processing filters can be applied (Jol, 2009).

3.2.1.2.- Dewow

A common feature in commercialized GPR equipment is the appearance of a continuous or very low frequency component (DC component) in the traces recorded by the radar, since the averaged level of the signal is moved from zero amplitude to a different value (Fig. 3.12A). The appearance of this component is usually associated with either inductive phenomena or possible instrumentation dynamic range limitations (Annan, 2003). DC-levels often vary depending on the medium under the antenna and then antenna-surface distance, so it is common for this component to differ slightly from one trace to another in a continuous profile. The elimination of this component is a prerequisite not only visually, but also for subsequent application of other processing filters because otherwise, the results may differ significantly from what is expected (Sandmeier, 2007). This can be accomplished with different filters although the main one employed in this work was DC-shift. This filter computes and removes from every single trace an average value based on the low energy in the last part of the trace. Values between 1/3 and 1/5 of the trace length, starting from the bottom, are usually recommended. An example before and after applying this filter is shown in Figure 3.9

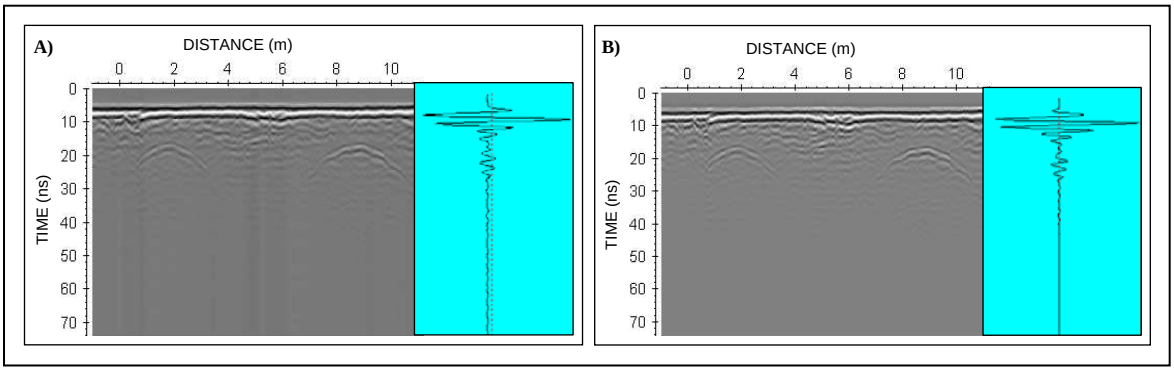

Figure 3.12.- Example of the use of dewow filtering on a 500 MHz GPR section collected. A) Raw-data. B) Data after dewow.

3.2.1.3.- Band-pass

Sometimes, the energy of reflected signals is placed in a particular frequency range whereas most of noise sources and background noise are in a different frequency range. Therefore, distinguishing noise form useful information is often possible in the frequency domain. A band-pass filter is a combination of high-pass filters –for removing signal drift and low frequency noise– and low-pass filters –for high frequency noise–. Band-pass filters are very common and there are several types, each with different parameters that define the shape and form of the pass band (Figure 3.13).

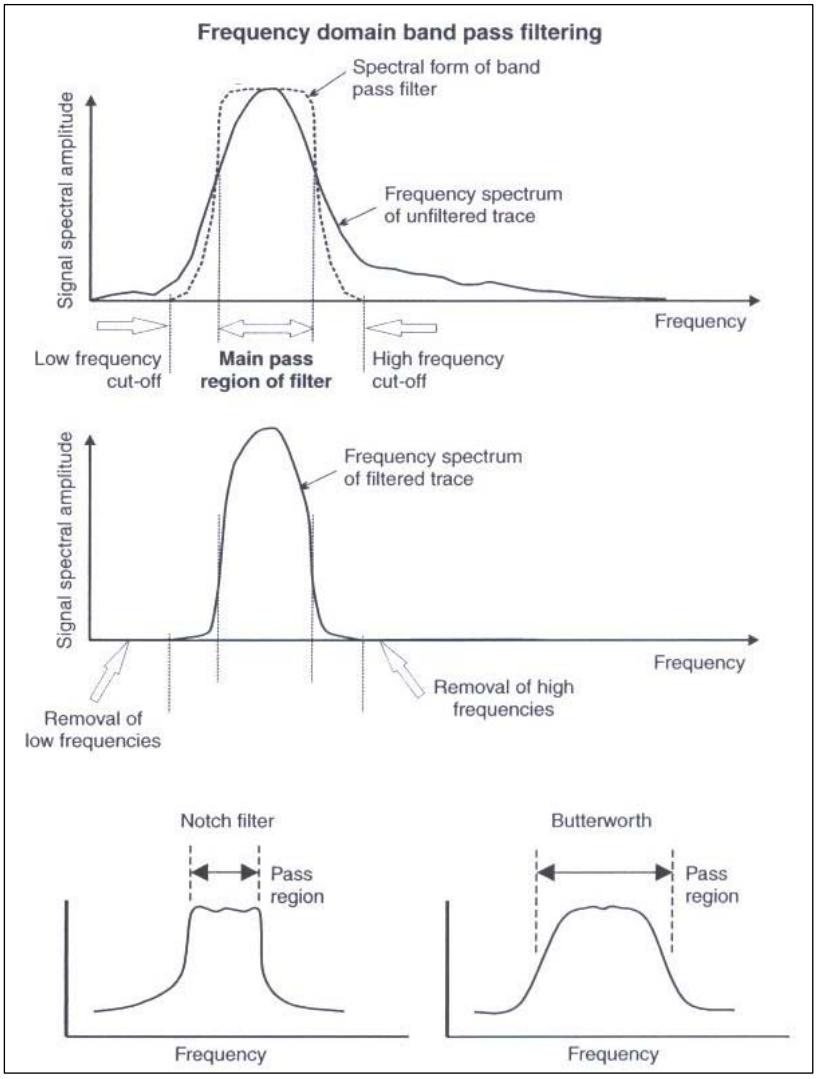

Figure 3.13.- Principle of a simple band-pass filter in the frequency domain and the form of two common filter functions: a notch filter and a Butterworth filter (*From Jol, 2009*).

Band-pass filters are generally defined by setting two frequency values. The first point determines the low-cut frequency while the second one the high-cut frequency. Figure 3.14A shows a radargram recorded with a 250 MHz antenna in which low-frequency noise,

especially placed on consecutive groups of traces as vertical bands, is clearly seen. After applying a butterworth temporal band-pass filter, this noise is mostly removed (Fig. 3.14B).

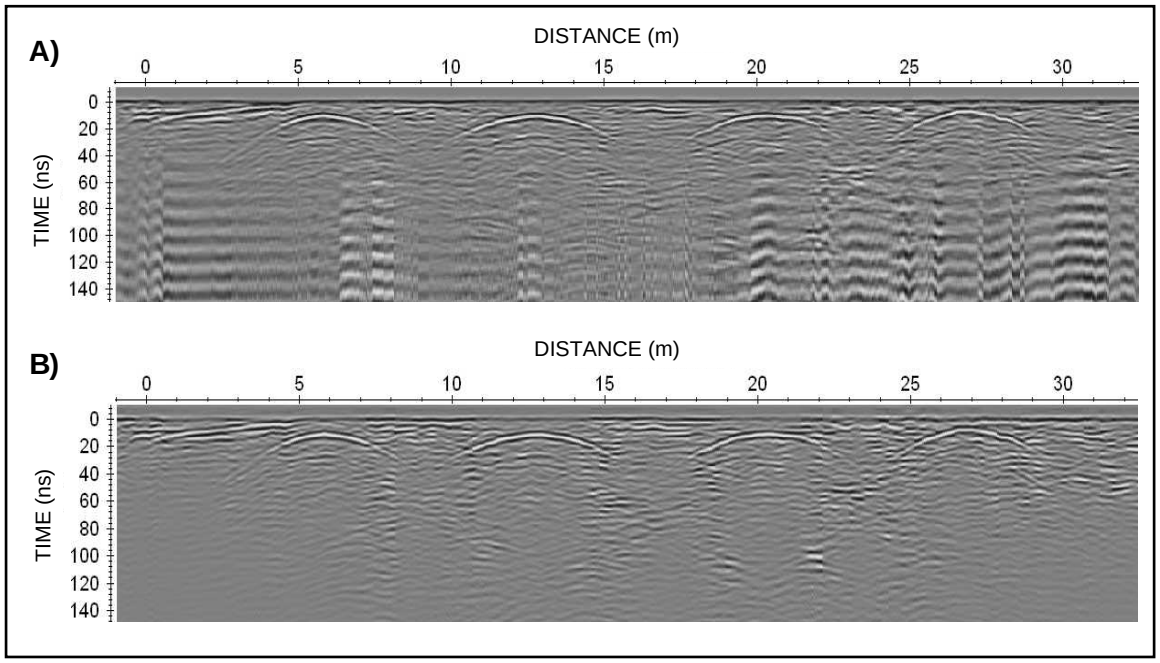

Figure 3.14.- Example of band-pass filtering (butterworth) on a 250 MHz GPR section. A) Before band-pass filtering and B) After band-pass filtering (100/300 MHz).

3.2.2.- Gain

Gaining consists on amplifying the received signal by multiplying the data by using a mathematical function or manually entering gain values (Fig. 3.15). Radar signals are very rapidly attenuated as they propagate into the ground. Signals at greater depths have very low energy due to signal attenuation and geometrical spreading. Equalizing amplitudes by applying some sort of time dependent gain function compensates for the rapid fall off in radar signals from deeper depths.

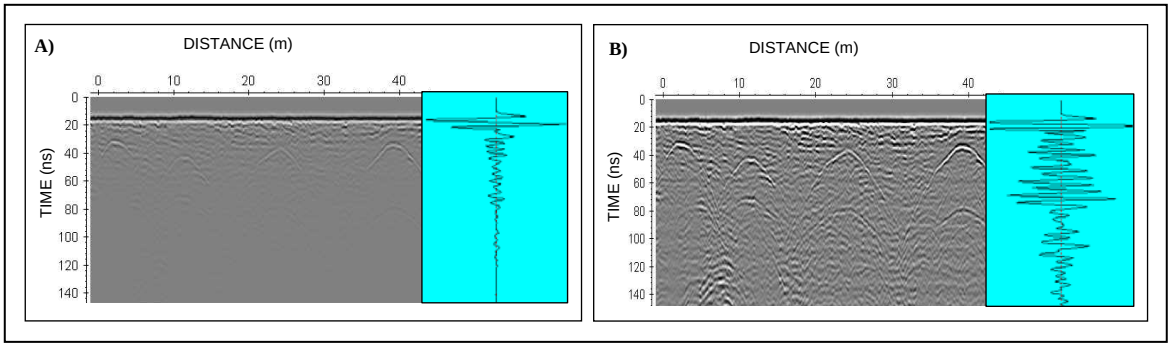

Figure 3.15.- Example of gain applied to a 250 MHz GPR section recorded. A) Raw-data and B) Radargram after gain.

3.2.3.- 2D Filters

3.2.3.1.- Spatial filtering (Subtracting average)

The main objective of these filters is to remove potential low-frequency noise which appears in form of continuous horizontal bands along the recorded traces or only in some parts of them (Fig 3.16). The aim of these filters is to estimate an average of all traces in a window and remove it from every single trace. The main effect in the data is to suppress flat-lying reflectors emphasizing smaller reflections (Jol, 2009). Spatial filters are good at removing noise originated by bad coupling between antenna and medium and to eliminate ringing from the datasets.

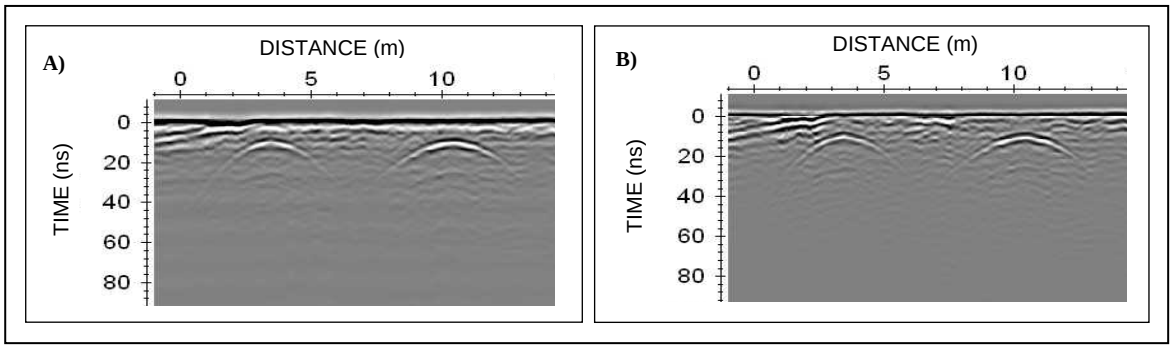

Figure 3.16.- Example of the use of subtracting average filtering on a 250 MHz GPR section. A) Raw-data and B) GPR data after subtracting average (100 traces).

This method should be applied with care in locations where the subsurface features of interest are horizontal layers, since after applying this process most of the signals caused by planar interfaces have been removed (Daniels, 2004).

3.2.4.- Velocity determination

The importance of having an accurate estimate of the radar pulse velocity through the material is well known. To estimate this velocity, a hyperbolic fitting was used by adaptation of the diffraction hyperbola (Sandmeier, 2007). Here, the path length to the object was varied and the radar system moved perpendicular to the axis of the arch (Annan, 2003). The operation was used to visually fit a model hyperbolic shape to the GPR data. The radius parameter was set from the expeditious geometric measurements of the bridge or from the 3D model of the structure generated by photogrammetric or laser scanning techniques. This adjustment provided an estimation of pulse velocity. Combining velocity and time delay, made it possible to obtain an estimate of the depth to the top of the target.

The reflections generated in the arch-air interface sometimes presented an asymmetric pattern on either side of the keystone (Fig. 3.17A). This irregularity can be caused by the presence of different filling materials on each side over the arch resulting in different GPR signal velocities. Furthermore, hyperbolic reflections can offer deformations by low frequency fluctuations due to inhomogeneities in a single material (Fig. 3.17B). High frequency fluctuations can also produce deformation owing to the internal staircase shape of the ring stones as well the ring separation (Fig. 3.17C).

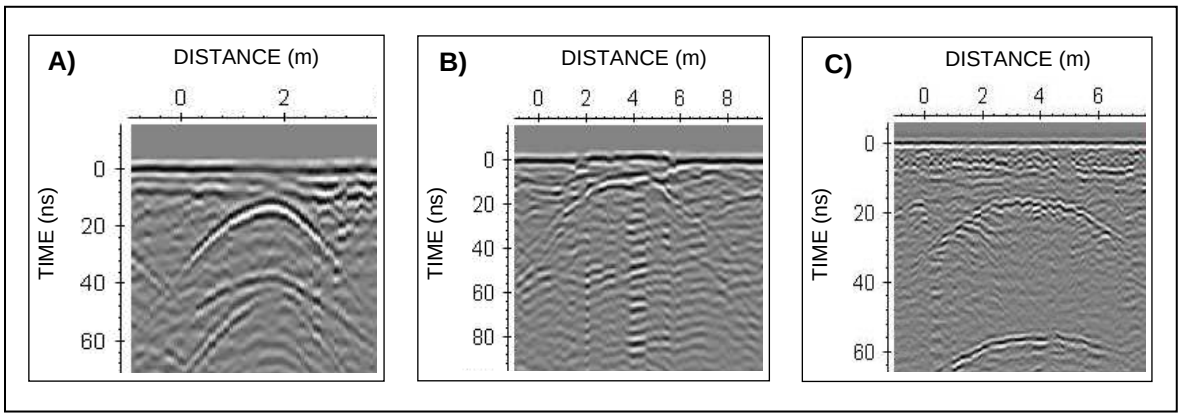

Figure 3.17.- Examples for deformations of hyperbolic reflections. A) asymmetric pattern by different fillings at both sides over the arch, B) deformations due to inhomogeneities in own material, C) deformation owing to the internal staircase shape of ring stones as well ring separation.

The general procedure for velocity determination is to fit a model hyperbolic shape to the reflection pattern generated in the arch-air interface, as illustrated in Figure 3.18(R3). However, the irregularities mentioned made the adjustment difficult. Thus, although the first arch was a barrel arch, the reflection generated in the arch-air interface for this arch presented an irregular hyperbolic shape (Fig. 3.18). This can be a consequence of different fills over the arch. For such circumstances, the velocity was estimated by adapting a hyperbolic shape to each half of the reflection resulting in two different signal velocities as shown in 3.18(R1). This measure allows for the consideration of possible restorations or reconstruction tasks carried out on the structure.

Segmental arches in the Roman period and Gothic pointed arches at medieval period represent the usual arch geometries for historical bridges. These irregular geometries generated asymmetric reflection patterns in the arch-air interfaces at both sides of the keystone. For such circumstances, the velocity is estimated by the adaptation of the diffraction hyperbola for each half of the reflection. An example of a hyperbolic adjustment for velocity estimation with Gothic arches is illustrated in Figure 3.18(R2).

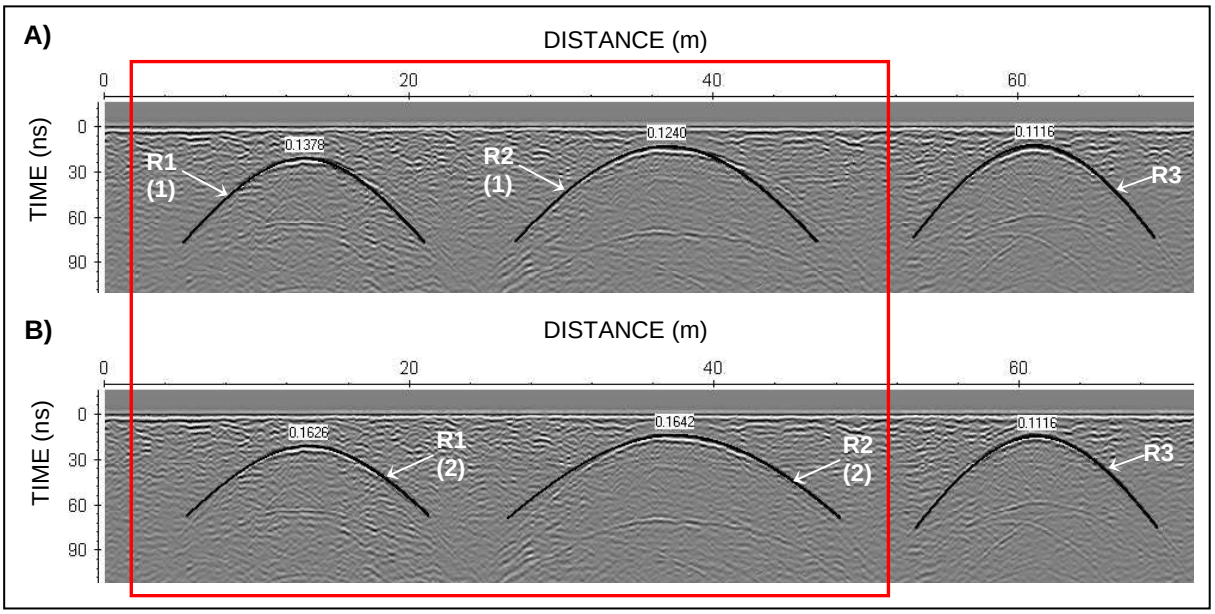

Figure 3.18.- Example of velocity determination by hyperbolic fitting in the radargram obtained with 250 MHz antenna in San Clodio bridge.

[R1: determination for an irregular pattern shape by different fillings over a barrel arch]
[R2: determination for an irregular pattern shape by a gothic arch]
[R3: determination for a regular pattern shape]

3.2.5.- Topography and tilt corrections

Compensating for topography is often important in improving the accuracy of imaging subsurface features. Features that are not directly underneath the antenna are recorded as if they actually were. A topographic relief tilts the antenna and therefore its footprint. Thus, recording data away from where it is actually seen on the screen during data acquisition can lead to misinterpretation of targets. A tilt of antennas is recommended even for abrupt topographies (Goodman et al, 2007; Leckebusch and Rychener, 2007). Without topography and tilt corrections, the location of subsurface structures can change and their shapes become distorted (Fig. 3.19). An average signal velocity of 13 cm/ns was assumed in applying these static corrections. This velocity was estimated by adapting a hyperbolic shape to each half branch of the reflection generated in the arch-air interface as detailed in the previous section (Fig. 3.20). Additionally, GPR-SLICE software (Goodman, 2009) was employed to integrate the influence of the topography and the tilt of the antenna.

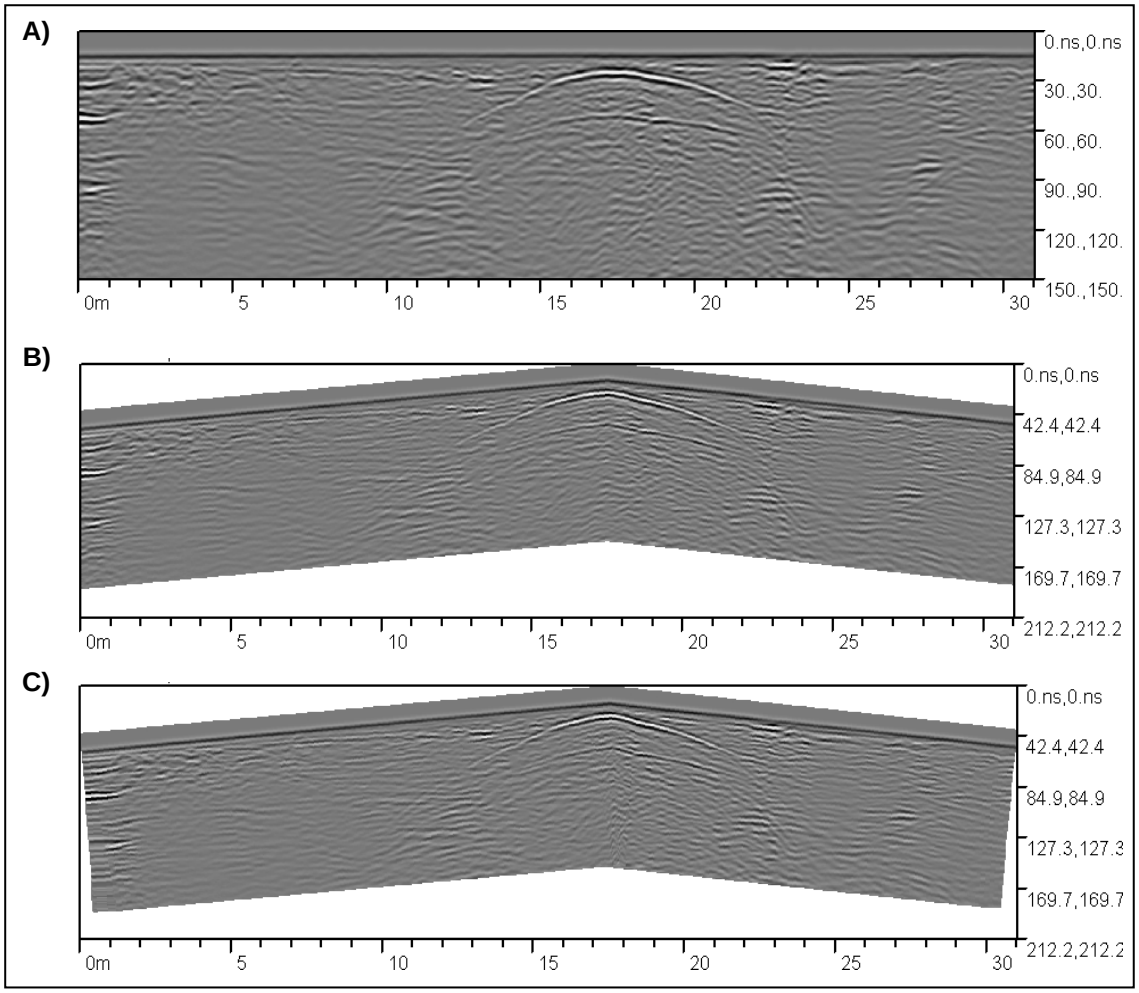

Figure 3.19.- Processed radargram for Liñares bridge (Pontevedra). A) Without topographic and tilt corrections, B) with topographic correction and C) with topographic and tilt corrections.

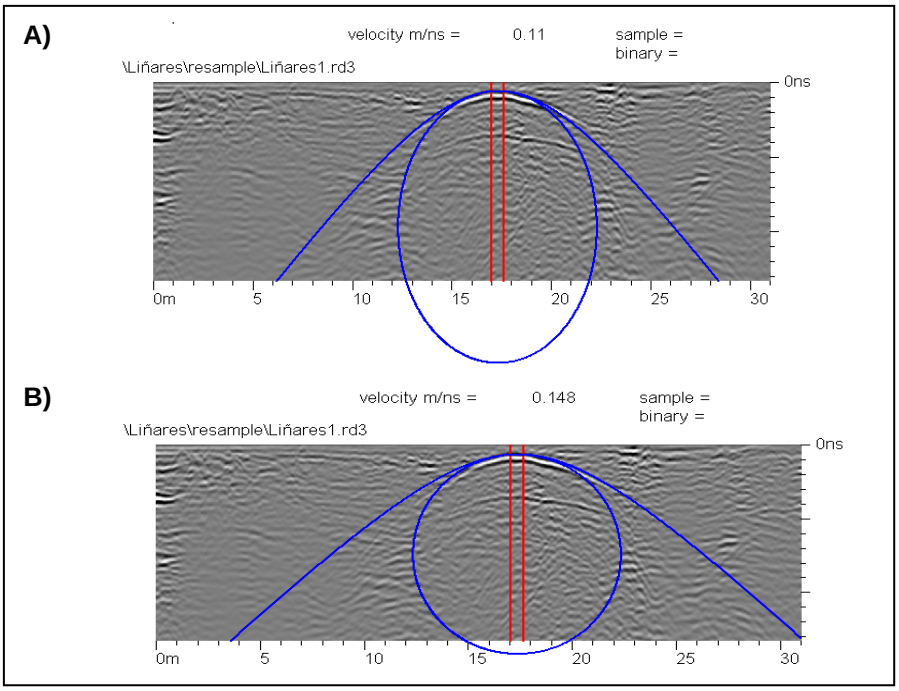

Figure 3.20.- Velocity determination by adapting a hyperbolic shape to each half part of the reflection. A) Adjustment at the left branch, and B) adjustment at the right branch.

Theoretically, the velocity determination must be applied before static corrections. However, the signal velocity determination by hyperbolic fitting methods can be affected due to the change in the shape of features after applying topographic and tilt corrections. Figure 3.21 illustrates the influence of previously applied topographic and tilt corrections on the value of the signal velocity, where the hyperbolic adjustment was made for the left branch of the reflection after static corrections. In this way, the velocity estimated after applying topographic correction was 9 cm/ns (Fig. 3.21A), whereas the value after both topographic and antenna tilt corrections was 8.2 cm/ns (Fig. 3.21B). Therefore, the results show how the estimated signal velocity can be modified when the topography and the tilt of the antenna are corrected for. While the difference in imaging accuracy was not clearly affected by the tilt of the antenna as shown in Figure 3.19, the influence of the tilt of the antenna on the velocity value was significant (Fig. 3.21B).

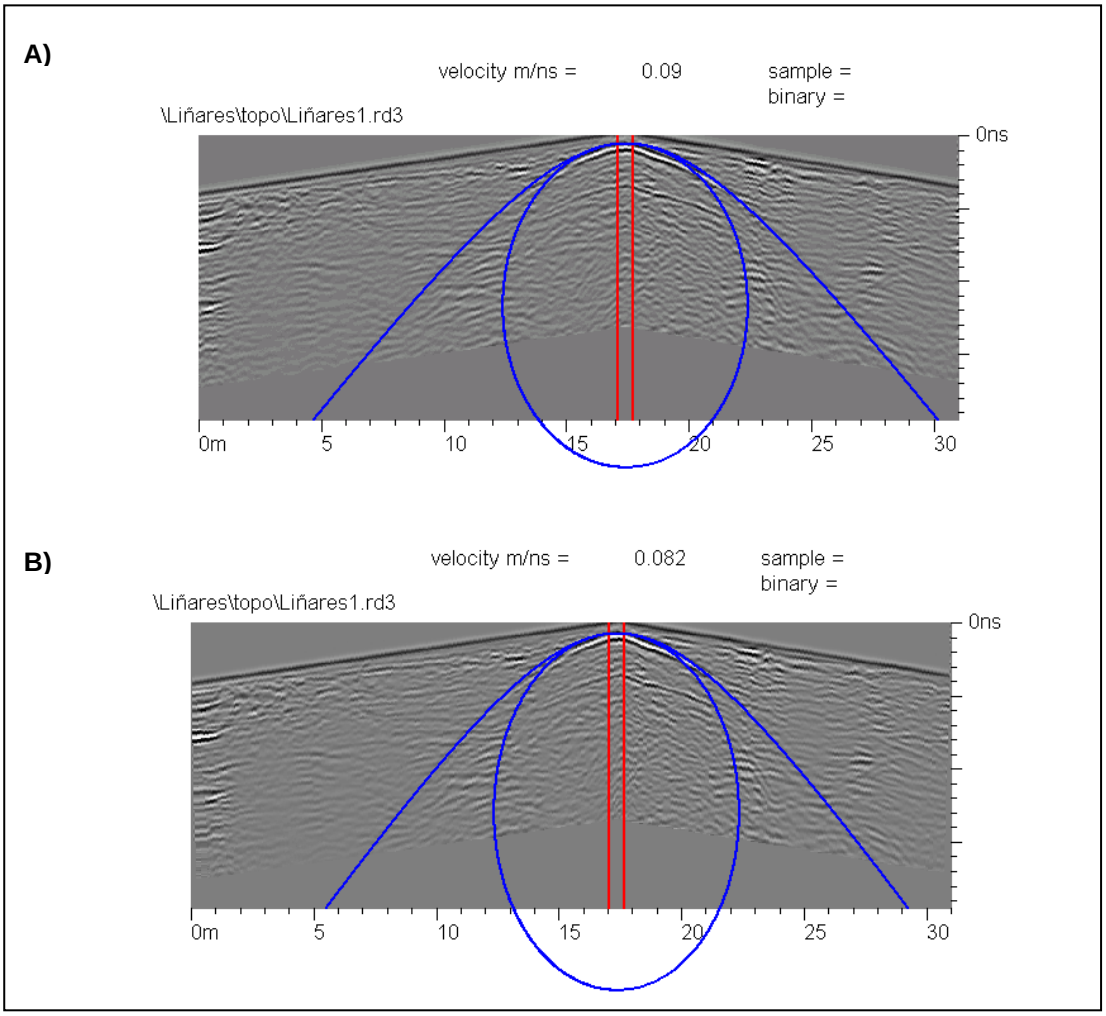

Figure 3.21.- Velocity determination after static corrections by adapting a hyperbolic shape at the left branch of the reflection. A) With topographic correction, and B) with topographic and tilt corrections.

It was of interest to test the influence of these static corrections on the signal velocity in detail. To this end, corrections for the topography and the tilt of the antenna were again applied considering the new signal velocity value obtained after static corrections; thus, an average velocity of 8.6 cm/ns was estimated for the left branch according the values obtained in Figure 3.21. The purpose was to make an iterative procedure. Consequently, a new velocity determination was carried out to check the difference achieved after the procedure. Figure 3.22 shows a lower difference between the initial velocity and those estimated after static corrections.

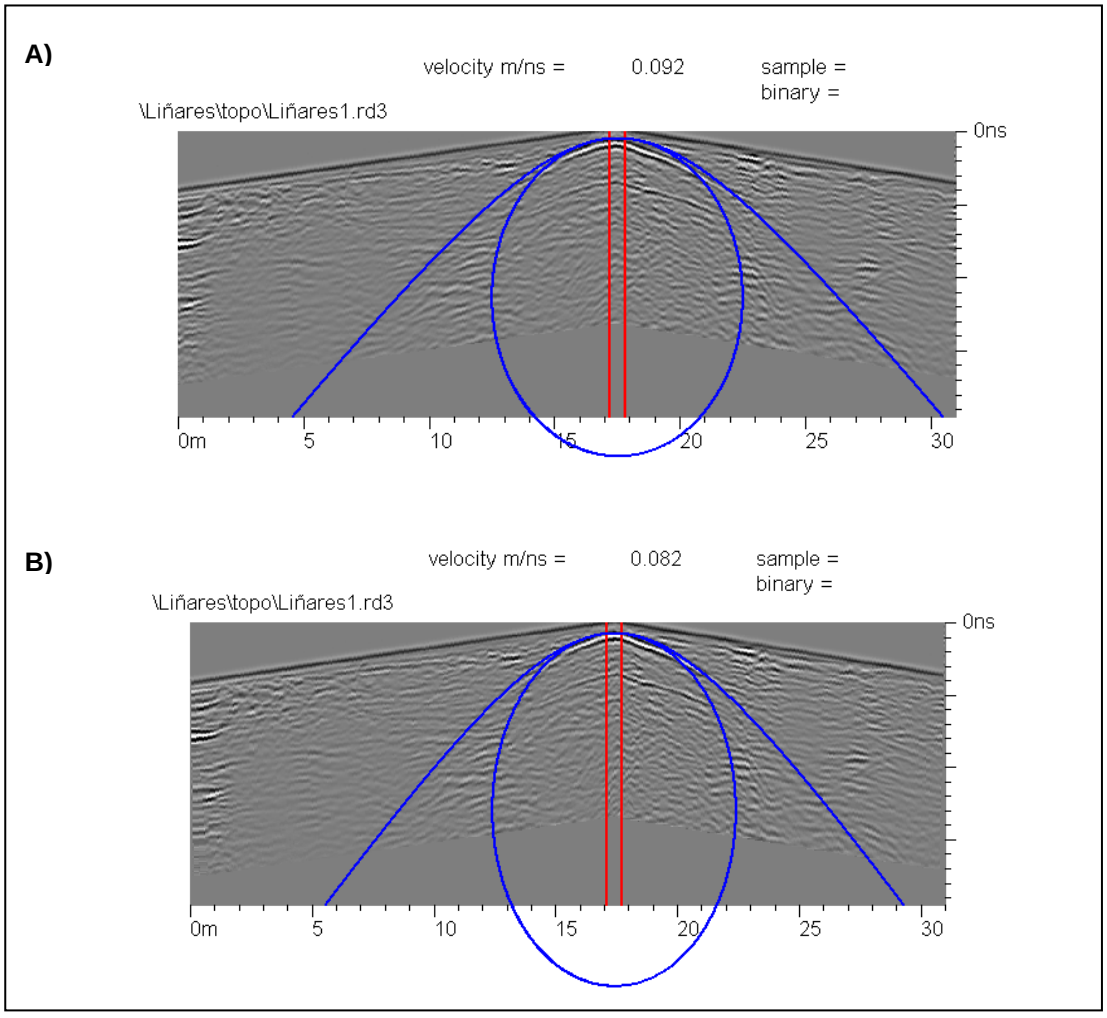

Figure 3.22.- Second velocity determination process. A) With topographic correction, and B) with topographic and tilt corrections.

In conclusion, this procedure can be of use when an accurate velocity value is required. However, velocity determination can be avoided due to the geometry of the arch, the usual pointed profile of ancient bridges, and the heterogeneity in building materials, among others. For these cases, an exhaustive velocity determination is not critical because a reliable accurate velocity value is difficult to obtain for these historical constructions.

3.3.- FDTD MODELLING

In complex, heterogeneous environments, the evaluation, interpretation and analysis of ground-penetrating radar (GPR) data is often complicated by the influence of near-field antenna coupling/induction effects, variations in antenna radiation patterns, the presence of inhomogeneous, anisotropic and lossy materials and the inevitable 'survey error' that arises during data collection. As a result, numerical modelling has become an increasingly popular interpretational tool to more thoroughly understand radar wave propagation phenomena in complex structures (Millard et al., 1998; Cassidy, 2005).

There are many different numerical modelling methods available to simulate the propagation of the GPR wave. Various numerical methods include boundary integral equations, frequency domain volume integral equations, finite-elements and finite-difference (Chen and Huang, 1998). When more sophisticated interpretations are required, then the finite-difference, time domain (FDTD) technique has evolved into one the most popular of the advanced modelling tools, particularly in more complex environments (Daniels, 2004; Jol, 2009). This allows extracting subtle interpretational information from the real data (such as the timing and presence of multiples, the dispersive characteristics of the subsurface media, target material properties).

3.3.1.- Basic theory

The finite-difference, time domain method was introduced by Yee (1966) and is also known as the Yee scheme. The FDTD approach to the numerical solutions of Maxwell's equations is to discretize both the space and time continua. Thus, the spatial Δx, Δy and Δz and temporal Δt discretization steps play a very significant role since the smaller they are the closer the FDTD model is to a real representation of the problem. However, the values of the discretization steps always have to be finite, since computers have a limited amount of storage and finite processing speed. Hence, the FDTD model represents a discretized version of the real problem and of limited size. The building block of this discretized FDTD grid is the Yee cell (Yee, 1966) and it is illustrated for the 3D case in Figure 3.23. The 2D FDTD cell is a simplification of the 3D one and is depicted in Figure 3.24.

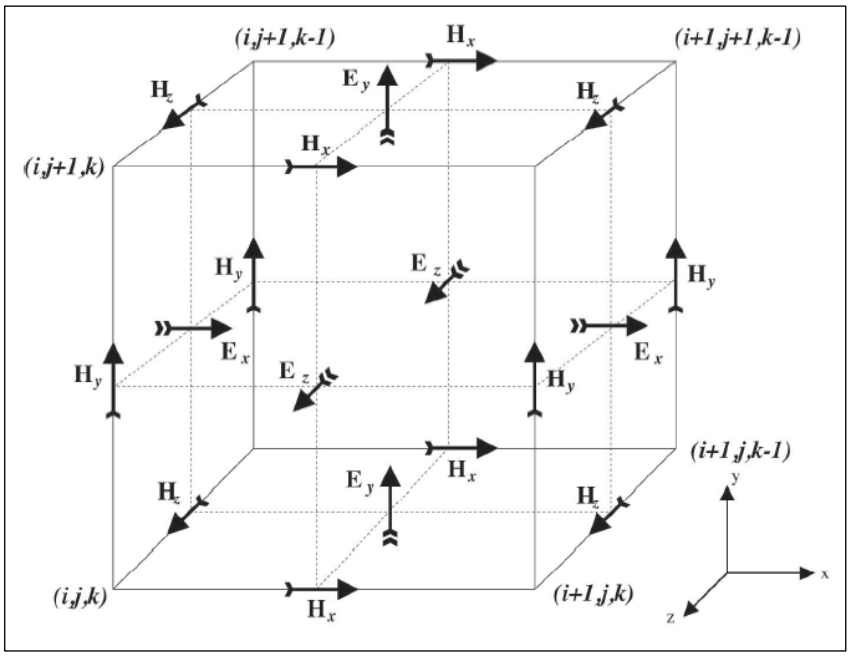

Figure 3.23.- The 3D FDTD Yee cell. E_x, E_y, and E_z are the electric field components and H_x, H_y, and H_z are the magnetic field components at the *x*, *y* and *z* directions, respectively. The indices *i*, *j*, *k* denote the position of the cell in the computational grig. *(From Diamanti, 2008)*

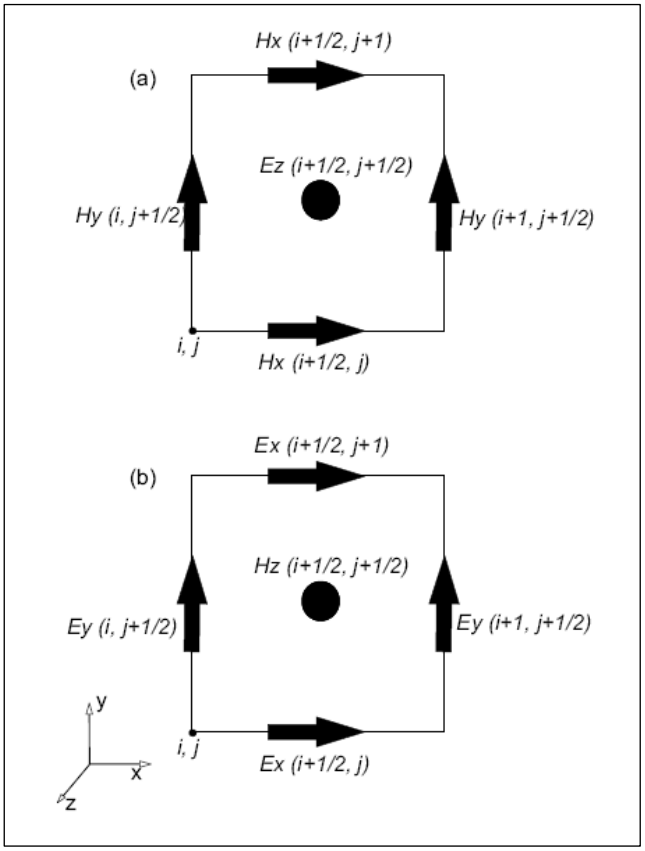

Figure 3.24.- Electromagnetic field configuration. (a) for the TM_z mode and (b) for the TE_z mode. *(From Diamanti, 2008)*

Figure 3.24 illustrates the configuration of the fields for the 2D case for the transverse magnetic (TM_z) and the transverse electric (TE_z) modes. For the TM_z mode, the electric fields are located in the middle of the cell while the magnetic fields are located at the cell edges, and vice versa for the TE_z mode.

Each cell is assigned with individual medium properties represented by the material's constitutive parameters (i.e., its permittivity, conductivity and permeability). This way, complex shaped targets can be included easily in the models. However, objects with curved boundaries are represented using a staircase approximation.

The numerical solution is obtained directly in the time domain by using a discretized version of Maxwell's curl equations which are applied in each FDTD cell. Since these equations are discretized in both space and time, the solution is obtained in an iterative fashion. In each iteration, the electromagnetic fields advance (propagate) in the FDTD grid and each iteration corresponds to an elapsed simulated time of one Δt. Hence by specifying the number of iterations one can instruct the FDTD solver to simulate the fields for a given time window.

The price one has to pay of obtaining a solution directly in the time domain using the FDTD method is that the values of Δx, Δy, Δz and Δt, cannot be assigned independently. FDTD is a conditionally stable numerical process. The stability condition is known as the CFL condition after the initials of Courant, Freidrichs and Lewy and is:

$$\Delta t \leq \frac{1}{c\sqrt{\frac{1}{(\Delta x)^2}+\frac{1}{(\Delta y)^2}+\frac{1}{(\Delta z)^2}}} \tag{3.1}$$

Where c is the speed of light. Hence Δt is bounded by the values of Δx, Δy and Δz. The stability condition for the 2D case is easily obtained by letting $\Delta z \rightarrow \infty$.

3.3.2.- GprMax

GprMax2D and GprMax3D are two computer software programs that implement the FDTD method for GPR modelling in 2D and 3D, respectively (Giannopoulos, 2005). Some of their key features are: an easy to use command interface, the ability to model dispersive materials, the modelling of complex shaped targets as well as the simulation of unbounded space using powerful absorbing boundary conditions.

GprMax2D is freely available for teaching and research purposes and can be downloaded in either Windows™ or Linux (http://www.gprmax.org/) and was developed by Dr Antonis Giannopoulos of the University of Edinburgh.

3.3.2.1.- General input file structure

The program runs in an MS Windows environment. To run a 2D model using GprMax you have to create an input file in which the parameters of the model are specified. This input file is a plain ASCII text file. Any linear, isotropic media with constant constitutive parameters can be included in the model.

It is important to note that GprMax2D converts spatial and temporal parameters given in meters and seconds respectively to integer values corresponding to FDTD cell coordinates and iteration number (Giannopoulos, 2004). Detailed description of the general commands used for this work to create input files are described below.

- General commands which include the ones used to specify the size and discretization of the model:

#title: str. With this command you can include a title for your model.

#domain: f1 f2. It should be used to specify the size in meters of the model. The parameters f1 and f2 are the size in meters of your model in the x and y direction respectively.

#dx_dy: f1 f2. It is used to specify the discretization of space in the x and y directions respectively. f1 is the spatial step in the x direction and f2 is the spatial step in the y direction. This command combined with the #domain command determines the number of cells which are going to be used in the model.

#time_window: f1. Used to specify the total required simulated time. The f1 parameter determines the required simulated time in seconds.

#geometry_file: file1.geo. It is possible to specify a file in which information about the model's geometry is stored in binary format. This information can be used to create an image of the model and check if it is properly constructed. The parameter file1 is the filename of the geometry file.

#messages: c1. This command can partially control the amount of information displayed on the screen at run time. The parameter c1 can be either y (yes) or n (no) which turns on or off the messages on the screen.

- Media and Object construction commands which are used to introduce different media in the model and construct simple geometric shapes with different constitutive parameters:

#medium: f1 f2 f3 f4 f5 f6 str1. This command introduces into the model a set of constitutive parameters describing a given medium. The parameters of the command are:

f1 – the DC (static) relative permittivity of the medium.

f2 – the relative permittivity at theoretically infinite frequency.

f3 – the relaxation time of the medium (seconds).

f4 – the DC (static) conductivity of the medium (Siemens/meter).

f5 – the relative permeability of the medium.

f6 – the magnetic conductivity of the medium.

str1 a string characterizing the medium (medium identifier).

If a medium is non-magnetic you can set f5 to 1.0 and f6 to zero. The parameters for free_space and pec are internally specified.

#box: f1 f2 f3 f4 str1. This command introduces a rectangle of specific properties in the model. The parameters f1 f2 are the lower left (x,y) coordinates of the rectangle in meters. Similarly, the f3 f4 are the upper right (x,y) coordinates of the rectangle. The parameter str1 is a medium identifier defined either with a #domain command.

#cylinder: f1 f2 f3 str1. This command introduces a circular disk in the model. The parameters f1, f2 are the (x,y) coordinates of the centre of the circular disk in meters. The parameter f3 is its radius in meters and str1 is the medium identifier.

#triangle: f1 f2 f3 f4 f5 f6 str1. This command introduces a triangular patch with specific parameters in the model. The three apexes of the triangular patch are specified in pairs of (x,y) in meters as: f1 f2; f3 f4; f5 f6. The parameter str1 is the predefined medium identifier.

It is important to note that GprMax2D process all object construction commands in the order they appear in the input file.

- Excitation and Output commands which are used to place source and output points in the model:

#line_source: f1 f2 str1 str2. f1 and f2 are the amplitude in amperes of the line source's current and the frequency in Hertz of the source's excitation waveform respectively. The parameter str1 controls the type of the excitation waveform and str2 is a user supplied ID which will subsequently be used to relate the specification of that source with the point of its application in the model.

#analysis: i1 file1 c1. The parameter i1 is the number of new runs of the model. It means that the model will run again – after resetting all arrays and time to zero – for every single i1. The parameter file1 is the name of the file and the parameter c1 is a single character either a or b denoting that the format of the output file (file1) will be ASCII or BINARY, respectively.

#end_analysis: .Which denotes the end of an analysis section that was started using a #analysis command.

The commands #tx and #rx are used together in order to introduce a source position and output points respectively.

#tx: f1 f2 str1 f3 f4. The parameters f1 and f2 are the (x,y) coordinates in meters of the source in the model. The parameter str1 is the source ID that has been specified before using a source description command (#line_source). The parameter f3 is a delay in the source's initiation. The parameter f4 is the time of source removal. If the simulation runs for longer than the source's removal time the source will stop functioning in the model after f4 seconds.

#rx: f1 f2. The parameters f1 and f2 are the (x,y) coordinates in meters of the output (receiver) point.

To calculate the coordinates of a new step, we need to include the commands:

#tx_steps: f1 f2. f1 and f2 are the increments in meters of the x and y coordinates accordingly for all the sources specified using #tx commands.

#rx_steps: f1 f2. f1 and f2 are the increments in meters of the x and y coordinates accordingly for all the receivers specified using #rx commands.

In the input file the hash character (#) is reserved and is used to denote the beginning of a command which should be passed to the programs. If the line starts with any other character it is ignored by the program. More information about how to create an input file as well as the GprMax operation is available in the corresponding user's manual developed (Giannopoulos, 2004).

A schematic for a modelling process of a bridge with three arches is illustrated in Figure 3.25. The constitutive parameters of the media involved as well as the commands used are described in the input file shown in Figure 3.25A. Free space can be modelled without the need to specify their parameters. Using GprMax2D and the input file created, an image representation of the model's space constructed using the information stored in the geometry file is obtained (Fig. 3.25B). The simulated GPR scan has been also provided (Fig. 3.25C).

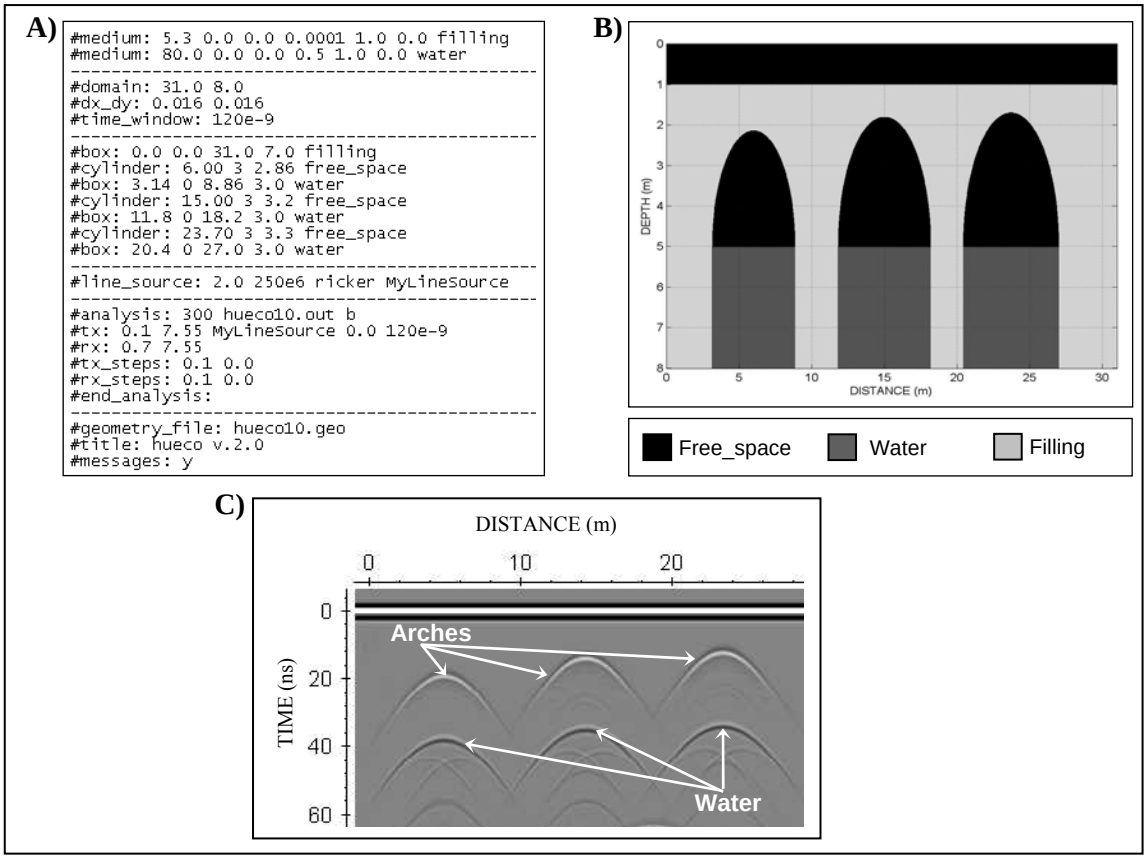

Figure 3.25.- FDTD simulation of a three arches bridge. A) Input file, B) model and C) synthetic radargram obtained.

The main disadvantages of the FDTD technique are: the need to discrete the volume of the problem space which could lead to excessive computer memory requirements and the

staircase representation of curved interfaces. Last GprMax version has been parallelized for shared memory machines and it allows the possibility of a combined approach where different traces (or lines in radar data) are computed at different nodes of a cluster. A significant reduction on computational time is achieved by using a mixed model of parallelization in GprMax based on MPI and OpenMP. The computational resources provided by the HPC-Europe2 program during my postgraduate researcher in the School of Engineering at the University of Edinburgh, under the supervision of Dr Antonis Giannopoulos, have allowed simulating large scale and realistic models. The inputs to create the synthetic models were generated by the orthophoto of the bridge produced by laser scanning or photogrammetric data (Fig. 3.26). The synthetic results (Fig. 3.27) have shown that even a relatively basic FDTD model can provide important additional information for the advanced interpretation of radar data. Although, the model is only two-dimensional it encompass the complete bridge structure in fine detail.

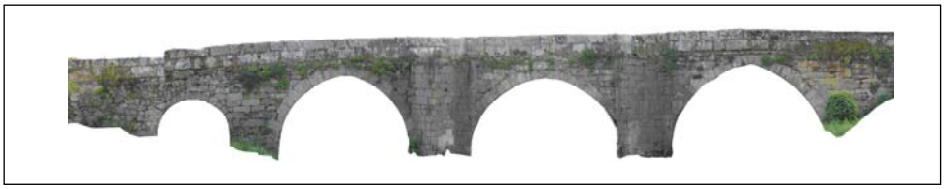

Figure 3.26.- Orthophoto of Traba bridge generated by laser scanning data.

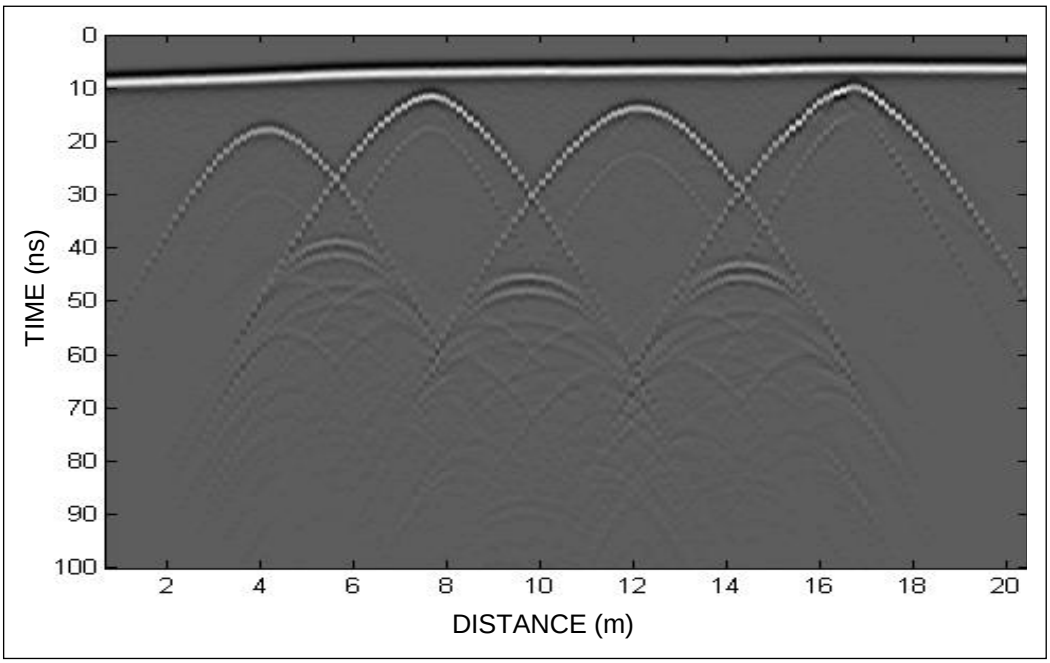

Figure 3.27.- Synthetic radargram of Traba bridge from the Orthophoto generated by laser scanning data.

3.4.- GPR DATA INTERPRETATION

Data interpretation is the last important task in a GPR survey. As described in the previous section, the quality of information contained in GPR data can be improved by the application of appropriate simple and/or more advanced signal processing techniques. However, the amount of information contained in GPR data sets cannot be maximized by signal processing approaches and the extraction of valid and sufficient information from GPR data is highly dependent on the knowledge and the experience of the interpreter. To avoid GPR pitfalls and assist interpretation, several factors should be taken into account. The establishment of clearly defined survey objectives, the gathering of the available structural and geometrical information about the bridge as well as the building materials employed for its construction and the possible restorations performed on the bridge under survey are very important factors. For example, knowledge of the arch span would help to establish an estimate of the electromagnetic wave velocity in the stone ashlars. Moreover, a correlation of GPR data with construction and/or restoration information, if available, is a very helpful step for the interpretation procedure.

Numerical modelling can also play a very important role in extracting valid and useful information from GPR data sets as a scenario for the expected GPR response can be developed through the use of modelling tools. Finally, a very thorough knowledge of the applicability, as well as the limitations of the GPR system is essential.

3.4.1.- Data interpretation pitfalls

There are many factors that can adversely affect a GPR survey. Owing to these unfavorable events, the later data interpretation becomes very complex in some circumstances. The main pitfalls in GPR data interpretation concerning to this dissertation are briefly described below.

3.4.1.1.- Ringing noise

Ringing is a term generally used for GPR signals which reverberate in a regular fashion as nearly horizontal and periodic events. This effect appears when the signal interacts with a metal object creating repeatedly bounces into the object or between two or more objects (Fig. 3.28). Deeper structures may be completely masked when its effect is strong and is

not properly removed (Kim et al., 2007). Ringing represents a common type of noise in GPR data.

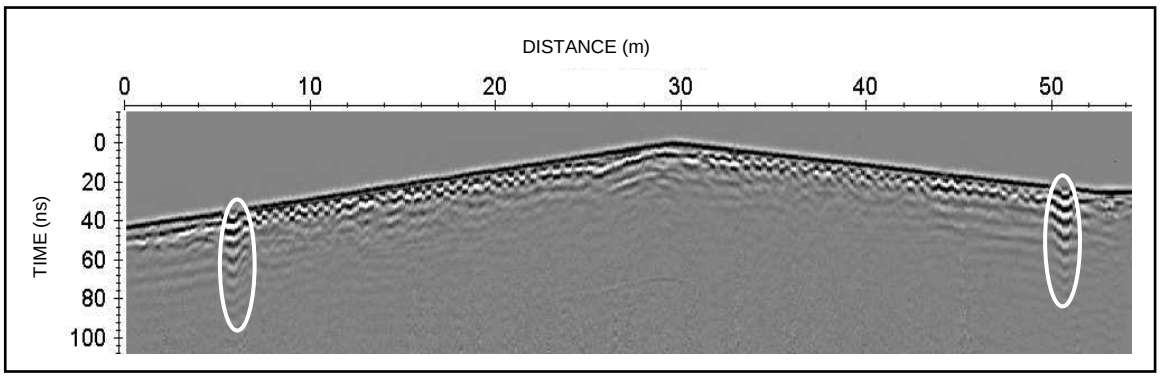

Figure 3.28.- The 250 MHz radargram acquired in Loña bridge shows ringing owing to both sewers along the pathway.

3.4.1.2.- X Marks the spot

This effect appears when the GPR system is placed close to a long wire such as fence or cable since the energy couples from the transmitter onto the wire. The energy travels along the wire in both directions until it reaches the end of the wire and the bounces back out (Annan, 2003). This signal noise is illustrated in the 250 MHz radargram acquired in Sarela bridge due to the presence of an electrical cable inside its pathway (Fig. 3.29).

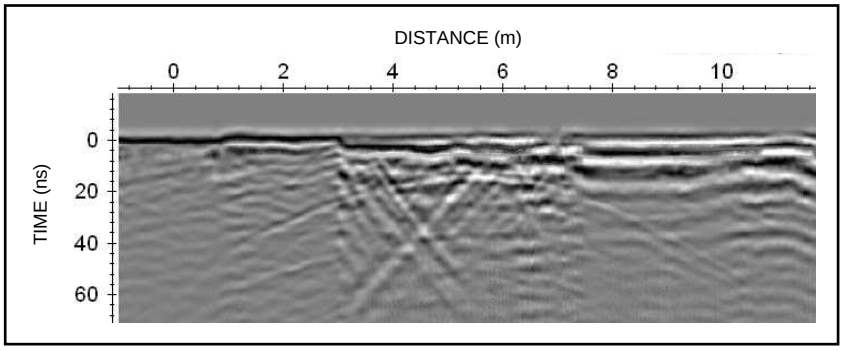

Figure 3.29.- Example of X Marks the spot in Sarela bridge data.

3.4.1.3.- Airwave events

Events on GPR data which are associated with energy that leaks into the air and gets reflected back into the GPR receiver. The source of these airwave reflections can be any above surface objects such as overhead wires, walls, vehicles, etc. Due to the higher electromagnetic wave velocity in the air than in the ground, their arrival time could be in the time window of interest (Nuzzo, 2003). Consequently, airwaves can produce a wrong interpretation in two different ways since they may be identified as a buried object as well as to make difficult or impossible to observe relevant surface reflections. The radargram

shown in Figure 3.30 is an example of airwave noise produced by the existence of reinforcing beams from a metal parapet structure.

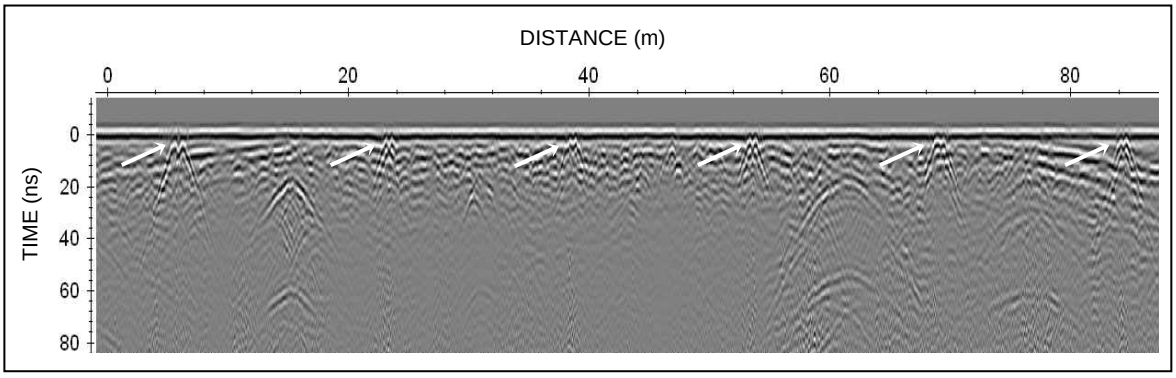

Figure 3.30.- Airwave events in a radargram gathered with the 250 MHz antenna in Lugo bridge.

3.4.1.4.- Signal attenuation

During the propagation of radar signal through the subsurface media, several factors results in a decrease of the signal's strength and the electromagnetic signal will experience attenuation. The attenuation of the electromagnetic signal's energy is a complex function of the electric and magnetic properties of the medium through which it is travelling hence the electromagnetic signal is not attenuated in the same way depending on ground materials. Besides that, signal attenuation is also frequency dependent and, therefore, a higher attenuation of the signal is expected when using GPR systems with high frequency antennas. Concerning to the assessment of historical masonry arch bridges, some modern materials used for restoration –such as reinforced concrete, soil-cement, metal mesh and geo-textile fabrics–, can be an important cause of the signal attenuation and loss of target resolution that result in a difficult data interpretation. Figure 3.31 illustrates the GPR data acquired with the 250 MHz antenna in the restored San Alberte bridge. The radargram shows a severe signal attenuation probably caused by using a mix of soil-cement for the subgrade reinforcing and protecting.

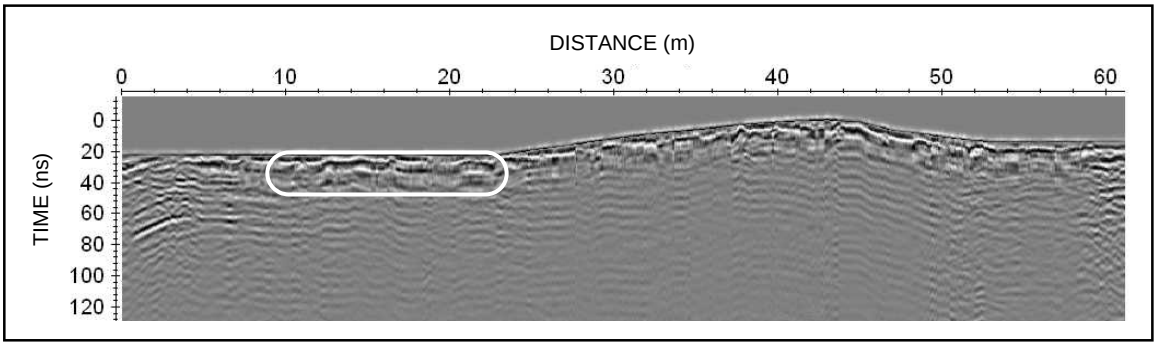

Figure 3.31.- Example of a severe signal attenuation in San Alberte bridge probably caused by the presence of a soil-cement mixture under the pathway.

4

Results

After an indepth review and selection of the most representative historical bridges around the whole Galician territory (NW Spain), a total of 36 ancient bridges were surveyed with GPR. This chapter is composed of an detailed inventory including a brief summary of the GPR results obtained for the evaluated bridges as well as a selection of four case studies representative of the most interesting GPR results acquired.

The radargrams are shown from the upstream side and the arches are named from the left to the right margin following the usual nomenclature.

4.1.- INVENTORY

This section presents an inventory of the historical Galician bridges selected for diagnosis, maintaining a balanced representation of the four Galician provinces. The main purpose was to develop a catalogue for characterization and diagnosis of these structures providing information useful to civil engineers in evaluating and predicting their states of conservation and considering any maintenance or rehabilitation tasks. It was based on historical and conservation criteria and thus can serve as a useful information resource for the legal protection of this heritage.

The existing documentation such as articles, single publications, specialized books, etc., was reviewed to locate and analyze the history of the bridges inventoried. Alvarado et al.

(1989), among others, provided valuable information about the state of these historical bridges.

The inventory consists of catalogue cards supplying the most relevant information for each bridge. A total of 36 masonry arch bridges with sufficient monumental entity, artistic value and technical interest are included. Each card provides the following remarks: a general description of the bridge including its location, the external structure and restorations effected over time. The GPR survey conducted for the assessment of each bridge is also described, including the methodology employed as well as the survey parameters and processing flow used. Finally, the best results obtained with GPR are shown together with an interpretation of the main reflectors detected.

Figure 4.1.- Location of Galicia in Europe.

4.1.1.- CORUÑA

4.1.1.1.- Carmen de Abajo Bridge (Santiago de Compostela).

4.1.1.2.- Brozos Bridge (Arteixo).

4.1.1.3.- Lubians Bridge (Carballo).

4.1.1.4.- Furelos Bridge (Melide).

4.1.1.5.- Ames Bridge (Ames).

4.1.1.6.- Sarela Bridge (Santiago de Compostela).

4.1.1.7.- Traba Bridge (Noia). CASE STUDY 4.2.2.

Figure 4.2.- Surveyed bridges distribution.

4.1.1.1.- CARMEN DE ABAJO BRIDGE

GENERAL DESCRIPTION

A single span arch bridge of the 17th century over the river Sarela in the town council of Santiago de Compostela (Fig. 4.2). It has an elliptical arch of 2.7 m span (Fig. 4.3). The whole structure is 36 m long and 3.60 m wide. It presents granitic stonework and a double slope shale path.

Figure 4.3.- View of Carmen de Abajo bridge from the downstream side.

GPR SURVEY

- **Methodology**

Carmen de Abajo bridge was surveyed in agreement with the common methodology proposed with the survey parameters shown in Table 4.1. The radargrams obtained were corrected for topography with (x,y,z) data from a total station.

Antenna	250 MHz	500 MHz
Number of Samples	439	479
Time Window	170 ns	70 ns
Trace Interval	0.02 m	0.02 m

Table 4.1.- GPR survey parameters.

- **Processing flow**

The processing sequence applied was: time-zero correction, dewow filtering, gain function, spatial filtering (subtracting average), band-pass filtering (butterworth) and topographic correction.

- **Results and interpretation**

The best results were obtained with the 250 MHz antenna, having its pulse enough energy and an adequate resolution. In the processed radargram obtained with the 250 MHz

antenna (Fig. 4.4A) were easily identified the reflections due to the arch-air and air-water interfaces. It was important to distinguish that between 22 and 27 meters to 130 ns, it could be differentiated another interesting reflection. This reflection could be correlated with the presence of a hidden spillway (Fig. 4.4B), which can be currently concealed according to the testimony of some residents.

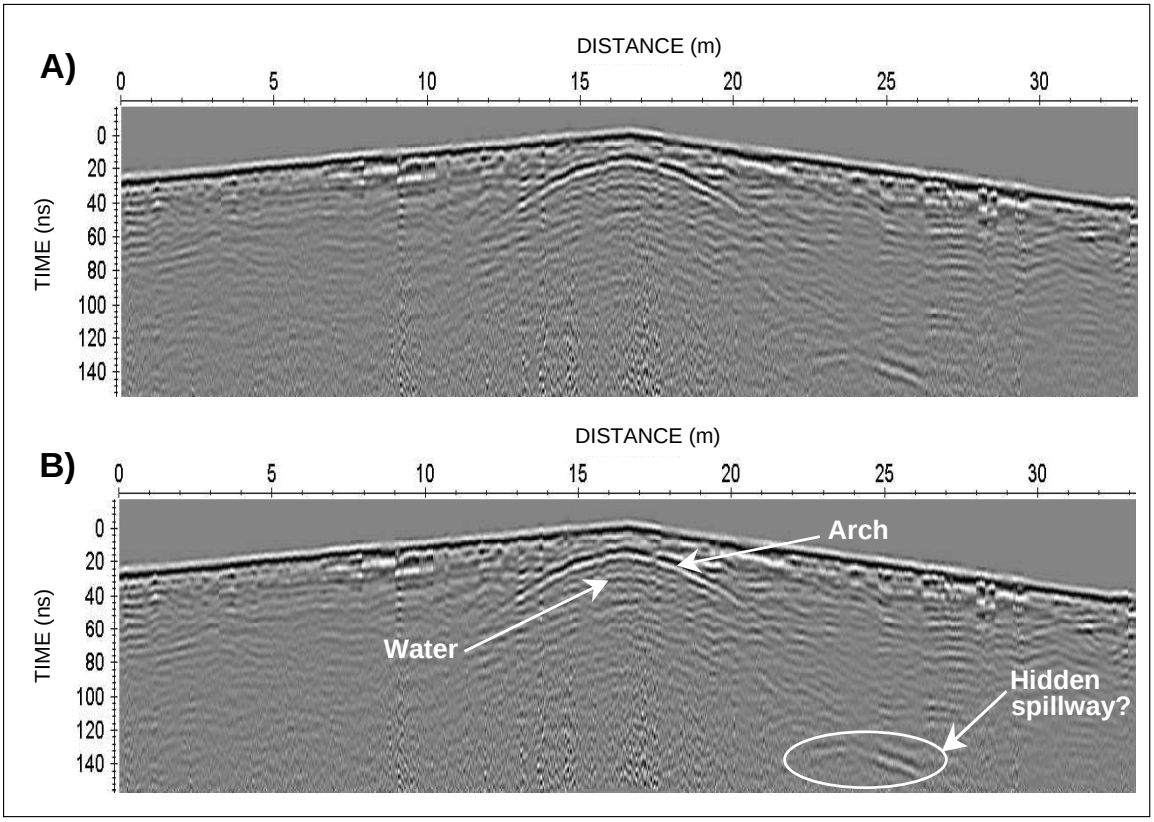

Figure 4.4.- Radargram obtained with 250 MHz antenna in Carme de Abajo bridge.
A) Processed data. B) Interpretation of the main reflectors detected.

4.1.1.2.- BROZOS BRIDGE

GENERAL DESCRIPTION

Brozos bridge is a 17th century masonry bridge across Bolaños river, located in the council of Arteixo (Fig. 4.2). As shown in Figure 4.5, it has two barrel arches of 4.40 m span, a triangular buttress and a slightly pointed profile. Additionally, it has a flagstone path between 4.0 and 4.6 meters wide. Last restoration tasks were made at the end of the 20th century.

Figure 4.5.- View of Brozos bridge from the upstream side.

GPR SURVEY

- **Methodology**

The common methodology proposed for surveying masonry arch bridges was assumed. The survey parameters used are mentioned in Table 4.2. (x,y,z) data from a total station were employed to correct the radargrams acquired for topography.

Antenna	250 MHz	500 MHz
Number of Samples	673	677
Time Window	200 ns	100 ns
Trace Interval	0.03 m	0.02 m

Table 4.2.- GPR survey parameters.

- **Processing flow**

The processing sequence applied was: time-zero correction, dewow filtering, gain function, spatial filtering (subtracting average), band-pass filtering (butterworth) and topographic correction.

- **Results and interpretation**

Observing the processed radargram acquired with the 250 MHz antenna (Fig. 4.6A), the reflections due to the arch-air and air-river bed interfaces were recognized. In addition, the reflection because of the dielectric contrast between the filling material and the stone

layer as well as the reflection from the foundation were identified (Fig. 4.6B).

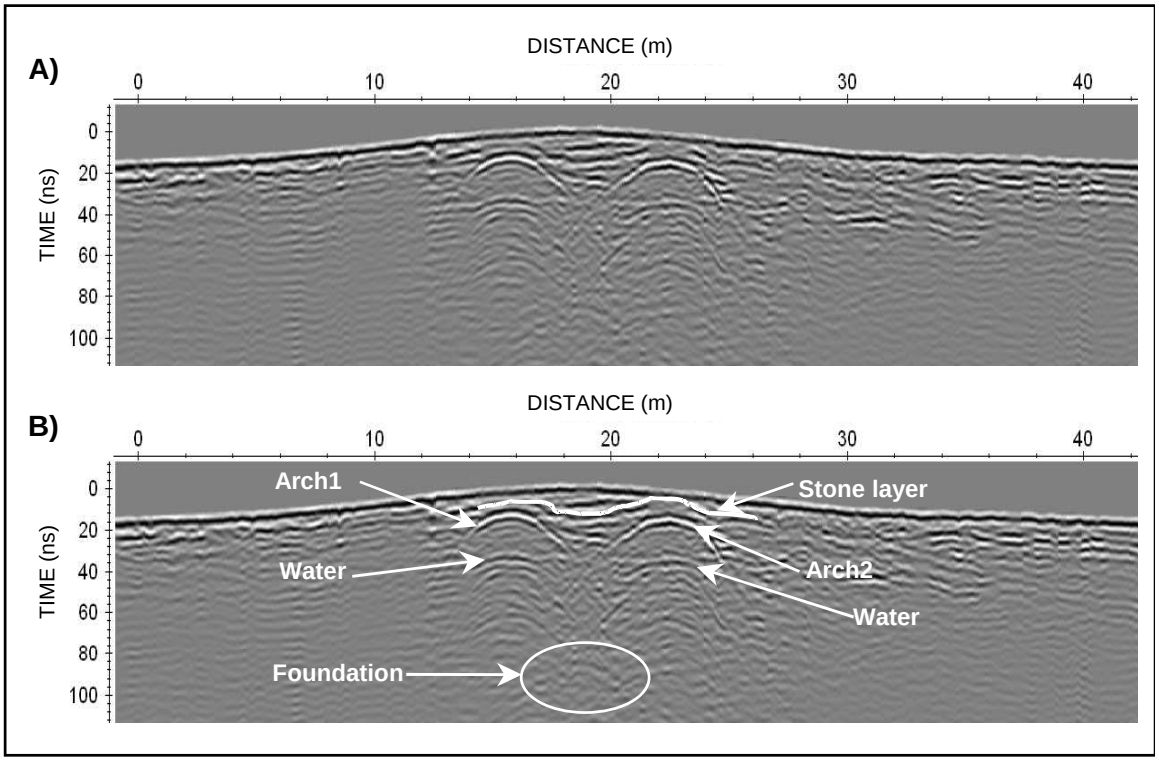

Figure 4.6.- Radargram obtained with 250 MHz antenna in Brozos bridge.
A) Processed data. B) Interpretation of the main reflectors detected.

4.1.1.3.- LUBIANS BRIDGE

GENERAL DESCRIPTION

The Lubians bridge was built in the 15th century over the Rosende river in the council of Carballo (Fig. 4.2). It has four barrel arches among 6.7 and 3.1 meters, a slightly pointed profile and a medieval flagstone path 2.5 m wide (Fig. 4.7).

Figure 4.7.- View of Lubians bridge from the upstream side.

This bridge was restored in the 17-18th centuries. In addition, the second vault in the left margin from the upstream side was recently rebuilt as a consequence of a flood. Some authors, who are specialized in the documentation and study of this kind of bridges, have referenced that the original bridge had five arches (Alvarado et al., 1989).

GPR SURVEY

- **Methodology**

The common methodology proposed was employed for surveying the Lubians bridge with the survey parameters mentioned in Table 4.3. The radargrams acquired were corrected for topography by using (x,y,z) data recorded by means of a total station.

Antenna	250 MHz	500 MHz
Number of Samples	626	677
Time Window	200 ns	100 ns
Trace Interval	0.03 m	0.02 m

Table 4.3.- GPR survey parameters.

- **Processing flow**

The processing sequence applied was: time-zero correction, dewow filtering, gain function, spatial filtering (subtracting average) and topographic correction.

- **Results and interpretation**

The best results were acquired with the 500 MHz antenna. Observing the processed radargram in Figure 4.8A it was possible to identify the reflections from the arch-air and air-water interfaces and the typical corner reflections generated in this kind of arches (Martinaud et al., 2004).

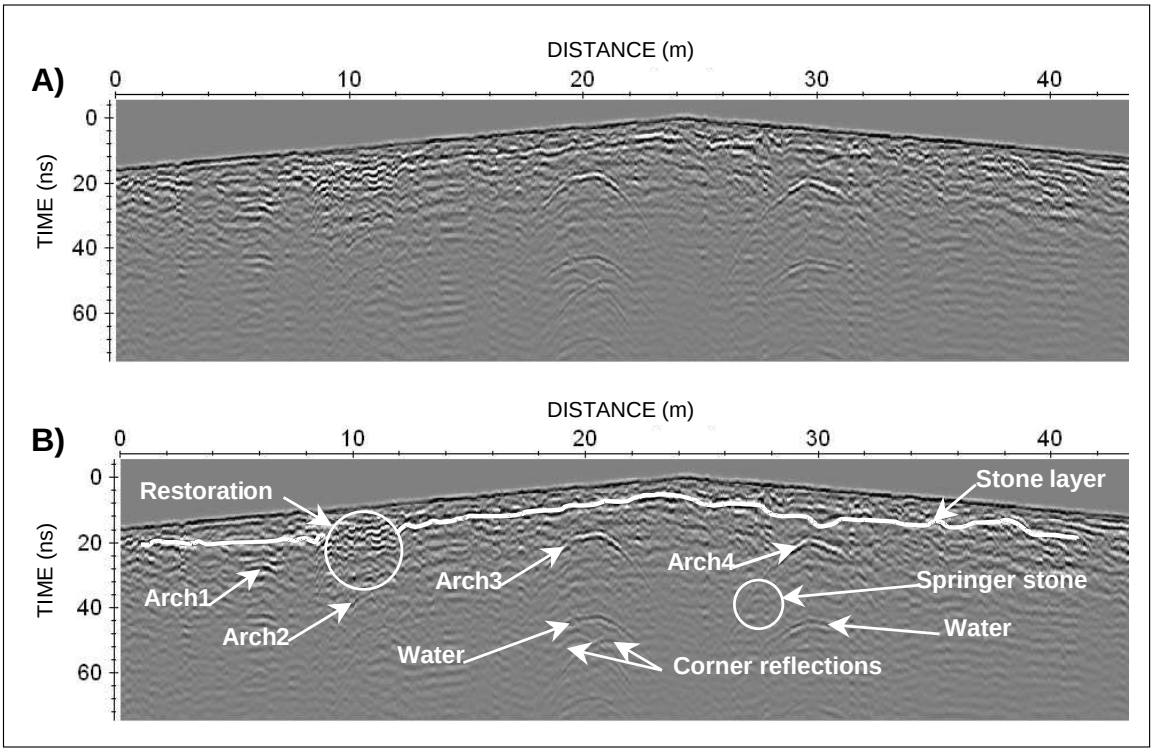

Figure 4.8.- Radargram obtained with 500 MHz antenna in Lubians bridge.
A) Processed data. B) Interpretation of the main reflectors detected.

An interesting reflection is the one just above the second arch. This effect is probably caused by the presence of building materials which are different than the original ones and were used for restoration according to the literature (Alvarado et al., 1989). Observing the radargram carefully, it was possible to identify the reflection owing to the dielectric contrast among the filling and the stone layer (Fig. 4.8B). Despite there being some historical references regarding the existence of a fifth arch in the original bridge, in the radargram there were no clear evidences of this fact.

4.1.1.4.- FURELOS BRIDGE

GENERAL DESCRIPTION

A 12th century bridge across the Furelos river, close to the council of Melide (Fig. 4.2). It presents four barrel arches between 5.3 and 12.05 meters, a slightly pointed profile and a flagstone path 2.6 m wide (Fig. 4.9).

Figure 4.9.- View of Furelos bridge from the upstream side.

Probably, this bridge was restored several times (Alvarado et al., 1989). It is a bridge of granite and shale ashlars maybe owing to the restorations before mentioned.

GPR SURVEY

- **Methodology**

The common methodology proposed was used for assessing this bridge with the survey parameters described in Table 4.4. In addition, the radargrams obtained were corrected for topography by using (x,y,z) data from a total station.

Antenna	250 MHz	500 MHz
Number of Samples	512	612
Time Window	200 ns	90 ns
Trace Interval	0.02 m	0.02 m

Table 4.4.- GPR survey parameters.

- **Processing flow**

The processing sequence applied was: time-zero correction, dewow filtering, gain function, spatial filtering (subtracting average), band-pass filtering (butterworth) and topographic correction.

- **Results and interpretation**

The best results were acquired with the 250 MHz antenna. The reflections from the arch-air interfaces were relatively recognized (Fig. 4.10A). The reflection due to the air-water interface was only identified under the main arch (Fig. 4.10B).

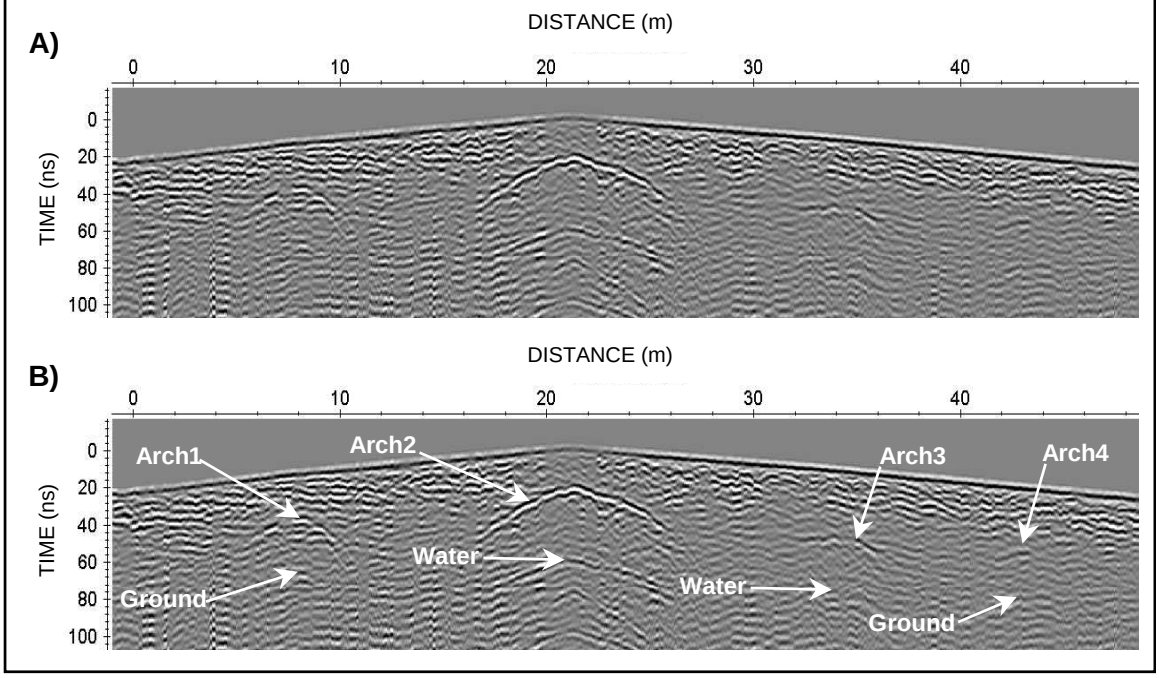

Figure 4.10.- Radargram obtained with 250 MHz antenna in Furelos bridge.
A) Processed data. B) Interpretation of the main reflectors detected.

4.1.1.5.- AMES BRIDGE

GENERAL DESCRIPTION

An elliptical arch bridge 3.0 m span with a medieval origin. It is located in the council of Ames (Fig. 4.2) over the Augapesada stream. Besides it presents two spillways, a slightly pointed profile and a flagstone path as shown in Figure 4.11.

Figure 4.11.- View of Ames bridge from the downstream side.

GPR SURVEY

- **Methodology**

The common methodology proposed was employed for surveying the Lubians bridge with the survey parameters mentioned in Table 4.5. Furthermore, the radargrams obtained were corrected for topography by using (x,y,z) data recorded from a total station.

Antenna	250 MHz	500 MHz
Number of Samples	512	683
Time Window	200 ns	100 ns
Trace Interval	0.05 m	0.02 m

Table 4.5.- GPR survey parameters.

- **Processing flow**

The processing sequence applied was: time-zero correction, dewow filtering, gain function, spatial filtering (subtracting average) and topographic correction.

- **Results and interpretation**

In the processed radargram in Figure 4.12, the reflections due to the arch-air and air-water interfaces were easily identified as well as the reflections generated in the spillway-air interfaces. The radargrams obtained with the 500 MHz antenna did not provide additional information.

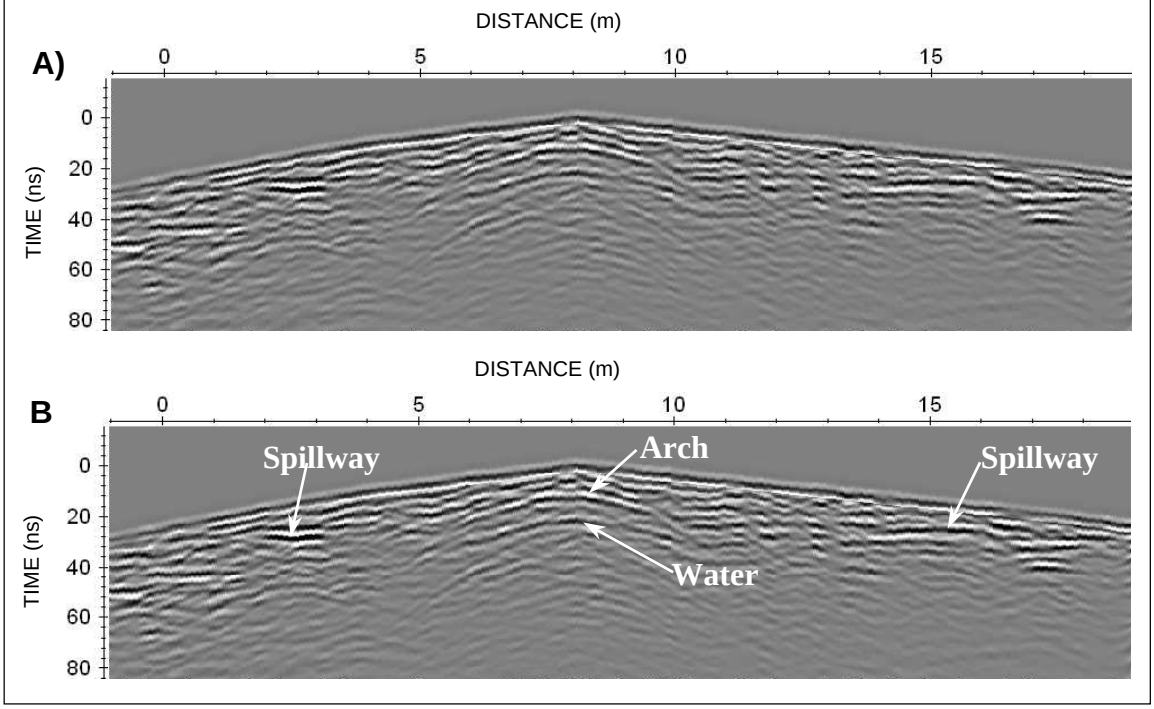

Figure 4.12.- Radargram obtained with 250 MHz antenna in Ames bridge.
A) Processed data. B) Interpretation of the main reflectors detected.

4.1.1.6.- SARELA BRIDGE

GENERAL DESCRIPTION

A granite stone bridge with an elliptical arch and a spillway (Fig. 4.13). It is in the town council of Santiago de Compostela (Fig. 4.2) over the Sarela river.

Figure 4.13.- View of Sarela bridge from the downstream side.

GPR SURVEY

- **Methodology**

The assessment was performed with the common methodoly proposed by means of the 250 MHz antenna and the survey parameters in Table 4.6. The radargrams acquired were corrected for topography by using (x,y,z) data recorded by means of a total station.

Antenna	**250 MHz**
Number of Samples	512
Time Window	200 ns
Trace Interval	0.05 m

Table 4.6.- GPR survey parameters.

- **Processing flow**

The processing sequence applied was: time-zero correction, dewow filtering, gain function, spatial filtering (subtracting average), band-pass filtering (butterworth) and topographic correction.

- **Results and interpretation**

Observing the processed radargram in Figure 4.14, it was possible to identify the reflections from the arch-air and air-water interfaces as well as the spillway-air interface generated.

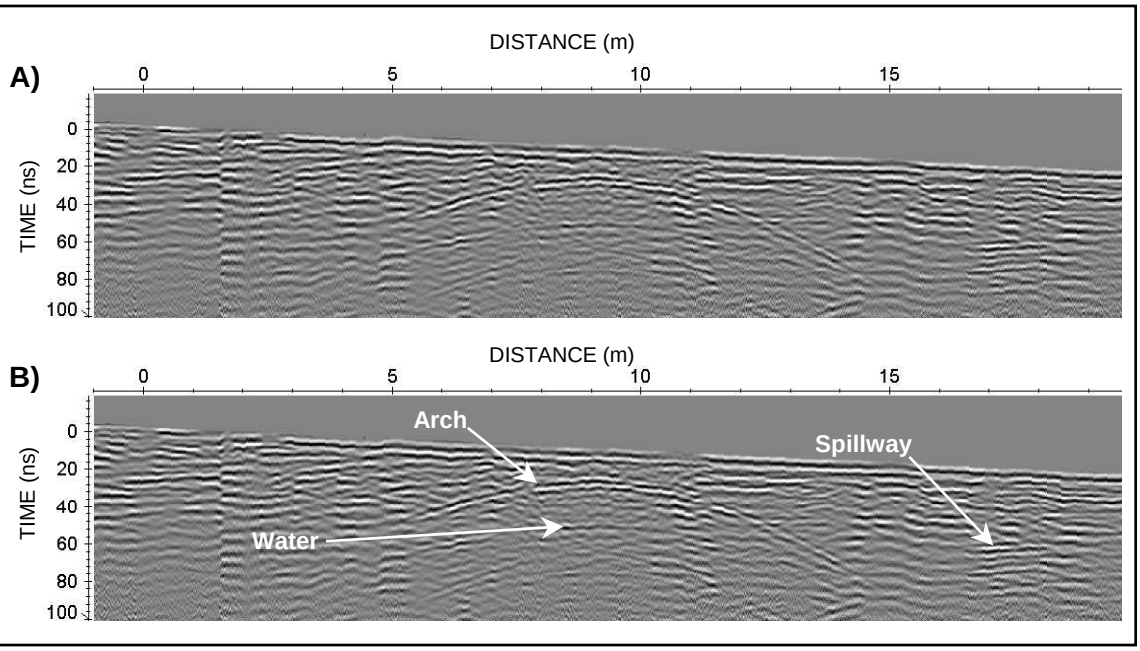

Figure 4.14.- Radargram obtained with 250 MHz antenna in Sarela bridge.
A) Processed data. B) Interpretation of the main reflectors detected.

4.1.1.7.- TRABA BRIDGE

GENERAL DESCRIPTION

Medieval arch bridge built in the 14th century. It is located in Noia across the Traba river (Fig. 4.2). It has four barrel or gothic arches between 4.8 and 7.0 meters span (Fig. 4.15).

Figure 4.15.- View of Traba bridge from the upstream side.

GPR SURVEY

- **Methodology**

Carmen de Abajo bridge was surveyed following the common methodology proposed with the survey parameters shown in Table 4.7. The radargrams obtained were corrected for topography with (x,y,z) data from a total station.

Antenna	250 MHz	500 MHz
Number of Samples	567	678
Time Window	200 ns	100 ns
Trace Interval	0.05 m	0.02 m

Table 4.7.- GPR survey parameters.

- **Processing flow**

The processing sequence applied was: time-zero correction, dewow filtering, gain function, spatial filtering (subtracting average), band-pass filtering (butterworth) and topographic correction.

- **Results and interpretation**

The best results were obtained with the 250 MHz antenna. Observing the processed radargram obtained with the 250 MHz antenna (Fig. 4.16A), the reflections due to the arch-air and air-water interfaces were easily identified, although it was possible to appreciate a severe attenuation of the signal in the first and third arches. This effect was probably caused by the presence of building materials which are different than the original ones and were used for restoration according to the historical references (Alvarado et al.,

1989). It could be differentiated a reflection pattern in form of consecutive small hyperbolas over the two restored arches (Fig. 4.16B), most likely generated by reinforced concrete which could be an important cause of the signal attenuation previously mentioned.

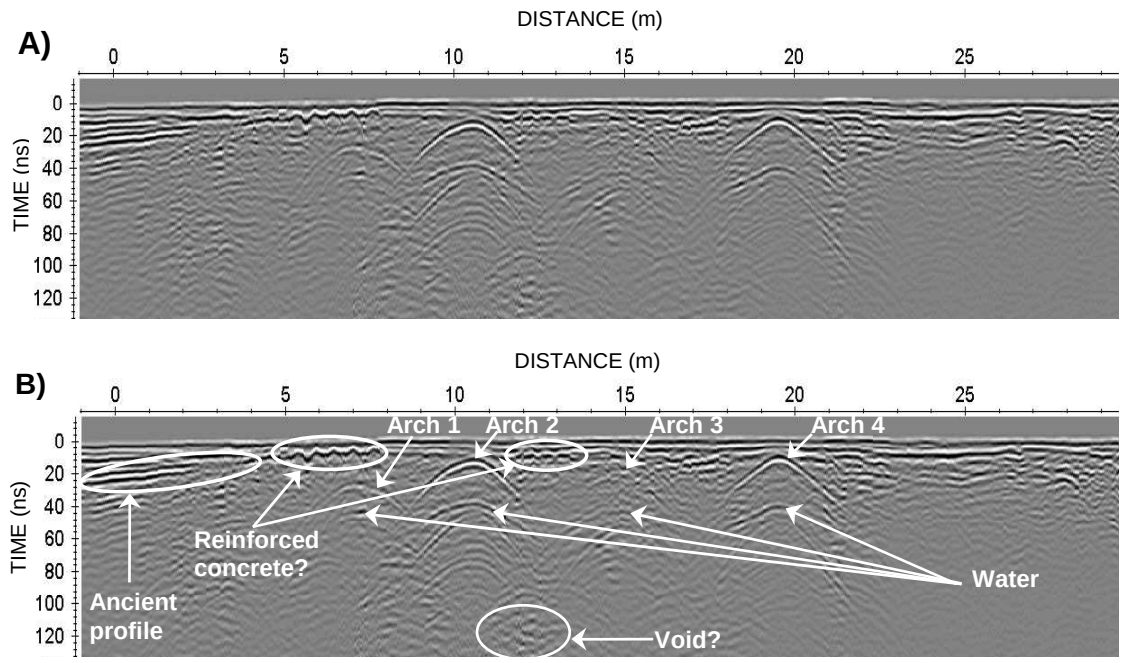

Figure 4.16.- Radargram obtained with 250 MHz antenna in Traba bridge.
A) Processed data. B) Interpretation of the main reflectors detected.

Another interesting reflection is located at the beginning of the radargram shown in Figure 4.16B and it may be generated by an ancient profile of the bridge more pronounced than the actual one. Additionally, it was possible to identify an anomaly in the second pier of the bridge from the left margin upstream which was named in Figure 4.16B as a probable void location.

Remark: An extended analysis of Traba bridge is described in subchapter 4.2.2.

4.1.2.- LUGO

4.1.2.1.- Lugo Bridge (Lugo). CASE STUDY 4.2.4.

4.1.2.2.- Aspera Bridge (Sarria).

4.1.2.3.- San Alberte Bridge (Guitiriz-Begonte).

4.1.2.4.- Madalena Bridge (Vilalba).

4.1.2.5.- Saa Bridge (Vilalba).

4.1.2.6.- Cabalar Bridge (Guntin).

4.1.2.7.- Carracedo Bridge (Lancara).

4.1.2.8.- Monforte Bridge (Monforte de Lemos).

Figure 4.17.- Surveyed bridges distribution.

4.1.2.1.- LUGO BRIDGE

GENERAL DESCRIPTION

A Roman bridge over the Miño river in the city council of Lugo (Fig. 4.17). It presents eight gothic or barrel arches from 5.6 to 10.4 meters span (Fig. 4.18). Some of these arches have a granite vault (1, 2, 4, 7 and 8 from the left margin in the upstream side), whereas the rest have a slate vault.

Figure 4.18.- View of Lugo bridge from the downstream side.

This bridge was restored and rebuilt several times up to now (Alvarado et al., 1989). Even it had a doble slope until the end of the XX century (Durán, 2005).

GPR SURVEY

- **Methodology**

Lugo bridge was surveyed according to the common methodology with the survey parameters shown in Table 4.8.

Antenna	250 MHz	500 MHz
Number of Samples	540	677
Time Window	210 ns	100 ns
Trace Interval	0.02 m	0.02 m

Table 4.8.- GPR survey parameters.

- **Processing flow**

The processing sequence applied was: time-zero correction, dewow filtering, gain function, spatial filtering (subtracting average) and band-pass filtering (butterworth).

- **Results and interpretation**

Figure 4.19 shows a radargram acquired with the 250 MHz antenna. It was possible to appreciate different signal responses over the arches. Additionally, signal attenuation was observed over some of them. Also, the fifth and eighth arches were practically attenuated

(Fig. 4.19B). The different signal behaviour could indicate the presence of several building materials in the structure as well as the existence of different filling materials over the arches. This effect could be caused by restoration tasks carried out over its lifetime. Moreover, it was possible to identify the ancient profile of Lugo bridge according to the specialized literature (Durán, 2005). This event could be useful to verify a probable pathway leveling. Finally, the typical corner reflections generated in this kind of arches were detected.

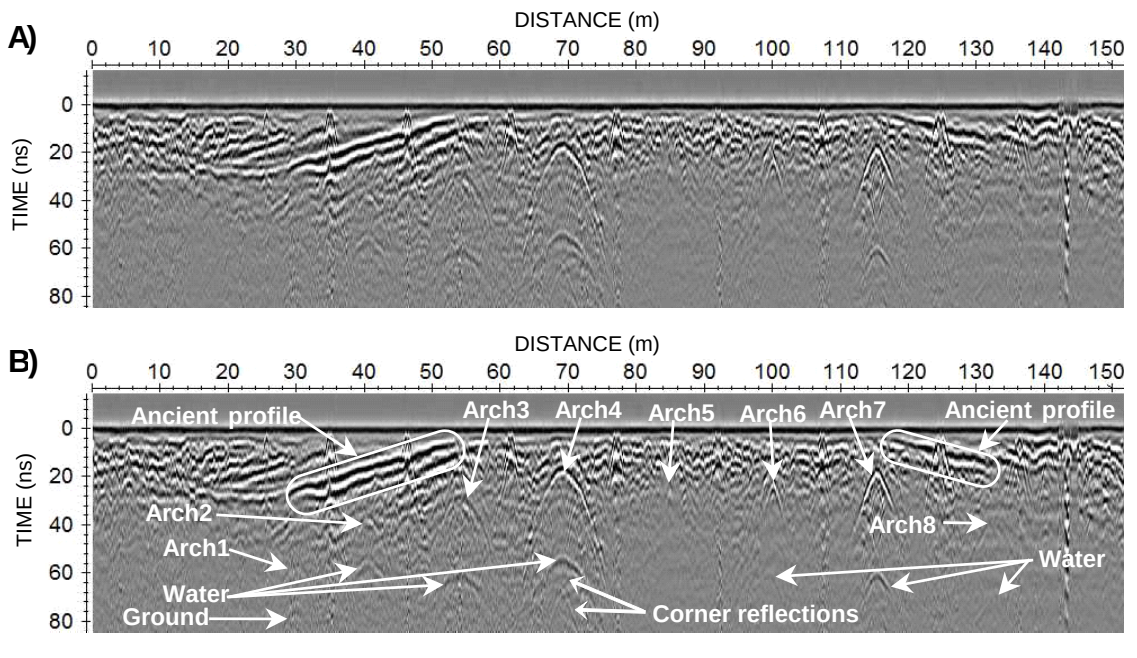

Figure 4.19.- Radargram obtained with 250 MHz antenna in Lugo bridge.
A) Processed data. B) Interpretation of the main reflectors detected.

Remark: An extended analysis of Lugo bridge is described in subchapter 4.2.4.

4.1.2.2.- ASPERA BRIDGE

GENERAL DESCRIPTION

A granite-slate arch bridge built in the 13th century with four arches among 3.5 and 4.7 m span (Fig. 4.20). It is located in Sarria (Fig. 4.17) across the Celeiro river. It presents granite arch rings whereas the spandrel walls were restored with slate ashlar. It has the former flagstone path 2.3 m wide and it an irregular profile.

Figure 4.20.- View of Aspera bridge from the upstream side.

GPR SURVEY

- **Methodology**

The common methodology exposed previously for surveying masonry arch bridges was carried out. The survey parameters used are given in Table 4.9. (x,y,z) data from a total station were employed to correct the radargrams acquired for topography.

Antenna	250 MHz	500 MHz
Number of Samples	789	678
Time Window	180 ns	100 ns
Trace Interval	0.05 m	0.02 m

Table 4.9.- GPR survey parameters.

- **Processing flow**

The processing sequence applied was: time-zero correction, dewow filtering, gain function, spatial filtering (subtracting average), band-pass filtering (butterworth) and topographic correction.

- **Results and interpretation**

The best results were recorded with the 250 MHz antenna, where the habitual reflections from the arch-air and air-water interfaces were distinguished(Fig. 4.21).

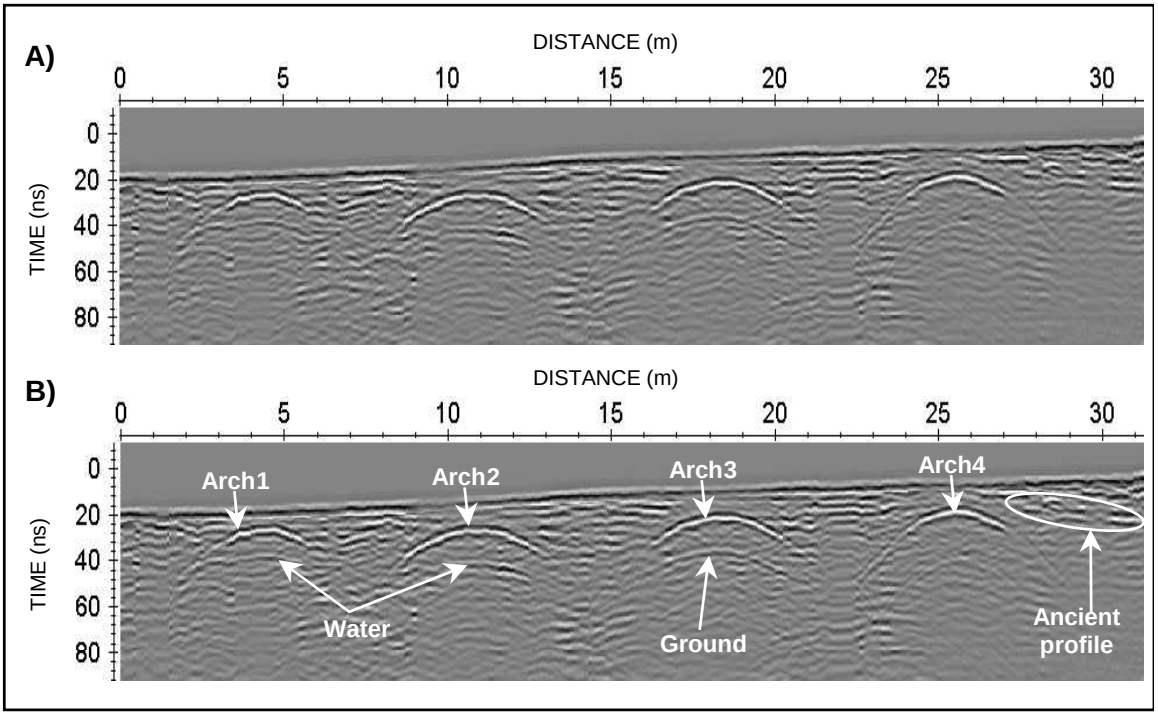

Figure 4.21.- Radargram obtained with 250 MHz antenna in Aspera bridge.
A) Processed data. B) Interpretation of the main reflectors detected.

4.1.2.3.- SAN ALBERTE BRIDGE

GENERAL DESCRIPTION

San Alberte bridge was built in the 14th century over the Parga river among Guitiriz and Begonte councils (Fig. 4.17). It is a granite-slate arch bridge with two gothic arches of 8.30 m span and some spillways in both margins (Fig. 4.22). It presents a double slope and it was restored recently.

Figure 4.22.- View of San Alberte bridge from the upstream side.

GPR SURVEY

- **Methodology**

The GPR survey was realized following the common methodoly proposed but, in this case, the 200 and 250 MHz antennas were employed. The survey parameters selected are shown in Table 4.10. In addition, the radargrams acquired were corrected for topography by using (x,y,z) data recorded by means of a total station.

Antenna	200 MHz	250 MHz
Number of Samples	547	643
Time Window	250 ns	250 ns
Trace Interval	0.02 m	0.02 m

Table 4.10.- GPR survey parameters.

- **Processing flow**

The processing sequence applied was: time-zero correction, dewow filtering, gain function, spatial filtering (subtracting average), band-pass filtering (butterworth) and topographic correction.

- **Results and interpretation**

The radargram acquired with the 250 MHz antenna showed a severe signal attenuation in the GPR data obtained resulting in a impossible identification of reflectors (Fig. 4.23). This effect could be caused by the presence of filling materials used for pathway restoration wich are different than the original ones. The most probable hypothesis for the backing employed could be soil-cement. It is a mix of pulverized natural soil with small amount of portland cement and water compacted to high density which supposes voids left. Soil-cement is frequently used in pathway construction as a subbase layer for reinforcing and protecting of the subgrade. Similar results were observed by Lorenzo (1996).

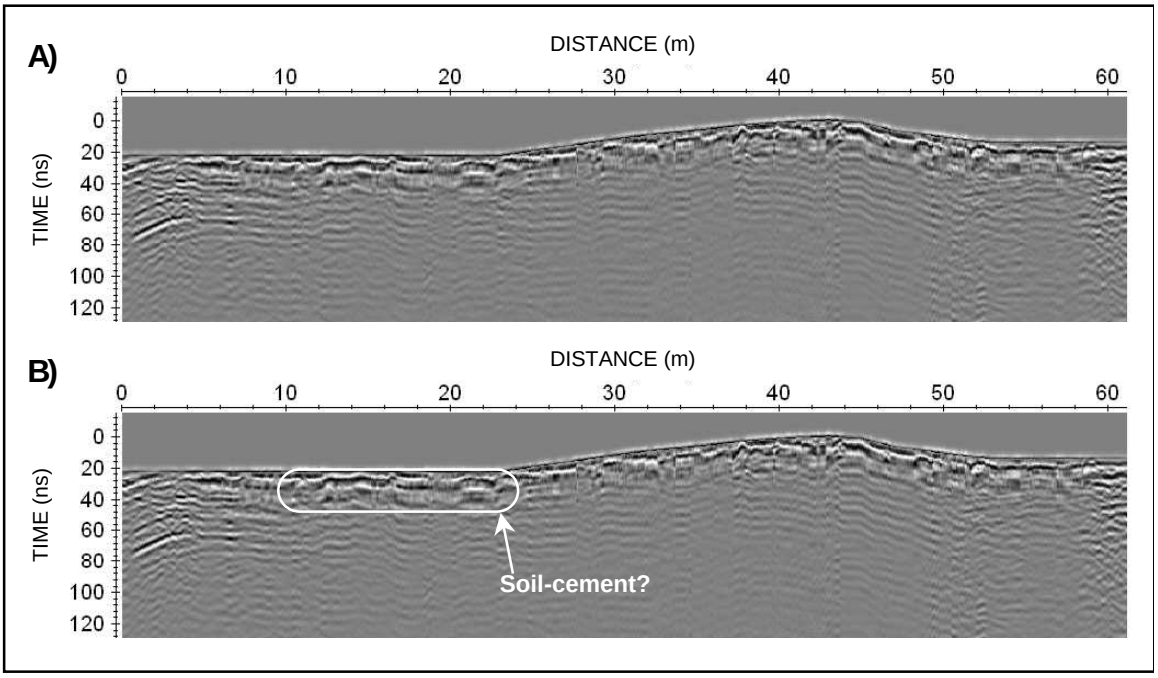

Figure 4.23.- Radargram obtained with 250 MHz antenna in San Alberte bridge.
A) Processed data. B) Interpretation of the main reflectors detected.

4.1.2.4.- MADALENA BRIDGE

GENERAL DESCRIPTION

Masonry arch bridge located in Vilalba council through the Ladra river (Fig. 4.17). Observing Figure 4.24, this bridge presents two gothic arches of 6.2 m span.

Figure 4.24.- View of Madalena bridge from the upstream side.

GPR SURVEY

- **Methodology**

The assessment was performed with the common methodology proposed by means of the 250 MHz antenna with the survey parameters in Table 4.11.

Antenna	**250 MHz**
Number of Samples	643
Time Window	250 ns
Trace Interval	0.02 m

Table 4.11.- GPR survey parameters.

- **Processing flow**

The processing sequence applied was: time-zero correction, dewow filtering, gain function, spatial filtering (subtracting average) and band-pass filtering (butterworth).

- **Results and interpretation**

In the processed radargram on Figure 4.25, the reflections due to the arch-air and air-water interfaces were easily identified as well as the reflection generated in the stone-filling interface along the bridge. Another reflection identified was the one caused by the presence of a possible ancient profile of Madalena bridge (Fig. 4.25B). The reflection from the foundation of the first arch in the left margin was also interpreted.

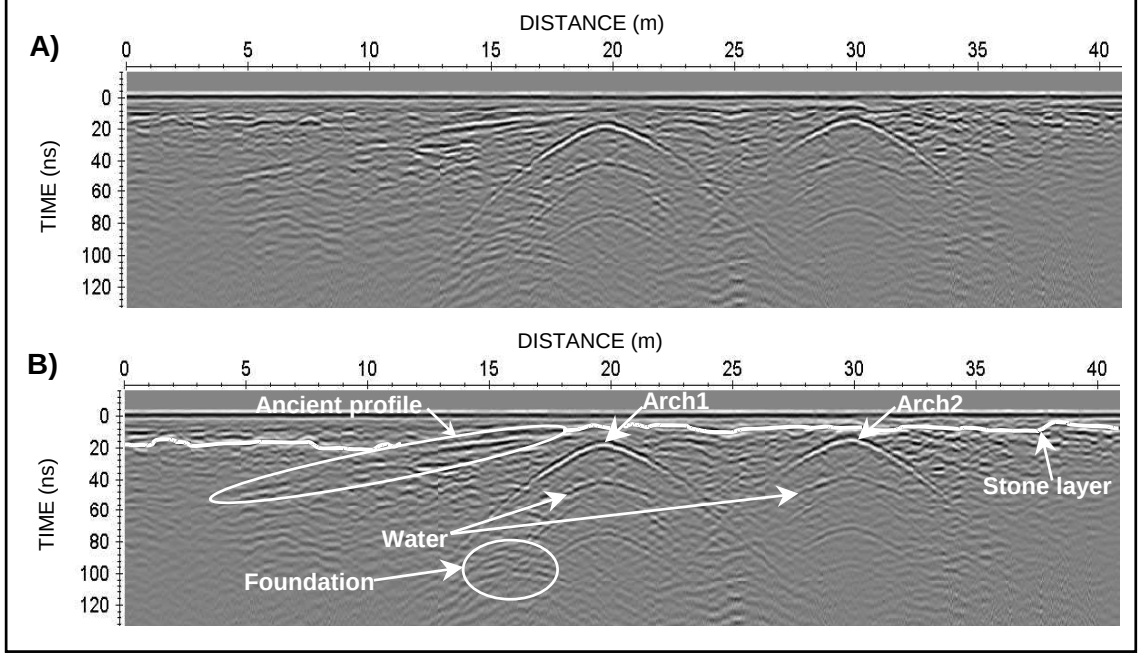

Figure 4.25.- Radargram obtained with 250 MHz antenna in Madalena bridge.
A) Processed data. B) Interpretation of the main reflectors detected.

4.1.2.5.- SAA BRIDGE

GENERAL DESCRIPTION

Medieval masonry arch bridge in Vilalba across the Labrada river (Fig. 4.17). It has two arches with 5.4 and 1.7 meters span and a long wing wall with ten spillways (Fig. 4.26). The stonework is slate, only the arch rings were built with granite. In addition, Saa bridge presents a very slightly pointed profile.

Figure 4.26.- View of Saa bridge from the downstream side.

GPR SURVEY

- **Methodology**

The methodology employed in this bridge envolved the use of 250 and 500 MHz frequencies although only one profile was recorded with each antenna due to the narrowness of the bridge. The survey parameters are mentioned in Table 4.12. The radargrams acquired were corrected for topography by using (x,y,z) data recorded by means of a total station.

Antenna	250 MHz	500 MHz
Number of Samples	387	479
Time Window	150 ns	70 ns
Trace Interval	0.02 m	0.02 m

Table 4.12.- GPR survey parameters.

- **Processing flow**

The processing sequence applied was: time-zero correction, dewow filtering, gain function, spatial filtering (subtracting average), band-pass filtering (butterworth) and topographic correction.

- **Results and interpretation**

The reflections due to the arch-air and air-water interfaces were easily identified in

Figure 4.27, as well as the reflections generated in the spillway-air interfaces. The radargram obtained with the 500 MHz antenna did not provide interesting additional information.

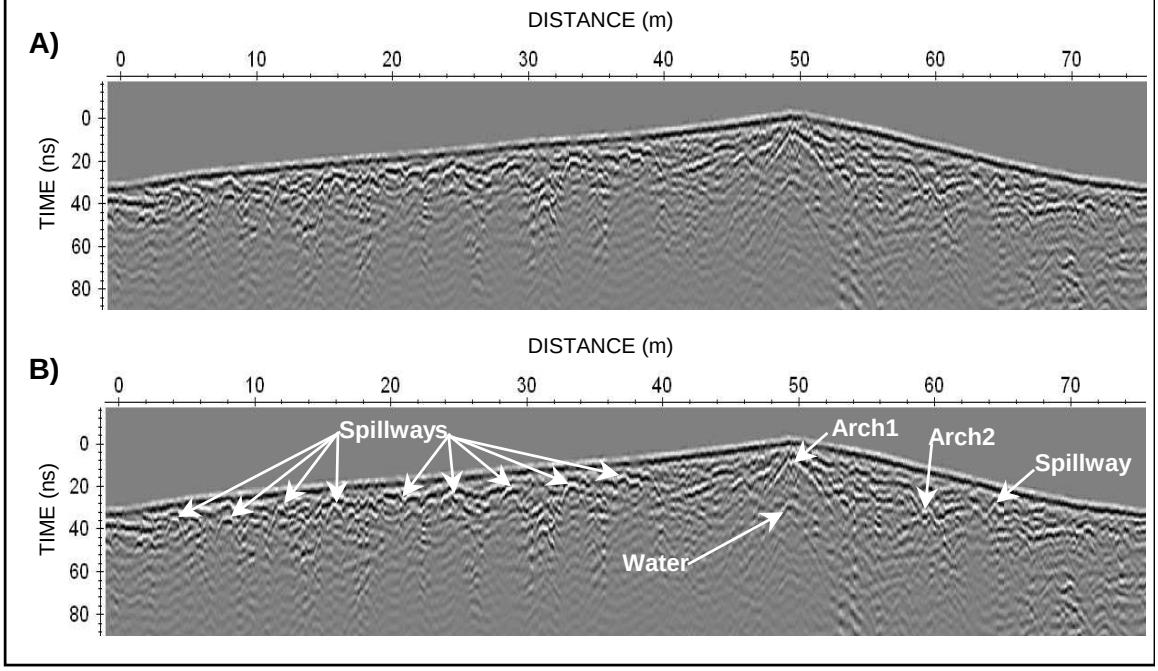

Figure 4.27.- Radargram obtained with 250 MHz antenna in Saa bridge.
A) Processed data. B) Interpretation of the main reflectors detected.

4.1.2.6.- CABALAR BRIDGE

GENERAL DESCRIPTION

A granite-slate arch bridge over the Ferreira river in the town council of Guntin (Fig. 4.17). It was built with four arches between 2.7 and 8.0 meters span (Fig. 4.28).

Figure 4.28.- View of Cabalar bridge from the downstream side.

GPR SURVEY

- **Methodology**

The common methodology proposed was employed for surveying the Cabalar bridge with the survey parameters mentioned in Table 4.13.

Antenna	250 MHz	500 MHz
Number of Samples	512	683
Time Window	200 ns	100 ns
Trace Interval	0.05 m	0.02 m

Table 4.13.- GPR survey parameters.

- **Processing flow**

The processing sequence applied was: time-zero correction, dewow filtering, gain function and spatial filtering (subtracting average).

- **Results and interpretation**

Observing the processed radargram obtained (Fig. 4.29A), the usual reflections due to the arch-air and air-water interfaces were identified, although the reflection from the first arch was not easily appreciated at first glance. Other reflection interpreted was the one caused by the stone-filling interface inside the bridge (Fig. 4.29B).

An interesting event was observed for the second arch of the bridge. It was possible to detect the reflection from the arch-air interface at the pathway level (Fig. 4.29B). This effect could inform us about an internal staircase shape of the ring stones.

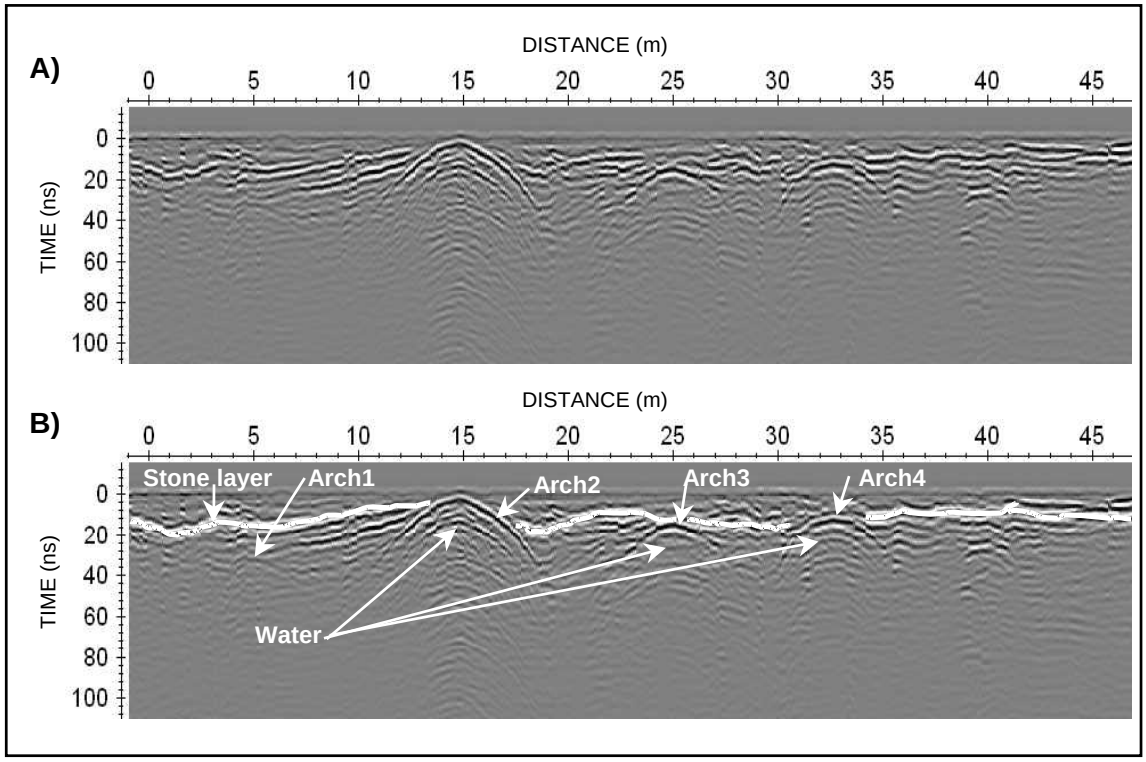

Figure 4.29.- Radargram obtained with 250 MHz antenna in Cabalar bridge.
A) Processed data. B) Interpretation of the main reflectors detected.

4.1.2.7.- CARRACEDO BRIDGE

GENERAL DESCRIPTION

A 16th masonry arch bridge over the Neira river in the council town of Lancara (Fig. 4.17). It has four arches among 1.7 and 11.6 meters span and a slightly pointed profile (Fig. 4.30). It presents a flagstone path 3.5 m wide.

Figure 4.30.- View of Carracedo bridge from the upstream side.

GPR SURVEY

- **Methodology**

The common methodology proposed was employed for surveying the Carracedo bridge with the survey parameters mentioned in Table 4.14. The radargrams acquired were corrected for topography by using (x,y,z) data recorded by means of a total station.

Antenna	250 MHz	500 MHz
Number of Samples	516	682
Time Window	200 ns	100 ns
Trace Interval	0.05 m	0.02 m

Table 4.14.- GPR survey parameters.

- **Processing flow**

The processing sequence applied was: time-zero correction, dewow filtering, gain function, spatial filtering (subtracting average), band-pass filtering (butterworth) and topographic correction.

- **Results and interpretation**

Observing the processed radargram obtained (Fig. 4.31A), the usual reflections due to the arch-air and air-water/air-ground interfaces were identified as well as the corner

reflections generated in this kind of arches (Martinaud et al., 2004). Other relevant structural reflections shown in Figure 4.31 were the ring stone reflections produced in arches due to their internal staircase shape (Alvarado et al., 1989) and the springer stone reflections due to their bigger size in relation to the other ring stones that compose the arch (Durán, 2005).

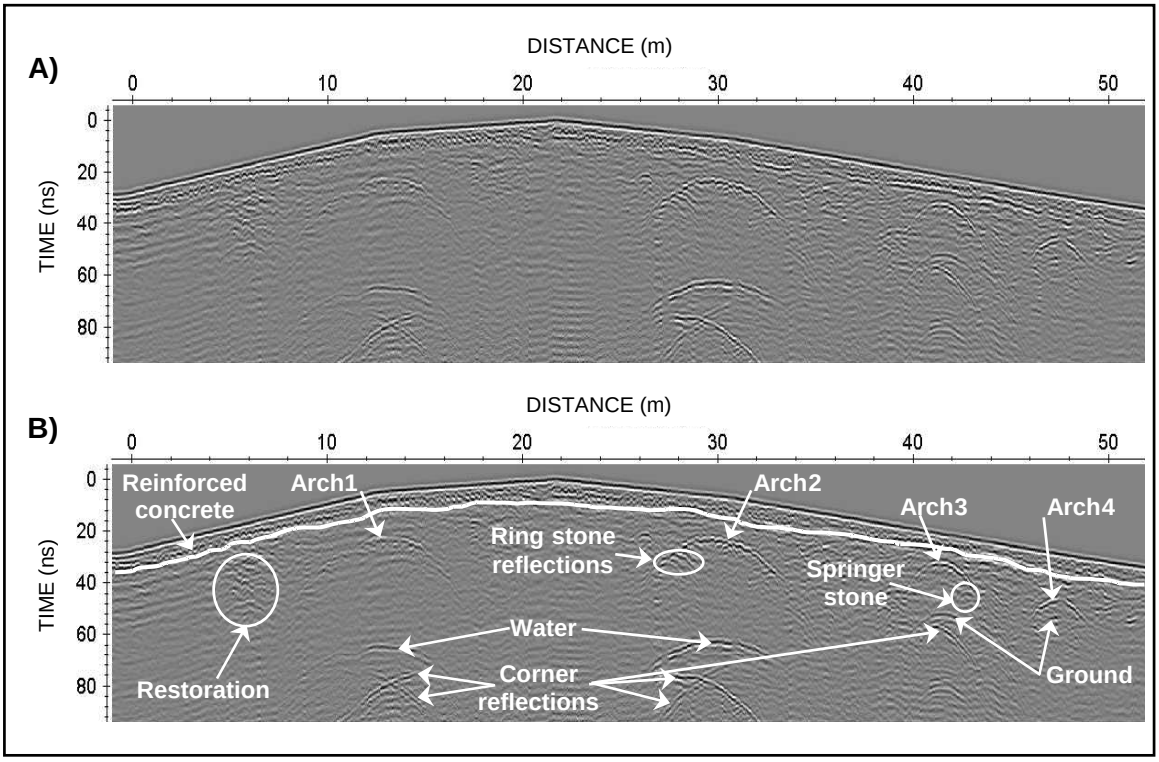

Figure 4.31- Radargram obtained with 500 MHz antenna in Carracedo bridge.
A) Processed data. B) Interpretation of the main reflectors detected.

An interesting reflection was identified and interpreted as a restoring intervention at the beginning of the radargram (Fig. 4.31B). It could be produced by the use of inhomogeneous building materials, which are different than the original ones, for the abutment restoration. Also, it was possible to observe the reinforced concrete layer employed for restoration along the bridge.

4.1.2.8.- MONFORTE BRIDGE

GENERAL DESCRIPTION

A 16th century masonry arch bridge over the Cabe river in the council town of Monforte de Lemos (Fig. 4.17). It has four segmental arches between 7.0 and 11.0 meters span and a slightly pointed profile as shown in Figure 4.32. Some authors have referenced that the original bridge had six arches (Alvarado et al., 1989).

Figure 4.32.- View of Monforte bridge from the downstream side.

GPR SURVEY

- **Methodology**

The common methodology developed in this work for surveying masonry arch bridges was carried out. The survey parameters used are given in Table 4.15. (x,y,z) data from a total station were employed to correct the radargrams acquired for topography.

Antenna	250 MHz	500 MHz
Number of Samples	515	678
Time Window	200 ns	100 ns
Trace Interval	0.02 m	0.02 m

Table 4.15.- GPR survey parameters.

- **Processing flow**

The processing sequence applied was: time-zero correction, dewow filtering, gain function, spatial filtering (subtracting average), band-pass filtering (butterworth) and topographic correction.

- **Results and interpretation**

The radargram acquired with the 250 MHz antenna (Fig. 4.33) showed the reflections caused by the arch-air and air-water interfaces and the typical corner reflections generated in this kind of arches (Martinaud et al., 2004). Six big hyperbolic reflections were easily identified, although this bridge has only four visible arches (Fig. 4.32). These two unexpected reflections could be interpreted as hidden arches (Fig. 4.33B) according to the historical references (Alvarado et al., 1989). Other relevant structural reflections

were the ring stone reflections produced in arches due to their internal staircase shape and the springer stone reflections due to their bigger size in relation to the other ring stones that compose the arch (Durán, 2005). Also, it was possible to distinguish a reflection along the bridge mentioned in the interpreted radargram as a stone layer (Fig. 4.33B). This effect is probably caused by a possible restoration. Monforte bridge could be emptied and filled for backing materials which are different than the original ones.

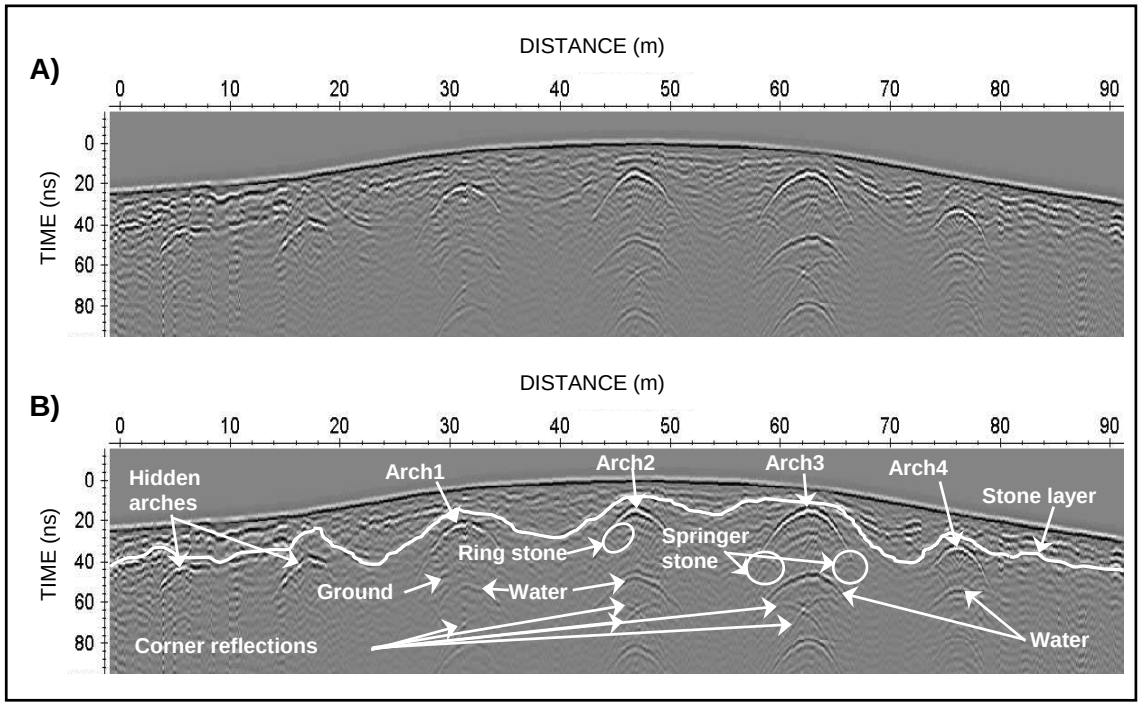

Figure 4.33.- Radargram obtained with 250MHz antenna in Monforte bridge.
A) Processed data. B) Interpretation of the main reflectors detected.

4.1.3.- OURENSE

4.1.3.1.- Bibei Bridge (Trives-Quiroga). CASE STUDY 4.2.3.

4.1.3.2.- Navea Bridge (Trives).

4.1.3.3.- Vilariñofrío Bridge (Montederramo).

4.1.3.4.- Brués Bridge (Boborás).

4.1.3.5.- San Clodio Bridge (Leiro).

4.1.3.6.- Molgas Bridge (Baño de Molgas).

4.1.3.7.- Loña Bridge (Ourense).

4.1.3.8.- Vilanova Bridge (Allariz).

4.1.3.9.- Freixo Bridge (Cartelle-Celanova).

4.1.3.10.- A Cigarrosa Bridge (Petín-A Rúa).

4.1.3.11.- Ourense Bridge (Ourense).

Figure 4.34.- Surveyed bridges distribution.

4.1.3.1.- BIBEI BRIDGE

GENERAL DESCRIPTION

A roman bridge over the Bibei river among Trives and Quiroga councils (Fig. 4.34). It presents three barrel arches of 6.09 – 18.51 – 8.77 meters span (Fig. 4.35).

Figure 4.35.- View of Bibei bridge from the upstream side.

Historical references inform about a possible restoration of the first arch from the left margin to the right margin in the upstream side in the 19th century (Durán, 2005). In addition, the pathway was filled to get a horizontal profile.

GPR SURVEY

- **Methodology**

Bibei bridge was surveyed following the common methodology proposed with the survey parameters shown in Table 4.16.

Antenna	250 MHz	500 MHz
Number of Samples	567	683
Time Window	220 ns	100 ns
Trace Interval	0.02 m	0.02 m

Table 4.16.- GPR survey parameters.

- **Processing flow**

The processing sequence applied was: time-zero correction, dewow filtering, gain function, spatial filtering (subtracting average) and band-pass filtering (butterworth).

- **Results and interpretation**

Observing the processed radargram acquired with the 250 MHz antenna (Fig. 4.36), it was possible to identify the reflections from the arch-air, air-water and air-ground interfaces , as well as the typical corner reflections generated in this kind of arches (Martinaud et al., 2004). Another interesting reflection was the one just above the arches probably caused by a pathway restoration. Bibei bridge could be emptied and consequently filled for different filling materials than the original ones. This event is named in the interpreted radargram as a stone layer (Fig. 4.36B). Moreover, the supposed ancient profile of this bridge was detected for each margin of the bridge which can ratify the restoration task for pathway leveling carried out in order to get a horizontal profile as mentioned in the specialized bibliography (Durán, 2005). Finally, other relevant information distinguished was the ring stone thickness of the second and third arches (Fig. 4.36B).

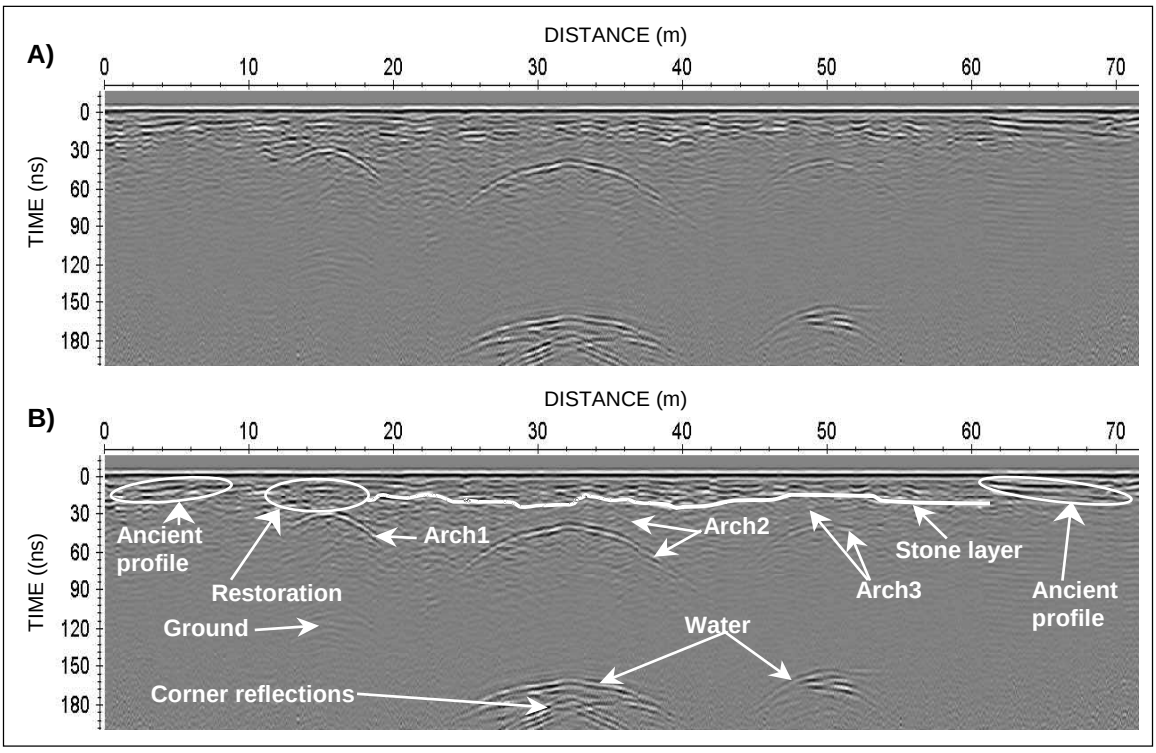

Figure 4.36.- Radargram obtained with 250 MHz antenna in Bibei bridge.
A) Processed data. B) Interpretation of the main reflectors detected.

Remark: An extended analysis of Bibei bridge is described in subchapter 4.2.3.

4.1.3.2.- NAVEA BRIDGE

GENERAL DESCRIPTION

A Roman arch bridge 46.5 m long over the Navea river close to the council of Trives (Fig. 4.34). It has a single arch 18.15 meters span, a slightly pointed profile and 3.9 m wide (Fig. 4.37).

Figure 4.37.- View of Navea bridge from the downstream side.

Navea bridge was restored in the medieval period. The arch was rebuilt. Beside that, its flagstone path was restored in 1986 (Durán, 2005).

GPR SURVEY

- **Methodology**

The common methodology developed for surveying masonry arch bridges was carried out. The survey parameters used are given in Table 4.17. (x,y,z) data from a total station were employed to correct the radargrams acquired for topography.

Antenna	**250 MHz**	**500 MHz**
Number of Samples	566	682
Time Window	220 ns	100 ns
Trace Interval	0.02 m	0.02 m

Table 4.17.- GPR survey parameters.

- **Processing flow**

The processing sequence applied was: time-zero correction, dewow filtering, gain

function, spatial filtering (subtracting average), band-pass filtering (butterworth) and topographic correction.

- **Results and interpretation**

Observing the processed radargram acquired with 250 MHz antenna (Fig. 4.38), it was possible to identify the reflections owing to the arch-air and air-water interfaces. Furthermore, the corner reflections generated in this kind of arches were distinguished (Fig. 4.38B). The radargram showed a low signal attenuation probably caused by the presence of some modern building material such as geotextile fabrics employed in the pathway restoration mentioned.

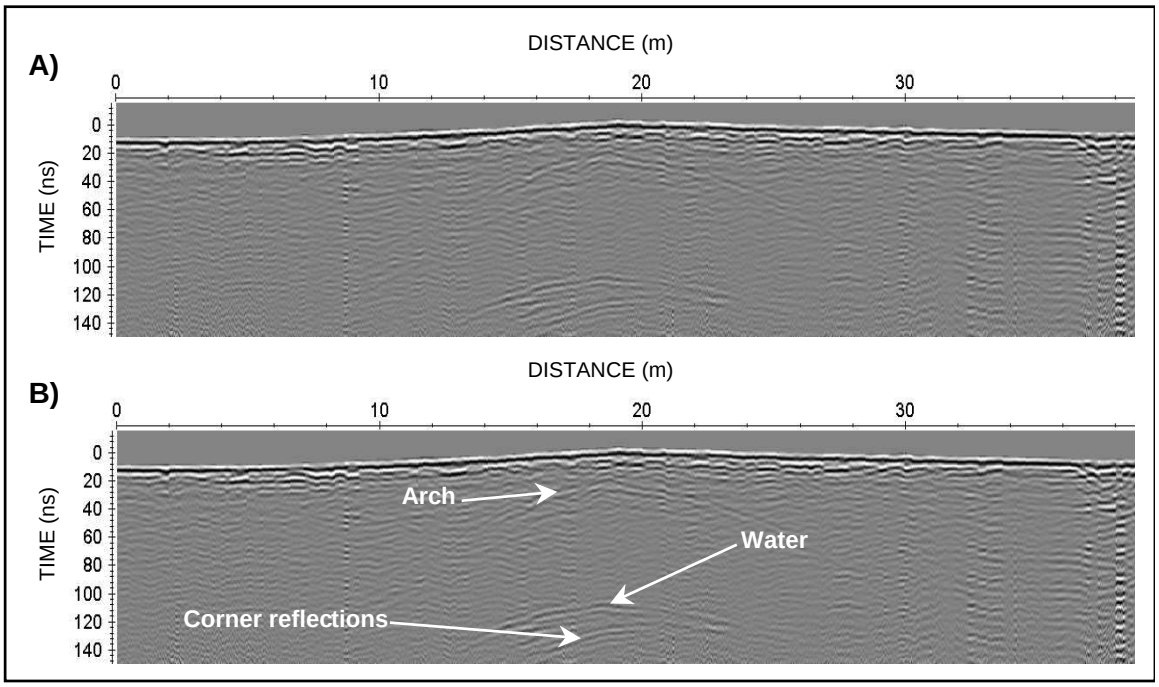

Figure 4.38.- Radargram obtained with 250 MHz antenna in Navea bridge.
A) Processed data. B) Interpretation of the main reflectors detected.

4.1.3.3.- VILARIÑOFRIO BRIDGE

GENERAL DESCRIPTION

A 18th century bridge located in the town council of Montederramo through Covas river (Fig. 4.34). It has three barrel arches of 3.35 – 5.20 – 2.57 meters span and a slightly pointed profile (Fig. 4.39).

Figure 4.39.- View of Vilariñofrío bridge from the upstream side.

GPR SURVEY

- **Methodology**

The common methodology developed for surveying masonry arch bridges was carried out. The survey parameters used are given in Table 4.18. (x,y,z) data from a total station were employed to correct the radargrams acquired for topography.

Antenna	250 MHz	500 MHz
Number of Samples	516	682
Time Window	200 ns	100 ns
Trace Interval	0.02 m	0.02 m

Table 4.18.- GPR survey parameters.

- **Processing flow**

The processing sequence applied was: time-zero correction, dewow filtering, gain function, spatial filtering (subtracting average) and topographic correction.

- **Results and interpretation**

In Figure 4.40B, the reflections owing to the arch-air and air-water interfaces were interpreted as well as the reflections from the foundation of the first pier upstream.

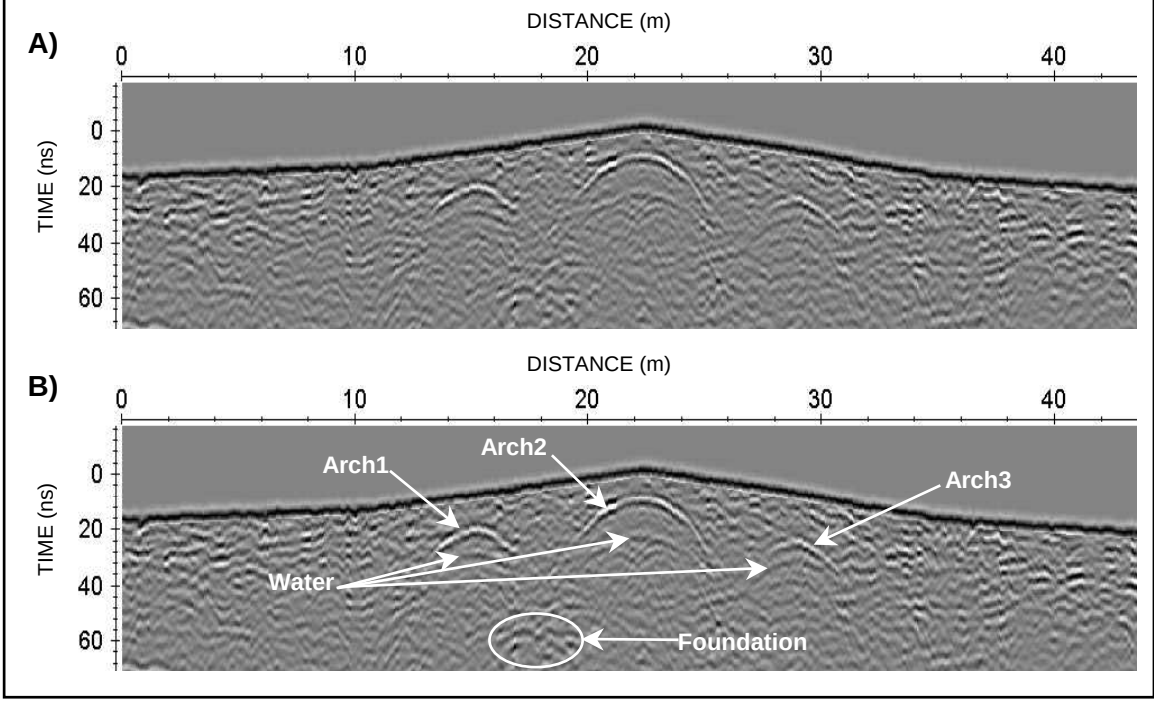

Figure 4.40.- Radargram obtained with 250 MHz antenna in Vilariñofrío bridge.
A) Processed data. B) Interpretation of the main reflectors detected.

4.1.3.4.- BRUES BRIDGE

GENERAL DESCRIPTION

Medieval arch bridge over the Viñao river in the Boborás council (Fig. 4.34). Observing Figure 4.41, this bridge has two gothic arches of 7.2 m span, a slightly pointed profile and a flagstone path.

Figure 4.41.- View of Brues bridge from the upstream side.

GPR SURVEY

- **Methodology**

The common methodology proposed was employed for surveying this bridge with the survey parameters mentioned in Table 4.19. The radargrams obtained were corrected for topography with (x,y,z) data from a total station.

Antenna	250 MHz	500 MHz
Number of Samples	512	678
Time Window	200 ns	100 ns
Trace Interval	0.02 m	0.02

Table 4.19.- GPR survey parameters.

- **Processing flow**

The processing sequence applied was: time-zero correction, dewow filtering, gain function, spatial filtering (subtracting average) and topographic correction.

- **Results and interpretation**

Observing the processed radargram obtained (Fig. 4.42A), the usual reflections due to the arch-air and air-water interfaces were identified. Also the reflection caused by the pier foundation was interpreted (Fig. 4.42B).

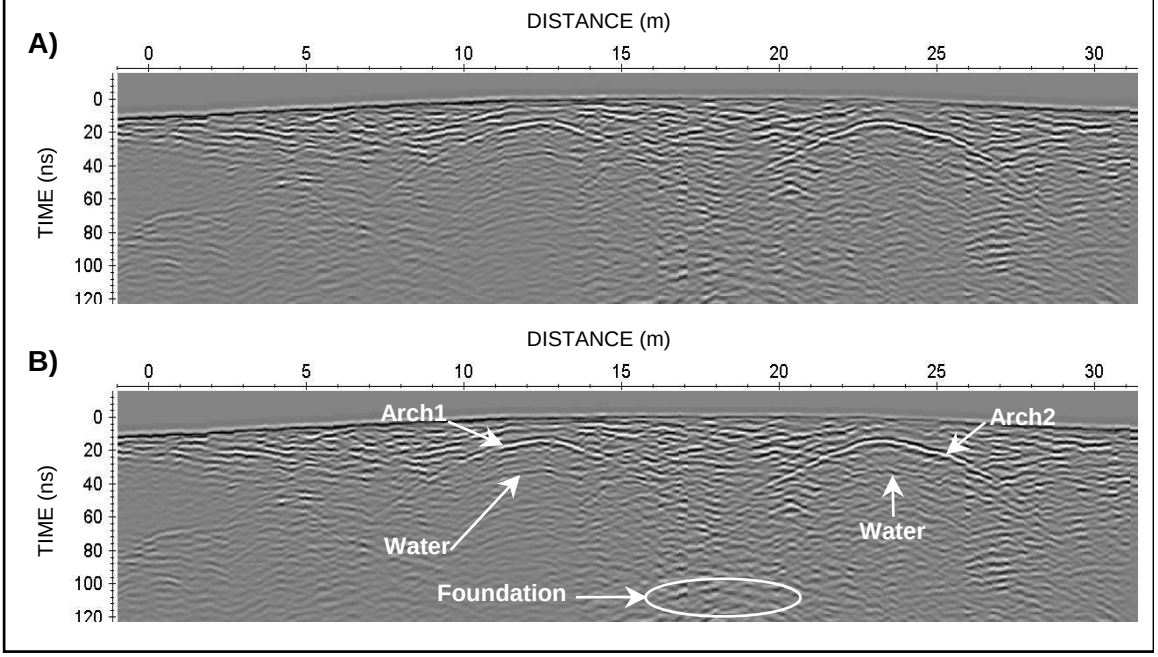

Figure 4.42.- Radargram obtained with 250 MHz antenna in Brues bridge.
A) Processed data. B) Interpretation of the main reflectors detected.

4.1.3.5.- SAN CLODIO BRIDGE

GENERAL DESCRIPTION

A 15th century masonry arch bridge in Leiro across the Avia river (Fig. 4.34). This brigde presents three arches of 10.75 – 18.98 – 13.50 m span and a slightly pointed profile (Fig. 4.43). It suffered several restorations over the time. Like this, its stonework was restored in the 18th century. In addition, its flagstone path was rebuilt in 1978 (Alvarado et al., 1989).

Figure 4.43.- View of San Clodio bridge from the upstream side.

GPR SURVEY

- **Methodology**

The common methodology was employed following the survey parameters mentioned in Table 4.20. The radargrams acquired were corrected for topography by using (x,y,z) data recorded by means of a total station.

Antenna	250 MHz	500 MHz
Number of Samples	567	677
Time Window	220 ns	100 ns
Trace Interval	0.02 m	0.02 m

Table 4.20.- GPR survey parameters.

- **Processing flow**

The processing sequence applied was: time-zero correction, dewow filtering, gain function, spatial filtering (subtracting average), band-pass filtering (butterworth) and topographic correction.

- **Results and interpretation**

In the processed radargram, the reflections generated in the arch-air and air-water interfaces were identified (Fig. 4.44B). Also, it was possible to observe the typical corner reflections produced in this kind of arches (Martinaud et al., 2004) as well as the ones from the foundations of both piers.

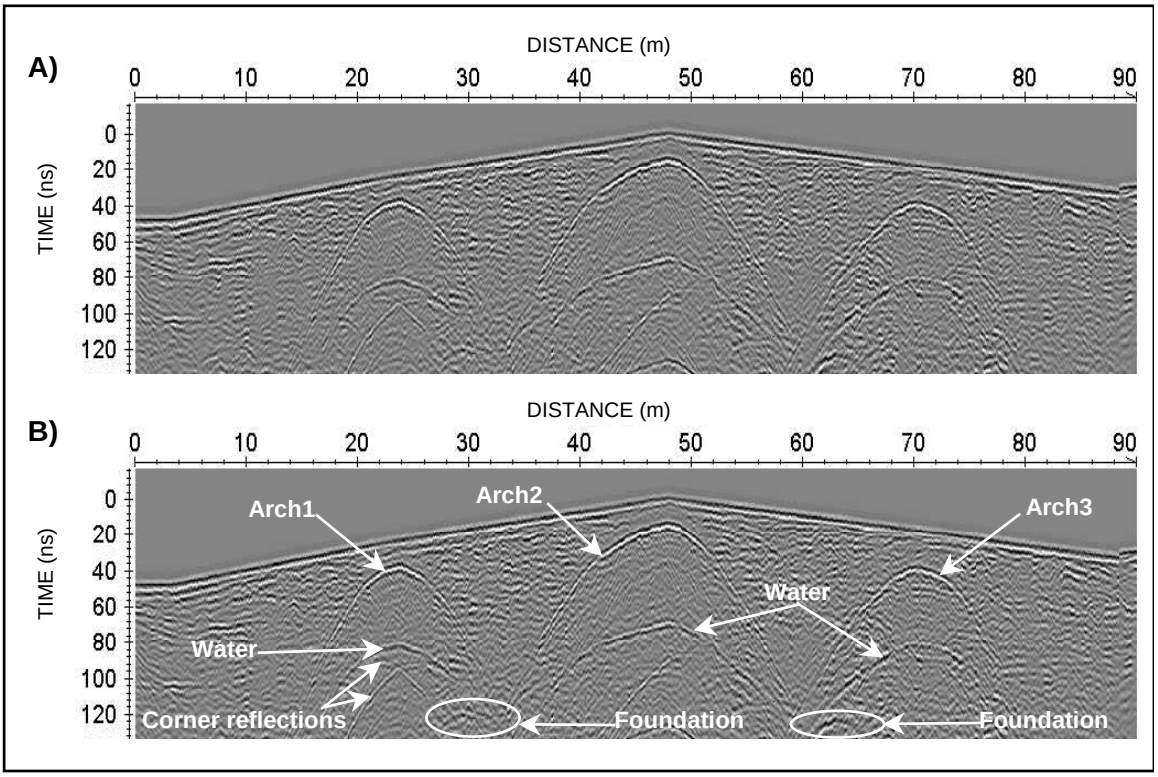

Figure 4.44.- Radargram obtained with 250 MHz antenna in San Clodio bridge.
A) Processed data. B) Interpretation of the main reflectors detected.

4.1.3.6.- MOLGAS BRIDGE

GENERAL DESCRIPTION

A Roman bridge across the Arnoia river in the town council of Baño de Molgas (Fig. 4.34). It is a single span arch bridge of 10.7 m (Fig. 4.45) and it has four spillways in the right margin from the upstream side. Its profile is slightly pointed and it has a flagstone path over 3.5 m wide restored in 1985. In this intervention, the vault was also restored (Durán, 2005).

Figure 4.45.- View of Molgas bridge from the upstream side.

GPR SURVEY

- **Methodology**

The common methodology proposed was employed for surveying this bridge with the survey parameters mentioned in Table 4.21. The radargrams acquired were corrected for topography by using (x,y,z) data recorded by means of a total station.

Antenna	250 MHz	500 MHz
Number of Samples	516	678
Time Window	200 ns	100 ns
Trace Interval	0.02 m	0.02 m

Table 4.21.- GPR survey parameters.

- **Processing flow**

The processing sequence applied was: time-zero correction, dewow filtering, gain function, spatial filtering (subtracting average) and topographic correction.

- **Results and interpretation**

Observing the processed radargram obtained (Fig. 4.46A), the usual reflections produced in the arch-air and air-water interfaces were interpreted. It was very difficult to identify

each spillway individually, even though a confluence of reflections from 21 to 23 meters were appreciated (Fig. 4.46B). These reflections could be generated by the presence of spillways in this location.

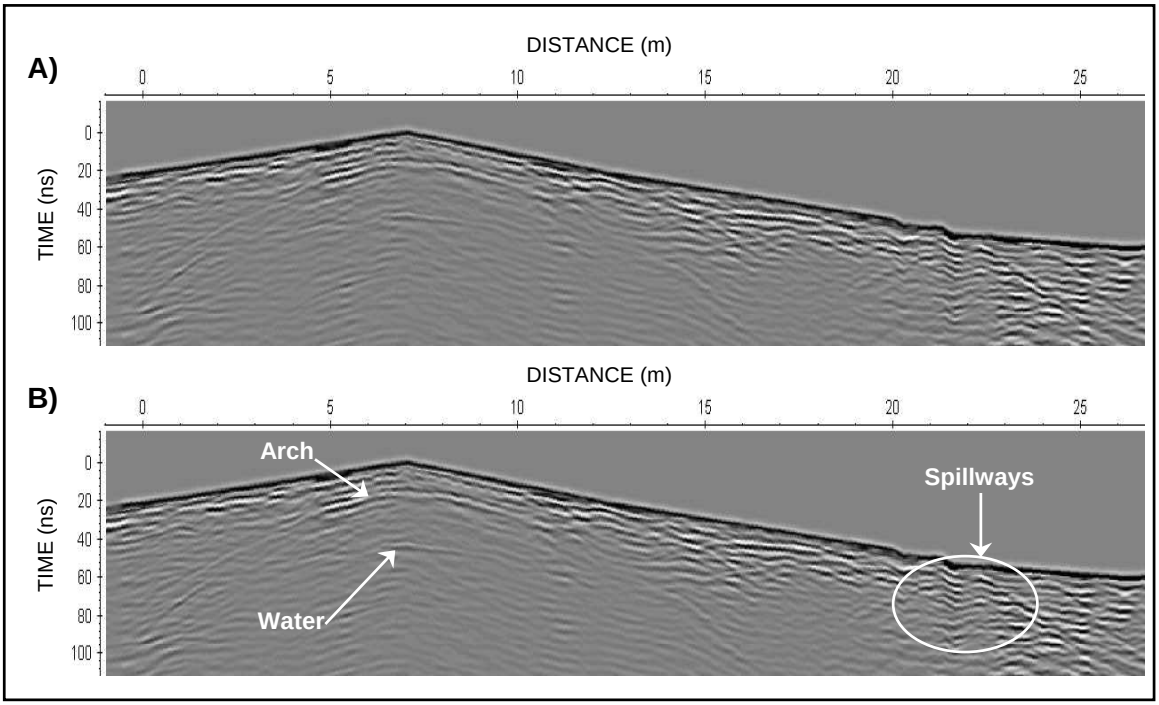

Figure 4.46.- Radargram obtained with 250 MHz antenna in Molgas bridge.
A) Processed data. B) Interpretation of the main reflectors detected.

4.1.3.7.- LOÑA BRIDGE

GENERAL DESCRIPTION

A 13th century masonry arch bridge over the Loña river in the council town of Ourense (Fig. 4.34). It has a single gothic arch 12.9 m span and a slightly pointed profile (Fig. 4.47).

Figure 4.47.- View of Loña bridge from the upstream side.

The last restoration made in Loña bridge dating back to 1985. In this occasion, the wing walls were rebuilt and the flagstone path was replaced. With this intervention, the aerial electrical installation was channeled under the new one and the paviment was strengthened employing a metallic joint and reinforced concrete (Alvarado et al., 1989).

GPR SURVEY

- **Methodology**

Loña bridge was surveyed following the common methodology proposed although the 500 MHz antenna was not used in this case. The survey parameters employed are mentioned in Table 4.22. The radargrams acquired were corrected for topography by using (x,y,z) data recorded by means of a total station.

Antenna	**250 MHz**
Number of Samples	669
Time Window	260 ns
Trace Interval	0.05 m

Table 4.22.- GPR survey parameters.

- **Processing flow**

The processing sequence applied was: time-zero correction, dewow filtering, gain function, spatial filtering (subtracting average) and topographic correction.

- **Results and interpretation**

The reflections from the arch-air and air-water interfaces were interpreted (Fig. 4.48A). These reflections were not easily identified due to signal attenuation. This effect is probably due to the use of a metallic joint in reinforced concrete for restoration (Alvarado et al., 1989). Similar results were observed by Lorenzo (1996). Also, it was possible to observe the reflections produced by two sewers placed in the bridge pathway (Fig. 4.48B).

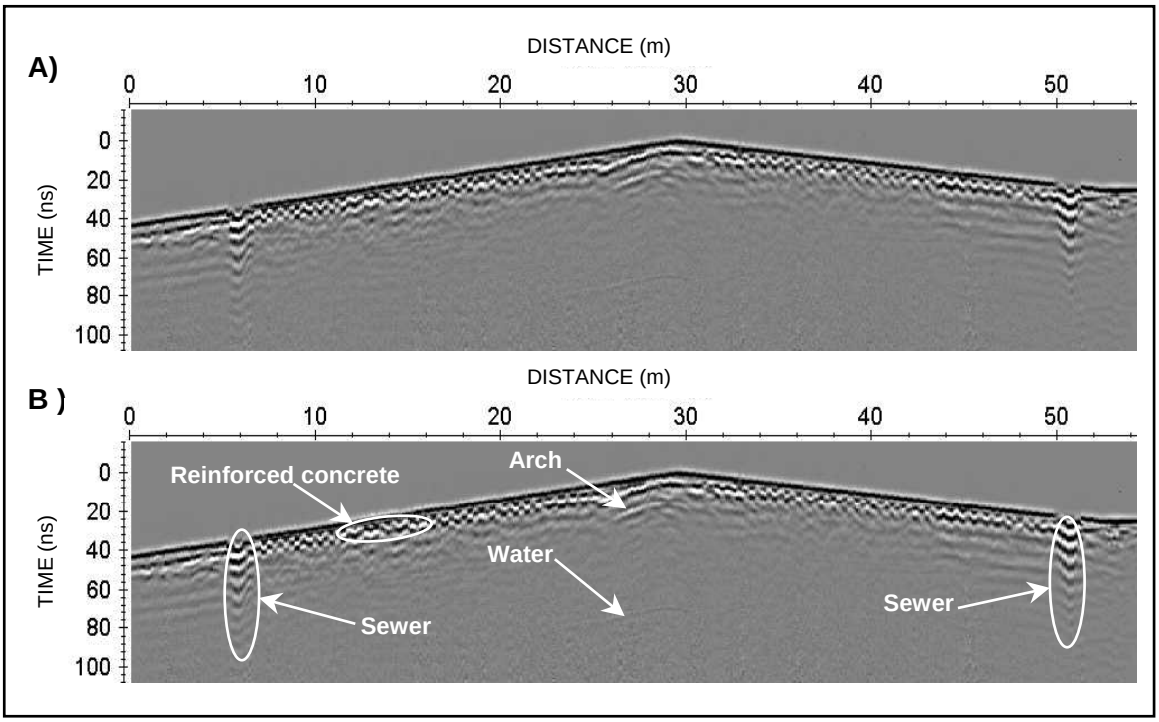

Figure 4.48.- Radargram obtained with 250 MHz antenna in Loña bridge.
A) Processed data. B) Interpretation of the main reflectors detected.

4.1.3.8.- VILANOVA BRIDGE

GENERAL DESCRIPTION

A 14th century arch bridge over the Arnoia river in the council town of Allariz (Fig. 4.34). It has two barrel arches about 11.3 m span and a slightly pointed profile (Fig. 4.49). Vilanova bridge was rebuilt several times (Alvarado et al., 1989).

Figure 4.49.- View of Vilanova bridge from the upstream side.

GPR SURVEY

- **Methodology**

The common methodology proposed was employed for surveying the Vilanova bridge with the survey parameters mentioned in Table 4.23. The radargrams acquired were corrected for topography by using (x,y,z) data recorded by means of a total station.

Antenna	250 MHz	500 MHz
Number of Samples	568	677
Time Window	220 ns	100 ns
Trace Interval	0.02 m	0.02 m

Table 4.23.- GPR survey parameters.

- **Processing flow**

The processing sequence applied was: time-zero correction, dewow filtering, gain function, spatial filtering (subtracting average), band-pass filtering (butterworth) and topographic correction.

- **Results and interpretation**

The best results were recorded with the 250 MHz antenna, where the reflections from the arch-air and air-water interfaces as well as the corner reflections generated were

identified (Fig. 4.50B).

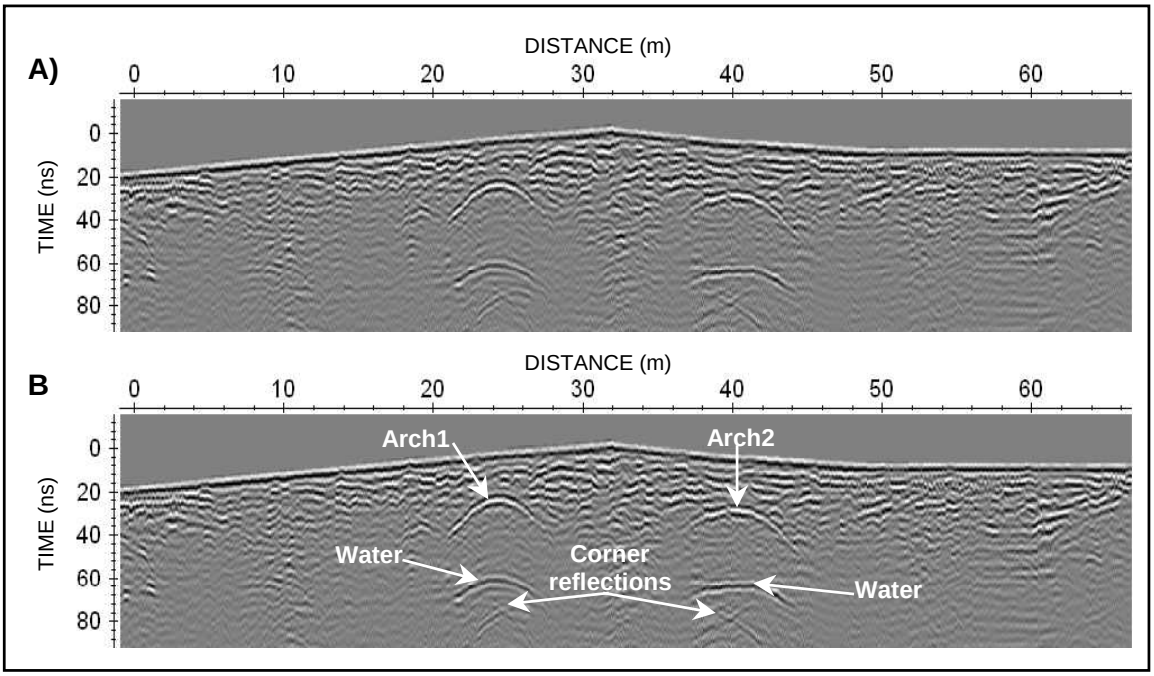

Figure 4.50.- Radargram obtained with 250 MHz antenna in Vilanova bridge.
A) Processed data. B) Interpretation of the main reflectors detected.

4.1.3.9.- FREIXO BRIDGE

GENERAL DESCRIPTION

Roman bridge over the Arnoia river between the councils of Cartelle and Celanova (Fig. 4.34). It has four barrel arches of 4.7 – 7.7 – 7.7 – 4.7 meters span (Fig. 4.51). This bridge was restored in 1988 (Durán, 2005).

Figure 4.51.- View of Freixo bridge from the upstream side.

GPR SURVEY

- **Methodology**

The common methodology developed for surveying masonry arch bridges was carried out. The survey parameters used are given in Table 4.24.

Antenna	250 MHz	500 MHz
Number of Samples	579	677
Time Window	225 ns	100 ns
Trace Interval	0.02 m	0.02 m

Table 4.24.- GPR survey parameters.

- **Processing flow**

The processing sequence applied was: time-zero correction, dewow filtering, gain function, spatial filtering (subtracting average) and band-pass filtering (butterworth).

- **Results and interpretation**

Observing the processed radargram obtained with the 250 MHz antenna (Fig. 4.52A), it was possible to identify the reflections caused by the arch-air and air-water interfaces and the typical corner reflections generated in this kind of arches (Martinaud et al., 2004).

Other interesting structural reflection was the springer stone reflection observed in the first arch due to their bigger size in relation to the other ring stones that compose the arch ring (Durán, 2005). Also, the ring stone thicknesses were provide from the GPR data acquired (Fig. 4.52B).

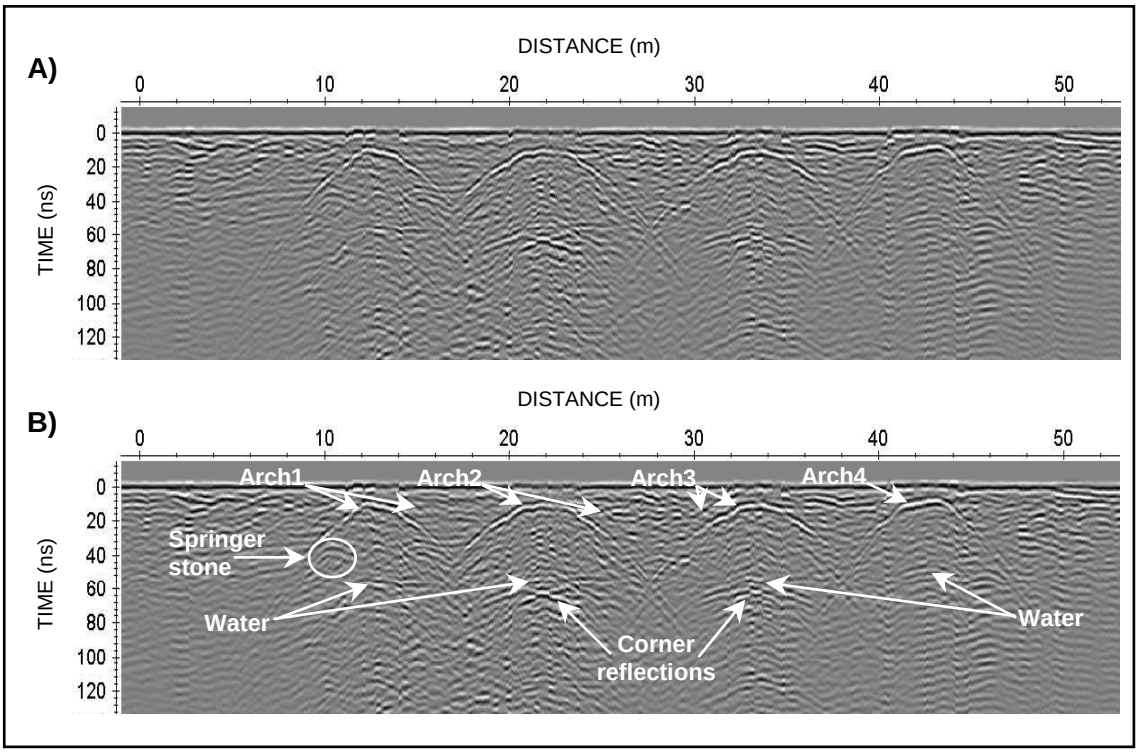

Figure 4.52.- Radargram obtained with 250 MHz antenna in Freixo bridge.
A) Processed data. B) Interpretation of the main reflectors detected.

4.1.3.10.- A CIGARROSA BRIDGE

GENERAL DESCRIPTION

Roman bridge over the Sil river between the councils of Petín and A Rúa (Fig. 4.34). It has five arches of 10.4 – 20.3 – 4.4 – 10.7 – 9.9 meters span (Fig. 4.54).

Figure 4.54.- View of A Cigarrosa bridge from the downstream side.

This bridge was restored in several circumstances over the time. The presence of gothic arches in its structure indicates a reconstruction in the 13th or 14th century. However, the geometry of the main arch means a later reconstruction.
Furthermore, a consolidation intervention was carried out in the first arch from the right margin in 1956 and the vault was covered with concrete (Durán, 2005).

GPR SURVEY

- **Methodology**

A Cigarrosa bridge was surveyed following the common methodology with the survey parameters shown in Table 4.25. The radargrams obtained were corrected for topography by using (x,y,z) data recorded acquired from a total station.

Antenna	250 MHz	500 MHz
Number of Samples	567	678
Time Window	220 ns	100 ns
Trace Interval	0.02	0.02 m

Table 4.25.- GPR survey parameters.

- **Processing flow**

The processing sequence applied was: time-zero correction, dewow filtering, gain function, spatial filtering (subtracting average), band-pass filtering (butterworth) and topographic correction.

- **Results and interpretation**

Observing the processed radargram obtained (Fig. 4.55A), only the reflections due to the

arch-air and air-water interfaces were easily identified for the second arch. These reflections could be attenuated in the other ones probably caused by the use of filling materials such as soil-cement for the restoration in the middle of the 20th century (Durán, 2005). This event is mentioned in the interpreted radargram as a soil-cement layer (Fig. 4.55B). The characteristics assumed for this material were mentioned in San Alberte bridge. A Similar signal response was observed by Lorenzo (1996).

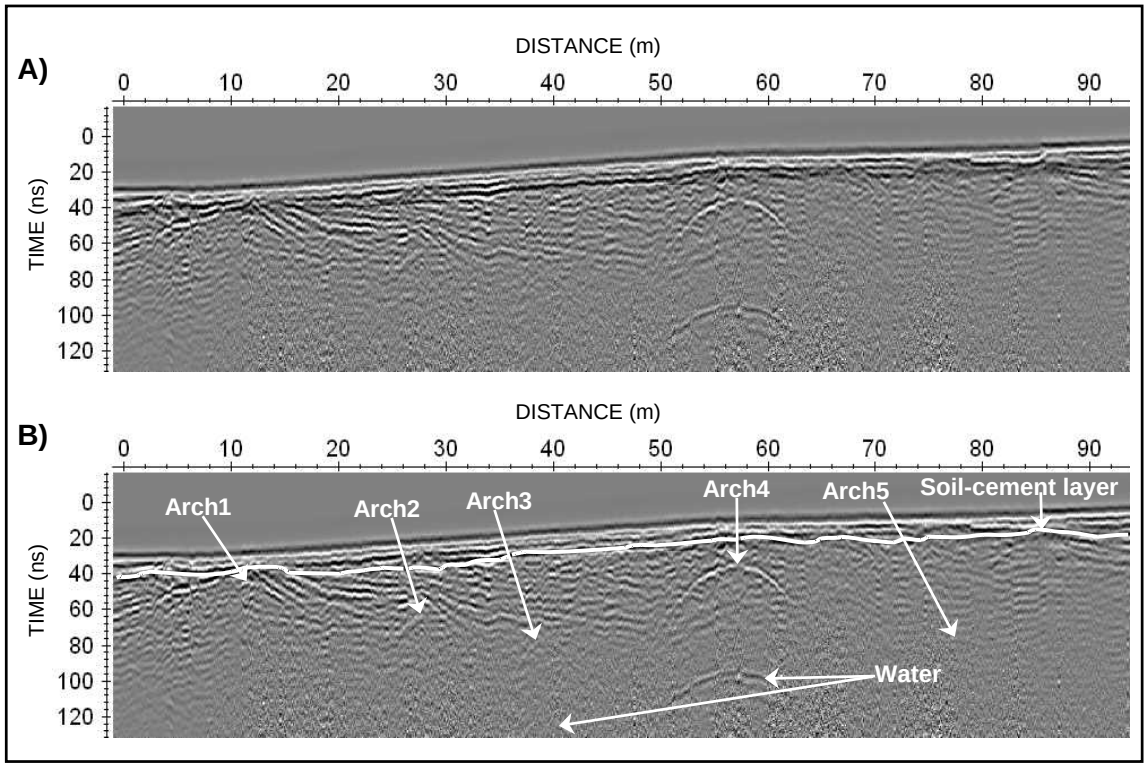

Figure 4.55.- Radargram obtained with 250 MHz antenna in A Cigarrosa bridge.
A) Processed data. B) Interpretation of the main reflectors detected.

4.1.3.11.- OURENSE BRIDGE

GENERAL DESCRIPTION

Roman bridge in the city council of Ourense (Fig. 4.34), across the Miño river. It has seven arches from 8.4 to 38 meters span (Fig. 4.56). This bridge was restored and/or rebuilt in several circumstances throughout the time (Durán, 2005).

Figure 4.56.- View of Ourense bridge from the downstream side.

GPR SURVEY

- **Methodology**

Ourense bridge was surveyed by the common methodology developed using the survey parameters shown in Table 4.26. The radargrams obtained were corrected for topography by using (x,y,z) data recorded acquired from a total station.

Antenna	250 MHz	500 MHz
Number of Samples	542	677
Time Window	210 ns	100 ns
Trace Interval	0.05 m	0.02 m

Table 4.26.- GPR survey parameters.

- **Processing flow**

The processing sequence applied was: time-zero correction, dewow filtering, gain function, spatial filtering (subtracting average), band-pass filtering (butterworth) and topographic correction.

- **Results and interpretation**

The radargram acquired with the 500 MHz antenna showed a severe GPR signal attenuation (Fig. 4.57) resulting in a non-identification of reflections from all arches of the bridge (Fig. 4.57B). This effect could be caused by the presence soil-cement used for backing in the a probable pathway restoration performed. This material was described before in San Alberte bridge. Similar results were observed by Lorenzo (1996).

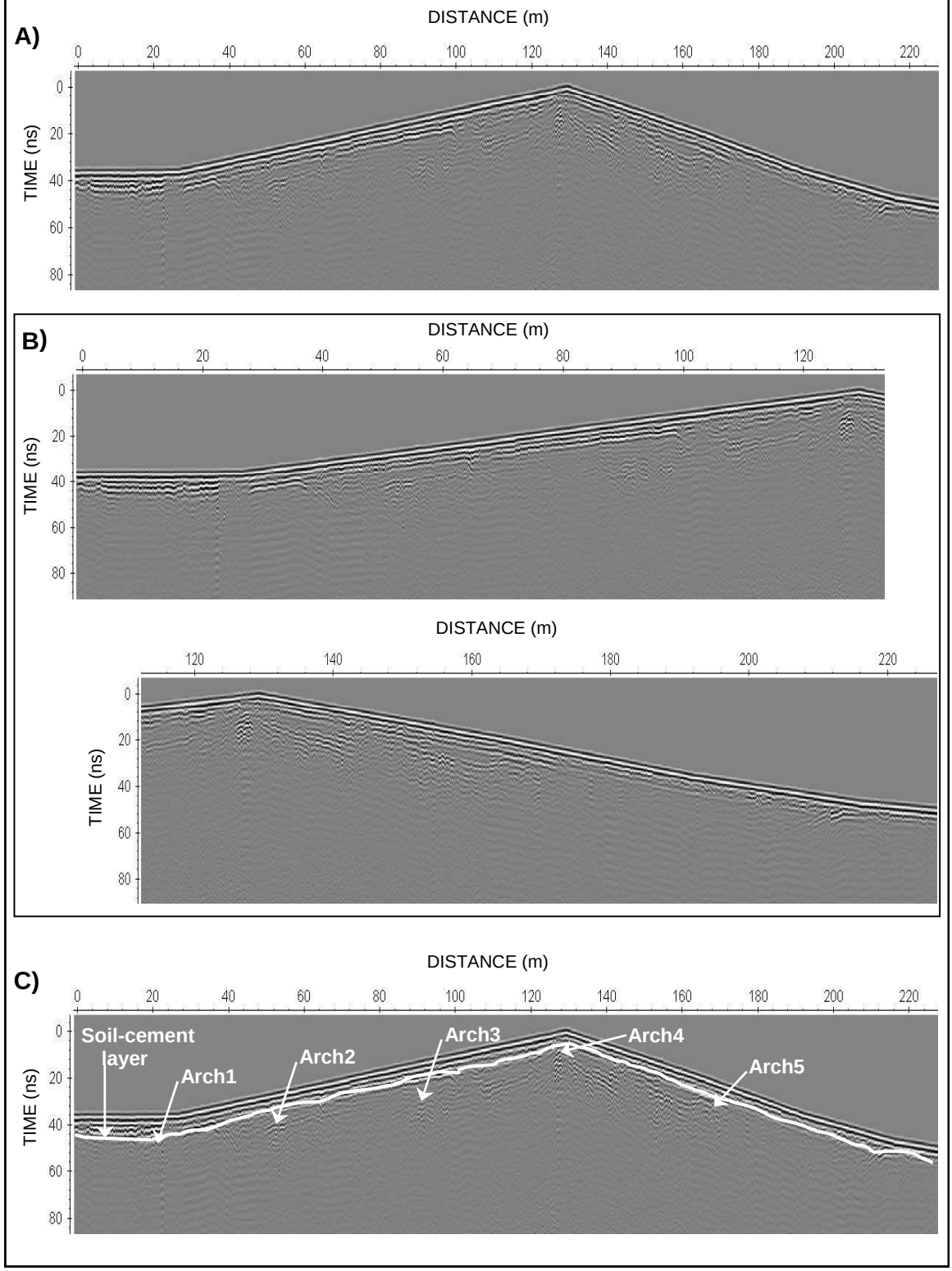

Figure 4.57.- Radargram obtained with 500 MHz antenna in Ourense bridge.
A) Processed data, B) Radargram in detail, and C) Interpretation of the main reflectors.

4.1.4.- PONTEVEDRA

4.1.4.1.- Bermaña Bridge (Caldas de Reis).

4.1.4.2.- Liñares Bridge (A Estrada).

4.1.4.3.- Carboeiro Bridge (Silleda-Vila de Cruces).

4.1.4.4.- Taboada Bridge (Lalín-Silleda).

4.1.4.5.- Das Partidas Bridge (Ponteareas).

4.1.4.6.- Areas Bridge (Ponteareas).

4.1.4.7.- Fillaboa Bridge (Salvaterra).

4.1.4.8.- Cernadela Bridge (Pontevedra).

4.1.4.9.- O Burgo Bridge (Pontevedra).

4.1.4.10.- San Antón Bridge (Cerdedo). CASE STUDY 4.2.1.

Figure 4.58.- Surveyed bridges distribution.

4.1.4.1.- BERMAÑA BRIDGE

GENERAL DESCRIPTION

It is a masonry arch bridge located in the village of Caldas de Reis over the river Bermaña (Fig. 4.58) dating back to the 13th century. It has three barrel arches between 4.0 and 4.8 m. span (Fig. 4.59) with a double slope flagstone path 3.9 m wide. This bridge was restored at the end of the 16th century (Alvarado et al., 1989).

Figure 4.59.- View of Bermaña bridge from the upstream side.

GPR SURVEY

- **Methodology**

Bermaña bridge was surveyed following the common methodology with the survey parameters shown in Table 4.27. The radargrams obtained were corrected for topography using (x, y, z) data acquired with a total station.

Antenna	250 MHz	500 MHz
Number of Samples	567	609
Time Window	220 ns	90 ns
Trace Interval	0.05 m	0.02 m

Table 4.27.- GPR survey parameters.

- **Processing flow**

The processing sequence applied was: time-zero correction, dewow filtering, gain function, spatial filtering (subtracting average), band-pass filtering (butterworth) and topographic correction.

- **Results and interpretation**

The radargram obtained with the 250 MHz antenna showed the usual reflections due to

the arch-air and air-water interfaces (Fig. 4.60A). Another relevant structural reflection was the one owing to the bigger size of the springer stone (Fig. 4.60B) in relation to the other ring stones that compose the arch (Durán, 2005).

The radargrams acquired with the 500 MHz antenna did not provide interesting additional information.

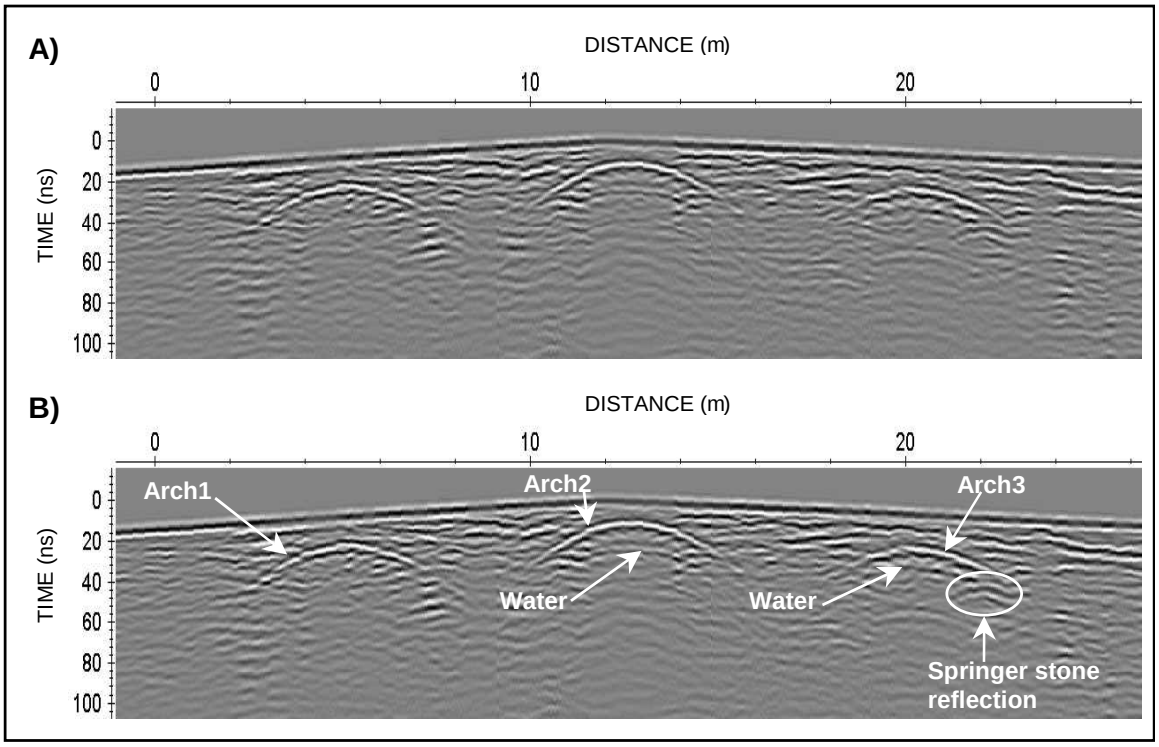

Figure 4.60.- Radargram obtained with 250 MHz antenna in Bermaña bridge. A) Processed data. B) Interpretation of the main reflectors detected.

4.1.4.2.- LIÑARES BRIDGE

GENERAL DESCRIPTION

A single span arch bridge built between the 17-18th centuries through Liñares river in the council of A Estrada (Fig. 4.58). It presents a barrel arch 9.5 m span and a pointed profile (Fig. 4.61).

Figure 4.61.- View of Liñares bridge from the upstream side.

GPR SURVEY

- **Methodology**

The common methodology developed in this work for surveying masonry arch bridges was assumed. The survey parameters used are given in Table 4.28. (x,y,z) data from a total station were employed to correct the radargrams acquired for topography.

Antenna	250 MHz	500 MHz
Number of Samples	516	637
Time Window	200 ns	120 ns
Trace Interval	0.05 m	0.02 m

Table 4.28.- GPR survey parameters.

- **Processing flow**

The processing sequence applied was: time-zero correction, dewow filtering, gain function, spatial filtering (subtracting average) and topographic correction.

- **Results and interpretation**

The best results were recorded with the 250 MHz antenna, where it could be identified the reflections from the arch-air and air-water interfaces as well as the reflections due

to the bridge foundations (Fig. 4.62).

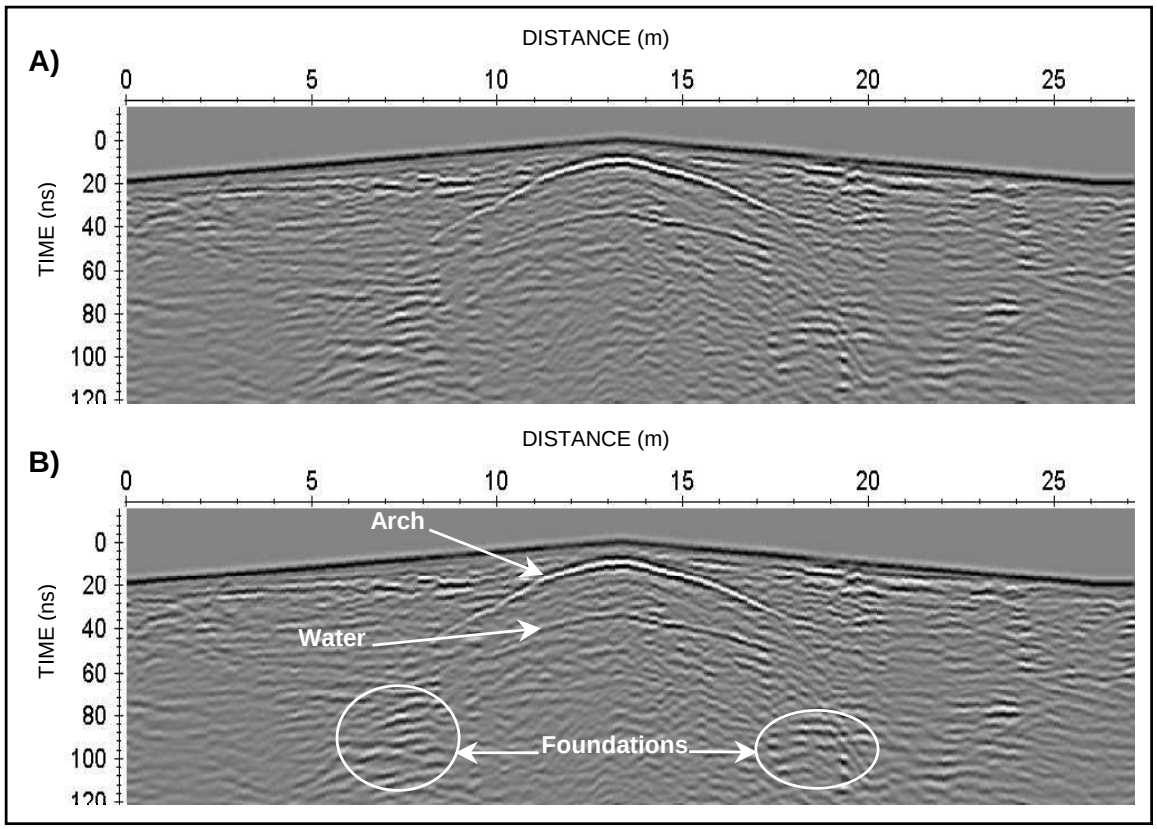

Figure 4.62.- Radargram obtained with 250 MHz antenna in Liñares bridge.
A) Processed data. B) Interpretation of the main reflectors detected.

4.1.4.3.- CARBOEIRO BRIDGE

GENERAL DESCRIPTION

The Carboeiro bridge was built in the 16th century over the Deza river among Silleda and Vila de Cruces councils (Fig. 4.58). It is a single arch bridge of 12.0 m span with a slightly pointed profile (Fig. 4.63). This bridge was restored at the end of the 20th century.

Figure 4.63.- View of Carboeiro bridge from the downstream side.

GPR SURVEY

- **Methodology**

The common methodology proposed was employed for surveying the Carboeiro bridge with the survey parameters mentioned in Table 4.29. The radargrams acquired were corrected for topography by using (x,y,z) data recorded by means of a total station.

Antenna	250 MHz	500 MHz
Number of Samples	644	683
Time Window	250 ns	100 ns
Trace Interval	0.05 m	0.02 m

Table 4.29.- GPR survey parameters.

- **Processing flow**

The processing sequence applied was: time-zero correction, dewow filtering, gain function, spatial filtering (subtracting average) and topographic correction.

- **Results and interpretation**

Besides the usual reflections from the arch-air and air-water interfaces, the typical corner

reflections generated in this kind of arches (Martinaud et al., 2004) were observed in the radargram acquired with the 250 MHz antenna (Fig. 4.64B).

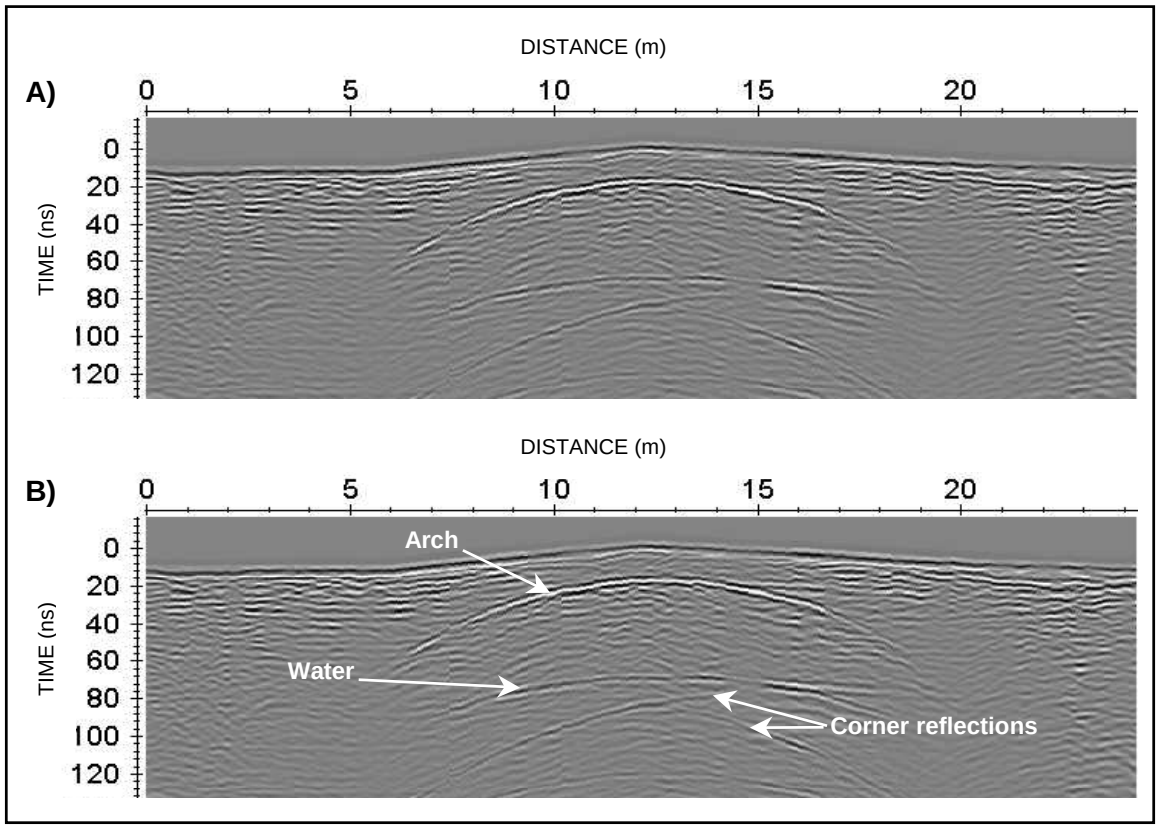

Figure 4.64.- Radargram obtained with 250 MHz antenna in Carboeiro bridge.
A) Processed data. B) Interpretation of the main reflectors detected.

4.1.4.4.- TABOADA BRIDGE

GENERAL DESCRIPTION

A 10th century masonry bridge located between Lalín and Silleda councils through the Deza river (Fig. 4.58). Observing Figure 4.65, this bridge presents a pointed arch of 10.5 m span and a double slope granite flagstone path.

Figure 4.65.- View of Taboada bridge from the downstream side.

GPR SURVEY

- **Methodology**

The common methodology proposed was employed for surveying this bridge with the survey parameters mentioned in Table 4.30. The radargrams acquired was corrected for topography by using (x,y,z) data recorded by means of a total station.

Antenna	250 MHz	500 MHz
Number of Samples	644	677
Time Window	250 ns	100 ns
Trace Interval	0.050 m	0.025 m

Table 4.30.- GPR survey parameters.

- **Processing flow**

The processing sequence applied was: time-zero correction, dewow filtering, gain function, spatial filtering (subtracting average) and topographic correction.

- **Results and interpretation**

Observing the processed radargram obtained (Fig. 4.66A), only the usual reflections due

to the arch-air and air-water interfaces were distinguished.

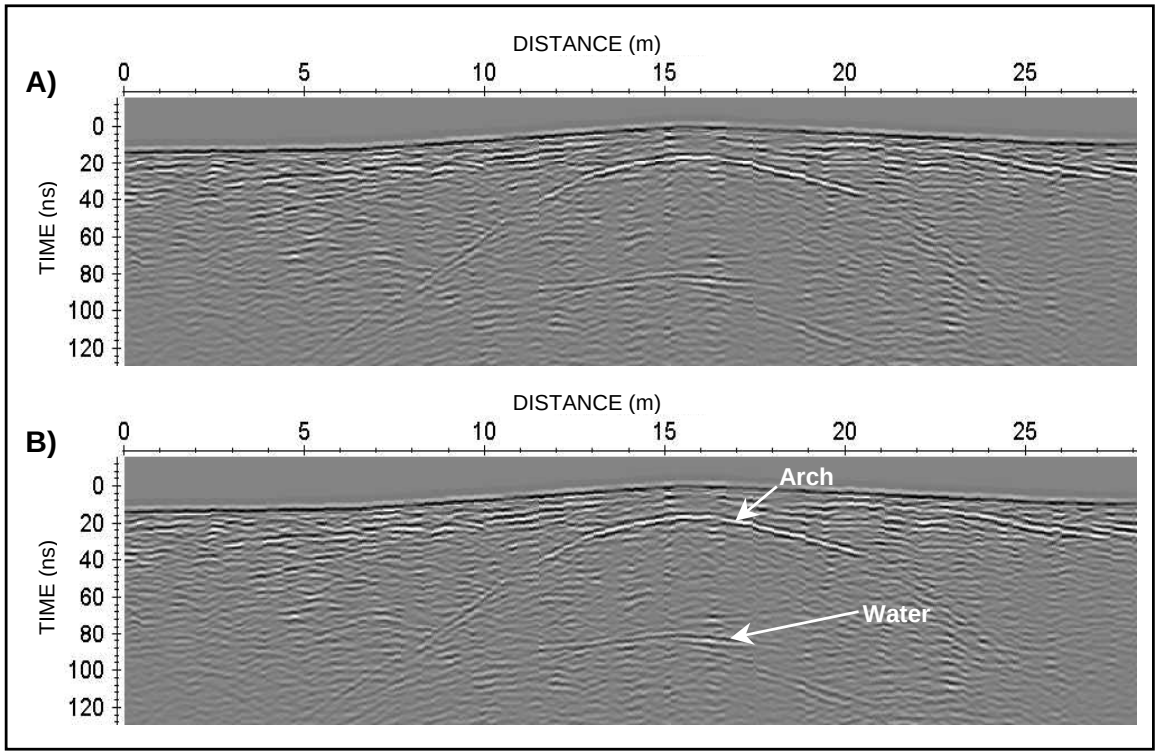

Figure 4.66.- Radargram obtained with 250 MHz antenna in Taboada bridge.
A) Processed data. B) Interpretation of the main reflectors detected.

4.1.4.5.- DAS PARTIDAS BRIDGE

GENERAL DESCRIPTION

A 16th century bridge located in the town council of Ponteareas over the Tea river (Fig. 4.58). It presents three barrel arches and another gothic one among 7.30 and 13.50 meters span. It has two spillways in the right margin from the upstream side and a slightly pointed profile (Fig. 4.67). This bridge was restored several times.

Figure 4.67.- View of Das Partidas bridge from the downstream side.

GPR SURVEY

- **Methodology**

The common methodology exposed previously for surveying masonry arch bridges was carried out. The survey parameters used are given in Table 4.31. (x,y,z) data from a total station were employed to correct the radargrams acquired for topography.

Antenna	250 MHz	500 MHz
Number of Samples	566	681
Time Window	220 ns	100 ns
Trace Interval	0.05 m	0.02 m

Table 4.31.- GPR survey parameters.

- **Processing flow**

The processing sequence applied was: time-zero correction, dewow filtering, gain function, spatial filtering (subtracting average), band-pass filtering (butterworth) and topographic correction.

- **Results and interpretation**

Observing the processed radargram obtained (Fig. 4.68A), only the reflections due to the arch-air and air-water interfaces were easily identified for the first and third arches. These reflections were attenuated in the other ones probably caused by the presence of soil-cement as a subbase layer used for pathway reinforcement (Fig. 4.68B). A Similar signal response was observed by Lorenzo (1996).

In addition, the reflections generated by the existence of two spillways in the right margin were observed, as well as the usual reflections generated by the bridge foundations (Fig. 4.68B).

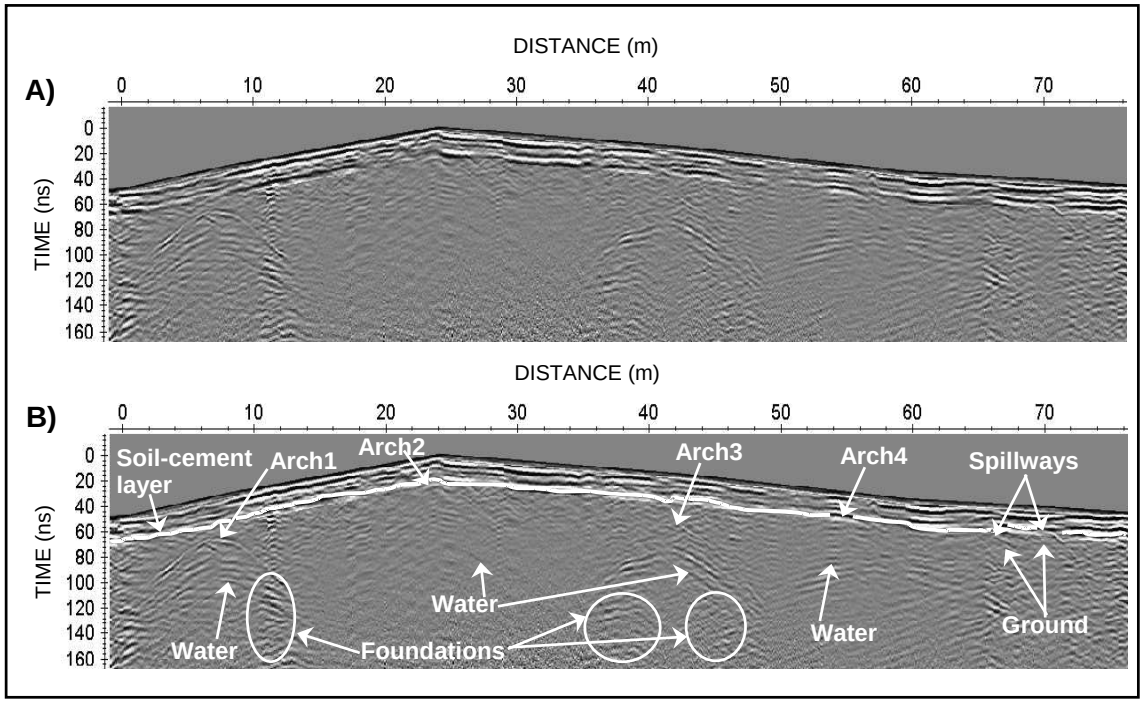

Figure 4.68.- Radargram obtained with 250 MHz antenna in Das Partidas bridge. A) Processed data. B) Interpretation of the main reflectors detected.

4.1.4.6.- AREAS BRIDGE

GENERAL DESCRIPTION

The ancient Areas bridge, built in the 14th century, is located in the town council of Pontareas across the Tea river (Fig. 4.58). It has four arches from 4.10 to 10.20 m span. Both in the left margin from the upstream side are pointed arches, whereas the other ones in the right margin are barrel arches (Fig. 4.69). Some authors have referenced the possible restoration of these two arches in the right margin (Alvarado et al., 1989). Areas bridge presents a very slightly pointed profile.

Figure 4.69.- View of Areas bridge from the upstream side.

GPR SURVEY

- **Methodology**

The common methodology proposed was employed for surveying the Areas bridge with the survey parameters mentioned in Table 4.32. The radargrams acquired was corrected for topography by using (x,y,z) data recorded by means of a total station.

Antenna	250 MHz	500 MHz
Number of Samples	566	681
Time Window	200 ns	100 ns
Trace Interval	0.05 m	0.02 m

Table 4.32.- GPR survey parameters.

- **Processing flow**

The processing sequence applied was: time-zero correction, dewow filtering, gain function, spatial filtering (subtracting average) and topographic correction.

- **Results and interpretation**

The reflections from the arch-air and air-water/air-ground interfaces as well as the usual reflections generated by the bridge foundations were easily identified in the processed radargram shown in Figure 4.70A. Also, it was possible to distinguish a relevant

reflection along the bridge named in the interpreted radargram as a stone layer (Fig. 4.70B). This effect is probably caused by a possible restoration. This bridge could be emptying and filling with backing materials which are different than the original ones.

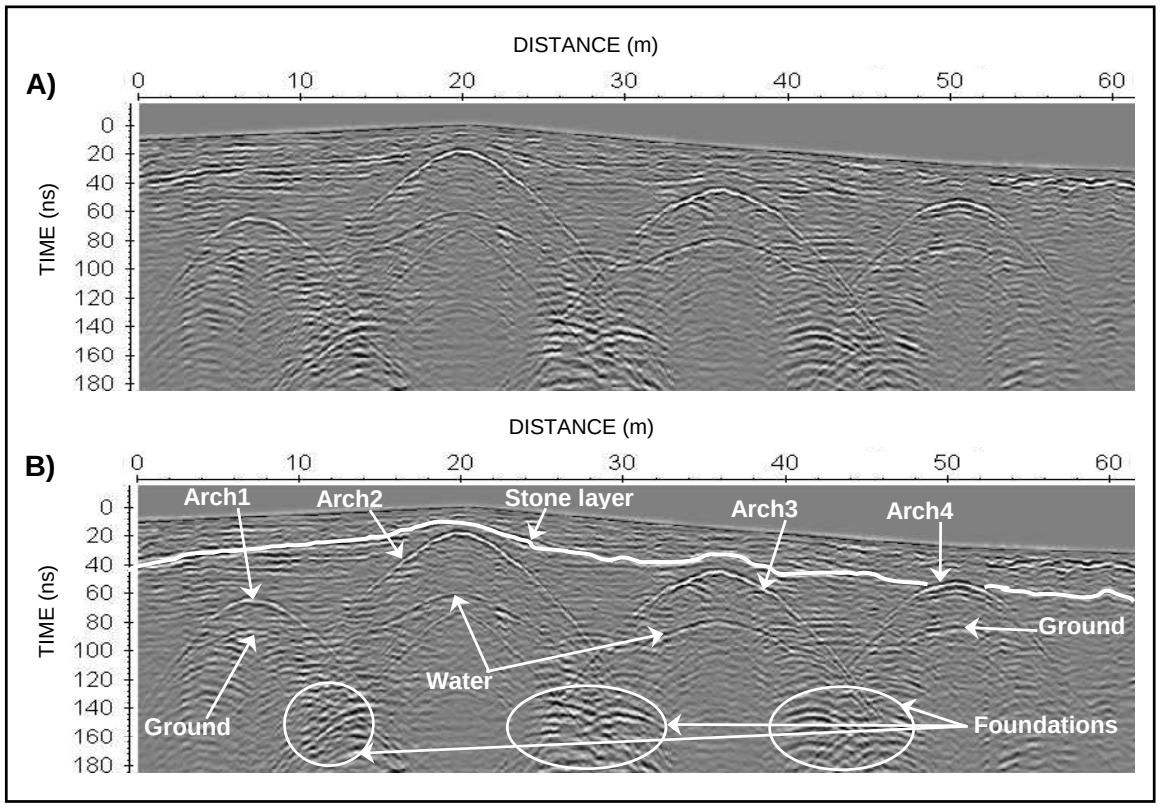

Figure 4.70.- Radargram obtained with 250 MHz antenna in Areas bridge.
A) Processed data. B) Interpretation of the main reflectors detected.

4.1.4.7.- FILLABOA BRIDGE

GENERAL DESCRIPTION

Medieval bridge built in the council of Salvaterra over the river Tea (Fig. 4.58). It has four arches among 4.2 and 4.7 m. span (Fig. 4.71) with a double slope flagstone path. The first arch from left to right in the upstream side was restored in 1915 (Alvarado et al., 1989).

Figure 4.71.- View of Fillaboa bridge from the downstream side.

GPR SURVEY

- **Methodology**

Fillaboa bridge was surveyed according to the common methodology with the survey parameters shown in Table 4.33. The radargrams obtained were corrected for topography using (x, y, z) data acquired with a total station.

Antenna	250 MHz	500 MHz
Number of Samples	512	813
Time Window	200 ns	120 ns
Trace Interval	0.05 m	0.02 m

Table 4.33.- GPR survey parameters.

- **Processing flow**

The processing sequence applied was: time-zero correction, dewow filtering, gain function, spatial filtering (subtracting average), band-pass filtering (butterworth) and topographic correction.

- **Results and interpretation**

The radargram obtained with the 250 MHz antenna showed the usual reflections due to the arch-air and air-water or air-ground interfaces, although it was possible to appreciate

a severe attenuation of the signal in the first arch (Fig. 4.72). This effect was probably caused by the presence of filling materials which are different than the original ones used for restoration. This hypothesis is in agreement with the historical references (Alvarado et al., 1989). Also the typical corner reflections generated in this kind of arches were observed (Martinaud et al., 2004).

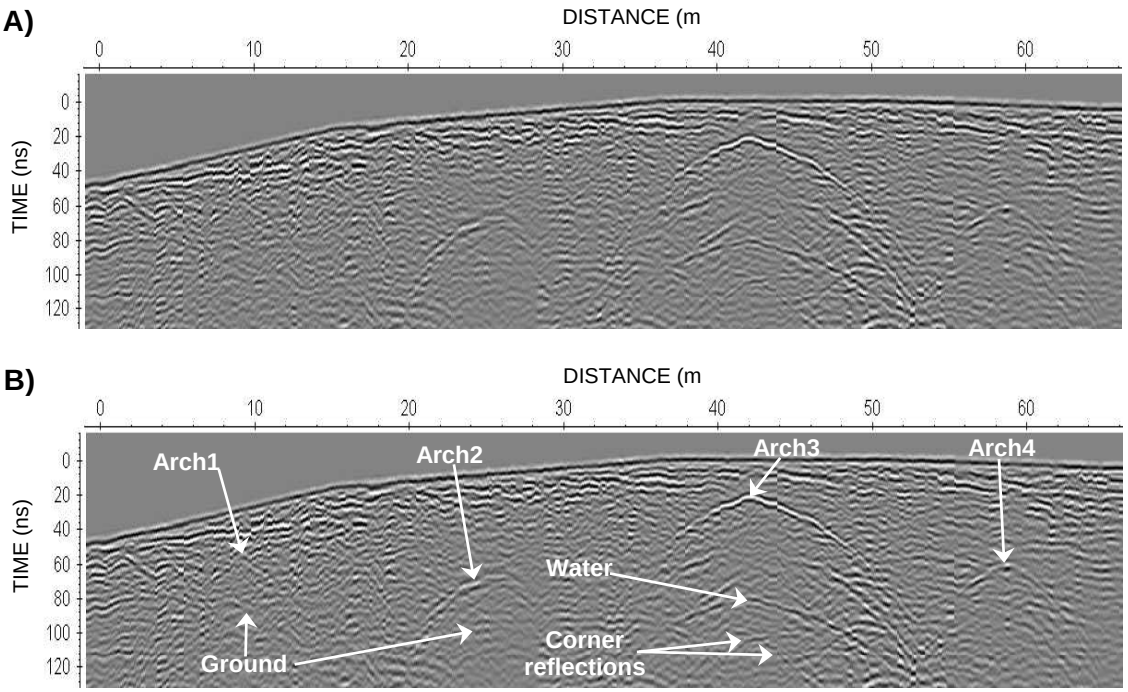

Figure 4.72.- Radargram obtained with 250 MHz antenna in Fillaboa bridge.
A) Processed data. B) Interpretation of the main reflectors detected.

The radargrams acquired with the 500 MHz antenna did not provide interesting additional information.

4.1.4.8.- CERNADELA BRIDGE

GENERAL DESCRIPTION

Cernadela bridge was built in the 15th century over the Tea river in the council of Mondariz (Fig. 4.58). It has five arches from 3.6 to 11.4 meters span with a slightly pointed profile (Fig. 4.73). According to the literature, this bridge was restored in several circumstances throughout time (Alvarado et al., 1989).

Figure 4.73.- View of Cernadela bridge from the upstream side.

GPR SURVEY

- **Methodology**

The common methodology proposed was employed for surveying Cernadela bridge with the survey parameters mentioned in Table 4.34. The radargrams acquired were corrected for topography by using (x,y,z) data recorded by means of a total station.

Antenna	250 MHz	500 MHz
Number of Samples	566	677
Time Window	220 ns	100 ns
Trace Interval	0.05 m	0.02 m

Table 4.34.- GPR survey parameters.

- **Processing flow**

The processing sequence applied was: time-zero correction, dewow filtering, gain function, spatial filtering (subtracting average), band-pass filtering (butterworth) and topographic correction.

- **Results and interpretation**

Observing the radargram obtained with the 250 MHz antenna, it was possible to identify the reflections from the arch-air and air-water or air-ground interfaces (Fig. 4.74A). Another interesting reflection interpreted was the springer stone reflection due to their

bigger size in relation to the other ring stones that compose the arch (Durán, 2005). Also the reflections from the bridge foundations were observed (Fig. 4.74B).

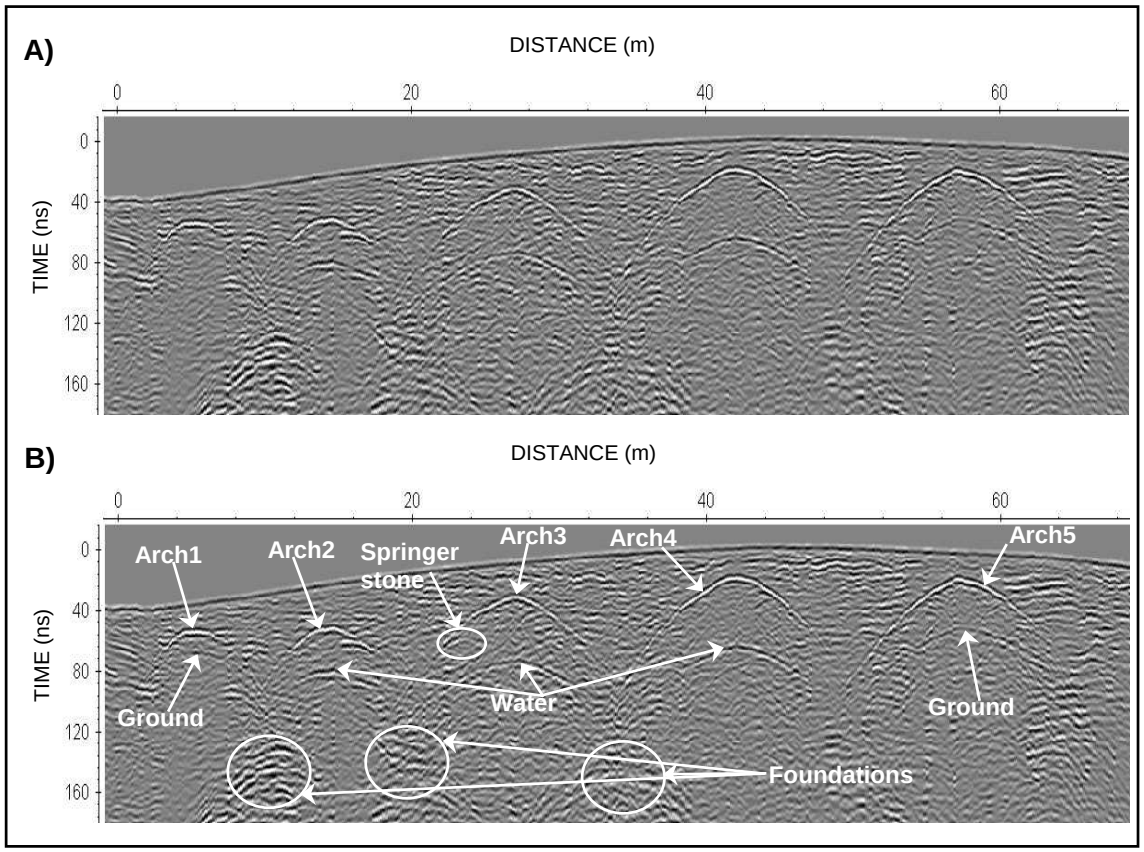

Figure 4.74.- Radargram obtained with 250 MHz antenna in Cernadela bridge.
A) Processed data. B) Interpretation of the main reflectors detected.

4.1.4.9.- O BURGO BRIDGE

GENERAL DESCRIPTION

This is a medieval bridge built in the 14th century in the council city of Pontevedra, over the Lérez river (Fig. 4.58). It presents eleven arches between 6.6 and 1.1 meters span (Fig. 4.75). This bridge was restored several times throughout the time (Llanso de Viñals, 1955).

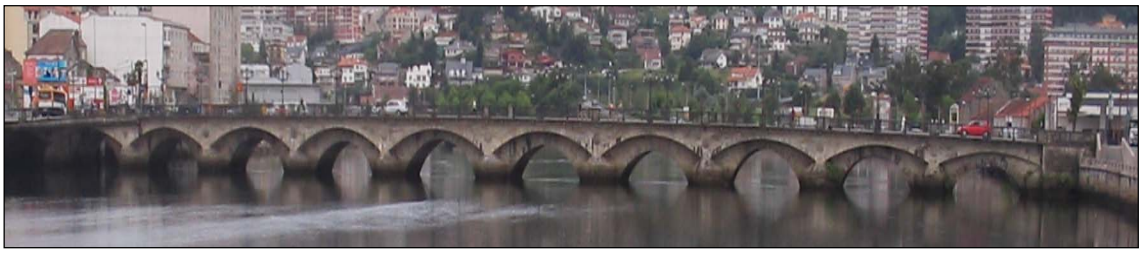

Figure 4.75.- View of O Burgo bridge from the upstream side.

GPR SURVEY

- **Methodology**

The common methodology proposed was employed for surveying this bridge with the survey parameters mentioned in Table 4.35.

Antenna	250 MHz	500 MHz
Number of Samples	516	678
Time Window	200 ns	100 ns
Trace Interval	0.05 m	0.02 m

Table 4.35.- GPR survey parameters.

- **Processing flow**

The processing sequence applied was: time-zero correction, dewow filtering, gain function, spatial filtering (subtracting average) and band-pass filtering (butterworth).

- **Results and interpretation**

In the processed radargram acquired with 250 MHz antenna, it was possible to identified the arch-air interfaces, except the last one (Fig. 4.76C). This identification resulted in a difficult task due to the use of an in-homogeneous filling material inside this bridge. A severe attenuation in the signal have been appreciated for the first and second piers of the structure. This effect can be produced by the presence of a reinforced concrete beam in these locations. These beams were placed for reinforcementcrosswise from the upstream buttress to the downstream one in a restoration carried out in the middle of the 20th century (Llanso de Viñals, 1955).

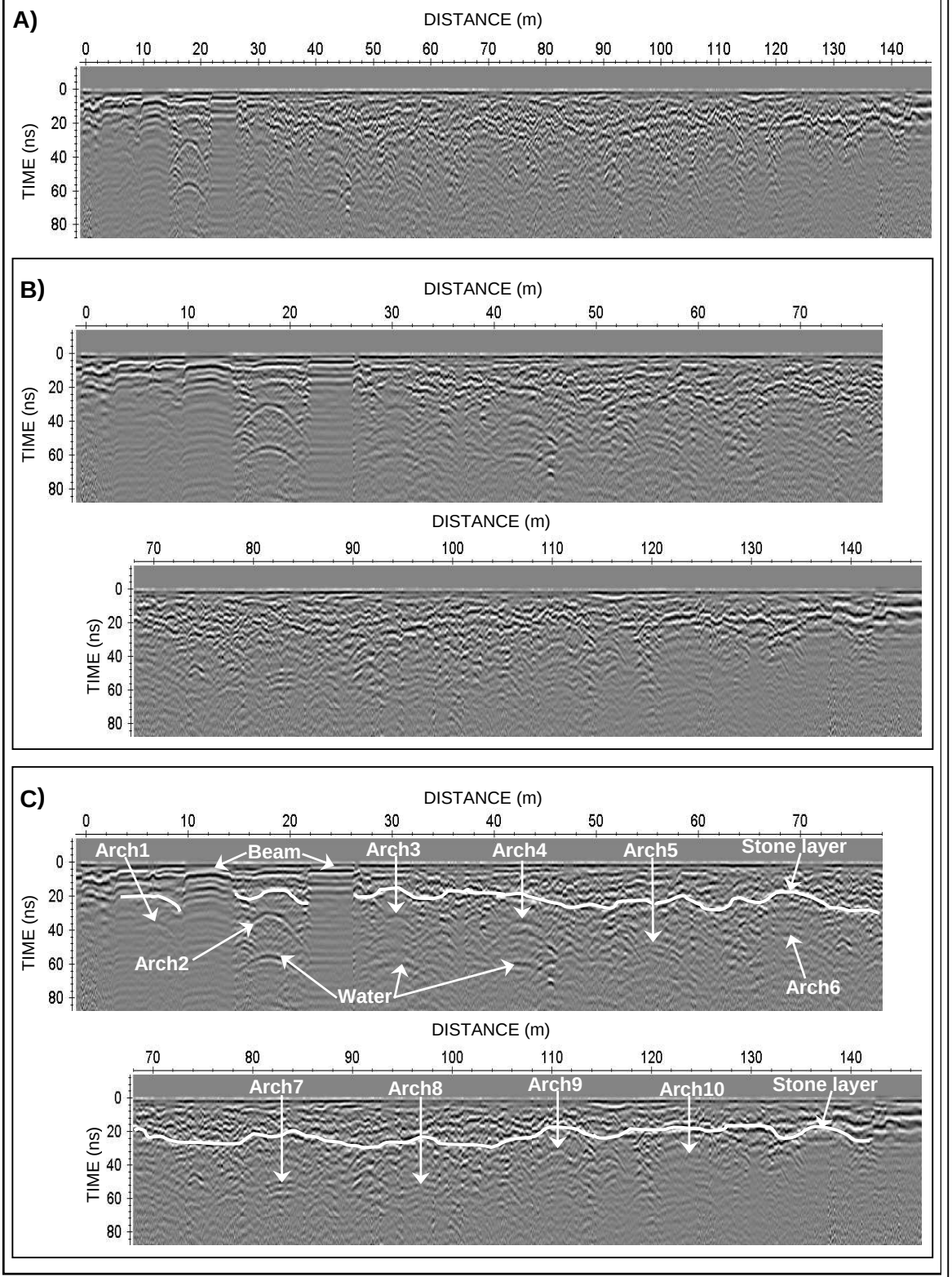

Figure 4.76.- Radargram obtained with 250 MHz antenna in O Burgo bridge.
A) Processed data, B) Radargram in detail, and C) Interpretation of the main reflectors.

4.1.4.10.- SAN ANTÓN BRIDGE

GENERAL DESCRIPTION

A 13th century bridge located in Cerdedo across the Lérez river (Fig. 4.58). This bridge has two arches 10.2 and 4 meters span. It is 31 m long and has a slightly pointed profile (Fig. 4.77). There is a medieval flagstone path over the bridge 3.5 meters wide.

Figure 4.77.- View of San Antón bridge from the upstream side.

GPR SURVEY

- **Methodology**

First, the 200 MHz antenna was chosen as the most suitable to research the foundations of the bridge and to analyse the material homogeneity within the structure. A total of three parallel lines were carried out. The survey parameters used are given in Table 4.26. (x,y,z) data from a total station were employed to correct the radargrams acquired for topography. After that, in order to verify the results acquired with 200 MHz antenna as well as to obtain more detailed information of the shallower filling material of the bridge, two surveys were performed with 250 and 500 MHz shielded antennas.

Antenna	200 MHz	250 MHz	500 MHz
Number of Samples	512	512	610
Time Window	234 ns	200 ns	90 ns
Trace Interval	0.10 m	0.05 m	0.05 m

Table 4.36.- GPR survey parameters.

- **Processing flow**

Each radargram obtained with 250 and 500 MHz antenna, was filtered applying the following processing sequence before interpretation: time-zero correction, dewow filtering, gain function, spatial filtering (subtracting average), band-pass filtering (butterworth) and topographic correction.

- **Results and interpretation**

The radargram acquired with the 250 MHz antenna showed the usual reflections due to the arch-air and air-water or air-ground interfaces (Fig. 4.78B). Another relevant event was located at the beginning of the radargram (Fig. 4.78A). An explanation to this might be a bridge modification which caused a partial destruction of a third arch and subsequent filling –including contiguous zones–. Below this unexpected reflection there was another reflection which could be associated with the old river-bed (Fig. 4.78B). All this area seemed to have a more homogeneous filling material.

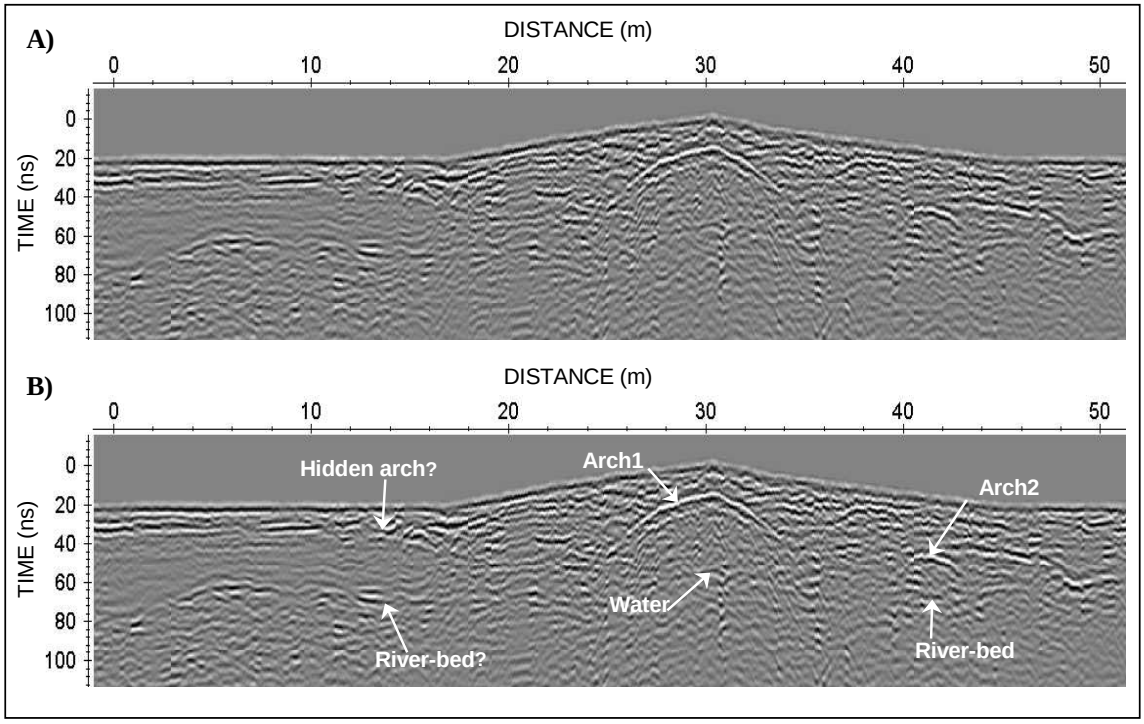

Figure 4.78.- Radargram obtained with 250 MHz antenna in San Antón bridge.
A) Processed data. B) Interpretation of the main reflectors detected.

The radargrams obtained with the 500 MHz antenna did not provide additional information.

Remark: An extended analysis of San Antón bridge is described in subchapter 4.2.1.

4.2.- SELECTED CASE STUDIES

This section is composed of four case studies selected from the inventory developed. The San Antón, Traba, Bibei and Lugo bridges were chosen due to their interesting structural information provided by GPR, which can be useful for civil engineers in terms of conservation and restoration. The GPR results obtained for these bridges are fully described in this section. FDTD modelling was used for an exhaustive data interpretation. The inputs to create the synthetic radargrams were usually elaborated with the external geometry of the bridge acquired by photogrammetric or laser scanning methods.

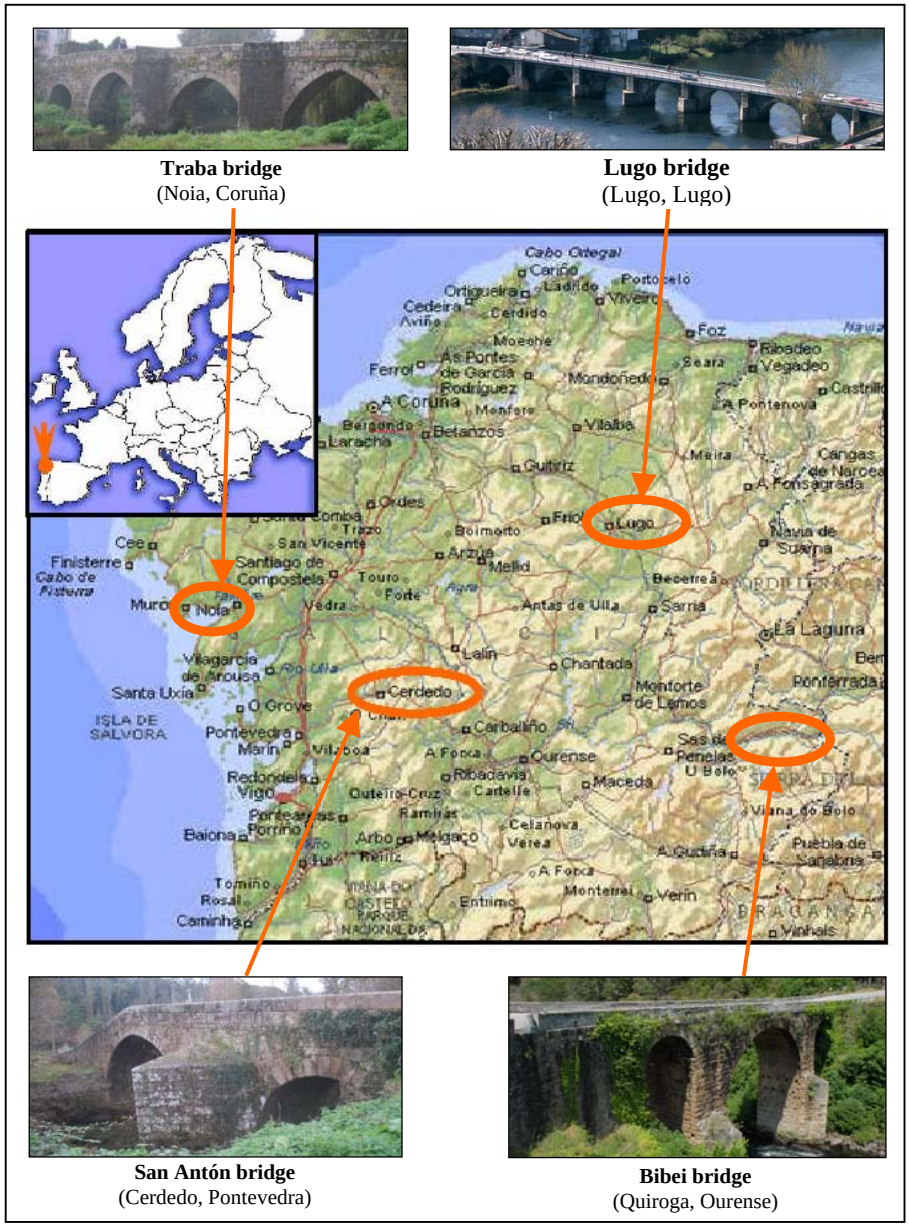

Figure 4.79.- Location of San Antón, Traba, Bibei and Lugo bridges in Galicia.

4.2.1.- SAN ANTÓN BRIDGE

A 13th century bridge located in Cerdedo across the Lérez river (Fig. 4.79). This bridge has two arches 10.2 and 4.0 meters span. It is 31 m long and has a slightly pointed profile (Fig. 4.80). It presents a medieval flagstone path 3.5 meters wide over the bridge (Alvarado et al., 1989).

Figure 4.80.- General view of the San Antón bridge from the upstream side.

San Antón bridge was the first one selected for assessing by means of GPR. The main goal of this survey was to analyze what kind of information is possible to obtain of the whole bridge. Our purpose was to evaluate the filling material homogeneity, identify different zones, detect hidden features –such as internal holes or cracks–, and define the internal construction characteristics.

4.2.1.1.- FIRST GPR SURVEY

Previously, a topographic survey along the bridge was carried out with a total station model Leica TCR110 for later correction of GPR data for topography and the tilt of the antenna.

Data acquisition

Due to its optimum compromise between penetration and resolution, the 200 MHz antenna was chosen as the most suitable to research the foundations of the bridge and to analyze the material homogeneity within the structure. The GPR survey was carried out following the common-offset mode. A total of three parallel lines, 45 m long each one, were carried out

with 1 m distance between transects (Fig. 4.81A). The offset between transmitter and receiver antennas was set to 0.6 m (Fig. 4.81B). Common-offset point-to-point data was acquired with 10 cm in-line spacing, time window of 234 ns, and 512 samples per trace.

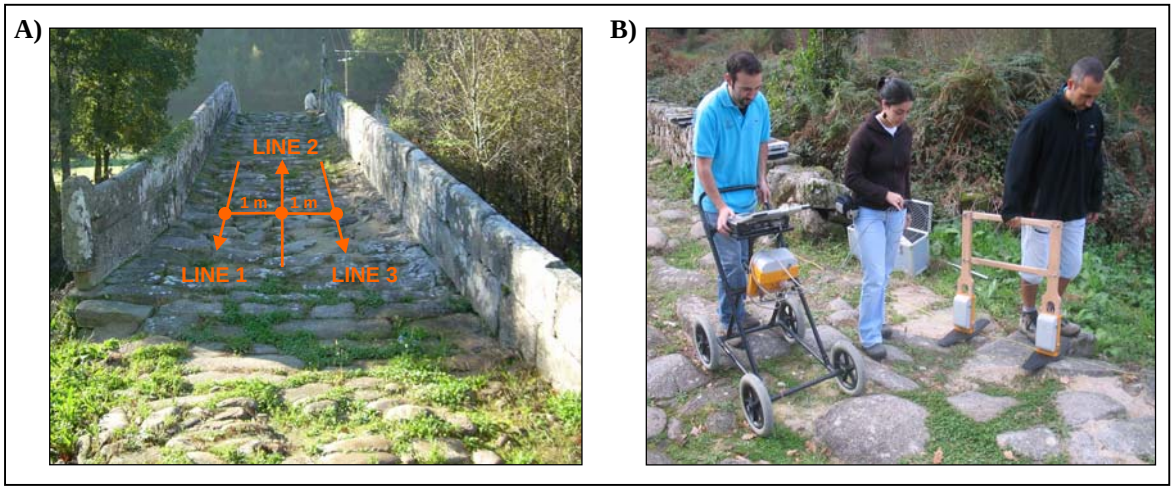

Figure 4.81.- GPR survey. A) GPR profiles direction in the right margin from the upstream side and B) data acquisition setup composed by 200 MHz unshielded antenna.

Processing flow

Each radargram was filtered applying the following processing sequence before interpretation: time-zero correction, dewow filtering, gain function, spatial filtering (subtracting average) and topographic correction. As well, the radargram was also corrected for the tilt of the antenna to make a suitable estimation of the signal velocity in different zones into the structure.

Results and interpretation

Figure 4.82A shows an unprocessed radargram obtained with the 200 MHz unshielded antenna. The interpretation of the processed radargram presenting some structural characteristics that can be easily identified as the arches and bridge foundations is shown in Figure 4.82C. A semi-flat reflection located between the two arches could be interpreted as an internal structural element for pier reinforcement –as documented in engineering books specializing in the topic (Durán, 2005)– as a solid pier or even as filled with a compact material. Other relevant structural reflections observed are the ring stone reflections produced in arches due to their internal staircase shape as shown previously in Figure 2.4a and the springer stone reflections due to their larger size in relation to the other ring stones composing the arch (Durán, 2005).

Observing the radargrams in Figure 4.82, it is possible to identify three large hyperbolic reflections even though the bridge has only two visible arches (Fig. 4.80). The unexpected third reflection, located between meters 0 and 6, could be related to the presence of a hidden arch; however, there were no historical references of this third arch in the literature. Furthermore, this interpretation could be ratified by the external geometry –the bridge is quite symmetric respect to the first arch– and the presence of a dike in the left margin from the upstream side, gaining land from the river-bed (Fig. 4.80). Below this unexpected reflection there was another reflection which could be associated with the old river-bed (Fig. 4.82C).

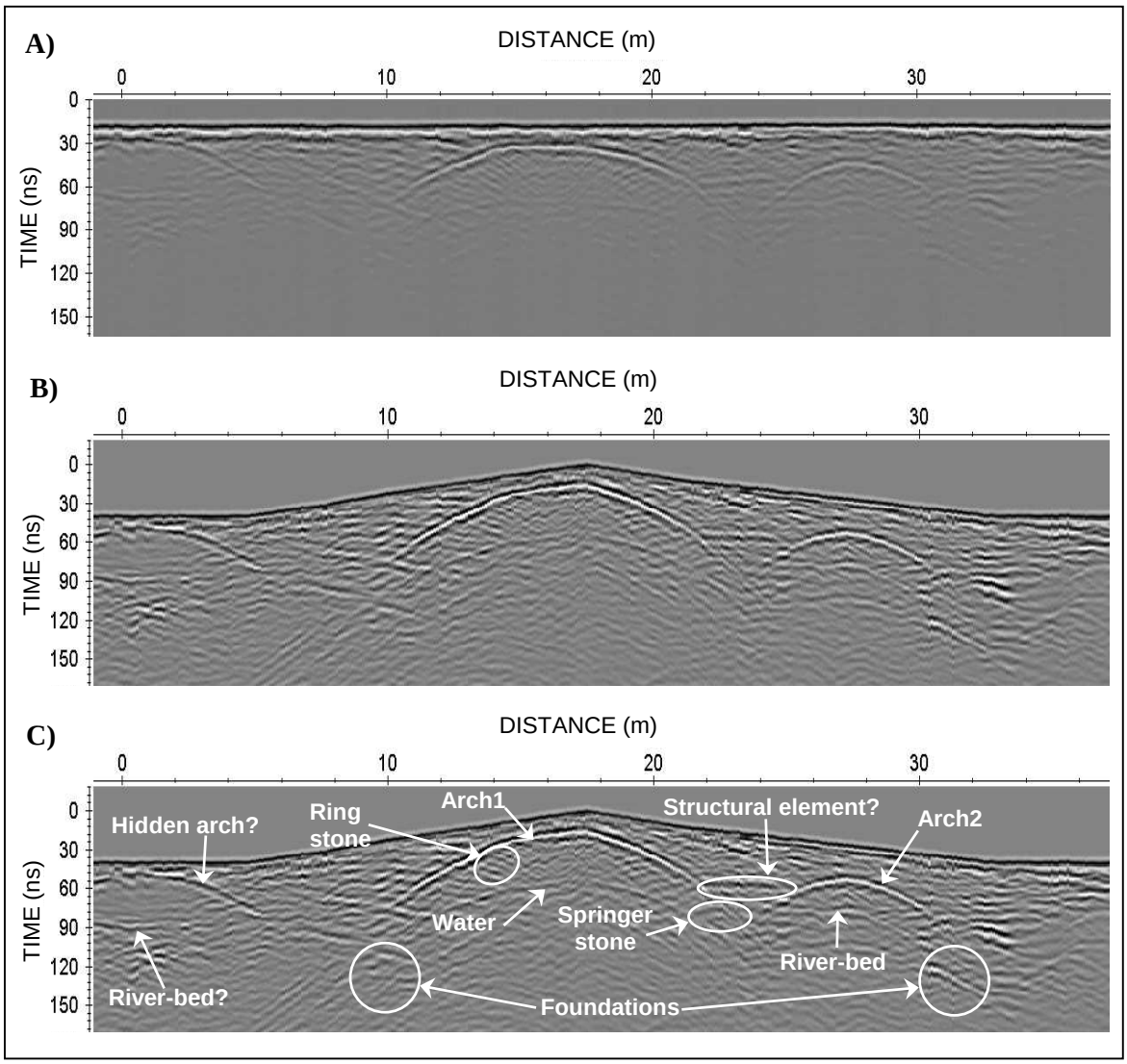

Figure 4.82.- Radargram acquired with the 200 MHz antenna. A) Raw data, B) processed data and C) interpretation of the main reflectors detected.

Considering this reflection as a hidden arch, the following step was to obtain some information regarding whether it was empty or filled. Measuring the delay between the reflections from its keystone and the old river-bed (about 40 ns), considering air as the

propagation medium, would result in an 6 m high arch, that is, much higher than the right one. Furthermore, if the arch was empty the polarity of the reflection in the arch-air interface should be the same as in the other two arches, which did not happen in this case (Fig. 4.82C) –that is, the arch is not empty–, and the signal velocity in the filling material was lower than in the arch. The filling material seemed quite homogeneous as it was not possible to differentiate significant internal reflections.

Using the structural dimensions provided by laser scanning (Table 4.37), it was possible to estimate the signal velocities in different zones of the bridge, ranging from 7.5 to 11.5 cm/ns. These were calculated according the procedures described in section 3.2. The typical average velocity of a GPR pulse in dry masonry is reported in the literature as 14.0-15.0 cm/ns (Colla et al., 1997b; Maierhofer et al., 2003a). Thus, the velocities found in this case were significantly lower, which could indicate moisture into the structure. This hypothesis was confirmed by the existence of vegetation growing in the stonework of the bridge (Fig. 4.80).

Figure 4.83.- Orthophoto of the upstream wall generated by laser scanning data.

Arches	1	2
Pathway-arch distance (m)	0.19	0.85
Ring stone thickness (m)	0.64	0.61
Arch-water/ground distance (m)	6.33	2.8
Distance between keystones (m)	10.80	

Table 4.37.- External measures of Traba bridge geometry in the upstream wall.

4.2.1.2- FDTD MODELLING

The FDTD simulations were elaborated from the precise geometry provided by the laser scanning process to verify the radar results acquired using the GprMax software v.2.0.(Giannopoulos, 2006). Numerical models were developed to analyze the differences between an empty arch (Fig. 4.84A,B) and a filled arch (Fig. 4.85A,B). These were

generated by simulating an arch with the same dimensions as the second arch and two meters between keystone and river-bed. The electromagnetic parameters used for media characterization are described in the input file, shown in Figures 4.84A and 4.85A.

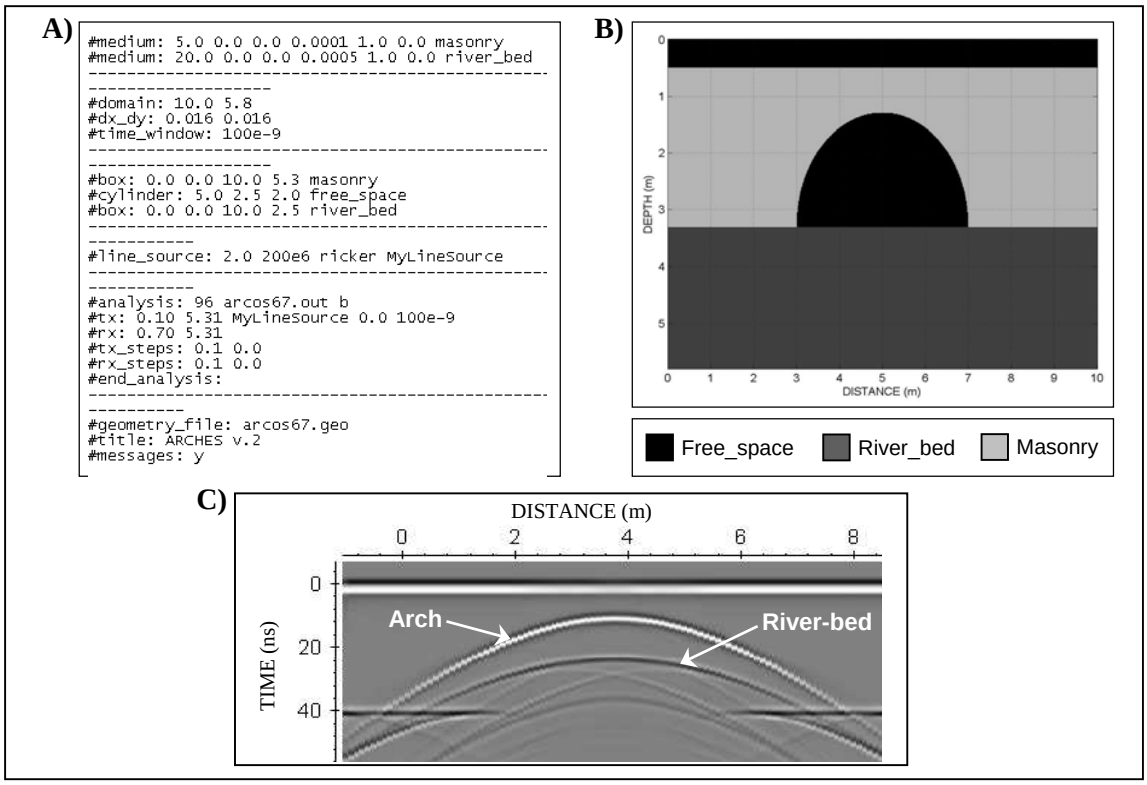

Figure 4.84.- FDTD simulation showing the GPR signal response in an empty arch. A) Input file, B) model and C) synthetic radargram obtained.

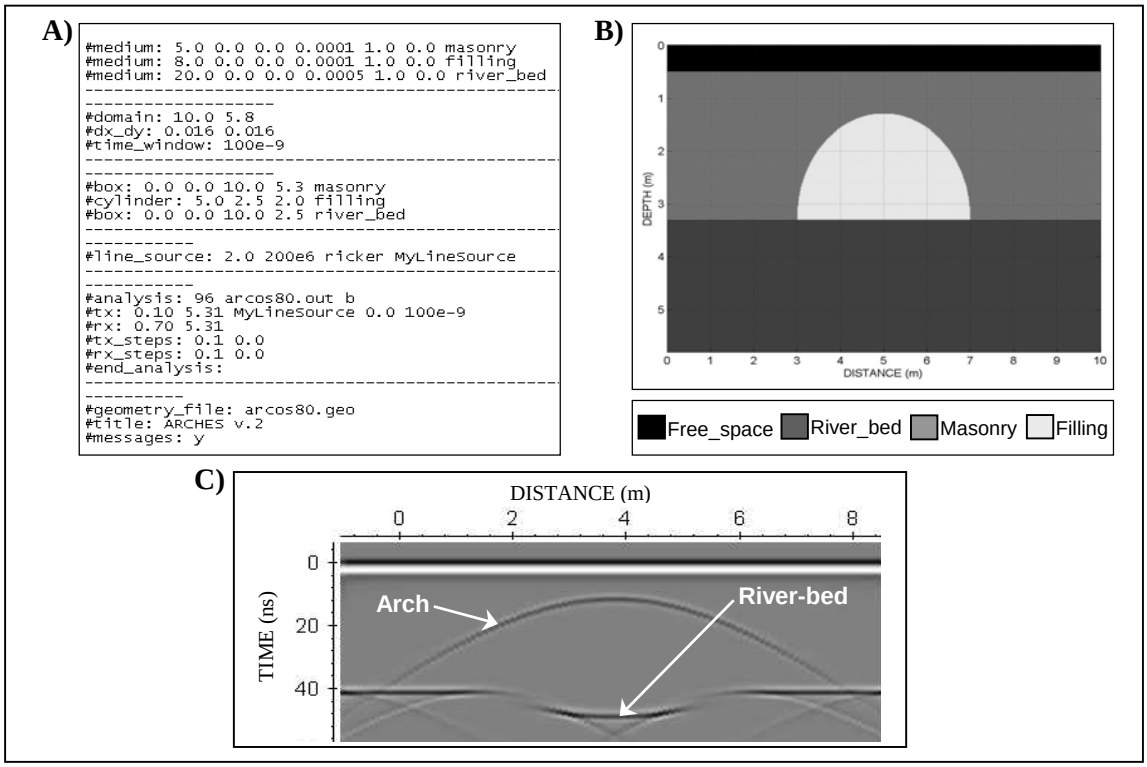

Figure 4.85.- FDTD simulation showing the GPR signal response in a filled arch. A) Input file, B) model and C) synthetic radargram obtained.

A comparison of both models showed how the polarity of the arch-air interface (Fig. 4.84C) was different from the arch-fill interface (Fig. 4.85C). Also, the river-bed reflection interpreted in the GPR results (Fig. 4.82C) was very similar to the one identified in the synthetic radargram (Fig. 4.85C).

Based on the interpretation provided by the numerical simulations shown in Figures 4.84 and 4.85 and the GPR results acquired, it was possible to create a synthetic model of the whole bridge to facilitate the interpretation of the radargram obtained. Therefore, it was elaborated including the presence of a filled arch with the same characteristics as the small one as well as a solid pier between arches (Fig. 4.86B). The electromagnetic parameters employed are described in Figure 4.86A. The accurate external geometry of the bridge measured in the orthophoto generated with laser scanning data (Fig. 4.83) was used to elaborate this synthetic model.

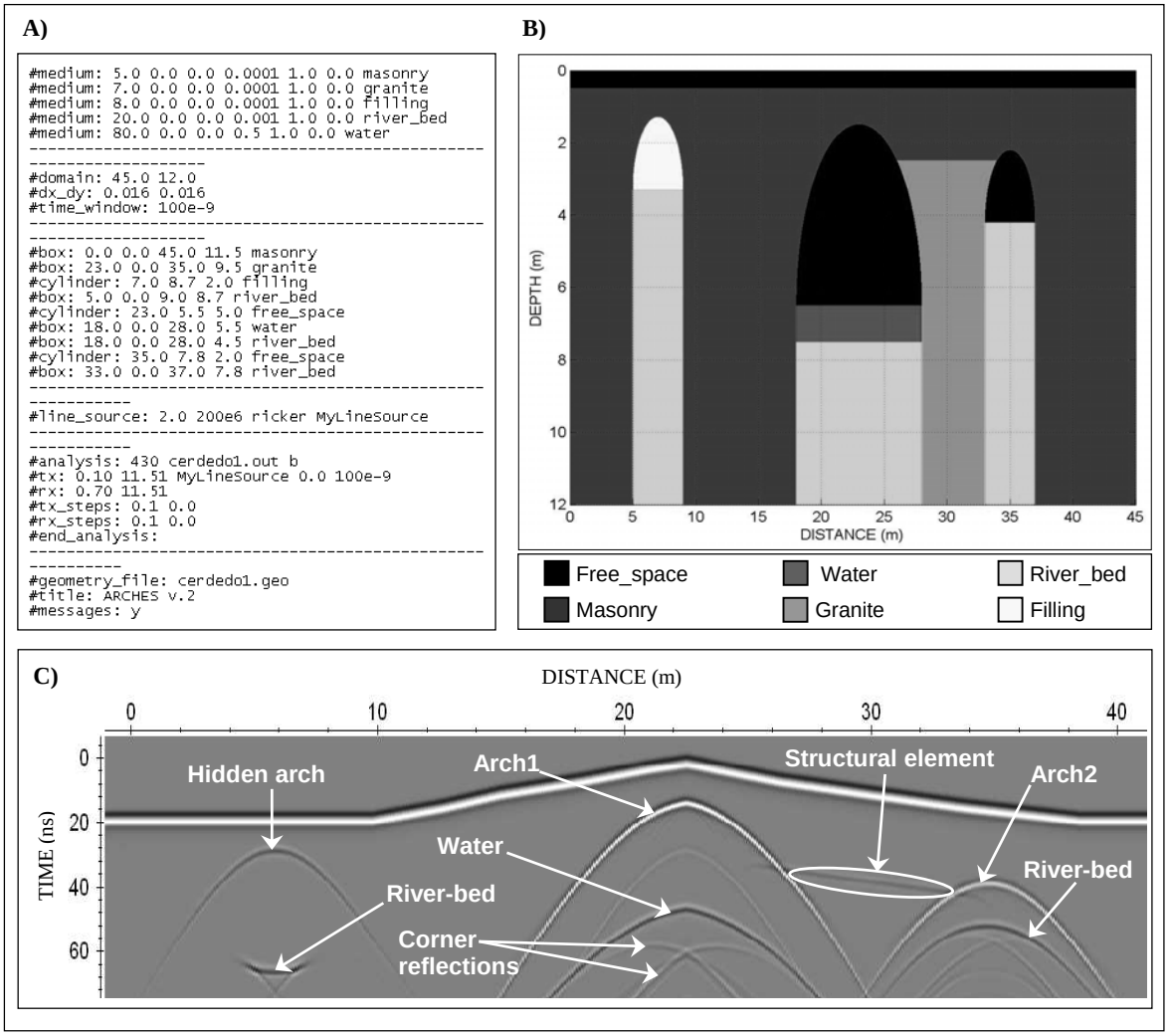

Figure 4.86.- Numerical simulation of the whole bridge. A) Input file, B) model and C) synthetic radargram obtained.

The synthetic radargram shows reflections produced by the structural elements of the bridge (Fig. 4.86C) and also the presence of multiples from the arch and the typical corner reflections produced in arches of this kind (Martinaud et al., 2004). These complex reflection patterns can hinder the detection of other interesting reflectors by cluttering. Thus, it can be difficult to obtain clear information in the radar data about the foundations or filling material between the arches.

The ring and springer stone reflections produced in this kind of arch (Fig. 4.82C), are explained by the FDTD model shown in Figure 4.87. Despite the usual external uniform surface of the ring stones, their internal structure usually presents an irregular staircase shape. In addition, the springer stones are generally larger than the other ring stones which compose the arch-ring (Durán, 2005). The synthetic radargram created illustrated reflection patterns similar to the radar radargram as well the usual hyperbolic deformation caused by high-frequency fluctuations (Fig. 82C).

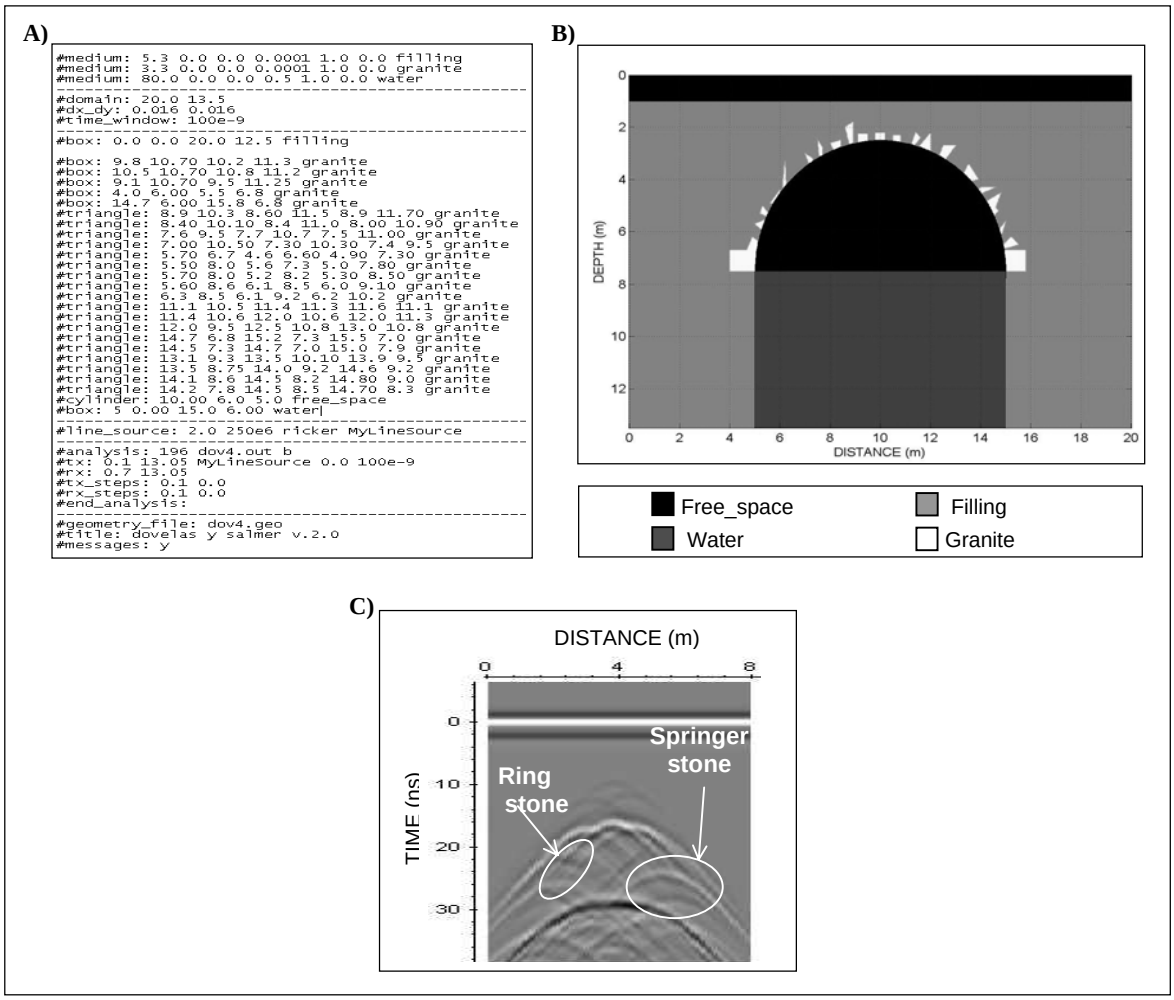

Figure 4.87.- FDTD model showing the effect produced by the existence of an internal staircase shape and the springer stones in the arch-ring. A) Input file, B) model and C) synthetic radargram obtained.

In order to verify the results acquired with 200 MHz antenna as well as to obtain more detailed information of the shallower filling material of the bridge, two surveys were performed with 250 and 500 MHz shielded antennas.

4.2.1.3.- SECOND GPR SURVEY

Data acquisition

The GPR data acquisition was based on constant distance intervals. An odometer wheel attached on the back was used for measuring the profile length. Two longitudinal parallel profiles, 75 m long each, were gathered twice following the common methodology proposed for this work and described in subchapter 3.1. First dataset with the 250 MHz shielded antenna, 5 cm in-line spacing, 200 ns time window, and 512 samples per trace. The second dataset with the 500 MHz shielded antenna, 5 cm in-line spacing, 90 ns time window, and 610 samples per trace.

Owing to the bridge's floor consists on large irregular rocks (Fig. 4.81A), the measurements can result in a difficult task since the continuos movement of the survey wheel can be interrupted. Calibration of the wheel is recommended before starting surveying for mitigating this factor which affects the accuracy of radar trace location.

Processing flow

Each radargram was filtered applying the following processing sequence before interpretation: time-zero correction, dewow filtering, gain function, spatial filtering (subtracting average), band-pass filtering (butterworth) and topographic correction.

Results and interpretation

The profiles recorded with the 250 and 500 MHz antennas were started a few meters before the 200 MHz survey, with the goal of verifying the continuity of the reflected structure which previously was interpreted as a possible hidden arch. However, as can be noticed in the radargram acquired with the 250 MHz antenna (Fig. 4.88), there was not a clear reflection from a hidden arch and it appears that the reflected structure has a certain continuity to the left. This entire area seemed to have a more homogeneous filling material. An explanation for this might be a bridge modification which caused a partial destruction of the arch and subsequent filling –including contiguous zones–. The radargrams obtained with the 500 MHz antenna did not provide any additional useful information.

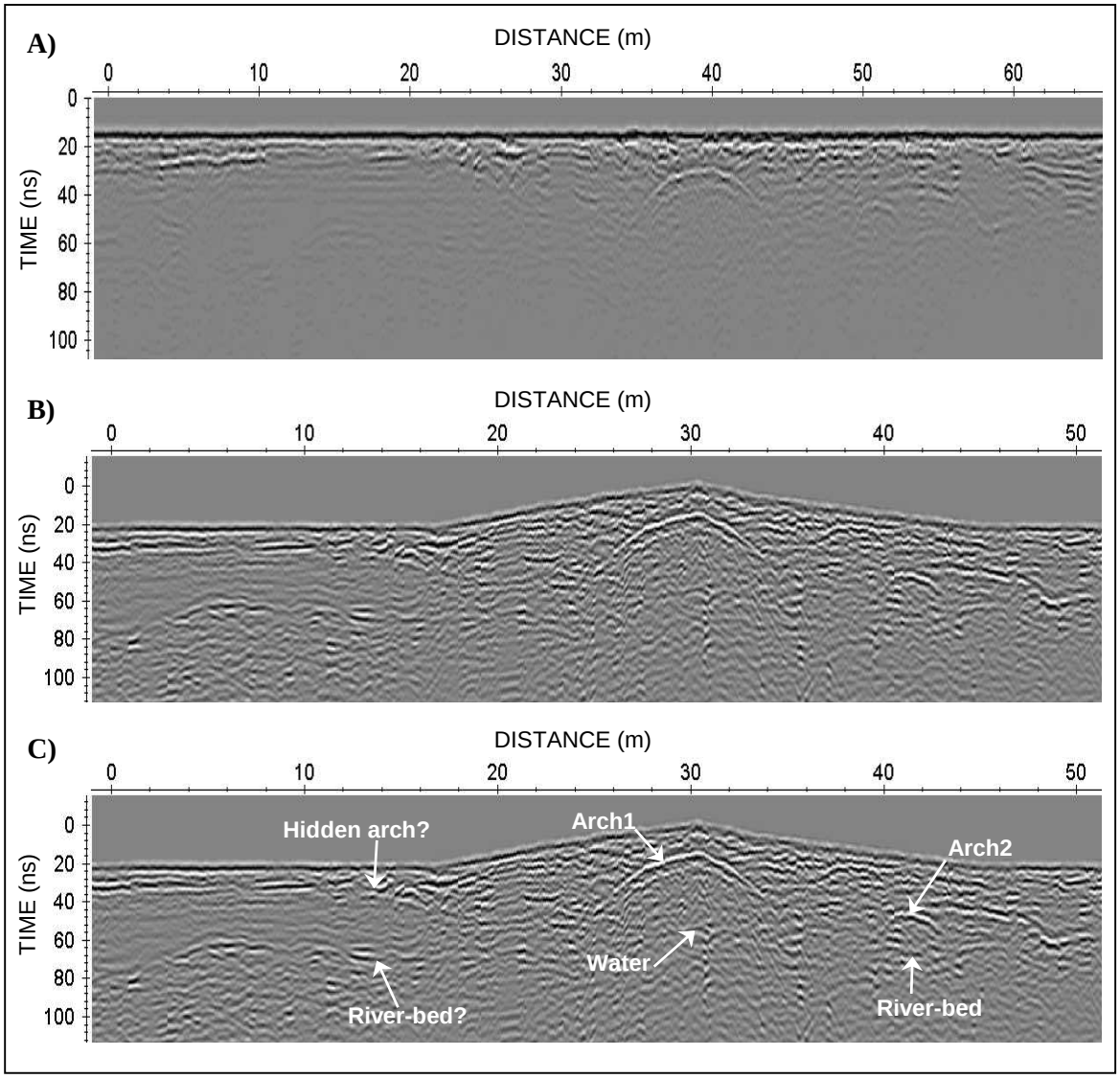

Figure 4.88.- Radargram acquired with the 250 MHz antenna. A) Raw data, B) processed data and C) interpretation of the main reflectors detected.

4.2.1.4.- DISCUSSION AND CONCLUSIONS

The results acquired for this bridge confirmed that GPR is an effective NDT method for historical bridge inspection. It proved useful for revealing structural details and possible modifications over time.

<u>From a historical-archaeological point of view:</u>

Considering the GPR data acquired with the 250 MHz antenna and the synthetic models created, it was hypothetically possible that the San Antón bridge was composed of three arches in ancient times. However, the second survey did not reveal a clear reflection from a hidden arch. The final explanation may be a bridge modification resulting in a partial

destruction of this hidden arch and subsequent filling including contiguous areas. This modification could have been produced by the construction of a dike on the left margin of the upstream side to reclaim land from the river-bed. This information can be an impetus for historians and civil engineers to take conservation steps because there are no historical references regarding this third arch in the specialized literature. Therefore, it would be interesting to realize an exhaustive survey such as a 3D mesh in this location to investigate this hypothesis, although the presence of an ancient flagstone path built of large irregular blocks could hinder data acquisition for 3D surveys.

From a civil-structural point of view:

The irregular pattern observed for the reflection generated in the arch-air interface of the first arch informed us about the existence of different filling materials on either side over the arch. The differences in bridge fills may also indicate restoration tasks carried out on the San Antón bridge.

A continuous semi-flat reflection between the two arches was interpreted as an internal structural element for pier reinforcement. According to engineering books specialized in the topic, the pier would be solid or filled with a compact material to yield a better structural behavior of the bridge in terms of stability.

Additionally, GPR detected the presence of moisture content in the structure, which is very important due to its influence on the durability and strength of the materials involved. The moisture content can be related to the existence of faults such as voids and cracks. However, the confluence of many reflections from the inhomogeneous filling material between arches makes their identification difficult. This information can be helpful for engineers attempting to take strengthening measures.

4.2.2.- TRABA BRIDGE

A medieval arch bridge built in the 14th century. It is located in Noia across the Traba river (Fig. 4.79). It has four arches between 4.8 and 7.0 meters span (Fig. 4.89). The first and third arches from the left margin upstream are barrel, whereas the other ones are gothic arches. This event is probably caused by two different times for the stonework construction. The gothic arches from the original bridge and the barrel ones owing to a later restoration. Some authors apprise of the existence of a fifth arch in the right margin in its original structure (Alvarado et al., 1989). Currently, the original pathway is covered by an asphalt paving.

Figure 4.89.- General view of the Traba bridge from the upstream side.

Traba bridge was surveyed in order to assess its state of conservation and to verify the hypothesis about the existance of a fifth arch within the structure according to the bibliography (Alvarado et al., 1989).

4.2.2.1.- GPR SURVEY

Previously, a topographic survey along the bridge was carried out with a total station model Leica TCR110 for later correction of GPR data for topography.

Data acquisition

This bridge was surveyed using 250 and 500 MHz shielded antennas following the common methodology developed for this dissertation. Two longitudinal parallel profiles were acquired in opposite directions along the bridge. Survey parameters with the 250 MHz antenna were: 5 cm in-line spacing, time window of 200 ns, and 567 samples per

trace, whereas with the 500 MHz antenna the following parameters were selected: 2 cm in-line spacing, time window of 100 ns, and 678 samples per trace.

Processing flow

Reflex W software was used for data filtering, applying the following processing sequence before interpretation: time zero correction, dewow filtering, gain function, spatial filtering (subtracting average), band-pass filtering (butterworth) and topographic correction. The tilt of the antenna correction was not necessary since this bridge has a near horizontal profile and the effect would be very fine.

Results and interpretation

The best results were obtained with the 250 MHz antenna, having sufficient pulse energy to reach the foundations of the bridges and an adequate resolution to distinguish different inner features.

Observing the processed radargram obtained with the 250 MHz antenna (Fig. 4.90A), the reflections due to the arch-air and air-water interfaces are easily identified, although it is possible to distinguish a severe attenuation of the signal in the first and third arches. This effect was probably caused by the presence of filling materials which are different from the original ones and that were used for restoration according to the historical references (Alvarado et al., 1989). It is important to notice that a reflection pattern can be differentiated over the two restored arches in the form of consecutive small hyperbolas (Fig. 4.90B), more noticeable in the first arch in this particular profile. This effect was most likely generated by reinforced concrete, which could also be an important cause of the signal attenuation previously mentioned. A similar signal response was observed by other authors owing to the use of rebar in a concrete layer (Lorenzo, 1996).

Another interesting reflection is located at the beginning of the radargram shown in Figure 4.90B; this might be generated by an ancient profile of the bridge more pronounced than the present one. Despite the fact that there are no references to the existence of this former pointed profile, similar reflection patterns have been identified in other bridges in which a change in the original profile was documented (Solla et al., 2008a). On the contrary, several historical references (Alvarado et al., 1989), support the existence of a fifth arch inside the Traba bridge located at the right upstream margin, at the end of the radargram in Figure 4.90, although in the GPR data there was no clear evidence of this.

In an underwater inspection carried out a few days after the GPR survey, a cavity was found in the second pier of the bridge from the left margin upstream (Fig. 4.89). Observing the radar data obtained (Fig. 4.90A), this fault could be correlated with an anomaly identified in the same pier and interpreted in Figure 4.90B as a probable void location.

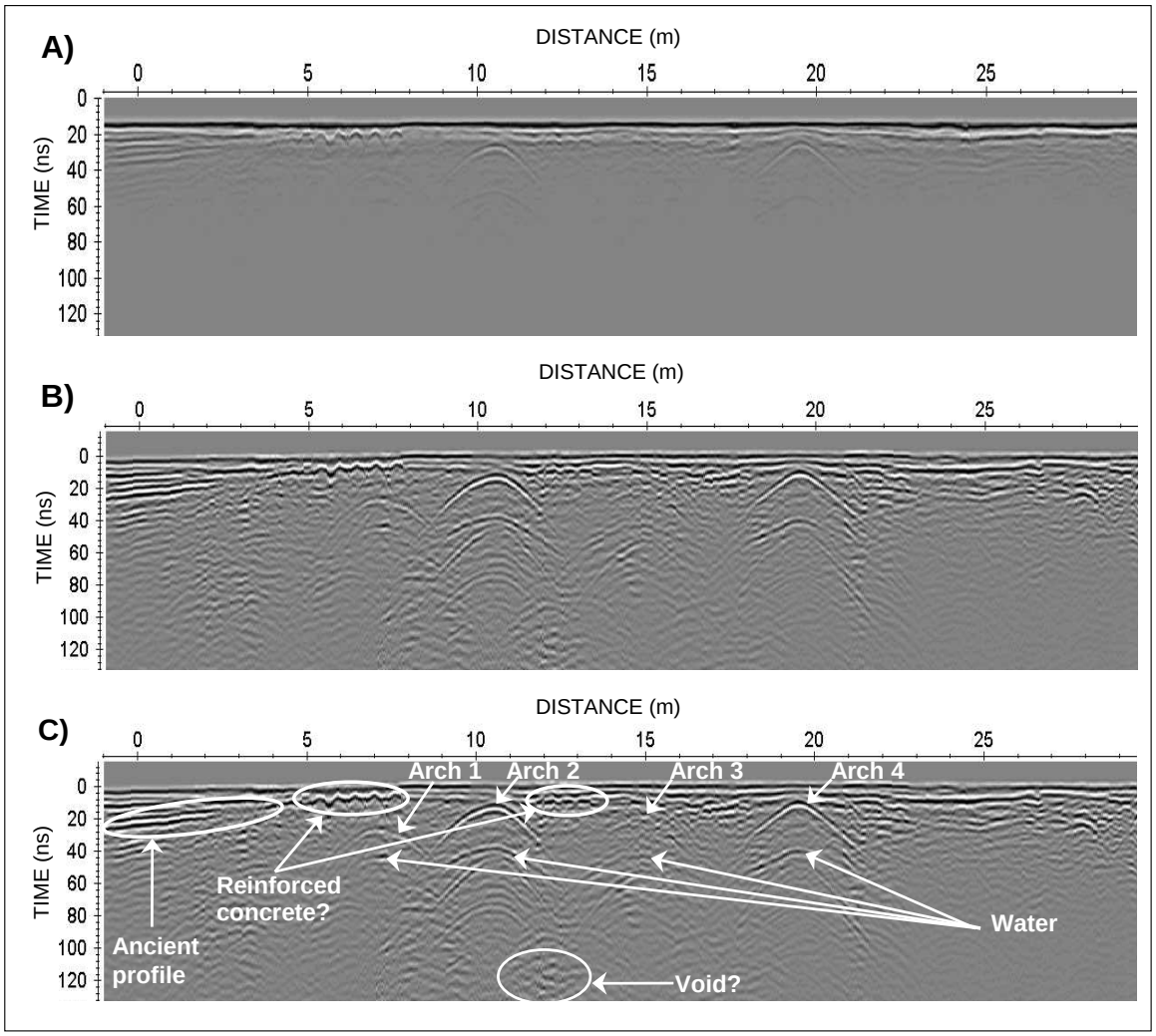

Figure 4.90.- Radargram acquired with the 250 MHz antenna. A) Raw data, B) processed data and C) interpretation of the main reflectors detected.

Utilizing the structural dimensions provided by laser scanning (Table 4.38), it was possible to estimate the signal velocities in different zones of the bridge, ranging from 7.25 to 11.05 cm/ns. Due to the asymmetric reflection patterns generated in the arch-air interfaces of the second and fourth arches produced by their gothic geometry, the signal velocities for these cases were calculated by adaptation of the diffraction hyperbola for each half of the reflection according to the procedures described in section 3.2. The typical average velocity of a GPR pulse in dry masonry is reported in the literature as 14.0-15.0 cm/ns (Colla et al., 1997b; Maierhofer et al., 2003a). Thus, the velocities found in this case were significantly lower, which could indicate moisture within the structure. The presence of

vegetation and lichens in the stonework of the bridge may be related to this possible moisture content inside the Traba bridge (Fig. 4.91); it may also be a consequence of the void identified in the GPR data acquired.

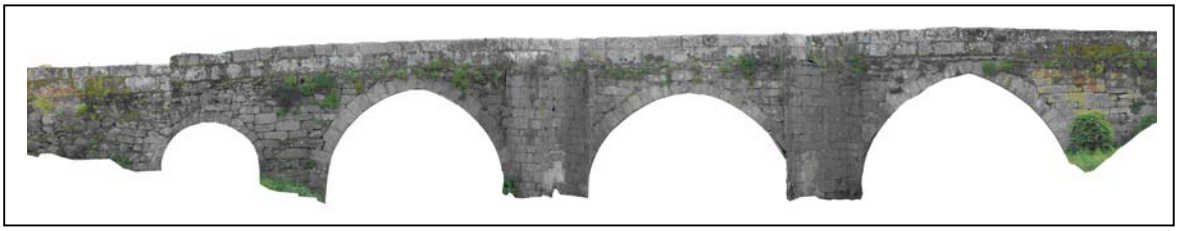

Figure 4.91.- Orthophoto of the upstream wall generated by laser scanning data.

Arches	1	2	3	4
Pathway-arch distance (m)	0.97	0.14	0.58	0.17
Ring stone thickness (m)	0.37	0.52	0.39	0.36
Arch-water/ground distance (m)	2.56	3.80	3.73	4.39
Distance between keystones (m)	6.79	8.67	9.02	

Table 4.38.- External measurements of Traba bridge geometry.

4.2.2.2.- FDTD MODELLING

To verify the radar results, FDTD models were developed simulating the presence of a void in one of the piers. The synthetic model shown in Figure 4.92 represents the best correlation obtained with the GPR data. This model was elaborated by simulating the three main arches and the existence of a void with characteristics similar to the one found (Fig. 4.92B). The electromagnetic properties assumed for the media characterization are detailed in Figure 4.92A according to the values proposed by previous authors (Table 2.2).

Observing the synthetic radargram generated (Fig. 4.92C), the existence of a void in the pier can be deduced from a strong reflection due to the high dielectric contrast between filling material and water. However, this effect is not easily appreciated in the radar results due to the confluence of many reflections –multiples, corner reflections and reflections from the foundations and filling material between the arches– which made the identification of the void difficult (Fig. 4.90B).

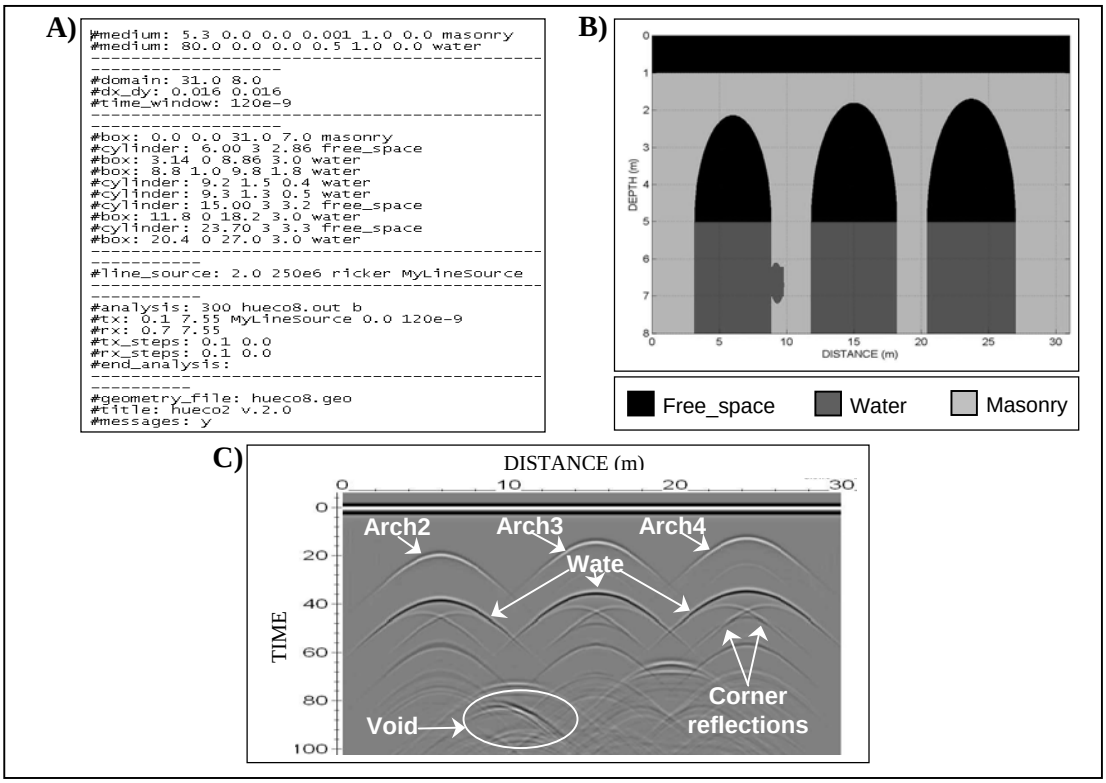

Figure 4.92.- FDTD model showing the effect produced by the existence of a void in one of the two piers. A) Input file, B) model and C) synthetic radargram obtained.

Moreover, another numerical model was created to simulate the habitual reflection pattern produced by reinforced concrete (Fig. 4.93).

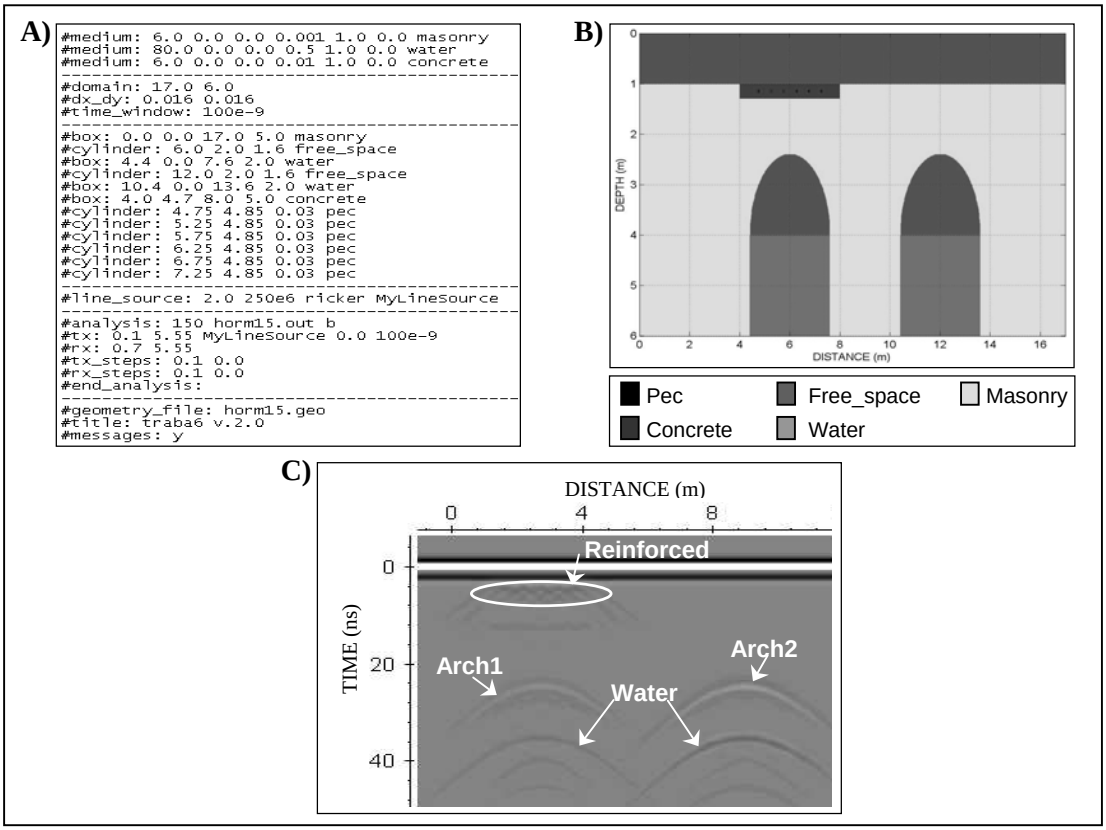

Figure 4.93.- FDTD model illustrating the reflection pattern produced by a reinforced concrete slab. A) Input file, B) model and C) synthetic radargram obtained.

The input file for this model and the electromagnetic properties assumed for the materials are shown in Figure 4.93A. Figure 4.93B illustrates the image generated from the information in this geometry file, simulating a reinforced concrete slab placed above the first arch containing 30 milimeter rebars. Observing the synthetic radargram acquired (Fig. 4.93C), it is possible to identify a signal response similar to the one recorded in the real radar data (Fig. 4.90C).

4.2.2.3.- DISCUSSION AND CONCLUSIONS

GPR investigations employing 250 and 500 MHz antennas were carried out on the medieval Traba bridge. This technique was shown to be useful in identifying the construction details as well as the modifications caused by restoration tasks over time.

From an archaeological point of view:

A slightly sloping constant reflector on the left margin of the bridge has been was identified. The geometry and size of this reflection informed us about the probable medieval profile of Traba bridge. This information can be of interest to historians owing to the fact that currently there are no references to the existence of this former pointed profile. As well, despite the existence of historical references supporting the hypothesis of the presence of a fifth arch located at the right margin upstream of the actual structure, the GPR data did not show clear evidence of this. Both interpretations have revealed interesting information for civil engineers engaged in developing future conservation and restoration tasks.

From a historical point of view:

The severe attenuation observed for the first and third arches, as well as their differing geometries in relation to the others, informed us about the execution of restoration or reconstruction tasks on both arches. Therefore, this attenuation was probably caused by the presence of different filling materials than the original ones that were used for restoration according to the historical references (Alvarado et al., 1989). Moreover, it was possible to identify, over both restored arches, the presence of modern materials such as reinforced concrete, which is frequently used in pathway construction for reinforcement and protection. The FDTD models showed their effectiveness in verifying the existence of

these materials in these locations, which may be the cause of the previously mentioned signal attenuation.

From a civil-structural point of view:

GPR surveying detected an isolated reflection close to the foundation of the second pier which was correlated with the existence of a cavity in the same location according to the observations of an underwater inspection carried out a few days after GPR survey. It would be very complicated to relate this reflection to the existence of a cavity without the additional information obtained. FDTD modelling was used to corroborate this fault and the synthetic radargram created yielded a good correlation with GPR data. Moreover, the moisture content detected by GPR was likely a consequence of this void as well as the presence of cracks or hollows in the stonework of the Traba bridge.

Although a GPR survey with the 500 MHz antenna was performed, the reflections from the inhomogeneous filling material between arches resulted in a complex identification of cracks and voids in the stonework. This is an interesting aspect to explore because it can provide useful information for civil engineers in developing strengthening measures. Consequently, a deep survey using a higher frequency antenna is required to obtain further information about possible faults in the structure. Additionally, the identification of the cavity in the second pier was not easily appreciated by observing the original radargram, probably due to the confluence of many reflections such as multiples, corner reflections, and reflections from the foundations and filling material between arches. Therefore, a 3D GPR survey would be useful to analyze the continuity of this cavity along the transverse direction of the pier as well as its dimensions.

4.2.3.- BIBEI BRIDGE

This is a roman bridge close to Quiroga council across the Bibei river (Fig. 4.79). It presents three barrel arches of 6.09-18.51-8.77 meters span (Fig. 4.94).

Historical references inform about a possible restoration of the first arch from the left margin to the right margin in the upstream side in the 19th century (Durán, 2005). As well, the pathway was filled to get a horizontal profile as a consequence of the restoration task carried out in the middle of the 20th century (Durán, 2005).

Figure 4.94.- General view of the Bibei bridge from the upstream side.

Bibei bridge was surveyed for evaluating the effectiveness of GPR in order to reach the bridge foundations when the structure presents high dimensions as well to obtain information concerning to the shallower filling material.

4.2.3.1.- GPR SURVEY

Data acquisition

This bridge was surveyed with 250 and 500 MHz shielded antennas following the common methodology carried out. Two longitudinal parallel profiles were acquired in opposite directions along its whole pathway. Survey parameters with the 250 MHz antenna were: 2 cm in-line spacing, time window of 220 ns, and 567 samples per trace, whereas with the 500 MHz antenna the following parameters were selected: 2 cm in-line spacing, time window of 100 ns, and 568 samples per trace.

Processing flow

Reflex W software was used for data filtering, applying the following processing sequence before interpretation: time zero correction, dewow filtering, gain function, spatial filtering (subtracting average) and band-pass filtering (butterworth).

Results and interpretation

Utilizing the structural dimensions provided by laser scanning (Table 4.39), it was possible to estimate the signal velocities in different zones of the bridge, ranging from 8.5 to 13.6 cm/ns.These were calculated according the procedures described in section 3.2. The typical average velocity of a GPR pulse in dry masonry is reported in the literature as 14.0-15.0 cm/ns (Colla et al., 1997b; Maierhofer et al., 2003a). Thus, the velocities found were significantly lower, which could indicate moisture in the structure. The presence of vegetation growing in the stonework of the Bibei bridge (Fig. 4.95), may be related to this possible moisture content inside the structure.

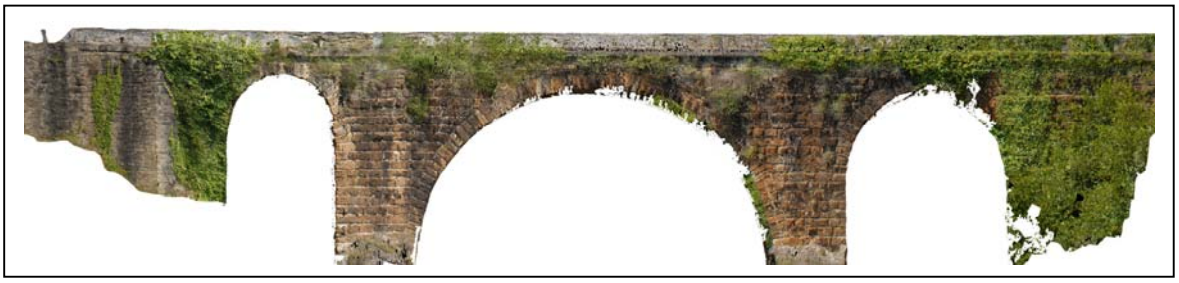

Figure 4.95.- Orthophoto of the upstream wall generated by laser scanning data.

Arches	1	2	3
Pathway-arch distance (m)	0.93	1.10	1.37
Ring stone thickness (m)	0.55	0.90	0.80
Arch-water/ground distance (m)	13.40	17.20	16.97
Distance between keystones (m)	16.85	17.88	

Table 4.39.- External measurements of Bibei bridge geometry.

In the processed radargram acquired with the 250 MHz antenna (Fig. 4.96B), it was possible to identify the reflections from the arch-air, air-water and air-ground interfaces as well as the typical corner reflections generated in these arches (Martinaud et al., 2004). An interesting pattern of reflections is the one just above the first arch, probably caused by the

presence of building materials which are different than the original ones (Fig. 4.96C). These materials may have been used for a restoration task as previously mentioned. Thus, this interpretation ratifies the hypothesis espoused by the historical references (Durán, 2005). Also, it was possible to distinguish a reflection along the arches probably caused by a pathway restoration. The Bibei bridge could have been emptied and consequently refilled with different filling materials than the original ones. This event is evidenced in the interpreted radargram as a stone layer (Fig. 4.96C). Moreover, a continuous, slightly pointed reflector was observed at each margin of the bridge, which can be caused by the supposed ancient profile of the Bibei bridge. This pointed profile could have been altered with the restoration task for pathway leveling carried out in the middle of the 20th century to obtain a horizontal profile, as mentioned in the specialized literature (Durán, 2005).

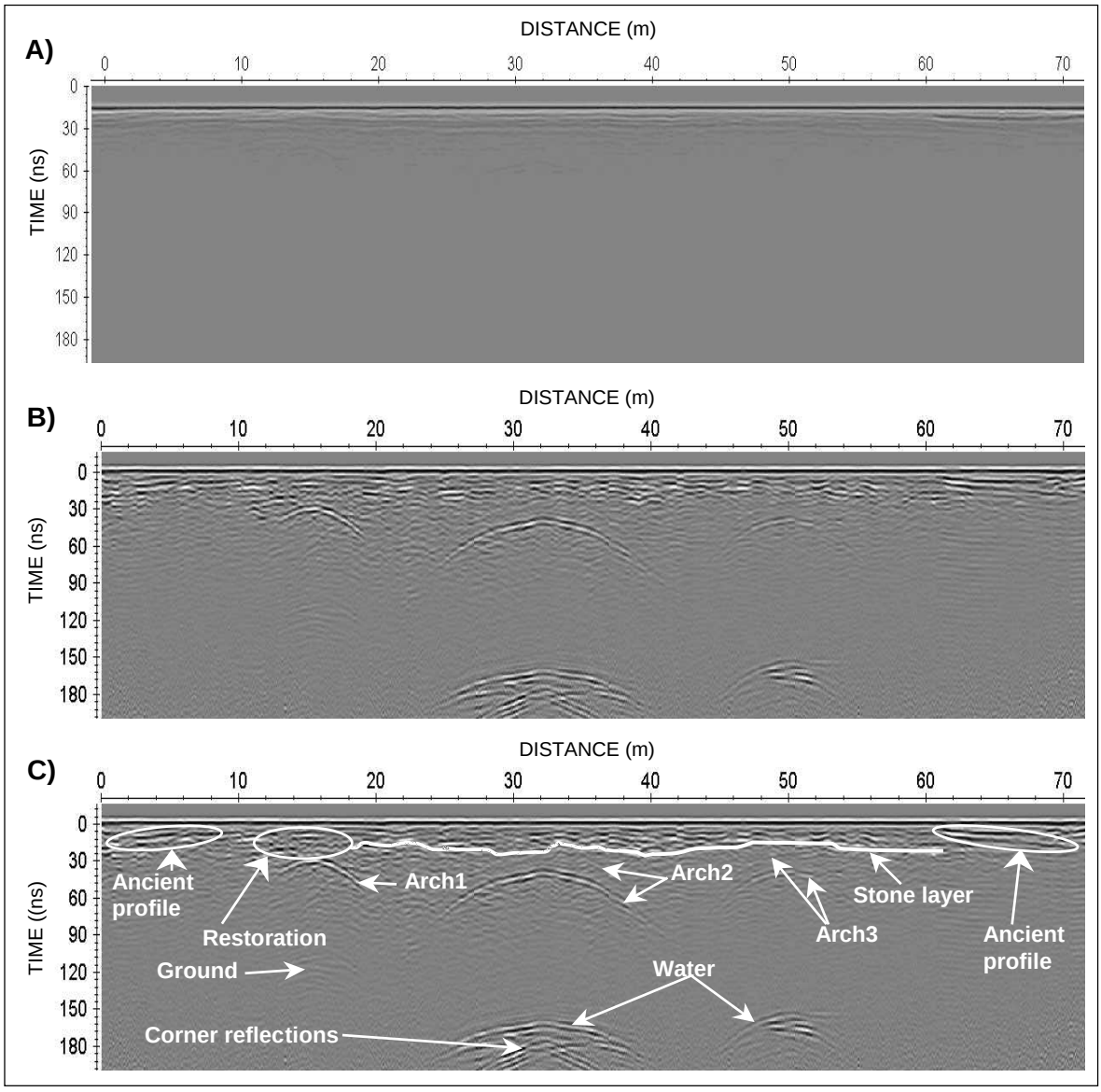

Figure 4.96.- Radargram acquired with the 250 MHz antenna. A) Raw data, B) processed data and C) interpretation of the main reflectors detected.

Other relevant information obtained was the ring stone thickness for the second and third arches, where it was possible to observe that the filling-stone interface was detected as well as the stone-air interface, with a consequent shift in the signal polarity (Fig. 4.96C). The stone-air interface was characterized by a rather strong signal due to the strong contrast between the dielectric properties of the stone and air media. However, the polarity of the signal in the filling-stone interface is not as evident due to the small dielectric contrast between media and probable irregularities in the interface such as the presence of voids or the usual internal staircase shape of the ring stones.

The reflection obtained from the filling-stone interface allowed us to estimate the pulse velocity in the filling situated over the arch. Figure 4.97 shows the velocity values for granite and filling media estimated by adapting a hyperbolic for the reflections from the filling-stone and stone-air interfaces corresponding to the first and second arches. The signal velocities for masonry were 13.46 and 13.06 cm/ns respectively (Fig. 4.97A), whereas the corresponding values for the filling were 12.24 and 12.36 cm/ns, respectively (Fig. 4.97B).

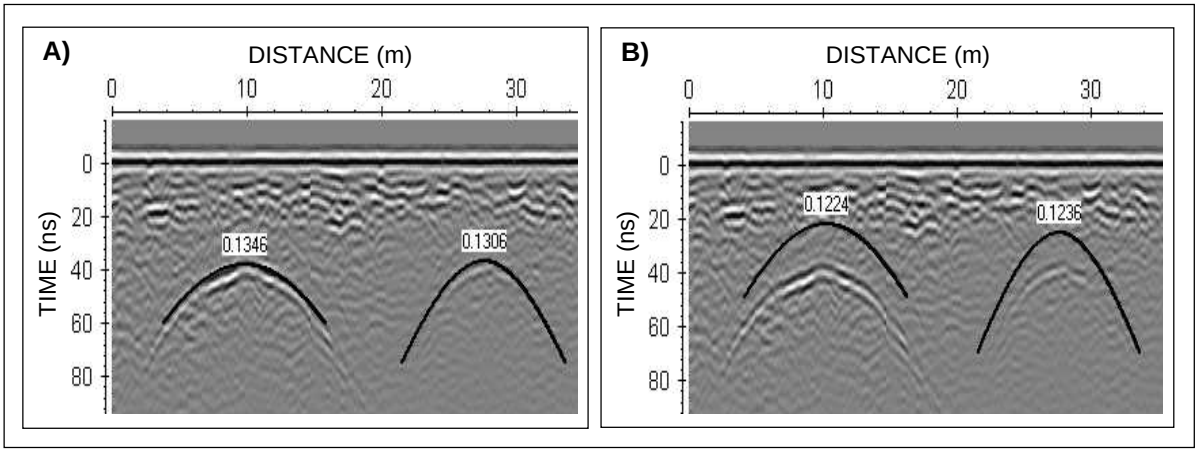

Figure 4.97.- Velocity determination by fitting a hyperbolic shape for the second and third arches of Bibei bridge. A) signal velocity for granite and B) signal velocity for filling.

Considering a signal velocity for masonry of 13.0 cm/ns, the ring stone thicknesses for the second and third arches at the keystone location are 1.26 and 0.91 meters, respectively, as shown in Figure 4.98. These values resulted in an error around 10-30% relative to the actual dimensions as measured from the exterior from the accurate external geometry of the bridge acquired with laser scanning methods (0.90 and 0.80 m, respectively (Table 4.39)). These differences between the thickness values obtained from GPR data and

accurate external geometry can be related to the usual internal staircase shape of the ring stones.

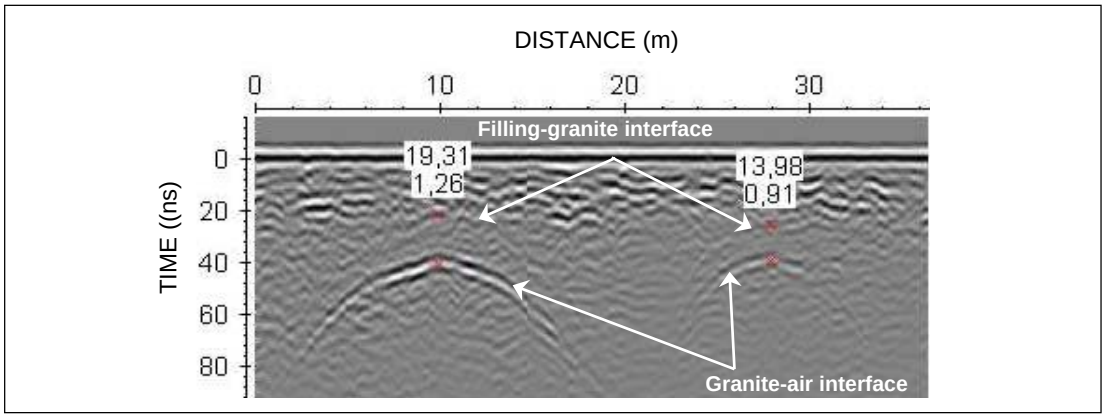

Figure 4.98.- Ring stone thickness for the second and third arches of Bibei bridge at the keystone location considering an average signal velocity of 13 cm/ns.

4.2.3.2.- FDTD MODELLING

Synthetic models were created simulating the ring stone thickness to evaluate the signal polarity in the filling-stone and stone-air interfaces. The accurate geometry provided by laser scanning was used to elaborate these models. The FDTD model shown in Figure 4.99 represents one of the best approximations to the real data.

The model was created assuming a permittivity value of 7 for filling and 11 for granite stone according to the values proposed by other authors (Table 2.2). The other electromagnetic properties assumed are detailed in Figure 4.99A. The ring stone thickness was assumed to be granite ashlars.

The synthetic radargram generated shows the reflection at the granite stone-air interface as well as the one generated at the filling-granite stone interface (Fig. 4.99C). The opposite signal polarity and the strongest signal in the stone-air interface are easily identified. However, this effect was not clearly appreciated from the real data (Fig. 4.96) probably due to the confluence of many reflections from the inhomogeneous filling material used. Also, an internal anathyrosis (irregular internal structure in the granite ashlar) together with the internal staircase shape of the ring stones can produce erratic reflection patterns making the data interpretation difficult.

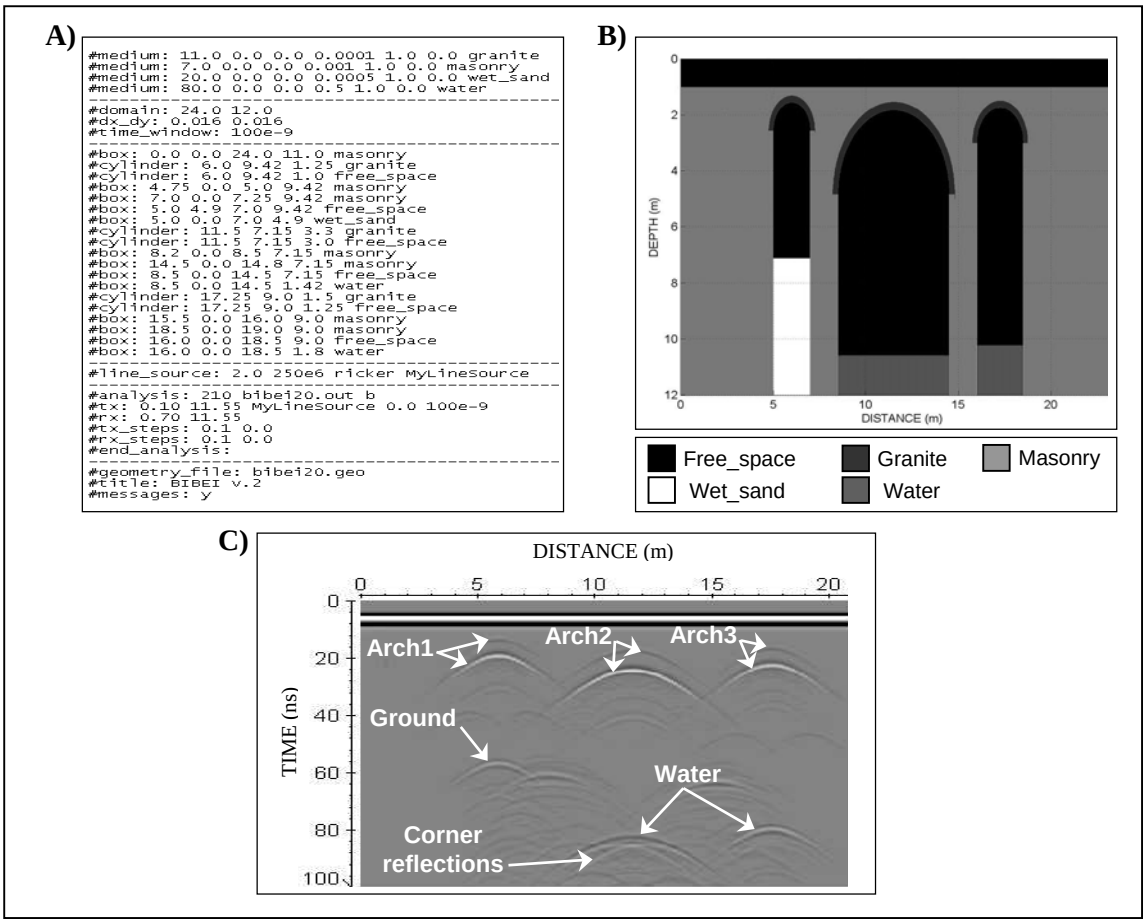

Figure 4.99.- FDTD model simulating the ring stone thickness. A) Input file, B) model and C) synthetic radargram obtained.

4.2.3.3.- DISCUSSION AND CONCLUSIONS

Although the GPR results did not reveal information about the bridge foundations, the 250 MHz antenna have provided enough energy to reach the river level despite the height of the Bibei bridge.

From an archaeological point of view:

A slightly sloping constant reflector was identified at both margins of the bridge. The geometry of this reflection informed us about an ancient pointed profile for this bridge. In agreement with this interpretation, there are historical references concerning the pathway leveling to obtain a horizontal profile during the restoration tasks carried out in the middle of the 20th century (Durán, 2005). This information can be valuable for historians, as the historical pointed profile of Bibei bridge is not well documented in the specialized literature. Also, a better understanding of the internal structure of this bridge can be useful for engineers in terms of future conservation tasks.

From a historical point of view:

It was possible to identify a continuous reflection over the arches, probably caused by an emptying and later refilling with different filling materials. This event, together with the continuous, slightly pointed reflector interpreted as an ancient profile, informs us about the execution of some pathway restoration tasks on the Bibei bridge. Moreover, a complex pattern of reflections above the first arch was distinguished. This could have been produced by the presence of filling materials differing from the original ones. It was possible to observe clearly different signal behavior for this location in relation to the other two arches. Thus, GPR data interpretation allowed us to ratify the hypothetical reconstruction of the first arch mentioned in the specialized literature (Durán, 2005).

From a civil-structural point of view:

The ring stone thickness was identified for the second and third arches. This value resulted in information of interest to civil engineers in terms of durability and stability and in the design of preservation guidelines. It was possible to determine differences between the thickness value at the keystone location obtained from GPR data and that measured from the 3D model of the bridge constructed by laser scanning methods. These differences informed us about the internal staircase shape of the ring stones. Also, comparing the real data to the synthetic radargram created, it was possible to distinguish a finer signal in the GPR data for the filling-stone. This effect may also have been caused by the internal staircase shape of the ring stones. Moreover, this could be produced by the presence of voids in the filling-stone interface. Additionally, the existence of voids in the structure could be a consequence of the moisture content detected by GPR through the estimated velocity values. While the 500 MHz antenna did not reveal additional information, an exhaustive research using higher frequency antennas is required for further research to identify probable cracks and voids in the bridge.

The non-identification of the ring stone thickness for the first arch can be explained by the presence of an inhomogeneous filling over the arch used for reconstruction tasks. The complex reflection pattern produced by these inhomogeneities together with the internal staircase shape of the ring stones prevented identification of the reflection from the filling-stone interface.

4.2.4.- LUGO BRIDGE

A roman bridge over the Miño river in the city council of Lugo (Fig. 4.79). It has eight gothic or barrel arches from 5.6 to 10.4 meters span (Fig. 4.100). Although all of them have granitic ring stones, some of these arches have a granitic vault (1, 2, 4, 7 and 8 from the left margin in the upstream side), whereas the other ones have a slater vault (Durán, 2005). The existence of different building materials into the stonework of Lugo bridge can be produced by several restorations and reconstructions performed throughout historical time (Alvarado et al., 1989).

Figure 4.100.- General view of the Lugo bridge from the downstream side.

This bridge had a medieval double slope until the end of the XIX century as shown in Figure 4.101. Due to this last repair intervention carried out in 1898, its pathway got wider by using cantilever metal parapets (Durán, 2005). These metallic structures are leaned in pilasters from the buttresses.

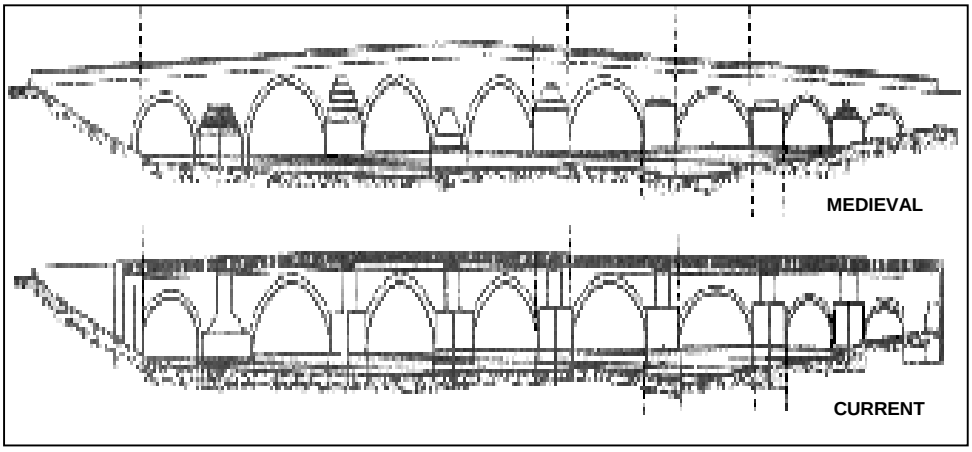

Figure 4.101.- Profile evolution in Lugo bridge throughout the time (*From Durán, 2005*).

This bridge was selected in order to evaluate the internal state of conservation since it supports an intensive traffic road.

4.2.4.1.- GPR SURVEY

Data acquisition

The assessment was carried out following the common methodology developed for this dissertation and described in subchapter 3.1. The survey parameters selected were: 2 cm in-line spacing, time window of 210 ns, and 540 samples per trace for 250 MHz antenna, whereas with the 500 MHz antenna the parameters used were: 2 cm in-line spacing, time window of 100 ns, and 677 samples per trace.

Processing flow

Reflex W software was used for data filtering, applying the following processing sequence before interpretation: time zero correction, dewow filtering, gain function, spatial filtering (subtracting average) and band-pass filtering (butterworth).

Results and interpretation

The raw data acquired show the reflections produced by the presence of several transverse reinforcing beams employed for supporting the metal parapet structures mentioned (Fig. 4.102B).

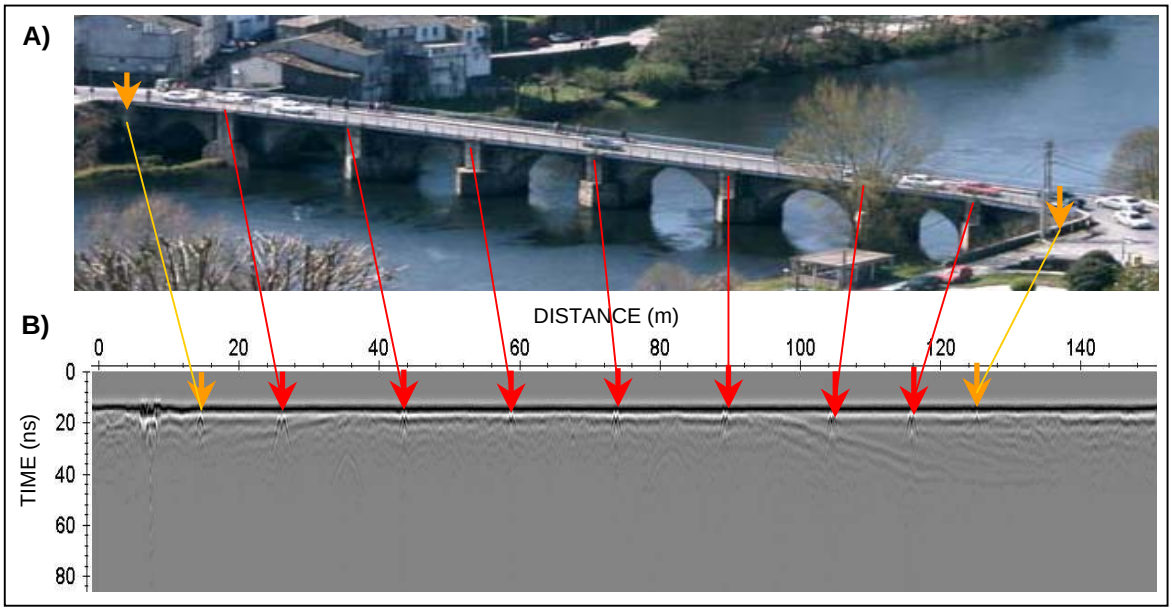

Figure 4.102.- Identification of reinforcing beams. A) Location on the structure from the downstream side and B) Association to the raw-data obtained with the 250 MHz antenna.

Figure 4.103 illustrates the processed radargram acquired as well the interpretation of the main reflectors detected. Observing the processed radargram, it is possible to appreciate

different GPR signal responses over the arches along the structure (Fig. 4.103B). Clear signal attenuation is observed over some arches. Thus, the reflections from the arch-air interfaces for the first, fifth and eighth arches were nearly completely attenuated, although they are placed at the same level as the others. The different signal behavior could be an indication of the presence of several building materials in the stonework of the Lugo bridge, as well the existence of different filling material over the arches. This effect was likely caused by several reconstructions and restorations performed throughout its lifetime (Durán, 2005). The following step would be identifying the materials involved. According to historical references, the stonework of this bridge is composed of granitic and slate materials (Durán, 2005). The signal attenuation produced can be explained by the presence of these materials over the arch because the vaults built of slater materials, such as arches 5 and 6, presented more attenuation than the other ones built with granitic materials (arches 4 and 7). In these sense, the numerical simulations described in the following can provide suitable information to corroborate this hypothesis.

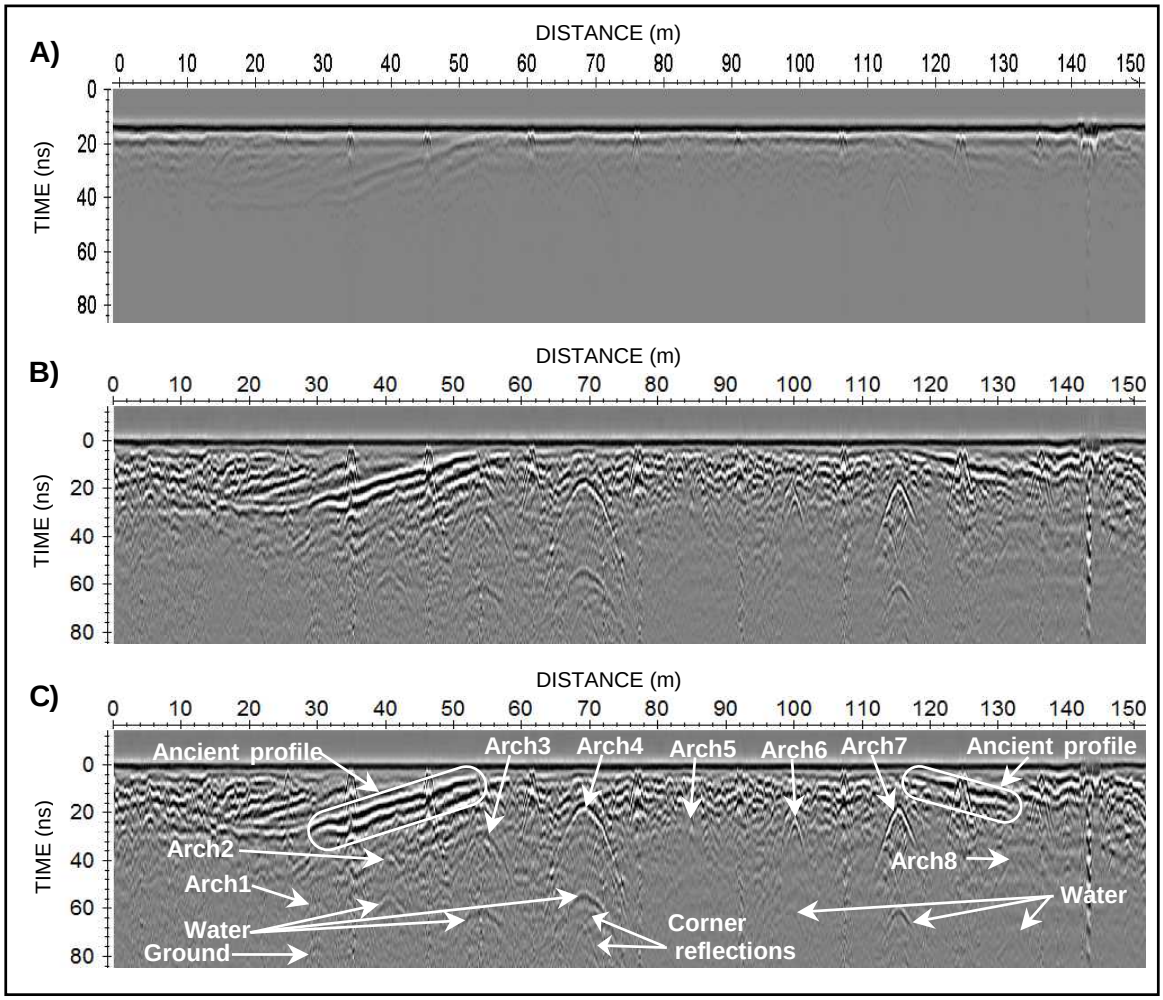

Figure 4.103.- Radargram acquired with the 250 MHz antenna. A) Raw data, B) processed data and C) interpretation of the main reflectors detected.

Besides an obvious longitudinal discontinuity in the filling materials, inhomogeneities can exist in a single material. Therefore, the irregular shape of the reflection generated by the arch-air interface for the fourth arch could be a consequence of this lack of homogeneity (Fig. 4.103B). This inhomogeneity resulted in several GPR signal velocities over the arch. In addition, different reflection patterns are observed depending on the geometry of the arch. Gothic arches (e.g., arches 6 and 7) produce a narrower reflection than barrel arches (such as arches 3 and 4), as shown in Figure 4.103C.

An interesting reflection was generated by an ancient profile of the bridge more pronounced than the present profile (Fig. 4.103C). The existence of a medieval profile of the Lugo bridge is documented in the specialized literature (Durán, 2005). Analyzing the processed radargram, this pointed profile was filled at both margins of the river to yield a horizontal pathway, as illustrated in Figure 4.103. The filling material used for leveling could also have produced the signal attenuation observed for the first, second and eighth arches (Fig. 4.103C). Furthermore, the typical corner reflections generated in this kind of arch were identified under the fourth arch (Martinaud et al., 2004).

4.2.4.2.- FDTD MODELLING

The FDTD simulations were elaborated for analyzing the influence of different filling materials on the signal response over the arches. According to some historical references and the construction materials present in the stonework, many simulations were tested to obtain the best fit with the bridge radargrams. The most realistic approximation to the GPR results was obtained using granitic and slater filling materials. The values for the permittivity and conductivity of the filling were selected from the literature (Table 2.2).

The FDTD model in Figure 4.104 shows one of the best correlations with the actual data. A two span bridge was simulated considering granitic and slater fillings over each arch (Fig. 4.104B). The permittivity values used for this model were 6 and 8, respectively (the other electromagnetic properties introduced into the model are shown in Figure 4.104A). Additionally, the arch rings of both arches were assumed to be granite ashlars. The result is a synthetic radargram showing a slight signal attenuation for the slater filling compared to the granitic filling (Fig. 4.104C). Thus, it allowed us to assume that the areas filled with

granitic materials provided less attenuation than those filled by slater filling. Most importantly for our study, it confirmed that the differing signal behavior in different fillings facilitates the mapping of those areas in bridges usually associated with reconstruction or restoration tasks.

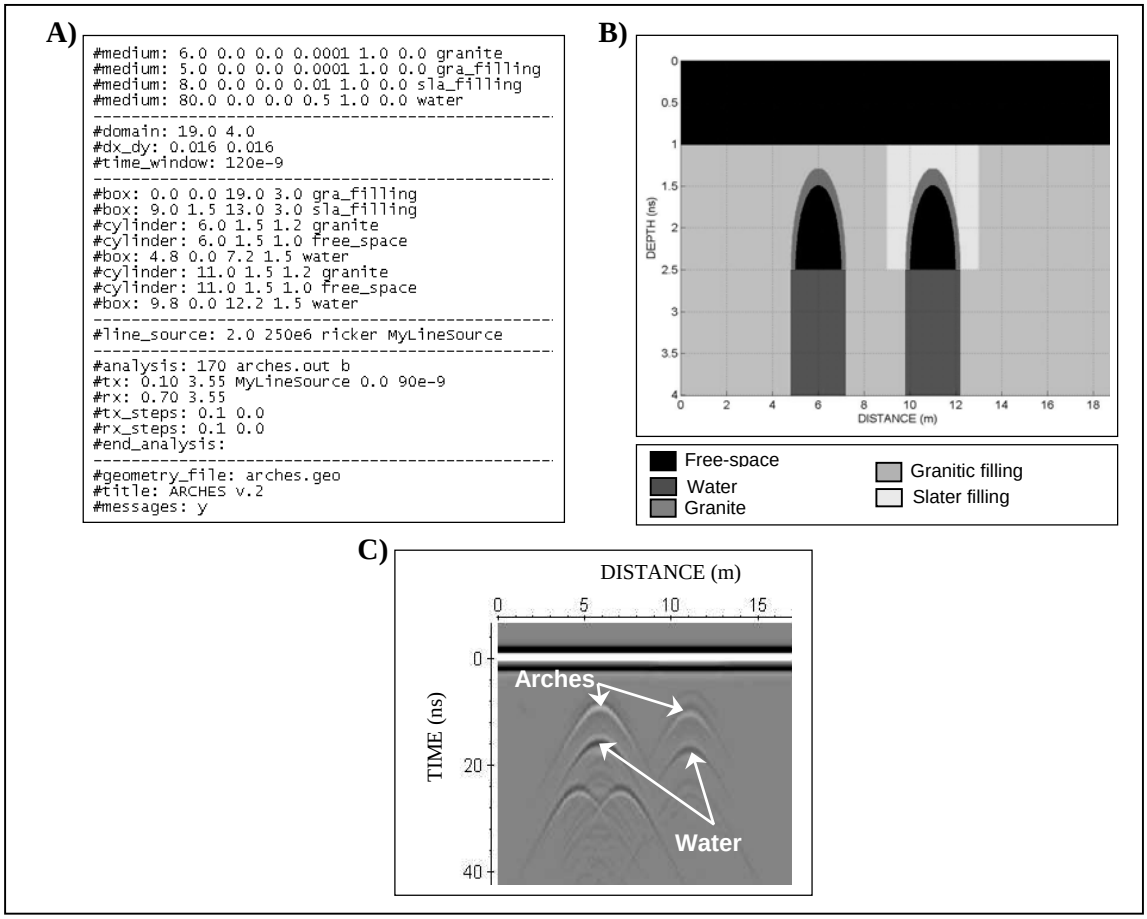

Figure 4.104.- FDTD model simulating the different signal response for granitic and slater materials. A) Input file, B) model and C) synthetic radargram obtained.

4.2.4.3.- DISCUSSION AND CONCLUSIONS

GPR was confirmed to be an effective NDT method to reveal inner bridge construction details and modifications over time. At first glance, this bridge presents a relatively homogeneous external geometry. However, the results acquired showed significant heterogeneity in the structure.

From a historical point of view:

The GPR data interpretation together with the synthetic models generated revealed the presence of diverse areas in the bridge depending on their different fills, especially, above

some arches. The most probable source for this inhomogeneity within the structure would be related to several restoration and reconstruction tasks throughout its history.

This hypothesis was corroborated by historical references. Although this information is perfectly documented, it is interesting to verify the relevant information provided by GPR.

From a civil-structural point of view:

The results acquired showed a different GPR signal response depending on the medium of propagation. The signal attenuation observed for some arches could be produced by the presence of slater materials over their vaults and a different filling material employed for leveling which is different than the original one. FDTD modelling showed its capabilities as an important interpretation tool. Thus, the synthetic models created displayed different signal behaviors for granitic and slater materials, and it is reasonable to assume that granitic arches provided a different signal response than slater arches. The existence of different building and/or filling materials over an arch can generate an irregularly shaped reflection pattern generated at the arch-air interface, making it difficult to estimate the velocity by hyperbolic fitting. This is produced by the confluence of several GPR signal velocities over the arch. In these cases, the velocity for the arch-air interface was determined by adapting a hyperbolic shape for each half of the reflection as described in section 3.2.4. The same procedure would be followed for the velocity determination of pointed arches.

Although GPR can usually distinguish between different subsoil zones depending on their composition, the specific identification of the materials involved is more difficult. Furthermore, the detection and accurate positioning of cracks, hollows or faults (some of them visible on the surface of the arches and piers) becomes challenging due to the significant filling heterogeneity within the structure of the bridge. Thus, an exhaustive study using higher frequency antennas is required for further research. The main purpose here was to define different areas within the bridge by their homogeneity in terms of signal response. The inhomogeneous results in many reflections and diffractions generally presented a very difficult data interpretation. Observing the GPR results acquired, it is possible to select several locations of interest at which to perform an endoscopy to obtain a general view of the materials involved. The information obtained will allow for an exhaustive data interpretation. The combination GPR-endoscopic survey is very useful to reduce invasive interventions if the endoscopy is perfectly set. This is an interesting aspect

to advance because it is important for civil engineers to analyze the internal state of conservation of these historical structures.

From an archaeological point of view:

It was possible to identify a slightly sloping constant reflector at both margins of the bridge. The geometry, condition and size of this reflection allowed us to conclude that it must be the ancient profile of this bridge. Additionally, GPR results informed us about its filling at both river margins to obtain the current horizontal profile. The medieval pointed profile of the Lugo bridge is perfectly documented in the literature (Durán, 2005). However, no archaeological survey or endoscopy had been made until now to verify the documentation. This may represent noteworthy information in taking steps for conservation and restoration.

5

General discussion

The main purpose of this thesis was to evaluate the viability and effectiveness of GPR as an NDT method for obtaining internal information in historical bridges from three points of view: historical, structural and archaeological. A total of 36 historical bridges were chosen throughout the whole Galician territory according to the selection criteria described in Chapter 3. As a general conclusion, the results presented confirmed that GPR is an effective NDT method for masonry arch bridge inspection, revealing construction details, modifications and problems which have arisen over time.

Additionally, this work attempted to develop an extended methodology to assess masonry arch bridges using GPR. The 250 and 500 MHz antennas were selected to reach the bridge foundations and to obtain information concerning the shallower filling material. These frequencies were selected as an optimum compromise between penetration and resolution. For each antenna, two longitudinal parallel profiles were acquired in opposite directions. Usually, historical bridges present a narrow pathway. Thus, the use of two profiles was assumed to be the most suitable. Sometimes, due to the heterogeneity in materials within the structure it was useful to have two profiles to corroborate the lateral continuity of the reflections detected and verify the subsequent data interpretation. Moreover, the field markers gathered over the keystones of the arches together with the geometric measurements acquired proved useful in performing a preliminary identification of the main reflections, such as those from the arch-air and air-water interfaces.

Several problems were revealed related to GPR field data acquisition. Due to the usual rough stone pathways of the ancient bridges, a previous calibration of the survey wheel

was necessary to obtain suitable radar-trace locations. Moreover, GPR data acquisition could take additional time owing to the fact that some of these structures support intensive road traffic. Sometimes, the great heights of the bridges presented a problem for data acquisition, necessitating the employment of higher peak power or lower frequency antennas. Thus, the unshielded 200 MHz antenna or shielded/unshielded 100 MHz antenna could be used to reach the bridge foundations. For this work, the best alternative was the unshielded 200 MHz antenna, which was sufficient to perform the structural diagnostics in these cases without a loss of resolution. Additionally, topographic correction revealed its importance for improving the accuracy of imaging subsurface features in pointed bridges. However, the antenna-tilt correction was not highly relevant given the slight variations in elevation of these structures; this correction is more recommended for abrupt topographies. Although GPS seemed to be the best option to collect the (x,y,z) data due to its centimeter accuracy and real-time positioning, it showed considerable limitations in achieving high accuracy in data processing, such as those related to the GPS antenna position and stability during GPR-GPS data collection. The GPS stability can be an issue during data acquisition due to the typical rough stone pathway of the historical bridges. In addition, historical bridges are often situated in wooden areas which impede good coverage for continuous RTK precision, reducing GPS data accuracy. In contrast, topographic surveys by means of a total station coupled with field markers and expeditious measurements proved to be a fast and simple method to provide suitable information.

The results showed how just a simple but careful data processing allowed for the extraction of significant information concerning the internal structure of the bridge, which made the GPR data interpretation easier. Besides the experience of the interpreter and their knowledge of the techniques required to obtain good results, it is important to understand the construction details of masonry arch bridges. In this way, interpretation of these data by historians, archaeologists and engineers specialized in this topic can be very useful. Additionally, the existing literature on the matter can provide relevant information to corroborate the interpretations made.

Several difficulties arose in signal velocity determination related to the presence of different fillings on either side over an arch or inhomogeneities in a single material as well as those caused by the usual internal staircase shape of ring stones and by ring separation. As a consequence, irregularities in the reflection patterns obtained from the arch-air interfaces were observed. To solve these difficulties, the velocity was estimated by

adapting a hyperbolic shape for each half of the reflection, resulting in two different signal velocities. Moreover, the segmental and gothic geometries assumed to exist in ancient times also provided irregular shapes; in such cases, the velocity was determined by the same procedure. It could be worthwhile to perform a survey in the common-mid-point acquisition mode (CMP) to estimate the velocity value, especially in the transverse direction to the bridge. However, this survey can be avoided owing to the typical pointed profile of ancient bridges as well as the difficult analysis produced by the complex inhomogeneity within the structure and the ignorance relating to the different building materials involved. In addition, some modern materials used for restoration such as reinforced concrete and soil-cement can be an important cause of signal attenuation and loss of target resolution, resulting in a difficult data interpretation. Examples of signal attenuation by reinforced concrete were encountered in the Carracedo and Loña bridges, whereas for soil-cement this effect was easily distinguished in the San Alberte and Ourense bridges.

The results revealed notable information from historical, archaeological and civil-structural view points. It was possible to detect and map the remains of restoration tasks performed on the bridges. In this way, reconstruction of the arches was observed in the Lubians and Bibei bridges as well as restoration tasks concerning the pathways of some bridges, as in the cases of the Monforte and Areas bridges. After restoration, these bridges were filled using backfilling materials different from the original ones. Moreover, as in the case of the Lugo bridge, different building materials were identified in the stonework. Sometimes, the existence of a different filling material and inhomogeneities in a single material over the arches were also found. These events were easily recognized by the asymmetric pattern across the two sides of the keystone and the deformations produced by low frequency fluctuations, respectively. Indirectly, this can also inform the surveyor about reconstruction or restoration tasks performed in the past. Additionally, it was possible to identify other interesting aspects from an archaeological point of view, such as the presence of possible hidden arches (as in the San Antón, Monforte and Carmen de Abajo bridges) or a different historical shape of the structure (as in the Lugo, Madalena and Traba bridges). This information may be useful for historians and civil engineers to corroborate the available historical information and to take steps for the preservation and restoration of historical bridges. Also, structural information was obtained such as structural elements for reinforcement (San Antón bridge), the ring stone thickness (Freixo and Bibei bridges) and information about the nature of the foundations (Cernadela, Areas and San Clodio bridges).

A probable cavity was even detected in one pier of the Traba bridge. Other relevant structural information obtained included the presence of modern materials frequently used in pathway construction for reinforcement in the subsurface of the bridge, such as reinforced concrete (Carracedo and Loña bridges), and soil-cement (A Cigarrosa and Ourense bridges). All this information can be useful for civil engineers in developing strengthening measures. In addition, an accurate signal velocity determination was essential because this value can indicate the presence of moisture in the structure, as in the cases of the Bibei, Traba and San Antón bridges. This moisture content can be related to the existence of cracks and voids within the bridge, which is an important aspect in terms of durability and stability.

The identification of cracks and hollows within the structure by GPR was not possible. This could be a consequence of the confluence of many reflections from the inhomogeneous filling material over and between the arches. Additionally, the river-bed level was not easily distinguishable for any bridge. For this case, the confluence of reflections was more complex because, in this location, there are unwanted reflections from the foundations and the filling between arches, as well as multiples from the arch-air and air-water interfaces and the typical corner reflections generated in these kinds of arches. Moreover, the identification of the ring stone thickness poses a difficult task due to this inhomogeneity. A GPR survey around the internal surface of the arch vault may be an effective way to solve this problem.

Improvements in the understanding and use of this technique applied to masonry structures as well as for GPR data interpretation are required in the near future due to a growing demand in the use of NDT methods in civil engineering. Thus, the FDTD models created in this work provide important additional information for the advanced interpretation of radar data. The proposal contemplates the use of accurate external bridge geometry obtained from photogrammetric or 3D laser scanning methods to design suitable models. An inconvenience in FDTD modelling was encountered when large-scale and realistic models were simulated because excessive computer memory was required. Therefore, further research on synthetic modelling is demanded to yield a better correlation between real GPR data and synthetic results as well as a significant reduction in computational time.

The 500 MHz antenna did not provide information about the existence of cracks or hollows in the structures due to the significant filling heterogeneity within them. Therefore, a

further, deeper study of historical bridges using higher frequency antennas is required to define these kinds of structural faults. A 3D survey could possibly be utilized to detect the presence of cracks and hollows. However, the data acquisition of a 3D mesh can be avoided for the usual rough stone pathways of historical bridges.

The results acquired sometimes revealed interesting structural information. In these cases, further studies are proposed to perform a deeper GPR survey or even a 3D survey to obtain detailed information. It may also be important to verify the continuity of some reflectors as well as their dimensions. Moreover, we would suggest a GPR survey on the spandrel walls of the bridge to obtain additional information such as the thickness of the granite ashlars. Additionally, GPR tomography methodologies placing the antennas on opposite spandrel walls of the bridge are proposed as complementary diagnostic tools to perform an internal evaluation of the filling compaction and moisture content within the structure. It may be interesting to test a combination of GPR with other NDT methods such as infrared thermography, sonic or conductivity, as each NDT method provides different information regarding the physical properties of the masonry structure. Thus, this complementary testing could be useful in detecting and monitoring the presence of cracks or voids in the structure as well as changes in internal moisture content together with inhomogeneity identification and layering within the bridge.

Finally, an extension of the inventory developed here is proposed by attaching more historical bridges in the Galician territory or even presenting additional GPR results obtained with higher and lower frequency antennas.

References

Al-Qadi, I.; Xie, W.; Roberts, R., 2010. Optimization of antenna configuration in multiple-frequency ground penetrating radar system for railroad substructure assessment. NDT&E International, Vol. 43, Issue 1, pp. 20-28.

Alvarado, S.; Durán, M.; Nárdiz, C., 1989. Puentes históricos de Galicia. Colegio Oficial de Ingenieros de Caminos, Canales y Puertos. Xunta de Galicia, Consellería de Cultura e Deportes, Dirección Xeral do Patrimonio Histórico e Documental.

Annan, P., 2003. GPR principles, procedures and applications. Sensors and Software Inc., 192 pp.

Aperio, F., 2008. http://www. aperio.co.uk.

Arias, P.; Armesto, J.; Di-Capua, D.; González-Drigo, R.; Lorenzo, H.; Pérez-Gracia, V., 2007. Digital Photogrammetry, GPR and Computational Analysis of structural damages in a medieval bridge. Engineering Failure Analysis, Vol. 14, pp. 1444-1457.

Bavusi, M.; Giocoli, A.; Rizzo, E.; Lapenna, V., 2009. Geophysical characterisation of Carlo's V Castle (Crotone, Italy). Journal of Applied Geophysics, Vol. 67, Issue 4, pp. 386-401.

Bertram, C.L.; Morey, R.M.; Sandler, S.S., 1974. Feasibility study for rapid evaluation of airfield pavements. Rep. No. AFWL-TR-71-178, U.S. Air Force Weapons Lab., Dayton, Ohio, 38p.

Bhandari, N.M.; Kumar, P., 2006. Structural health monitoring and assessment of masonry arch bridges. Advances in Bridge Engineering, March 24-25, pp. 115-132.

Bień, J.; Kamiński, T., 2007. Damages to masonry arch bridges – proposal for terminology unification. In: Proceedings of 5th International Conference on Arch Bridges (ARCH'07), pp. 341-348.

Binda, L.; Saisi, A.; Tiraboschi, C.; Valle, S.; Colla, C.; Forde, M.C., 2003a. Application of sonic and radar tests on the piers and walls of the cathedral of noto. Construction and Building Materials, Vol. 17, Issue 8, pp. 613-627.

Binda, L.; Lualdi, M.; Saisi, A.; Zanzi, L.; Gianinetto, M., Roche, G., 2003b. NDT applied to the diagnosis of historic buildings: a case history. Structural Faults & Repair.

Binda, L.; Lenzi, G.; Saisi, A., 1998. NDE of masonry structures: Use of radar tests for the characterisation of stone masonries. NDT&E International, Vol. 31, Issue 6, pp. 411-419.

Brink, A.; Maierhofer, C.; Röllig, M.; Wiggenhauser, H., 2002. Application of quantitative impulse thermography for structural evaluation in civil engineering – Comparison of

experimental results and numerical simulations. QIRT. Federal Institute for Materials Research and Testing (BAM).

Buderi, R., 1998. The invention that changed the World: How a small group of radar pioneers won the Second World War and launched a technological revolution. Simon & Schuster.

Bungey, J.H.; Millard, S.G., 1993. Radar inspection of structures. Journal of the Institute of Civil Engineers Structures and Buildings, 99, pp. 173-186.

Carrión, F.J.; Lomelí, M.G.; Quintana, J.A.; Martínez, M., 2003. La evaluación no destructiva de materiales estructurales y puentes. Instituto Mexicano del Transporte, Publicación Técnica No. 231.

Cassidy, N.J., 2005. The Practical Application of Numerical Modelling for the Advanced Interpretation of Ground-Penetrating Radar. In: Proceedings of 3th International Workshop on Advanced Ground Penetrating Radar (IWAGPR'05). pp. 105-112.

Chen, H.W.; Huang, T.M., 1998. Finite-difference time-domain simulation of GPR data. Journal of Applied Geophysics, Vol. 40, pp. 139-163.

Chong, K.P.; Carino, N.J.; Washer, G., 2003. Health monitoring of civil infrastructures. Smart materials and structures, Vol.12, pp. 483-493.

Clark, M.; Forde, M.C., 2003a. Infrared thermography assessment of masonry arch bridges laboratory and field case studies. In: Proceedings of the International Symposium on Non-Destructive Testing in Civil Engineering.

Clark, M.; Forde, M.C., 2003b. Using conductivity to determine the location of moisture in a masonry arch bridge. In: Proceedings of the International Symposium on Non-Destructive Testing in Civil Engineering.

Clark, M.R.; Crabb, G., 2003. Detection of water movement below a concrete road using ground penetrating radar". In: Proceedings of the 10th International Conference on Structural Faults & Repair.

Clark, M.R.; McCann, D.M.; Forde, M.C., 2003. Application of infrared thermography to non-destructive testing of concrete and masonry bridges. NDT&E International, Vol. 36, pp. 265-275.

Colla, C., 2003. Non-destructive evaluation of brick masonry via scanning impact-echo testing. In: Proceedings of the 9th North American Masonry Conference. Clemson, South Carolina, pp. 954-965.

Colla, C., 1997. NDT of masonry arch bridges, PhD Thesis, The University of Edinburgh, Dept. Civil and Environmental Engineering, Edinburgh, pp. 242.

Colla, C.; Das, P.C.; McCann, D.; Forde, M., 1997a. Sonic, electromagnetic and impulse radar investigation of stone masonry bridges. NDT&E International, Vol. 30, Issue 4, pp. 249-254.

Colla, C.; Forde, M.C.; Das, P.C.; Batchelor, A.J., 1997b. Radar tomography of masonry arch bridges. In: Proceedings of the 7th International Conference on Structural Faults & Repair. Vol. 1. Edinburgh, UK, pp. 143-151.

Colombo, S.; Giannopoulos, A.; Forde, M.C., 2002. Accuracy of radar testing of masonry arch bridges. In: Proceedings IABMAS'02, pp. 252-253.

Cook, J.C., 1995. Preface. Journal of Applied Geophysics 33 (1), pp. 1-3.

Daniels, D.J., 2004. Ground Penetrating Radar. The institution of Electrical Engineers, London.

Daniels, D.J.; Gunton, D.J.; Scott, H.F., 1988. Introduction to subsurface radar. Radar and Signal Processingg, IEE Proceedings F 135 (4), pp. 278-320.

David, J.; Annan, P., 1989. Ground-penetrating radar for high-resolution mapping of soil and rock stratigraphy. Geophysical Prospecting, Vol. 37, pp. 531-551.

Diamanti, N., 2008. An Efficient Ground Penetrating Radar Finite-Difference Time-Domain Subgridding Scheme and its Application to the Non-Destructive Testing of Masonry Arch Bridges. PhD Thesis. University of Edinburgh.

Diamanti, N.; Giannopoulos, A.; Forde, M., 2008. Numerical modelling and experimental verification of GPR to investigate ring separation in brick masonry arch bridges. NDT&E International, Vol. 41 (5), pp. 354-363.

Durán, M., 2005. La construcción de Puentes Romanos en Hispania. Xunta de Galicia.

Durán, M., 2004. Técnica y construcción de Puentes Romanos. Publicado en: Elementos de Ingeniería Romana. Congreso Europeo "Las Obras Públicas Romanas".

Durán, M., 2002. Análisis constructivo de los puentes romanos. Libro de ponencias del I Congreso sobre la Obras Públicas Romanas.

Fanning, P.J.; Boothby, T.E.; Roberts, B.J., 2001. Longitudinal and transverse effects in masonry arch assessment. Construction and Building Materials, Vol. 15, pp. 51-60.

Fernandes, F., 2006. Evaluation of two novel NDT techniques: microdrilling of clay bricks and ground penetrating radar in masonry. PhD thesis. Universidade do Minho.

Fernández, J.A, 1995. Obras Públicas y Monumentos. Revista de Obras públicas y Monumentos, 142 (3347), pp. 7-13.

Fernández, L., 2005. Morphological variants of Spanish Mediaeval bridges. Revista de Obras Públicas, nº 3459, pp. 11-32.

Flint, R.C.; Jackson, P.D.; McCann, D.M., 1999. Geophysical imaging inside masonry structures. NDT&E International, Vol. 32, pp. 469-479.

Forde, M.C.; McCavitt, N., 1993. Impulse Radar Testing of Structures. Journal of the Institute of Civil Engineers Structures and Buildings, 99, pp. 96-99.

Forde, M.C., 2008. Nondestructive Testing as Tool for Inspection of Concrete and Masonry Arch Bridges: International Practice. Transportation Research Board Annual Meeting.

Forde, M.C., 2004. Ground Penetrating Radar. In: Proceedings of Introduction to Non-destructive Evaluation Technologies for Bridges Conference. Transportation Research Board.

Forde, M.C., 1998. Bridge research in Europe. Construction and Building Materials, Vol. 12, Issues 2-3, pp. 85-91.

Fraile, J.M.; Gamallo, J., 2007. Conservación de puentes. Cimbra: Revista del Colegio de Ingenieros Técnicos de Obras Públicas, Issue 375, pp. 10-19.

Frunzio, G.; Monaco, M.; Gesualdo, A., 2001. 3D F.E.M. analysis of a Roman arch bridge. Historical Constructions, pp. 591-597.

García, F.; Ramírez, M.; Rodríguez, I.; Martínez, R.; Tort, I.; Benlloch, J.; Montalvá, J.L., 2007. GPR technique as a tool for cultural heritage restorations: San Miguel de los Reyes Hieronymite Monastery, 16th century (Valencia, Spain). Journal of Cultural Heritage, Vol. 8, Issue 1, pp. 87-92.

Genovese, R.A., 2005. Architectural, archaeological and environmental restoration planning methodology: historic researches and techniques of survey aiming to conservation. In: Proceedings of XX International Symposium of CIPA. CD-ROM.

Giannopoulos, A., 2006. GprMax2D/3D: Electromagnetic simulator for ground probing radar. http://www.grpmax.org/.

Giannopoulos, A., 2005. Modelling ground penetrating radar by GprMax. Construction and Building Materials, Vol. 19, pp. 755-762.

Giannopoulos, A., 2004. GprMax2D/3D. User's Manual. Version 2.0. (From: http://www.gprmax.org/).

Gibson, A.; Popovics, J.S., 2005. Lamb Wave Basis for Impact-Echo Method Analysis. Journal of Engineering Mechanics, Vol. 121, Issue 4, pp. 438-443.

Goodman, D., 2009. GPR-SLICE v6.0 Manual. From http://www.gpr-survey.com, January/2009.

Goodman, D.; Hongo, H.; Higashi, N.; Inaoka, H.; Nishimura, Y., 2007. GPR surveying over burial mounds: Correcting for topography and the tilt of the GPR antenna. Near Surface Geophysics Vol. 5 (6), pp. 383 – 388.

Goodman, D.; Nishimura, Y.; Hongo, H.; Higashi, N., 2006. Correcting for Topography and The Tilt of Ground-penetrating Radar Antennae. Archaeological Prospection, Vol. 13 (2), pp. 157-161.

Grandjean, G.; Gourry, J.C.; Bitri, A., 2000. Evaluation of GPR techniques for civil-engineering applications: study on a test site. Journal of Applied Geophysics 45, pp. 141-156.

Gupta, A.K., 2005. Non Destructive Testing of Bridges. Indian Railways institute of Civil Engineering, Pune 411001.

Hendry, A.W.; Sinha, B.P.; Davies, S.R., 1997. Design of Masonry Structures. E & FN Spon, London.

Hülsenbeck, & Co. (1926). German patent 489 434.

ICOMOS 2001. Recommendations for the analysis, conservation and structural restoration of architectural heritage.

Jol, H.M., 2009. Ground Penetrating Radar: Theory and Applications. Elsevier Science. 524 pp.

Kim, J.-H.; Cho, S.-J.; Yi, M.-J., 2007. Removal of ringing noise in GPR data by signal processing. Geosciences Journal, Vol. 11, No. 1, pp. 75-81.

Lataste, J.F.; Sirieix, C.; Breysse, D.; Frappa, M., 2003. Electrical resistivity measurement applied to cracking assessment on reinforced concrete structures in civil engineering. NDT&E International, Vol. 36, Issue 6, pp. 383-394.

Leckebusch, J.; Rychener, J., 2007. Verification and topographic correction of GPR data in three dimensions. Near Surface Geophysics, Vol. 5 (6), pp. 395-403.

Leucci, G.; Cataldo, R.; Nunzio, G., 2007. Assessment of fractures in some columns inside the crypt of the Cattedrale di Otranto using integrated geophysical methods. Jounal of Archaeological Science, Vol. 34, Issue 2, pp. 222-232.

Llanso de Viñals, J.; 1955. La reforma que el plan de modernización de carreteras ha efectuado en el milenario Puente del Burgo, de Pontevedra. Revista de Obras Públicas. 103, Tomo I (2878), pp. 73-79.

Lorenzo, H.; Arias, P.; Armesto, J.; Rial, F.I.; Pereira, M.; Novo, A.; Riveiro, B.; Solla, M., 2007. Documentation and evaluation of historic masonry arch bridges by means of geomatic techniques. In: Proceedings of 5th International Conference on Arch Bridges (ARCH'07), pp. 373-380.

Lorenzo, H., 1996. Prospección Geofísica de Alta Resolución mediante Geo-Radar. Aplicación a Obras Civiles. CEDEX, Centro de Estudio y Experimentación de Obras Públicas, Madrid, 198 pp.

Lourenço, P.B.; Oliveira, D.V., 2006. Conservation of ancient constructions and application to a masonry arch bridge. In: International Seminar Theory and Practice in Conservations, pp. 253-262.

Lourenço, P.B., 2004. Analysis and Restoration of Ancient Masonry Structures: Guidelines and Examples. University of Minho, Department of Civil Engineering.

Lubowiecka, I.; Armesto, J.; Arias, P.; Lorenzo, H., 2009. Historic bridge modelling using laser scanning, ground penetrating radar and finite element methods in the context of structural dynamics. Engineering Structures, Vol. 31, Issue 11, pp. 2667-2676.

Mabon, L., 2002. Assessment, strengthening and preservation of masonry structures for continued use in today's infrastructure. IABSE Reports, Issue 86, pp. 448-459.

Maierhofer, C.; Brink, A.; Röllig, M.; Wiggenhauser, H., 2005. Quantitative impulse-thermography as non-destructive testing method in civil engineering – Experimental results and numerical simulations. Construction and Building Materials, Vol. 19, pp. 731-737.

Maierhofer, C.; Wöstmann, J.; Hennen, C., 2003a. Non-destructive investigation of complex historic masonry structures with impulse radar. In: Proceedings of the International Symposium on Non-Destructive Testing in Civil Engineering.

Maierhofer, C.; Ziebolz, A.; Köpp, C., 2003b. Onsiteformasonry – A European Research Project: On-site investigation techniques for the structural evaluation of historic masonry. International Symposium. Non-Destructive Testing in Civil Engineering.

Maierhofer, C.; Leipold, S., 2001. Radar investigation of masonry structures. NDT&E International, Vol. 34, pp. 139 – 147.

Martin, J.; Hardy, M.S.A.; Usmani, A. S.; Forde, M.C., 1998. Accuracy of NDE in bridge assessment. Engineering Structures 20 (11), pp. 979-984.

Martinaud, M.; Frappa, M.; Chapoulie, R., 2004. GPR signal for the understanding of the shape and filling of man-made underground masonry. In: Proceedings of 10th International Conference on Ground Penetrating Radar.

Mathur, M.; Kumar, S.V.; Singh, K., 2006. Assessment and retrofitting of arch bridges.

McCann, D.M.; Forde M.C., 2001. Review of NDT methods in the assessment of concrete and masonry structures. NDT&E International, Vol. 34, pp. 71-84.

McKibbins, L.; Melbourne, C.; Sawar, N.; Gaillard, C.S., 2006. Masonry arch bridges: condition, appraisal and remedial treatment. Ciria, London.

McNeill, J.D., 1980. Electromagnetic terrain conductivity measurement at low induction numbers. Ontario, Geonics Limited, Technical Note TN-6, 15 pp.

Melbourne, C.; McKibbins, L.D.; Sawar, N.; Sicilia Gaillard, C., 2006. Masonry arch bridges: condition appraisal and remedial treatment. Documentation, CIRIA, London.

Meola, C., 2007. Infrared thermography of masonry structures. Infrared Physics & Technology, Vol. 49, pp. 228-233.

Meola, C.; Carlomagno, G.M., 2004. Recent advances in the use of infrared thermography. Measurement Science and Technology, Vol. 15, pp. R27-R58.

Millard, S.G.; Shaw, M.R.; Giannopoulos, A.; Soutsos, M.N., 1998. Modeling of Subsurface Pulsed Radar for Nondestructive Testing of Structures. ASCE J. Mater Civil Eng., Vol. 10, pp. 188-196.

Mullett, P.J.; Briggs, M.; Minton, K., 2006. Archtec-Strengthening and Preserving Masonry Arch Bridges in Cumbria. In: Proceedings of Structural Faults and Repair.

NASA, 2009. The electromagnetic spectrum. Modified from http://mynasadata.larc.nasa.gov/ElectromMag.html, last access on 5 November 2009.

Novo, A., 2009. 3D GPR Imaging for archaeological prospection. PhD Thesis. University of Vigo.

Nuzzo, L., 2003. Coherent noise attenuation in GPR data by linear and parabolic Radon Transform techniques. Annals of Geophysics, Vol. 46, No.3, pp. 533-547.

Olhoeft, G.R., 2000. Maximizing the information return from ground penetrating radar. Journal of Applied Geophysics 43, pp. 175-187.

Oliveira, D.V.; Lourenço, P.B., 2004. Repair of stone masonry arch bridges. In: Proceedings of International Conference on Arch Bridges (ARCH'04).

Orbán, Z.; Gutermann, M., 2009. Assessment of masonry arch railway bridges using non-destructive in-situ testing methods. Engineering Structures, Vol. 31, Issue 10, pp. 2287-2298.

Orbán, Z.; Yakovlev, G.; Pervushin, G., 2008. Non-Destructive Testing of masonry arch bridges – an overview. Bautechnick, Vol.85, Issue 10, pp. 711-717.

Orbán, Z., 2007. Non-Destructive Testing of Masonry Arch Bridges. UIC Workshop on Masonry Arch Bridges, Paris.

Orbán, Z., 2006. Increasing the reliability of the assessment of masonry arch bridges by non-destructive testing. Pollack Periodica. An International Journal for Engineering and Information Sciences. Vol.1, Issue 3, pp. 45-46.

Orlando, L.; Slob, E., 2009. Using multicomponent GPR to monitor cracks in a historical building. Journal of Applied Geophysics, Vol. 67, Issue 4, pp. 327-334.

Ozaeta, R.; Martín-Caro, J.A., 2006. Catalogue of damages for masonry arch bridges. Final Draft. International Union of Railways.

Page, L., 1993. Masonry arch bridges. State of the art review. HMSO, Transport Research Laboratory.

Pérez-Gracia, V.; Caselles, O.; Clapés, J.; Osorio, R.; Canas, J.A.; Pujades, L.G., 2009. Radar exploration applied to historical buildings: A case study of the Marques de Llió palace, in Barcelona (Spain). Engineering Failure Analysis, Vol. 16, Issue 4, pp. 1039-1050.

Pérez-Gracia, V., 2001. Radar de Subsuelo. Evaluación para Aplicaciones en Arqueología y en Patrimonio Histórico-Artístico. Tesis doctoral. Universidad Politécnica de Cataluña.

Perret, S.; Khayat, K.H.; Gagnon, E.; Rhazi, J., 2002. Repair of 130-year old masonry bridge using high-performance cement grout. Journal of Bridge Engineering 7 (1), pp. 31-38.

Peters, L.; Young, J.D., 1994. Ground Penetrating Radar as a Subsurface Environmental Sensing Tool. In: Proceedings of the IEEE, Vol. 82, Issue 12, pp. 1813-1822.

Popovics, J.S., 2003. NDE techniques for concrete and masonry structures. Prog. Struct. Engng. Mater. Vol.5, pp. 49-59.

Ranalli, D.; Scozzafava, M.; Tallini, M., 2004. Ground penetrating radar investigations for the restoration of historic buildings: the case study of the Collemaggio Basilica (L'Aquila, Italy). Journal of Cultural Heritage, Volume 5, Issue 5, pp. 91-99.

Reynolds, J.M., 2002. An introduction to applied and environmental geophysics. John Wiley & Sons, Chichester.

Rial, F.I., 2007. Characterization and analysis of GPR bowtie antennas. Application in road surveys. University of Vigo. PhD dissertation. 265 pp.

Rial, F.I.; Pereira, M.; Lorenzo, H.; Arias, P.; Novo, A., 2006. Accurate setting of the Time Zero Position in subsurface radar systems. 5ª Asamblea Hispano-Portuguesa de Geodesia y Geofísica.

Riveiro, B.; Arias, P.; Armesto, J.; Rial, F.; Solla, M., 2008. Multidisciplinar aproach to historical arch bridges documentation. In: Proceedings of the International Society for Photogrammetry and Remote Sensing (ISPRS). Vol. 37, Tome B5, Commission V, pp. 247-252.

Rusnak, C.J.; Boothby, T.E., 1998. Stone bridges and historic American landscapes. Arch Bridges, Sinopoli (ed.). Balkema, Rotterdam.

Saarenketo, T.; Soderqvist, M.K.; Insight, M.K., 1995. Ground penetrating radar applications for bridge deck evaluations in Finland. NDT&E International, Vol. 28, Issue 5, pp. 313.

Saisi, A.; Valle, S.; Zanzi, L.; Binda, L., 2000. Radar and sonic as complementary and/or alternative tests in the survey of structures. In: Proceedings of the International Congress Archi. Vol.1.

Sandmeier, K.J., 2007. ReflexW manual ver. 4.5. From http://www.sandmeier-geo.de. Sandmeier Scientific Software. 435 pp.

Sansalone, M.J.; Streett, W.B., 1997. Impact-Echo: Non-Destructive Evaluation of Concrete and Masonry. Bullbrier Press, New York.

Schuller, M.P., 2003. Non-destructive testing and damage assessment of masonry structures. Progress in Structural Engineering and Materials 5 (4), pp. 239-251.

Senker, J.H., 2007. Pennsylvania stone arch bridges: Evaluation and assessment. In: Proceedings of 5th International Conference on Arch Bridges (ARCH'07), pp. 257-265.

Skolnik, M.I., 2001. Introduction to Radar Systems (3rd Edition). McGraw-Hill, New York.

Skolnik, M.I., 1981. Introduction to Radar Systems. McGraw-Hill, New York.

Solla, M.; Lorenzo, H.; Rial, F.I.; Novo, A.; Riveiro, B., 2009. GPR Surveying of Historical Bridges in Spain. In: Proceedings of 5th International Workshop on Advanced Ground Penetrating Radar (IWAGPR'09). pp. 150-154.

Solla, M.; Lorenzo, H.; Rial, F.I.; Novo, A.; Riveiro, B., 2008a. Aplicabilidad del Georadar en el Estudio de Puentes Romanos. Actas del IV Congreso de las Obras Públicas en la Ciudad Romana. pp. 387-398.

Solla, M.; Lorenzo, H.; Rial, F.I.; Novo, A.; Riveiro, B., 2008b. GPR Survey in the medieval bridge of San Antonio (Cerdedo-Galicia). Actas de la 6ª Asamblea Hispano Portuguesa de Geodesia y Geofísica. Pp. 287-288.

Solla, M.; Lorenzo, H.; Rial, F.I.; Novo, A.; Riveiro, B., 2008c. GPR Survey on Masonry Arch Bridges: A Study Case in Galicia (NW Spain). In: Proceedings of 12th International Conference on Ground Penetrating Radar.

Sundberg, K., 1931. Gerlands Beitr. Geoph., Ergänzungs-Hefte, 1, pp. 298-361.

Tavukçuoğlu, A.; Düzgüneş, A.; Caner-Saltik, E.N.; Demirci, Ş., 2005. Use of IR thermography for the assessment of surface-water drainage problems in a historical building, Ağzikarahan (Aksaray), Turkey. NDT&E International, Vol. 38, Issue 5, pp. 402-410.

Ulriksen, P., 1982. Applicaton of impulse radar to civil engineering. PhD thesis. Department of Engineering Geology, Lund University of Technology.

Ural, A.; Oruç, Ş.; Doğangün, A.; İskender, Ö., 2008. Turkish historical arch bridges and their deteriorations and failures. Engineering Failure Analysis 15, pp. 43-53.

Wiggenhauser, H., 2002. Active IR-applications in civil engineering. Infrared Physics & Technology 43, pp. 233-238.

Wikipedia, 2009. Arkadiko bridge. http://en.wikipedia.org/wiki/Arkadiko_bridge. Last accessed on 08 of April, 2009.

Williams, T.S.; Sansalone, M.J.; Streett, W.B.; Poston, R.W.; Whitlock, A.R., 1997. Non-destructive evaluation of masonry structures using the impact echo method. The Masonry Society Journal 15 (1), pp. 47-57.

Woodham, D., 2002. Using infrared imaging to evaluate masonry. Masonry Construction 15 (4), pp. 25-28.

Yee, K.S., 1966. Numerical Solution of Initial Boundary Value Problems Involving Maxwell's Equations in Isotropic Media", IEEE Transactions on Antennas and Propagation, Vol. 14, pp. 302-307.

Yelf, R., 2004. Where is True Time Zero?. 10th International Conference on Ground Penetrating Radar.